UNIVERSITÀ
DEGLI STUDI
FIRENZE

DOTTORATO DI RICERCA IN
Area del Farmaco e Trattamenti Innovativi

CICLO XXVIII
COORDINATORE Prof. ssa Teodori Elisabetta

Design, optimization, characterization and performance of nanocarriers for brain delivery of natural compounds

Settore Scientifico Disciplinare CHIM/09

Dottoranda
Dott. ssa Guccione Clizia

Tutor
Prof. ssa Bilia Anna Rita

Coordinatore
Prof. ssa Teodori Elisabetta

Anni 2012/2015

To those who have always trusted me and

believed in my dreams

together with me

TABLE OF CONTENTS

List Of Figures

List Of Tables

List Of Abbreviations

AD: Alzheimer Disease
AG: Andrographolide
ALS: Amyotrophic lateral sclerosis
AME: Adsorptive-mediated endocytosis
APCI: Atmospheric pressure chemical ionization
Apo ER-2: Apolipoprotein receptor-2
Apo-E: Apo-lipoprotein E
ATM: adsorptive-mediated transcytosis
AUC: Area under the curves
BBB: Blood brain barrier
BCRP: Breast Cancer Resistance Protein
BCSFB: Blood–cerebrospinal fluid barrier
BSA: Bovine serum albumin
CAT1: Cationic amino acid transporter
CMT: Carrier mediated transport
CNS: Central Nervous System
CNT2: Nucleoside transporter
CSF: Cerebrospinal fluid
CSF: Cerebrospinal fluid
CV%: Coefficient of variation
D: Dextran 70,000
DF: Dilution factor
DMSO: Dimethyl sulfoxide
DLS: Dynamic light scattering
ECA: Ethyl cyanoacrylate
EE: Encapsulation efficacy
EMA: European Medicines Agency
ESI: Electrospray ionization
ESI-: Electrospray ionization in negative ion mode
EtOH: Ethanol
FA: Formic acid
F/T: Freeze and thaw
FDA: Food and Drug Administration
FITC-D: Fluorescein isothiocyanate dextran 70,000
FTD: Frontotemporal dementia

GLP: Good laboratory practice
GLUT1: Glucose transporter
HD: Herbal drug
HD: Huntington disease
HSA: Human serum albumin
HSAC NPs: Nanoparticle of albumin made by chemical cross-linking
HSAT NPs: Nanoparticle of albumin made by thermal cross-linking
IS: Internal standard
IAM: Immobilized artificial membrane
$K_{p,uu}$: Unbound brain-to-plasma ratio
K_p: Total brain-to-plasma ratio
LAT1: Large neutral amino acid transporter
LBD: Lewy body dementia
LC-MS/MS: Liquid Chromatography Coupled to Triple Quadrupole Mass Spectrometers
LC: Loading capacity
LDL: Low-density lipoprotein
LLE: Liquid-liquid extraction
LLOQ: Lower limits of quantification
LOD: Limits of detection
LogP: logarithm of partition coefficient
LOQ: Limits of quantification
LRP1: LDL receptor
MCT1: Monocarboxylic acid transporter
MRM: Multiple reaction monitoring
MRPs: Multidrug Resistance-associated Proteins
MW: Molecular weight
NaCl: Sodium chloride
NAF: Fluorescein sodium salt
NBM: Nucleus Basalis Magnocellularis
NPs: Nanoparticles
NVs: Nanovectors
OATPs: Organic anion transporting polypeptide family
OATs: Organic anion transporters
ORT: Object recognition test
PAMPAs: Parallel artificial membrane permeability assays
P*app*: Apparent permeability coefficient

P_e: Endothelial permeability coefficients
P-gp: P-glycoprotein
PBCA: Poly(butyl cyanoacrylate)
PBS: Phosphate buffered saline
PD: Parkinson Disease
PDI: polydispersity index
PECA-FITC-D-TW80 NPs: Fluorescent poly (ethyl-cyanoacrylate) nanoparticles coated with TW80
PECA-TW80 NPs: Poly (ethyl-cyanoacrylate) nanoparticles coated with Tween 80
PEG-PHDCA: Polymethoxyethyleneglycol cyanoacrylate-co-n-hexadecyl cyanoacrylate
PEG: Polyethylene glycol
RHB: Ringer HEPES buffer
PIHCA: Poly(isohexyl cyanoacrylate)
PLA): Poly(lactic acid)
PLGA: Lactide-co-glycolide acid
PP: Protein precipitation
PS: Surface area
PSA: Polar surface area
QCL, QCM, QCH: Quality control at low, medium, and high concentrations
QCs: Quality controls
R^2: Coefficient of determination
RE%: Relative error
RF: Radio frequency
RME: Receptor mediated endocytosis
SalB: Salvianolic acid B
SAR: Structure Activity Relationship
SEM: Scanning electron microscope
SIM: Selected ion monitoring
SiRNA: Small-interfering RNA
SLE: Supported-liquid extraction
SPE: Solid-phase extraction
SS: Stock solution
TEER: Transendothelial electrical resistance
TEM: Transmission electron microscope
TFA: Trifluoroacetic acid
TJ: Tight junction

TW80: Polysorbate 80
ULOQ: Upper limit of quantification
UPLC-MS/MS: Ultra-performance liquid chromatography tandem mass spectrometry
VD: Vascular dementia
VLDLR: Very low density lipoprotein receptor
WS: Working solution
Zh: Hydrodynamic diameter of the particles
ζ-potential: Zeta Potential
[14C]-PHDCA NPs: PEGylated [14C]-poly[methoxy poly (ethylene glycol) cyanoacrylate-co-hexadecyl cyanoacrylate] nanoparticles

ABSTRACT

The aim of my PhD project was the design, optimization, characterisation and performance of nanocarriers for brain delivery loaded with natural compounds.
Blood brain barrier (BBB) represents an important physio-chemical obstacle for the delivery of therapeutics into the brain and the limitations of conventional therapies increase the interest regard the use of nanotechnologies for neurodegenerative treatments.
Several natural products have been studied for the prevention and the treatment of brain diseases, frequently, with very interesting therapeutic effects but their poor solubility, bioavailability and BBB permeability have limited their use. To overcome these problematical aspects, different NPs that target and reach brain tissues were formulated and examined during this PhD thesis.
My investigation started from the analysis of BBB in order to establish formulative strategies. Two different endogenous mechanisms of transport across the BBB, and deliver therapeutics into the brain, were selected: receptor mediated endocytosis by Apo-lipoprotein E (Apo-E) and adsorptive transcytosis by plasmatic proteins.
One synthetic unit, ethyl-cyanoacrylate, and a protein, human serum albumin, were selected as materials for the design of brain delivery systems. In case of albumin nanoparticle, two distinctive method of preparations were investigated in order to reduce the use of toxic agents in the formulation, according with green chemistry criteria.
Nanocarriers were developed and fully characterized in term of size, superficial charge, encapsulation efficiency, loading capacity and morphology, using Dynamic Light Scattering (DLS) and Transmission Electron Microscopy (TEM).
The brain uptake of fluorescent NPs, their biodistribution and cellular-functional effects were evaluated *in vivo* in healthy rats, after intracerebral injection, while the ability of developed nanocarriers to cross BBB, after intraperitoneal and intravenous administration, were assessed. Behavioural studies were performed for the investigation of safety profile. After the results obtained from the *in vivo* examinations, Salvianolic acid B (SalB) isolated from *Salvia miltiorrhiza* Bge. and Andrographolide (AG) from *Andrographis paniculata*'s leaves were selected, for their pharmacological profile, to be loaded in developed NPs for the treatment of neurodegenerative disease.

The permeability across the BBB of AG in the free form and loaded in nanocarriers was evaluated using a well established *in vitro* BBB model based on monolayers of human immortalized endothelial cells hCMEC / D3, that expresses the receptors for Apo-E (LRP-1expression).

CHAPTER 1
INTRODUCTION

1.1 Biological aspects in Central Nervous System (CNS) drug delivery

The brain is a unique organ highly protected from the periphery by two major barriers (Figure 1), the BBB whit the largest surface area (approximately 20 m^2) and the blood–cerebrospinal fluid barrier (BCSFB). The first represents a wide permeability range, highly regulates intracellular and intercellular signalling pathways and maintains CNS homeostasis [1].

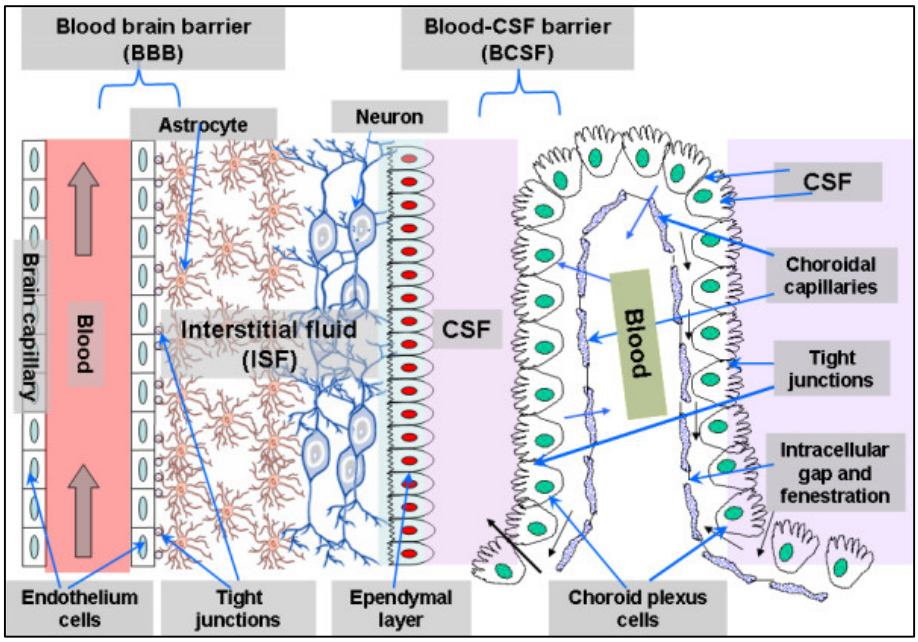

Figure 1: The two main barriers in the CNS: BBB and BCSF [36]

Several neuropathological conditions such as stroke, trauma, bacterial or viral infection, multiple sclerosis, Alzheimer's disease, Parkinson's disease, epilepsy and brain tumours can compromise the integrity of the BBB and as a result CNS permeability can be significantly altered [2]

Main drugs and large molecular weight particulate agents as recombinant proteins, peptides, monoclonal antibodies, small-interfering RNA (siRNA) and gene therapeutics do not readily permeate into brain parenchyma, so one of the most significant challenges facing CNS drug development, is the availability of effective brain drug targeting technology[3].

1.1.1 *BLOOD-BRAIN BARRIER (BBB)*

The BBB, was described for the first time by Paul Ehrlich in 1885, it is primarily composed of not fenestrated brain microvessel endothelial cells characterized by the presence of tight junctions which form a continuous almost impermeable cellular barrier that dramatically limits and regulates the traffic of immune surveillance cells (macrophages), xenobiotics and endogenous compounds. In particular, tight junction proteins (i.e., claudins, occludin) and adherent junction proteins (i.e., junctional adhesion molecule 1) expressed in brain microvessel cells are responsible for the high transendothelial electrical resistance (1500 to 2000 ohm cm^2) that restricts the paracellular entry of water and solutes [4]. The functional unit of the BBB includes more than just capillary endothelial cells. Several other cell types, as pericytes and perivascular astrocytes are in contact with the endothelium and maintenance of the brain capillary phenotype seems to be critically dependent on interactions with these other cells [5–7]. In addition, is present also a selective metabolism-driven barrier that largely reflects expression and function of several receptors, ion channels and influx/efflux transport proteins expressed prominently at the BBB. In particular, ATP-binding cassette (ABC) membrane associated transporters such as P-glycoprotein (P-gp), Multidrug Resistance-associated Proteins (MRPs) and Breast Cancer Resistance Protein (BCRP) play a significant role in restricting the permeability of several pharmacological agents including anti-cancer and anti-HIV agents [8–12]. The most extensively characterized transporter protein at the BBB is P-gp expressed at the luminal membrane of the brain capillary, it is an efflux pumps to extrude xenobiotics from the brain tissue back into the circulation [5]. Influx transporters such as members of the organic anion transporting polypeptide family (OATPs) and organic anion transporters (OATs) can facilitate both: substrate delivery into the brain as well as efflux [13]. In addition to transporters, the BBB also displays a metabolic barrier which together with influx and efflux transporter proteins can regulate the overall pharmacokinetic and pharmacodynamic profile of xenobiotics in the brain [14].

1.1.2 *BLOOD-CEREBROSPINAL FLUID BARRIER*

The BCSFB is composed by choroid plexus epithelial cells with much smaller surface area then BBB. The choroid plexus is a highly vascularized branched structure with numerous villi that project into all four cerebral ventricles [15].The capillaries are fenestrated and provide little resistance to the movement of water and solutes, a barrier is formed by a monolayer of polarized

epithelial cells surrounding the fenestrated capillaries that are joined together by tight junctional proteins that restricts the movement of molecules and ions [16,17] .The choroid plexus epithelial maintain the homeostatic composition of the cerebrospinal fluid (CSF), that fills the ventricles of the brain, the spinal canal and subarachnoid space and provides a drainage system for the brain known as the sink effect into which products of metabolism and molecules are diluted and subsequently removed. The sink effect is greater for large molecular weight and hydrophilic compounds. In humans, the total volume of CSF is approximately 140 ml and it is replaced four to five times daily [18–20]. Polarized expression of numerous receptors, ion channels and transporters has been reported at the level of epithelial cells [15,21–23].

1.2 DRUG TRANSPORT ACROSS THE BBB

The schematic endogenous transport mechanisms by which solutes move across membranes in and out of the brain, across the BBB, are shown in Figure 2.

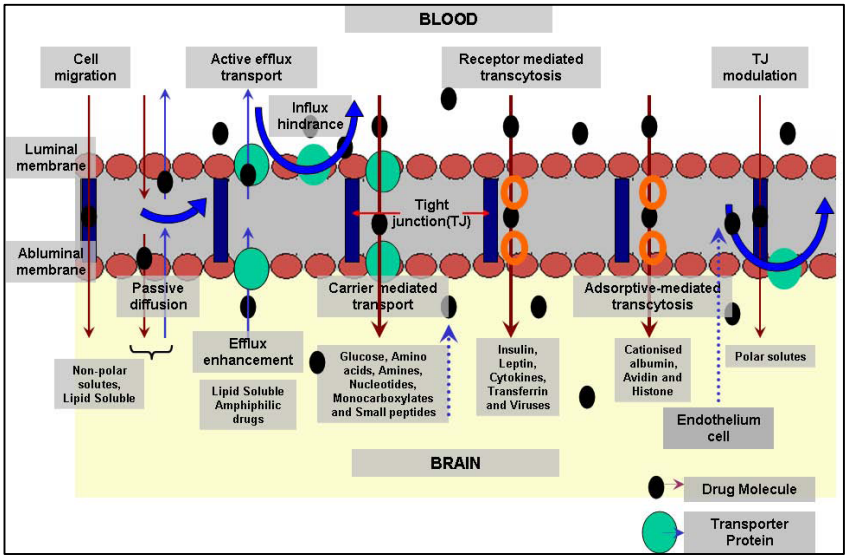

FIGURE 2: POTENTIAL TRANSPORT MECHANISM ACROSS BBB[24]

Firstly, the transport may occur due to diffusion, or simply diffusion or facilitated transport across aqueous channels. The primary bioenergy comes from a concentration gradient across the membranes, between cells (i.e., paracellular) or across cells (i.e., transcellular). This passive diffusion depending from size and lipophilicity of the substances. Secondly, active movement may be caused due

to the molecular affinity, fluid streams or magnetic fields. Carrier mediated transport (CMT) can be passive or active and include the unidirectional transport of drugs from the blood to the brain. It is mainly involved in the transport of many essential polar molecules, with the help of carrier systems or transporters, as glucose (GLUT1 glucose transporter), amino acids (the LAT1 large neutral amino acid transporter, the CAT1 cationic amino acid transporter), carboxylic acids (the MCT1 monocarboxylic acid transporter) and nucleosides (the CNT2 nucleoside transporter) into the brain. This type of transport involves extrusion of drugs from the brain in the presence of efflux transporters such as P-gp, MRPs, BCRP and other transporters, while the active efflux transport causes the active efflux of drugs from brain back to blood. It acts as a major obstacle in pharmacological drug delivery to the CNS.

Receptor mediated transport is primarily employed in the transport of macromolecules like peptides and proteins across the BBB by conjugating the substance with ligands such as lactoferrin, transferrin and insulin.

Adsorptive mediated transport is a type of endocytosis induced by electrostatic interaction with the anionic sites present on the membrane.

Finally, tight junction (TJ) modulation is caused by the relaxation of junctions, which facilitates selective aqueous diffusion across paracellular junctions in the BBB [24].

In our rational in the design of NPs for brain delivery, optimized during my PhD, two different endogenous transport mechanism across the BBB were evaluated:

- Receptor mediated endocytosis (RME), is a highly specific and energy mediated transport allowing eukaryotic cells to selective uptake macromolecules as specific cargo. For the BBB receptor-specific ligands have also been shown to be very effective to transport endogenous peptides like insulin and transferrin, albumin, and opioid peptides e.g. deltorphins, [D-penicillamine 2,5] encephalin and deltorphin II. Receptor-mediated drug delivery, is a promising Trojan horse approach for the release of therapeutics into neuronal cells, and tissues. Nanocarriers conjugated to different types of ligands of cell surface receptors expressed on brain endothelial cells, can accumulate and eventually be internalized by cells on the vascular side of the brain through the mechanism of receptor-mediated endocytosis. According with one possible fate of targeted receptors, the ligand conjugated nanocarrier gets collected in specialized areas of the plasma membrane known as coated pits. These clathrin coated pits

invaginate to form coated vesicles, upon endosomal processing of the vesicle, clathrin and associated proteins dissociate from the vesicle membrane (early endosome), to form new coated pits at the cell surface. The receptor dissociates from the ligand conjugated nanocarrier due to the acidification of the vesicle in the late endosome, and the nanocarrier complex degrades, hence releasing the drug to the cell. In addition, apolipoproteins B and E may be chiefly involved in the transport of NP-bound drugs into the brain. They concluded that by coating the NPs with polysorbate 80 (TW80), apolipoproteins B and E get adsorbed onto the NP surface from the blood after injection and thus seem to mimic lipoprotein particles that could be taken up by the brain capillary endothelial cells via receptor-mediated endocytosis. After endocytosis, drugs may be released within the endothelium cells and undergo further transportation into the brain by diffusion or through transcytosis [24].

- Adsorptive-mediated endocytosis (AME) is based on the electrostatic interaction between a positively charged substance and the negatively charged sites on the brain endothelial cell surface (e.g. glycoprotein). The concept of AME through the BBB originated from the observation that polycationic proteins such as protamine could not only bind to the endothelial cell surface but could also penetrate the BBB. Moreover, mixing protamine, poly-L-lysine or other cationic molecules with proteins (e.g. albumin) or enzymeas (e.g. horseradish peroxidase) greatly increased the permeability of these proteins across cerebral microvessels, probably for their binding affinity for polycations. In a similar manner, cationized proteins can be transported through the BBB. These findings were explained by adsorptive-mediated endocytosis triggered by electrostatic interactions between the positively charged moieties of the proteins and negatively charged membrane surface regions on the brain endothelial cells (ECs). As a consequence, the cationic net charge of a peptide/protein has gradually become recognized as an important determinant in the brain capillary uptake of these molecules. BBB is readily equipped for the AMT process: it provides both the potential for binding of cationic molecules to the luminal surface of endothelial cells, and then for exocytosis at the abluminal surface; the transcytotic pathways present at the BBB and its morphological and enzymatic properties, as well as the high content of mitochondria in

cerebral ECs provide the means for movement of the molecules through the endothelial cytoplasm [24].

1.3 NEURODEGENERATIVE DISEASE

Neurodegenerative diseases are some of the most debilitating disorders, affecting thinking, skilled movements, feelings, cognitive and memory. Today are the fourth leading cause of death in the developed world after heart diseases, cancer and stroke. Globally, each year, over 10 million people have neurodegenerative diseases. This figure is expected to grow by 20% over the next decade as the aging population increases and lives longer. Many similarities appear that relate these diseases to each other on a sub-cellular and molecular levels. These disorders have a high prevalence as well as short- and long-term impairments and disabilities. They include serious disorders such as Alzheimer Disease (AD), Parkinson Disease (PD), Lewy body dementia (LBD), Frontotemporal dementia (FTD), Vascular dementia (VD) and some rare disorders such as amyotrophic lateral sclerosis (ALS), Huntington disease (HD), spinocerebellar ataxia and prion diseases. There are important differences in clinical manifestation but neurodegenerative disorders share common features: their appearance late in life, the extensive neuronal loss and synaptic abnormalities, and the presence of cerebral deposits of misfolded proteins aggregates. Approximately 24 million people worldwide suffer from dementia, 60% of cases being due to AD, which occurs in 1% of individuals aged 50 to 70 and dramatically increases to 50% for those over 70 years. Dramatically, these numbers are estimated to increase to 15 million in the next 40 years [25].

AD is a chronic and progressive neurodegenerative disorder and the most cause of dementia. It is typified clinically by learning and memory impairment and pathologically by cerebral atrophy, indicative of neuronal loss, with numerous extracellular neuritic amyloid plaques and intracellular neurofibrillary tangles found predominantly in the frontal and temporal lobes, including the hippocampus. Although the mechanisms underlying AD are not completely clear yet several approaches aimed at inhibiting disease progression have advanced to clinical trials. AD in characterized by amyloid plaques extracellularly in the brain parenchyma and around the cerebral vessels walls and their main component is a 1-40 and 1-42 residues peptide termed beta-amyloid protein. It is well established that innocuous monomers of amyloid beta become neurotoxic upon aggregation and the toxicity of amyloid beta involved self aggregation of monomers into oligomers and higher aggregated forms. In the

last studies, a variety of post-transcriptionally modified variants have been identified but the predominant accumulation and initial peptide deposited in the brain parenchyma is a fibrillogenic amyloid-beta 1-42. Targeting amyloid-beta 1-42 in all its aggregation forms has been suggested for therapeutic and diagnostic purposes. Recently has been demonstrated that brain and blood amyloid-beta are in equilibrium through the BBB, and sequestration of amyloid- beta in the blood may shift this equilibrium, drawing out the excess from the brain[26–29].

PD is also a chronic disorder that involves the malfunction of dopaminergic neurons. The symptoms of the disease include tremors, stiffness and slow or hesitant speech and it is characterized by massive depletion of striatal dopamine as a result of degeneration of dopaminergic neurons in the substantia nigra pars compacta. Besides the lack of dopamine at the cellular level may appear the formation of Lewy bodies in the substantia nigra, which are cytoplasmic inclusions composed of fibrils, ubiquitin and alpha-synuclein. There are an estimated 7-10 million people living with PD in the world; 1.2 million people suffering from PD in Europe and over 1 million in US, however, medication only provides patients with temporary symptomatic relief, while access to care and treatment differs widely depending on where patients live [30–32].

LBD is the second most common type of progressive dementia after AD, causes a progressive decline in mental abilities; is characterized by fluctuations in cognition with variations in attention and alertness, recurrent formed visual hallucinations, visual spatial dysfunction and, like PD, LBD can result in rigid muscles, slowed movement and tremors. Variation in the distribution of Lewy body pathology is present in LBD, with more neocortical and limbic system Lewy bodies in both. The loss of cholinergic neurons originates the degradation of cognitive functioning, while the loss of dopaminergic neurons is thought to account for the degradation of motor control, as in PD: the overlap of neuropathologies and presenting symptoms (cognitive, emotional, and motor) can make an accurate differential diagnosis difficult. Current estimates are that about 60 to 75% of diagnosed dementias are of the AD and 10 to 15% are LBD [33–36].

FTD is a clinical syndrome associated with reduction of the frontal and temporal anterior lobes of the brain. The current designation of the syndrome groups together Pick's disease, primary progressive aphasia, and semantic dementia as FTD, in fact the symptoms of FTD are based in change in behaviour and problems with language. FTD affects parts of the brain containing microscopic

Pick bodies; abnormal protein-filled structures that develop within neurons. The histological features of FTD are the presence of neurofibrillary tangles of phosphor-Tau in the brain, a variety of mutations on several different genes such as MAPT, PGRN, FUS or VCP are involved and there isn't familiarity in more than half the people who develop FTD [37–39].

VD is widely considered the second most common and distinct type of dementia and these alterations occur in an already aged brain. VD develops when compromised blood flow to parts of the brain deprives cells of food and oxygen. The diagnosis may be clearest when symptoms appear soon after a single major stroke blocks a large blood vessel and disrupts the blood supply to a significant portion of the brain. This situation is sometimes called post-stroke dementia. Symptoms of VD can vary, depending on the specific brain areas deprived of blood. Impairment may occur in steps and memory problems may not be a prominent symptom, depending on whether brain regions important in memory are affected [40].

Other rare neurodegenerative diseases are:

- ALS is a form of motor neuron disease caused by the degeneration of neurons located in the ventral horn of the spinal cord and the cortical neurons that provide their afferent input. This disorder is characterized by rapidly progressive weakness, muscle atrophy and fasciculation, pasticity and respiratory compromise [41].
- HD is a rare fatal brain disorder caused by inherited changes in a single gene called huntingtin. The either of an individual's two copies of the gene. It is the most common genetic cause of abnormal involuntary writhing movements called chorea. These changes lead to destruction of neurons in certain brain regions [25].
- Spinocerebellar ataxia is a congenital disorder characterized by problems with coordination that often disturb legs, hands and speech. There are more than 20 types of spinocerebellar ataxia that have been described. All types of spinocerebellar ataxia are characterized by a progressive incoordination of walking. In addition, they are often associated with poor coordination of hand movements, eye movements, and speech. The symptoms usually occur after the age of 18 but condition gradually worsen over a period of years. Some types of spinocerebellar ataxia can progress more rapidly than others. Brain scans such as magnetic resonance imaging (MRI) and computerized tomography (CT) of affected persons often show reduction or

atrophy of the cerebellum that becomes more noticeable as the disease progresses [42,43].

- Prion diseases are conformational neurodegenerative disorders characterized by the structural modification of the normal cellular prion protein into a pathological conformer; can be inherited, infectious or sporadic. The transmissible pathogen for these diseases is a proteinaceous infectious particle (hence the term 'prion'). These disorders in humans are very rare, affecting only about one person per million worldwide each year but, transmissible prion proteins can reach epidemic proportions, as was seen in the UK. At this moment, there isn't effective therapy for this group of diseases [20,44].

1.4 NANOTECHNOLOGY FOR BRAIN DELIVERY

Nanotechnology, in the context of medicine, is defined as the technologies for making nanocarriers of therapeutics and imaging agents, nanoelectronic biosensors, nanodevices, and microdevices containing nanostructures. Unlike the definition in core nanotechnology field, which restricts the "nano" to at least 1–100 nm in one dimension, nanocarriers in the biomedical field are often referred to as particles with a dimension a few nanometers to 1000 nm; so, nanotechnology, when applied to biomedical and clinical applications, has a broader definition. Nanomedicine and nanotechnology share a common ground of basic science and technologies. Many techniques for making nanomaterials, especially those bottom-up techniques such as chemical synthesis, self-assembly, and positional assembly methods, are used to prepare nanocarriers for delivering therapeutics and imaging agents. Nanomedicine is generally defined as the application of nanotechnology in the clinical field. There are two main medical applications of nanotechnology: medical imaging/diagnosis and therapeutic delivery. In order to have the maximum therapeutic benefits, the carriers must be designed to delivery at target sites at the right time the right dose with the appropriate release kinetics. As discussed in this PhD thesis, multiple physiological, pathological and cellular barriers must be overcome before an adequate drug dose can reach the site of action[45].

1.4.1 DEFINITION OF NANOPARTICLES

According with the classical definition of NPs in the Encyclopedia of Pharmaceutical Technology and in the Encyclopedia of Nanoscience and Nanotechnology formulated already 40 years ago: "NPs for pharmaceutical

purposes are solid colloidal particles ranging in size from 1 to 1000 nm (1 µm) consisting of macromolecular materials in which the active principle (drug or biologically active material) is dissolved, entrapped, or encapsulated, or to which the active principle is adsorbed or attached" [46].
This definition diverges from the definition of physicists and material scientists who limit the upper size of NPs to 100 nm. However, up to 1000 nm size appears to be of no important influence concerning uptake into cells of the reticuloendothelial system (RES), i.e. macrophages and endothelial cells, and also most other parts of the body [46].
Schäfer et al. [47] demonstrated *in vitro* using electron microscopy that human macrophages endocytose NPs independent of size, while Gao and Jiang [48] reported small, i.e. 20%, increase in methotrexate delivery to the brain using 70 nm sized methotrexate loaded poly(butyl cyanoacrylate) NPs overcoated with TW80 after intravenous injection.
No differences in methotrexate brain delivery occurred between 170, 220, and 345 nm sized particles. This insignificant particle size influence can be attributed to the mechanism of NPs uptake and of bound drugs into the brain but the drug payload decreases with a reduced particles size. From other side, with sizes over 1000 nm the danger of embolization of the lung capillaries is increasing in size- and dose-dependent manner [46].

1.4.2 TYPES OF NANOPARTICLE POLYMERS

The main prerequisite for nanoparticulate brain delivery systems must be the biodegradability and the biocompatibility. In fact, non-degradable particles as fullerenes, metal particles or toxic systems such as quantumdots, or potentially risky needle-shaped delivery systems as carbon nanotubes, which may have dangerous effects similar to asbestos, therefore, are not useful. Similarly, silica particles also appear to be not suitable as they would import a very foreign material into the brain. Fumed silica has been used as an auxiliary material for oral application but appears to be not absorbed into the body in significant amounts. Silica NPs also are not a good model system as their body distribution is totally different from carbon chemistry-derived materials [46].
In this moment only three types of materials appear to be suitable for the formulation of nanocarriers: (poly(alky cyanoacrylates) as poly(butyl cyanoacrylate) PBCA, poly(lactic acid) (PLA) or its copolymer (lactide-co-glycolide) (PLGA), and human serum albumin (HSA) [46].

Numerous studies show that PBCA is the fastest biodegrading material. This rapid elimination, probably, depends to the low molecular weights of the poly(alkyl cyanoacrylates) in nanoparticulate form of around 2000–3000 Da while a minimal portion of higher molecular weight compounds also may be present in the particles. Degradation of the polymer occurs by enzymatic cleavage of the ester bond of the alkyl side chain of the polymer resulting in the formation of the low-toxic water-soluble products—poly(cyanoacrylate) acid and appropriate alcohol by esterases. Consequently, the molecular weights of the poly(alkyl cyanoacrylate) esters increase with increasing molecular weights whereas their degradation rate decreases. This reduced degradation significantly decreases their toxicity [46]. For all these reasons, poly(isohexyl cyanoacrylate) was chosen for clinical trials and is now in clinical phase III [49].

Biodegradation of the PLGA NPs also depends by enzymatic degradation by lipases due to their small size which is in contrast to larger PLA particles and materials where hydrolytic degradation is the prevailing degradation mechanism [50].

The degradation rate of HSA NPs also is quite rapid: if prepared by heat denaturation they were totally degraded within 3 days in macrophages, and if they are made by chemical- crosslinking, a rapid degradation also can be estimated, and the observed toxicity of the latter particles was extremely low [51].

In addition to the above materials, chitosan can be another advantageous polymer, because chitosan NPs also are biodegradable and biocompatible, possess good stability, low toxicity and can be manufactured by simple and mild preparation methods [52].

1.4.3 METHODS OF PREPARATION OF NANOPARTICLE

Some of the most commonly method of preparation of NPs are discussed below, as described by Goyal and co-workers [53]:

Nano-precipitation Method

The polymer is first dissolved in a water miscible solvent as acetone, tetrahydrofuran, methanol, ethanol, acetonitrile, DMF etc., then it is dispersed in the aqueous phase under constant stirring. The aqueous phase may contain surfactant. The organic phase will be removed to obtain the NPs in the aqueous phase. NPs quickly precipitate because the organic solvent is diffused in the aqueous phase. As the solvent diffuses from organic phase to the aqueous phase, it carries with it some polymeric chains, which aggregate to form NPs.

The size of NPs are affected by the concentration of polymer and the solvent system used.

Solvent Evaporation

This method is similar to nano-precipitation, the difference lies in the organic solvent in fact, in nano-precipitation is miscible with water, while in the solvent evaporation method is immiscible.

The organic phase is dispersed in the aqueous phase and it forms an oil-in-water emulsion. The emulsion is stabilized by using surfactants like TW80, poly vinyl alcohol, poloxamer-188, etc. and after the stabilization, the organic phase is evaporated under constant stirring.

Salting Out

In this process the polymer is slowly dissolved in a water miscible organic solvent. The aqueous phase contains high concentration of salt and emulsifiers due to which the mixing of organic phase and the aqueous phase is slowed down. These separate phases are emulsified by stirring. NPs are formed adding water rapidly to reduce the ionic strength. The excess salt must be removed before using it for therapeutic use. Sometimes the washing steps to remove excess salts and stabilizing agents became very extensive.

Emulsion Diffusion

The polymer is dissolved in an organic solvent, partially miscible with water (e.g. ethylacetate, polyprolylene carbonate, etc.). Aqueous phase containing stabilizer is added to this system. The mixture is constantly stirred with simultaneous addition of water. Copious quantity of water is added, until the formation of oil-in-water emulsion. The organic phase is removed by constant stirring, which results in the formation of NPs. This process has high reproducibility thanks the stabilizers that reduce the surface tension and makes the particle size smaller.

Emulsion Evaporation

An oil-in-water emulsion is done by dispersing the organic solvent containing polymer in the aqueous phase with stabilizers. A strong shear stress is applied to the emulsion droplets, which further breaks down the droplets into smaller size, then the organic phase is evaporated and polymer is precipitated to form the

NPs. Apply high shear stress is important to stop the migration of emulsion droplets towards each other and prevent their aggregation.

1.4.4 BRAIN DELIVERY SYSTEMS

In the last 35 years, with the advent of nanomedicine, different formulations have been proposed to enhance the delivery of therapeutics into the brain, as showed in the following highlights (Figure 3) and described below [53].

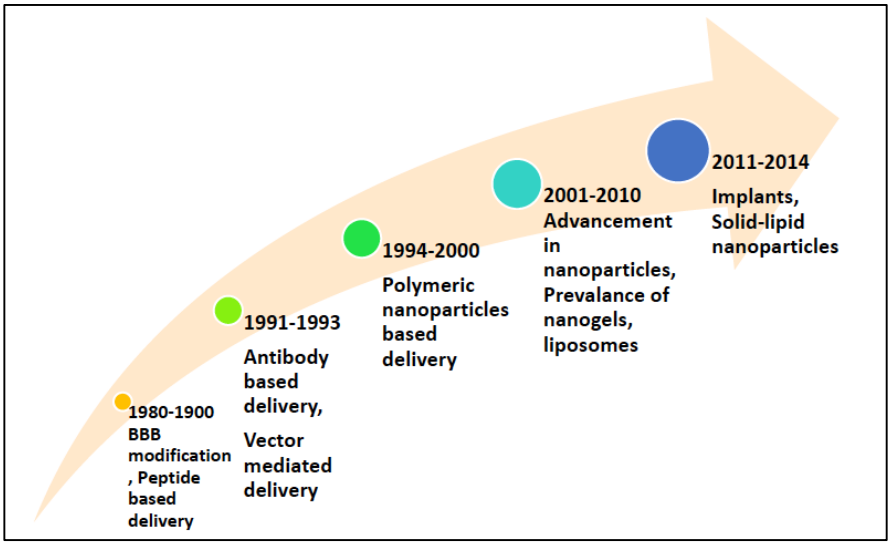

FIGURE 3: HIGHLIGHTS OF THE MAJOR DEVELOPMENT IN BRAIN DELIVERY SINCE 1980 [91]

Micelles

They are basically made of block copolymers, which self-assemble to from a dense hydrophobic core, which is surrounded by a hydrophilic brush like layer. The brush like outer structure prevents the micelles from adhering to proteins and cells, prevents opsonization and hence gives the micelles the advantage of having long circulation time in the body. Additional advantages of micelles are controlled drug release and good tissue penetrating ability. Various hydrophobic core are used in micelle formation, like poly(propylene oxide), PLA, poly(ε - caprolactone), poly(l-aspartate) and poloxamers and provide an excellent environment for the encapsulation of hydrophobic drugs. There are different disadvantages associated with micelles such as limited stability, difficult polymer synthesis, immature drug encapsulation technology, limitation to hydrophobic

drugs, slow extravasation and possible chronic liver toxicity due to slow metabolic processing.

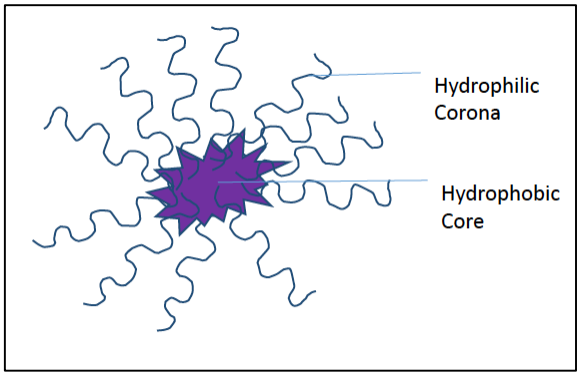

FIGURE 4: MORPHOLOGY OF POLYMERIC MICELLE [91]

Nanospheres

They are solid particle formed by polymeric matrix in which drugs can be dissolved, encapsulated or entrapped. The drugs can also be attached to the polymeric matrix by adsorption or chemical bonding. The hydrophobic surface of the nanospheres is susceptible to opsonization and hence it does not have long circulation time.

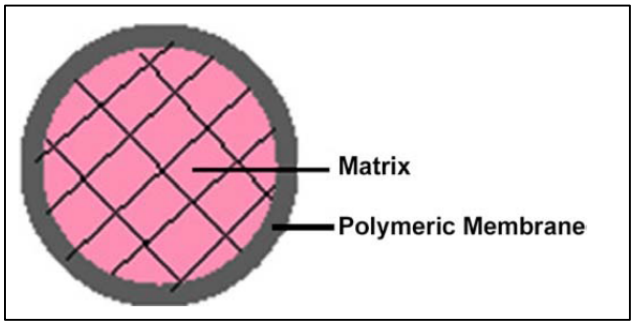

FIGURE 5: NANOSPHERES [91]

Nanocapsules

They have nanoscale vesicular structures, so are made up of polymeric membrane, which encapsulates the inner core. Concerning the size of nanocapsules, they are generally ranges from 10-1000 nm, as nanospheres too.

The drug is loaded into the inner core and should be both lipophilic and hydrophilic depending on the method of preparation of the nanocapsules.

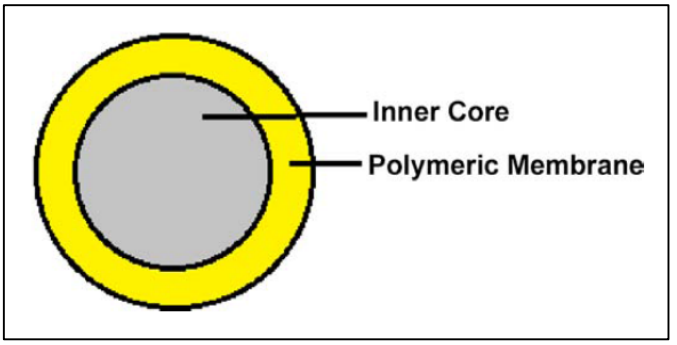

FIGURE 6: NANOCAPSULES [91]

Polymersomes

With a vesicular structure, they are composed by aqueous internal core surrounded by a polymeric membrane. The polymeric membrane can be viewed as a hydrophobic layer sandwiched between hydrophilic polymeric brushes. Thanks their thicker outer membranes, they are considered more stable vesicles if compared with the lipid based vesicles. The size are comprised between 5 nm and 5 µm.

The advantage of using the polymeric drug delivery system are related with their robustness and stability, with a high drug loading capacity and an opportunity with the possibility to control the drug release kinetics of the system.

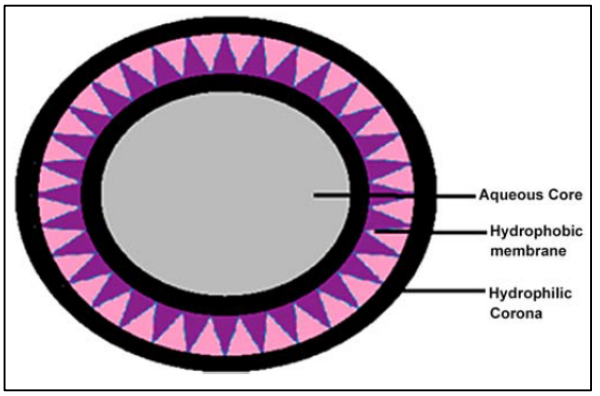

FIGURE 7: CROSS -SECTIONAL VIEW OF A POLYMERSOME [91]

Liposomes

The main advantage of this nanocarrier is the structure similar to cells with lipid bilayer. The vesicle has a hydrophilic core surrounded by a hydrophobic layer, decorated with hydrophilic groups on the outer surface. The bilayer is generally composed of the phospholipids. Liposomes can successfully act as nanocarriers to deliver drugs across the BBB. Liposomes were developed and conjugated with antibodies to work as immunoliposomes in the treatment of Alzheimer's disease, in this study, the antibodies against the transferrin receptor were conjugated onto the surface of the liposomes to cross the BBB.

Higher bioavailability, low cost, simplicity of preparation and the capability of transporting both hydrophobic and hydrophilic drugs makes liposomes an attractive nanocarrier for CNS drug delivery. The disadvantages are associated with the higher size.

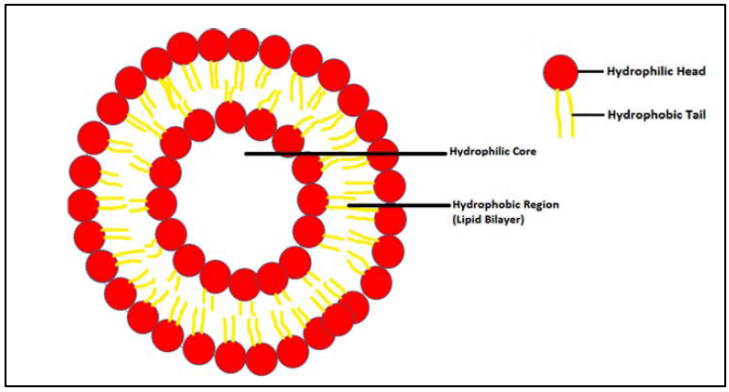

FIGURE 8: CROSS-SECTION OF LIPOSOME AND SINGLE UNIT OF PHOSPHOLIPIDS [91]

Microemulsions

These emulsions have droplet size at least 100 times less than the conventional emulsion system, they are thermodynamically stable blends of oil, water, and surfactant, and widely used for enhancing the bioavailability of the poorly soluble drugs. The small droplet size and low surface tension of microemulsions leads to higher absorption and permeation across the BBB.

Microemulsions are thermodynamically more stable and, therefore easy to store. They have higher skin penetration and diffusion rate but use of large amounts of surfactants to stabilize microemulsions is still a major concern.

Solid Lipid Nanoparticles (SLNPs)

They are nanoparticulate system with a solid core, synthesized from the solid lipids at room temperature. The main advantage of SLNPs is their very high drug loading capacities.
The surface of SLNPs loaded with carmustine was modified with monoclonal antibody to enhance the drug delivery across the BBB. This research provided promising breakthrough to the use of SLNPs for CNS drug delivery The nanocarrier is really advantageous for their control the drug release and for the incorporation of both hydrophilic and lipophilic drugs. Is very important consider that using the physiological lipids in the synthesis process, is possible reduce the risk of toxicity.

Nanogels

They are hydrogels with crosslinks of nanoscale size. The crosslinking is between hydrophilic or amphiphilic polymeric chains. The nanogel made from polyethyleneimine and polyethylene glycol (PEG) swells by making crosslinks when dispersed in a solution. As the drug binds to it through electrostatic interaction, the nanogel collapses. PEG plays a major role in stabilizing the structure and nanogels form a stabilized dispersion. Nanogels are prepared by the ionic gelation method using sodium tripolyphosphate and chitosan. If nanogels are modified with polysorbate 80, the drug loaded cross BBB [54].
In a recent study, it was shown that 5'-triphosphates of Nucleoside reverse transcriptase inhibitors encapsulated in cationized nanogels were more successful in suppressing the HIV-1 activity in CNS than NRTIs. The cationic drug-loaded nanogels exhibited less toxicity to the mitochondria [55].

Implants

They are the device used to replace a structure, support a damaged structure, or supplement an existing structure in human body. The implants are also used for diagnostic and drug delivery applications. They are traditionally made by silicon and use for investigating the neuronal firing but severe neuroinflammation are caused by the implant. It is hypothesized that the mechanical incompatibility between the rigid implant and soft brain tissue is the significant reason for neuroinflammation. In case of intracortical implants, it is seen that the implant caused tissue reactivity, which is probably for the oxidative stress created by the implant as well as its inflexibility. Its rigidity with respect to the softness brain tissue leads to the failure of the implant.

Recently, a group developed PVA based polymeric implants. These implants are mechanically adaptive and flexible, and designed to release curcumin. The two important parameters, which acted synergistically *in vivo* were: softening and flexibility of the implant and presence of an antioxidant [56]. The results of this investigation have opened up a new channel of flexible intracortical implants, where the neuroinflammation due to the rigidity of the implants has been minimized remarkably.
The implants are advantageous as they provide with maximum bioavailability but their implantation and removal requires surgical intervention, which is troublesome for the patient.

A considerable number of drugs have been already transported into the brain across BBB using nanocarriers. These drugs include anticancer, analgesic, cardiovascular drugs, protease inhibitors, several macromolecules etc. The majority of this drugs are listed in Table 1.

TABLE 1: DRUGS LOADED IN NPS FOR BRAIN DELIVERY [46]

Drug	Type of action	Core polymer	Surface modification	Size [nm]	Surface charge [mV]
Amphotericin B	Antifungal drug	PLA-PEG	PS80*	114–133	n/r****
BCNU	Anticancer drug	PLA	Transferrin	120	−35
Breviscapin	Cerebrovascular drug	PLA[a]	P188**	127	−34 to −56
				320	
Camptothecin	Anticancer drug	Poly-ε-caprolact.-PEG	PEG	130–280	0 to −20
Caspase-3 inhibitor	Caspase-3 inhibitor	Chitosan-PEG	PEG + anti-transferrin antibody	650	+18 to +20
Coumarin-6	Dye	PLGA-PEG	PS 80*	194	−23
			P188**	188	−21
			P407***	196	−20
					−
			PEG	200	22 to +2
			Glutathione	230–246	n/r****
			Phage-display peptide	104–121	−18 to −24
Dalargin	Analgesic drug	PBCA	PS 80*	230	n/r****
Dexamethasone	Steroidal drug	PLGA	Alginate hydrogel	400–600	n/r****
Dopamine	Anti-Parkinson drug	Chitosan	None (i.p. inject.)	98–148	+27 to +34
Doxorubicin	Anticancer drug	PBCA	PS 80*	270	n/r****
		PLGA	P188**	240–470	−11 to +16
Endomorpin-1	Analgesic drug	PBCA	PS 80*	27[a]	n/r****
Gemcitabine	Anticancer drug	PBCA	PS 80*	112	n/r****
Green fluorescent protein	Fluorescent dye	PBCA	PS 80*	150	n/r***
Horseradish peroxidase	Enzyme	PBCA	PS 80*	150	n/r****
Kyotorphin	Analgesic drug	PBCA	PS 80*	195–289	n/r****
Loperamide	Opiate receptor agonist	PBCA,	PS 80*	290	–, −35, −13
		HSA,	Apo E3, A1, B100	218–240	
		PLGA	P188**	178/290	−17 to −25
		PLGA	(R)-g7 peptide	139–182	−36 to +31
		PLGA-PEG	PEG	150	
Methotrexate	Anticancer drug	PBCA Chitosan	PS 80**	87[a]–318	n/r****
			PS 80*	125–263	+15 to +31
MRZ 2/576	NMDA reception antagonist	PBCA	PS 80*	251	n/r****
Nerve growth factor (NGF)	Growth factor	PBCA	PS 80*	250	n/r****
Obidoxime	Acetylcholinesterase reactivator	HSA	Apo E	230	n/r****
Paclitaxel	Anticancer drug	Poly-ε-caprolact.-PEG	Angiopep	90	n/r****
		PLA-PEG	Glutathione	230–246	n/r****
		Poly-ε-caprolact.-	Aptamer	156	−33
		PEG	PEG	73	−4
Rivastigmine	Anti-Alzheimer's drug	PBCA	PS 80*	41[a]	−35
		Chitosan	PS 80*	47[a]	+30 to +33
Ritonavir:	Protease inhibitor	PLA[a]	Trans-activating transcriptor peptide	175	+2
Saquinavir	Protease inhibitor	PBCA,	PS 80*	192–184	Medium negative
Sulpiride	Atypical antipsychotic drug	PLA[a]	Maleimide PEG	329	−39 to −19
Superoxide dismutase	Radical scavenger	PLGA	None (Infarcted animal)	291	−25
Tacrine	Anti-Alzheimer's drug	PBCA	PS 80*	36[a]	−40
		Chitosan		41[a]	+35 to +37
Temozolomide	Anticancer drug	PBCA	PS 80*	136	−25
Tubocurarine	Muscle relaxants	PBCA	PS 80*	230	n/r****
TGF-ß antisense oligonucleotide	Antisense oligonucleotide	PBCA	PS 80*	n/r***	n/r****
Valproic acid	Anticonvulsant and mood-stabilizing drug	PBCA	PS 80*	n/r****	n/r****

[a] these size are usually small,* PS 80 = polysorbate 80, ** PS 188 = poloxamer 188, *** P 407 = poloxamer 407, **** n/r = not reported

The next table reports the list of recent patents for NPs specifically formulated for the brain.

TABLE 2: PATENTS OF NANOCARRIERS DEVELOPED FOR THE BRAIN [25]

Class	Function Into Brain	Patent Number
Nanocapsules	Drug delivery	TW201006495 WO2009135853
Gold nanoparticle	Drug delivery	US2011262546
Magnetic nanoparticle	Drug delivery and imaging	US2011213193
Solid lipid nanoparticle	Drug delivery	US2011208161
Nanoparticle	Drug delivery	US2011195125
Gold nanoparticle	Drug delivery	US2011111040
HDL nanoparticle	Imaging	WO2011044545
Nanoparticle	Drug delivery	MX2010012137
Nanoemulsion	Drug delivery	CN101884614
Hydrophilic nanoparticle	Drug delivery	CN101701061
Dendritic conjugates	Diagnostic	WO2009142754
Gold nanoparticle	Imaging	WO2009136763
Chitosan nanoparticle	Imaging	US2010260686
Manganese oxide nanoparticle	Diagnostic	KR20100078508
Magnetic nanoparticle	Imaging	KR20070121788
Lipid nanoparticle	Drug delivery	WO2008024753
Lipid nanoparticle	Drug delivery	WO2008018932

1.4.5 *MECHANISM OF NANOPARTICLE-MEDIATED UPTAKE INTO THE BRAIN*

According with the last study of Kreuter [46], there are different proposed mechanisms of uptake of loaded NPs into the brain:

1. An increased retention of the NPs in the brain blood capillaries combined with an adsorption to the capillary walls. This could create a higher concentration gradient that would increase the transport across the ECs layer and as a result enhance the delivery to the brain.
2. The TW80 used as the coating agent could inhibit the efflux system, especially Pgp.
3. A general toxic effect on the brain vasculature.
4. A general surfactant effect characterised by the solubilisation of the EC membrane lipids that would lead to membrane fluidisation and to an enhanced drug permeability across the BBB.

5. Opening of the tight junctions between the brain blood vessel ECs. The drug could then permeate through the tight junctions in free form or together with the NPs in bound form.
6. Endocytosis by the ECs followed by the release of the drugs within these cells and delivery to the brain.
7. Transcytosis through the brain ECs layer.
8. A combination of the above effects.

NPs transport across the BBB seems to occur by endocytosis of the particles by the brain capillary ECs after intravenous injection followed by NPs transcytosis across these cells. In the previous reviews [57–60] was evidenced by the authors that the creation of high drug concentration gradients by adherence of the NPs to the inner surface of the blood capillary walls (mechanism 1) would not be sufficient for an effective and pharmacologically relevant drug transport across the ECs layer since the diffusing drug still would have been subjected to the highly efficient efflux transporters such as Pgp in the luminal membranes of these cells. These efflux transporters also cannot be blocked by the presence of the 1% TW80 in the injected NPs suspension because the pre-injection of polysorbate 80-coated empty NPs 5 or 30 min before injection of a dalargin solution did not induce any pharmacological effects and this fact negates the permeabilisation of the BBB by toxic effects (mechanism 3) or by membrane solubilisation caused by the surfactant (mechanism 4) and also opening of the tight junctions (mechanism 5). This conclusion was further verified by electron microscopic studies histological investigations and toxicological experiments [46].Moreover, a surfactant induced permeability enhancement appears to be unlikely as no pharmacological responses were observed after injection of dalargin loaded in NPs coated with other surfactants such as poloxamers 184, 338, 407, poloxamine 908, Cremophor® EZ, Cremophor® RH 40, and polyoxyethylene-(23)-laurylether (Brij® 35). Moreover, the electron microscopic studies by Kreuter et al. [61] showed that the tight junctions (mechanism 5) did not open after intravenous administration of the NPs. Mechanisms 6 and 7 are the principal mechanisms for the transport of drugs across the BBB into the brain [58].

Different *in vivo* experiments were performed with different apolipoproteins adsorbed directly onto uncoated or polysorbate 80-coated dalargin-loaded PBCA NPs prior to their intravenous injection, and the pharmacological responses (antinociceptive effects) were measured, demonstrating that,

especially apo E and B, yielded high antinociceptive effects. Consequently, it was concluded that TW80 and poloxamer 188 act as an anchor for the apolipoproteins and that these apolipoproteins then interact with lipoprotein receptors on the brain ECs cells [57,58,60]. Apo A-I is able to interact with the scavenger receptor class B type I and apo E and B with the LDL receptor (LRP1), for this reason, interaction with these receptors, followed by endocytosis and transcytosis across the brain capillary endothelial cells appears to be the principal mechanism for the drug delivery by surfactant-coated PBCA, polylactic acid, and HSA NPs with adsorbed or covalently linked targeting ligands such as the apolipoproteins A-I, B, and E. Accordingly NPs would mimic lipoprotein particles and act as Trojan horses. Zensi et al. [51] showed that only NPs with covalently bounded apolipoprotein A-I or apo E were found in brain capillary ECs as well as in neurons. Reimold et al. [62] developed rhodamine-123-, fluorescein-isothiocyanate-dextran-, or doxorubicin-labelled PBCA NPs and after the administration of TW80-coated NPs by carotic injection, fluorescence could first be detected in cryosections of the brain in capillary lumina with a progressive shift to capillary endothelial cells at 30 min followed by a rather evenly spread distribution across the brain tissue at 60 min after administration. Sixty minutes after administration into the tail vein, the fluorescent particles could be assigned to ECs, whereas after 2 h a rather evenly spread distribution across the he brain tissue was seen. No fluorescence in the brain was detectable with uncoated NPs. It is very important to note that endocytotic processes by ECs including brain capillary ECs are quite rapid processes, in fact NPs are observable in these cells of mice and rats already 15 min after i.v. injection and at the same time significant pharmacological effects are observed [46].
The transport of NPs across BBB appears to be also circadian phase-dependent in fact a circadian-time-dependent fluctuation in the permeability, or the transcytosis capacity, of the small cerebral vessels was observed by Ramge et al. [63].

1.4.6 Influence of surface proprieties

The surface properties of the NPs were found to be the key factor for successful brain delivery. In particular, endocytosis of the negatively charged 200–300 nm PBCA NPs by brain capillary ECs was clearly enabled by TW80 coating, which enhanced the adsorption of the plasma apolipoprotein on the surface of these particles. The Apo E participates in the transport of lipids into the brain by the low-density lipoprotein (LDL) receptors, which is essential for maintaining

cholesterol homeostasis. The Apo E binds to a number of receptors on the BBB such as LDLR, LRP-1, very low density lipoprotein receptor (VLDLR), apolipoprotein receptor-2 (Apo ER-2) and megalin/gp330, as well as receptors in other parts of CNS. Thus it is probable that the presence of Apo E on the NPS surface promoted internalization of these NPs in the brain capillary ECs via the LDL receptors expressed by these cells. As described previously, polysorbate 80, and also 20, 40, 60 and poloxamer 188 were able to achieve antinociceptive effects in mice after binding of dalargin following intravenous injection, whereas other surfactants such as poloxamers 184, 338, 407, poloxamine 908, Cremophor® EZ, Cremophor® RH 40, and polyoxyethylene-(23)-laurylether (Brij® 35) did not yield such effects [46].

Calvo et al. [64] showed that in mice and rats after intravenous injection of PEGylated [14C]-poly[methoxy poly (ethylene glycol) cyanoacrylate-co-hexadecyl cyanoacrylate]NPs ([14C]-PHDCA NPs), the 14C-concentrationin was enhanced considerably in different brain tissues. If NPs are PEGylated, they are called “stealth” and it means that they are characterized by a significant reduction in liver uptake and increase in blood circulation time and distribution into other organs and tissues. A species-dependent influence of the surfactants on the brain concentrations was observed: in mice the brain concentrations of the [14C]-PHDCA NPs were higher after coating with TW80 than with poloxamine 908 whereas in rats this order was reversed. After the reduction of the NPs dose, maintaining the same total polysorbate concentration, higher [14C] brain levels were observed with the TW80-coated NPs than with the PEGylated [14C]-PEG-PHDCA particles. In the studies of Brigger et al. [65] the tumour concentrations of the PEGylated NPs were about 3 times higher than with the normal particles and about 5–6 times higher than in the adjacent brain areas; in the tumour-bearing rats, the brain concentrations in the areas adjacent to the tumour as well as in the contralateral brain hemisphere also were increased significantly compared to normal animals without tumour, indicating a generally higher permeability in the diseased animals. In this context Huang et al. [66] found no difference in brain uptake between stealth and non-stealth [14C]-labelled polymethoxyethyleneglycol cyanoacrylate-co-n-hexadecyl cyanoacrylate (PEG-PHDCA) NPs in mice after intravenous injection, although the blood circulation time of the stealth particles again was significantly prolonged. Stealth properties alone, therefore, do not appear sufficient for enabling a NPs-mediated transport into the brain.

All these results underline the importance of the surface properties for brain drug delivery by intravenous injection.

1.4.7 *TOXICOLOGICAL RESULTS*

In the literature several studied has been made in order to investigate the toxicity of developed nanocarriers.

The toxicity of empty and loaded with doxorubicin PBCA NPs and control solutions of doxorubicin was investigated in many studies in normal and also in glioma 101/8-bearing rats. Doses up to 400 mg/kg of empty NPs did not cause any mortality within the period of observation (30 days) nor did they affect body weight or weight of internal organs after intravenous injection. Higher doses cannot be administered intravenously by bolus injection because of biological and technical limitations. Single intravenous injections of doxorubicin formulations caused dose-dependent mortality and weight loss. No significant difference in toxicity occurred between healthy and tumour-bearing animals. In addition, multiple intravenous injections (3 or 4 Å~ 1.5 mg/kg) were performed to assess body and internal organ weight, hematological parameters, blood biochemical parameters, and urinalysis. Morphological evaluations including macroscopic and histological investigations of heart, lung, spleen, testes, and liver revealed a considerably decreased toxicity in heart and testes of the animals treated with the doxorubicin bound to NPs compared to its solution. The lower toxicity of the nanoparticulate formulations of doxorubicin most probably is explained by the altered biodistribution of the drug mediated by the NPs. The reduced cardiotoxicity is the main goal because represents the limiting factor in the tumour therapy with doxorubicin. Additionally, a lower hepatotoxicity compared to the solutions occurred with the NPs although higher liver concentrations were determined in pharmacokinetic studies. Probably binding to NPs also leads to a different distribution of the doxorubicin within the liver increasing the Kupffer cell uptake thus making it less accessible to the more sensitive hepatocytes, thereby reducing its toxicity.

After autopsy, healthy animals treated with doxorubicin solution showed slight signs of lung oedema while these changes were not observed in animals treated with doxorubicin bound to the NPs. Indication of short-term neurotoxicity, such as increased apoptosis in areas distant from the tumour, increased expression of GFAP or ezrin on distant astrocytes or degenerative morphological changes of neurons, were entirely absent in NPs treated animals on day 12 as well as in long-term survivors. In addition, there was no indication of chronic glial

activation in areas distant from the tumour site in long-term surviving rats. Additionally, long-term survivors did not exhibit any obvious neurological symptoms [46].

1.5 MODELS TO PREDICT BRAIN PENETRATION

Brain penetration of drugs has two important mechanisms: *rate* (at the initial state) and *extent* (at steady state) (Figure 9) The *rate* of brain penetration depends on the permeability of the compounds across the BBB (by passive diffusion, active uptake and/or efflux). The *extent* of brain penetration is determined by the distribution of the drug between brain and plasma, and is affected by multiple factors including metabolic clearance, plasma protein binding, nonspecific binding to brain tissue, and drug clearance from brain ISF into CSF. Models to assess CNS penetration have typically been designed to measure either one of these two components (rate or extent) [67,68].

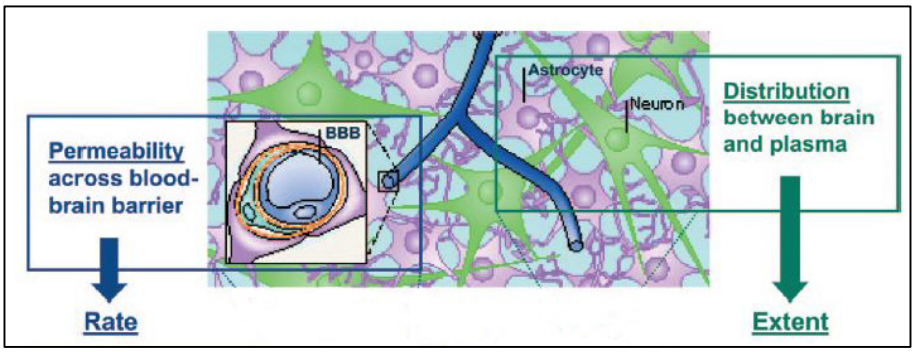

FIGURE 9:CNS PENETRATION OF A DRUG IS IMPACTED BY THE PERMEATION ACROSS THE BBB AND BY THE DISTRIBUTION TO AND WITHIN THE BRAIN [69]

In the last years, a wide spectrum of *in silico*, *in vitro* and *in vivo* models has been developed and employed in academia and industry, primarily dictated by two factors: (1) the need to advance the understanding of the complex molecular mechanisms regulating the brain environment and (2) facilitate the development of alternative and more effective pharmacological strategies aimed to CNS targets [70].

1.5.1 IN SILICO MODELLING AND PREDICTION

Recently computational models to predict rate and extent of brain penetration of drug molecules have become progressively popular. Methods based on

computer simulation are gained more and more interest in the research field as the incredible development of computer technology and advance algorithms are becoming available. Brain penetration of a molecule is influenced by its physicochemical properties such as lipophilicity, polar surface area (PSA), molecular weight (MW), hydrogen bonding and ionization state. One of the first set of rules for optimal brain penetration was introduced in 1995 by Pardridge [71] since he specified that BBB permeability of a drug is possible if the number of total H-bonds is < 8–10, the MW < 400–600 Da, and if the compound is not an acid [71]. Others studies have suggested that BBB permeation is favorited if the sum of oxygen and nitrogen is ≤ 5, the PSA < 60–70 Å2, the MW < 450 Da, and the LogD (at pH 7.4) between 1–3 [72–74].

Use of physico-chemical descriptors determining molecular partition (Abraham solvation equation) has proved to be one of the most reliable methods. A major problem has been the lack of biological experimental data, thus around 20 published computational modelling approaches have used variants of the same log BB training data set, or pooled data from different sources. There are even fewer reliable estimates of log PS, although this measure is expected to produce models better able to predict BBB permeability.

Until recently, lack of detailed knowledge on the Structure Activity Relationship (SAR) of transporter proteins and enzymes has made it difficult to generate predictive models for the 'transport' and 'metabolic' barrier functions of the BBB. That is beginning to change, with the appearance of hybrid (*in vitro/in silico*) models capable of predicting both passive and transporter-mediated function, and software tools for screening drugs for chemical features likely to make them P-gp substrates [70].

1.5.2 IN VITRO MODELS

In vitro models can be subdivided into physicochemical methods and cell-based methods. The functional and structural requirements for an ideal *in vitro* BBB model are reported in the subsequent table:

TABLE 3: REQUIREMENTS FOR AN IDEAL BBB *IN VITRO* MODEL [70]

Functional Features of An Ideal *In Vitro* BBB Model
Enable the expression of tight junctions between adjacent endothelial cells.
Negligible paracellular diffusion between endothelial cells.
Selective and asymmetric permeability to physiologically crucial ions (Na^+, K^+,CI^-).
Functional expression of efflux systems and selective transport mechanisms (e.g., P-gp, MRPs, hexose, aminoacid, monocarboxylic acid, and other relevant transporters).
Expression of drug-metabolizing enzymes (P450s, MAO, etc.).
Exposure to laminal shear stress (apical membrane), glia (basal membrane), and other permissive factors that promotes growth inhibition and differentiation of endothelial cells.
Responsiveness to permeation modulators (e.g., hyperosmolar mannitol) as well as other stimuli (endogenous and exogenous) that can affect BBB integrity and function.
Ability to reproduce the effect of a wide range of physiological and pathophysiogical stimuli (hypertension, flow arrest, inflammation, etc.) that affect the BBB *in vivo*.
User friendly, scalable, and cost effective.

The models of the BBB started to emerge in the early 1990s as potential new research tools complementary to *in vivo* and human studies in basic, translational, and clinical/pharmaceutical research bearing a number of desirable advantages:

1. cost effective—they are relatively inexpensive when compared with animal experimentation with a significantly higher throughput for drug permeability testing (a quality most desirable in the pharmaceutical industry);
2. simplified working environment—the artificial environment provided by these *in vitro* models allows studying and manipulating the BBB without the cumbersome number of additional variables to sort out when working with an entire organism;
3. versatility—they provide highly controllable and in some case quasi-physiological environments outside of a living organism in which cells or tissue can be manipulated to study and dissect out the response of a specific tissue/organ to a broad range of physiological and experimental stimuli otherwise difficult to reproduce *in vivo* [70].

1.5.2.1 Physicochemical methods

PAMPA-BBB

Parallel artificial membrane permeability assays (PAMPAs) have become a quite useful and versatile *in vitro* tool for predicting passive transcellular diffusion of a compound across the BBB. The system is based on the use of specially designed artificial lipid-impregnated membrane established on a solid filter support (e.g., polycarbonate) between a donor and an acceptor compartment. In this system a multiwell plate is placed at the bottom for the donor compartment, whereas the artificial lipid membrane/acceptor compartment is placed on top in a

"sandwich" like configuration. Initially, the test drug is added in the donor compartment and allowed to diffuse across the membrane. The drug diffused in the acceptor compartment is then measured and quantified. PAMPAs have some advantages such as: a high degree of versatility, automation compatibility, and assay reproducibility. The system can be modified to assess the effect of a wide range of pH on the permeability of the test drug of interest (e.g., gastric pH range 1.0–2.5, intestine pH range 6.6–7.0, etc.). The donor and/or acceptor compartments can be modified to emulate *in vivo* conditions by incorporating solubilizing agents or additives that bind the compounds as they diffuse across the lipid membrane. PAMPAs are considered suitable early stage absorption screening tool alternatives to more demanding and expensive cell-based assays.
The major limitation of PAMPA systems versus cell-based and *in vivo* studies is their inability to reproduce active transport mechanisms or metabolic transformations that a compound may incur during transcellular routing across physiological membranes. This may significantly affect predictability of bioavailability of the drug on the targeted site and thus use of PAMPAs alone would be insufficient. Their combination with in silico and the development of more complex algorithms that better reflect the behaviour of highly dynamic physiological membranes (e.g., BBB) can further extend the use of this broadly adopted technology beyond an early stage screening tool [70].

Immobilized artificial membrane (IAM) chromatography

This method mimic the membrane lipid environment found in living cells. This technology is more commonly used for purification of many biological substances but found other more specific applications in the study of drug–membrane interactions and drug permeability across the BBB. Originally developed at Purdue University by Charles Pidgeon, the IAM stationary phase consists of a monolayer of carboxyl phospholipids that bear interfacial functional groups identical to the membrane phospholipids forming the cell membranes (e.g., phosphatidylcholine, phosphatidylglycerol, phosphatidic acid, phosphatidylethanolamine, and phosphatidylserine) covalently immobilized on an inert silica support. The resulting IAM surface is a chemically stable chromatographic material, which mimics the lipid outer layer of a biological cell membrane. IAM chromatography can be used for the non-covalent immobilization as well as analytical and preparative separation of membrane-associated proteins, it also a method to estimate membrane permeability of

small drugs and to measure their specific phospholipophilicity. However, there are different limitations of this technique as a method to assess drug permeability: the IAM surface has limited ability to reproduce lateral membrane diffusion, which occurs at the cellular level in vivo, the IAM surface is a lipid monolayer, thus using this model to extrapolate solute diffusion across a physiological membrane bilayer is extremely difficult, IAM surface cannot mimic active efflux or drug metabolism, which normally occurs at the BBB level. Currently, IAM chromatography is primarily used as a single-step purification method for membrane proteins [70].

Equilibrium dialysis

This method consents to obtain information on protein binding in brain homogenate and plasma and, consequently, on the free (unbound) drug fractions in both matrices. Information on free drug fractions in plasma is important as only unbound molecules are available to cross the BBB. Thus, if plasma protein binding is too high, the extent of brain penetration may be insufficient [75]. However, attention must be paid when using *in vitro* data on plasma protein binding of compounds because that bound molecules within brain capillaries are able to dissociate more readily than in *in vitro* models, and thus the bioavailable fraction *in vivo* may be higher than expected [75]. Unbound drug fractions in the brain can be used for the calculation of unbound drug concentrations in the brain, if *in vivo* data on total brain levels are available [76]. Finally, the ratio of free plasma to free brain fraction has been suggested as a parameter to predict the *in vivo* extent of brain distribution [77].

1.5.2.2 Cell-based methods

Isolated brain capillaries

Brain microvessels from human or animal sources have been used in BBB research since their successful isolation more than three decades ago [78]. However, they are not suitable for *in vitro* BBB permeability screenings since the luminal side (blood side) of the capillaries is hardly accessible [79].

Cell culture models

Cell-based BBB models can be established with any type of cell source (human, animal, or cell line derivative) including the availability of BBB ECs and astrocytes freshly isolated from human brain tissue (e.g., from patients undergoing temporal lobectomies for drug refractory epilepsy, brain tumour resections, aneurisms, etc.). Is it important consider that cells cultured *ex situ* in an

artificially environment undergo dedifferentiation because of lack of exposure to physiological aspects. This can affect the expression (deregulation) of relevant cell biological features (e.g., transporters, ligands, enzymes, etc.), thus potentially altering the BBB physiology *in vitro* as well as its response to stimuli. Therefore, validation of *in vitro* findings in *in vivo* conditions is often necessary [70].

- Static models of BBB: ECs monocultures

The most common and usually utilized BBB model is based on a monolayer of highly specialized brain microvascular ECs. This system, known as the Transwell apparatus (e.g., Corning, Lowell, MA), is a vertical side-by-side diffusion system across a microporous semipermeable membrane that separates the luminal (vascular) and the abluminal (parenchymal side) compartments. Brain vascular ECs (from various sources) are grown to confluence on the upper (luminal) surface of the membrane immersed in their specific growth media. The advantages of cultured endothelium include the potential for using pure cell populations as well as their relative capability. The microporous membrane interface allows for nutrient exchange and the passage of cell-derived and exogenous substances but does not allow for cell-movement across the two compartments. Thanks to this model it is possible to test the drug permeability and also the binding affinity (receptor–ligand). In particular, they are ideal systems to study Michaelis–Menten kinetics of transport because of fixed volumes in each compartment. Of course this easy reconstruction of BBB lacks a number of critical features such as the absence of natural physiological stimuli as cell to cell interaction with perivascular astrocytes and other parenchymal cells (e.g., neurons). This non-physiological culture condition may accelerate endothelial dedifferentiation and increase the loss of the BBB characteristics with serial cell. ECs grown in Transwell tend to have irregular patterns of cell adhesion, which prompt the so-called “edge effect.” This term refers to a condition wherein the inability to form proper tight junctions between adjacent cells and between the endothelium beside the perimeter of the membrane and the inner wall of the luminal chamber leads to artefactual paracellular diffusion, affecting the reliability of permeability measurements across the endothelial monolayer, especially for compounds that are highly hydrophilic and poorly cross the lipid membrane bilayer of the cells [70]. Thus, various immortalized

cell lines from different origin have been used to model the BBB *in vitro* (Tables 4 and 5).

TABLE 4:CURRENTLY AVAILABLE IMMORTALIZED HUMAN BRAIN CAPILLARY ENDOTHELIAL CELL LINES USED FOR THE ESTABLISHMENT OF *IN VITRO* HUMAN BBB MODELS [69]

Brain capillary endothelial cell line	Transfection method	Year (first publication)	Reference
BB19	E6E7 genes of HPV	1996	Prudhomme et al. [80]
HBEC-5I	SV40T	1996	Xiao et al. [81]
SV-HCEC	SV40T	1997	Muruganandam et al. [82]
hBMEC	SV40T	2001	Stins et al. [83]
hTERT-HBEC	hTERT	2003	Gu et al. [84]
hCMEC/D3	hTERT and SV40T	2005	Weksler et al. [4]
NKIM-6	E6E7 genes of HPV type 16	2007	Ketabi-Kiyanvash et al. [85]
TY08	hTERT and temperature-sensitive SV40T	2010	Sano et al. [86]
TY09	hTERT and temperature-sensitive SV40T	2010	Sano et al. [86]
HBMEC/ciβ	hTERT and temperature-sensitive SV40T	2012	Kamiichi et al. [87]
TY10	hTERT and temperature-sensitive SV40T	2012	Maeda et al. [88]

TABLE 5:IMMORTALIZED ANIMAL AND NON-BRAIN HUMAN CELL LINES USED FOR BBB *IN VITRO* MODELS [69]

Cell line	Description	Origin	Remarks
Caco-2	Human epithelial colon adenocarcinoma cell line	Human (colon)	Limited prediction of BBB permeability (poor correlation of *in vitro* Caco-2 and *in vivo* BBB data) [89]

ECV304	Human endothelial umbilical vein (HUVEC) cell line [90]	Human (umbilical cord)	Non-brain origin, but cells show endothelial features, barrier tightness can be increased (up to TEER[1] of 200 Ωcm^2) by co-cultivation with immortalized rat glioma cells (C6 cell line) or C6 conditioned medium [91,92]
LLC-PK1	Porcine kidney epithelial cell line [93]	Pig (kidney)	Relatively tight monolayers, cell line can be transfected with transporter genes (e.g. MDR1) for efflux studies
MDCK	Madin Darby Canine Kidney epithelial cell line [94]	Dog (kidney)	Tight monolayers (high TEER[1] values), cell line useful for determination of passive permeation (due to low expression of transporters), assay straight forward (3–4 days of culture) [95,96]
MDR1-MDCK (type I or II) and BCRP-MDCK	MDCK transfected with human MDR1 gene (P-gp) or BCRP	Dog (kidney)	Tight monolayers (high TEER[1] values), polarized expression of P-gp/BCRP, useful for P-gp/BCRP efflux studies (bidirectional transport assays) [97]
RBE4	Rat brain capillary endothelial cell line [98]	Rat (brain)	Leaky monolayers (relatively high permeability to small molecules) [98]
cEND	Murine immortalized brain (cerebral) capillary endothelial cell line [99]	Mouse (brain)	Relatively tight monolayers depending on cultivation protocol (high TEER[1] values up to 1000 Ωcm^2) [99]
bEnd3 and bEnd5	Mouse brain microvascular endothelial cell lines [100,101]	Mouse (brain)	Leaky monolayers (relatively low TEER[1] values: bEnd3 40–130 Ωcm^2, bEnd5 around 120 Ωcm^2) [91,102]

Immortalized cell lines, from human brains are of greatest interest but the available cell lines often show deficits (e.g. low transendothelial electrical resistance (TEER) values, relatively high paracellular permeation of negative control compounds, insufficient expression of key transporter systems). Often, an optimization of culture conditions and a validation of cell line-based human *in vitro* BBB models is necessary. Significant advances in modelling the human BBB *in vitro* have been achieved recently by using endothelial cells derived from human pluripotent or hematopoietic stem cells [103,104]. As stem cells offer a high capacity of expansion by self-renewal while maintaining a homogenous genetic profile, stem cell-based models are promising, but require systematic benchmarking against established *in vitro* and *in vivo* models [105].

- **Static two-dimensional models of the BBB: coculture of ECs and glia**

The addition of abluminal astrocytes (Figure 10) facilitate the formation of more stringent interendothelial tight junctions and the overall expression of proprietary BBB features, that more closely resemble that of the BBB *in situ* [70].

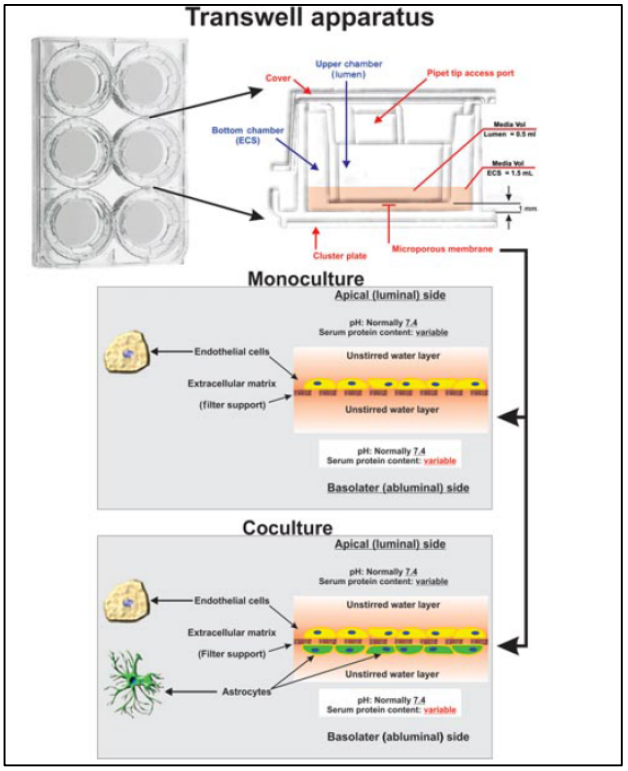

FIGURE 10: SCHEMATIC REPRESENTATION OF TRANSWELL APPARATUS [70]

Different evidences indicate that astrocyte interaction with the cerebral endothelium helps determine BBB function, morphology (i.e., tightness), and protein expression. Intercellular adhesion between astrocytes in the BBB has been observed in the form of gap and adheres junctions. The presence of glia and the interactions glial–endothelial have been shown to increase the expression of transporters (e.g., Glut-1 and MRPs such as P-gp) and tight junctions, and have also helped mimic the *in vivo* condition. A limited cell polarity is inducible in ECs when co-cultured with glia or in the presence of glial-conditioned medium. The exposure to glia promotes the expression of brain endothelial marker enzymes (e.g., OX-26, alkaline phosphatase, acetylcholinesterase, Na+ –K+ -ATPase) as well as that of a number of

specialized transport and efflux systems typically observed *in vivo*. TEER, should be higher in EC–glia coculture systems than EC monocultures. The difference in the measurement indicates formation of a more stringent and selective vascular bed [70].

1.5.3 IN VIVO MODELS

The last models provide some of the most reliable data to evaluate the permeability across the brain and the brain distribution [67]. Of course, the methods are labour-intensive and low throughput and frequently are not applicable to humans.

In situ brain perfusion

Represent a reliable method to determine BBB permeability of a drug [97]. A catheter is inserted into the common carotid artery of an anesthetized animal (rat, mouse, guinea pig, rabbit) and a solution containing the test drug is slowly perfused through the brain capillaries [106]. Drug concentrations are quantified in the perfused brain hemisphere of the sacrificed animals, and permeability surface area (PS) values, reflecting BBB permeability, are calculated [107]. Limitations of the method are that it is costly, labour-intensive, and requires surgical skills and expertise [67].

Total brain-to-plasma ratio (K_p)

Animals are dosed with a test drug, then they are sacrificed at designated time-point(s), and drug concentrations in brain homogenate and blood plasma are quantified. K_p values are calculated based on the respective drug concentrations or area under the curves (AUC) from both matrices ($K_p = C_{brain}/C_{plasma}$ or AUC_{brain}/AUC_{plasma}). K_p values based on AUC need money, more labor and animals but may is more useful [108]. A inconvenience of this method is that K_p values are firstly determined by non-specific binding of a substance to brain tissue [109].

Brain microdialysis

It is the best method to determine the free concentration of a compound in brain interstitial fluid [76]. A microdialysis probe with a semi-permeable membrane is implanted into a specific brain region of an animal (rat or mouse). Unbound molecules in brain interstitial fluid below a certain molecular weight freely diffuse through the membrane, and are captured in the fluid perfused

through the microdialysis probe [110]. The unbound brain concentration can then be related to the unbound drug concentration in plasma, providing the parameter $K_{p,uu}$ (unbound brain-to-plasma ratio), which has proved to be more predictive than K_p values (total brain-to-plasma ratios) [111]. This technique have various limitations: firstly the invasiveness, for this reason it is not suitable for humans; the probe used for the dialysis may damage locally and the BBB and lipophilic compounds should adsorb on the membrane of the probe [112].

Cerebrospinal fluid (CSF) sampling

This *in vivo* methods should be applicable to humans. As a lot of papers show, CSF concentrations could be used to predict free drug concentration in brain interstitial fluid but data interpretation of CSF levels is not easy because the molecules may enter the CSF compartment via the Blood-CSF barrier [113]. So, if a drug is subject to active uptake or efflux at only one of the two barriers, concentrations in CSF will not correctly predict free drug concentrations in brain interstitial fluid. There are others limitations: high turnover rate of CSF (around 6 hours in humans), which requires that CSF sampling is done at very specific time points, and that the CSF compartment is not well-mixed, resulting in varying concentrations depending on the site of sample collection [108,114].

1.6 BIOANALYSIS

Bioanalysis is a section of analytical chemistry for the qualitative and quantitative analysis in biological matrices, like plasma, serum, urine, saliva, tissue etc. Development and validation of bioanalytical method is important to understand the pharmacokinetics of any drug and/or its metabolites.

Bioanalytical method validation includes all of the procedures that demonstrate that a particular method used for quantitative measurement of analytes in a given biological matrix, such as blood, plasma, serum, or urine is reliable and reproducible for the intended use [115].

1.6.1 LIQUID CHROMATOGRAPHY COUPLED TO TRIPLE QUADRUPOLE MASS SPECTROMETERS (LC-MS/MS)

LC-MS/MS is a combination of two techniques: LC for the separation of a mixture between two immiscible phases based on the physical properties of the constituents and triple quadrupole MS for selective and sensitive detection of analytes. Is possible choice between different LC system: HPLC or UHPLC (the acronym, while UPLC is used only for Waters Corp. UHPLC instruments are able

to operate at higher back-pressure than conventional HPLC systems, allowing the use of shorter columns with smaller particles as stationary phase [116,117].
LC system is principally coupled to the triple quadrupole detector via electrospray ionization (ESI) or atmospheric pressure chemical ionization (APCI) interfaces [118]. ESI and APCI are both soft ionization techniques, by which the analytes eluting from the LC column are ionized to positively (M+H+) or negatively (M-H-) charged ions which are transferred into gas phase, and finally introduced into the MS [119]. APCI sources are more suited for ionization of less polar and non-polar compounds [119] while ESI sources are capable of ionizing almost any polar molecule.
Triple quadrupole mass spectrometers consist of three quadrupoles connected in series (Figure 11) [120,121]. A quadrupole typically consists of four molybdenum rods on which alternating DC (direct current) and RF (radio frequency) voltages are applied [121]. At a particular DC/RF ratio, only ions with a certain m/z value have a stable trajectory and are able to pass through the quadrupole [121]. In quantitative bioanalysis, triple quadrupole detectors are primarily operated in MRM mode. In this mode, the first (Q1) and third (Q3) quadrupole act as selective mass filters, while the second quadrupole (Q2), located between Q1 and Q3, serves as collision cell (RF voltage applied only) (Figure 1) [122]. Thus, only selected precursor ions with specific m/z values are allowed to pass through Q1. They subsequently collide in the collision cell (Q2) with inert gas (argon or nitrogen) and are fragmented into numerous product ions, a process called collision induced fragmentation (CID) [120]. Only selected product ions with certain m/z values are allowed to pass through Q3 and are finally detected typically by some type of electron multiplier (Figure 11) [123].

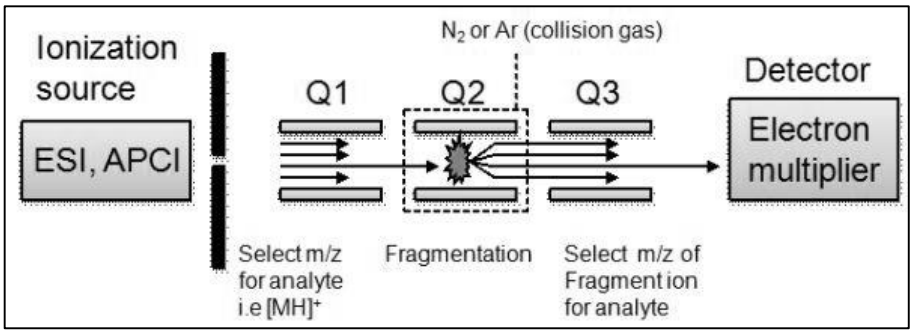

FIGURE 11: SCHEMATIC DIAGRAM OF A TRIPLE QUADRUPOLE MASS DETECTOR [124]

1.6.1.1 Sample preparation for LC-MS/MS

The purpose of sample preparation is to clean up the sample before analysis and/or to concentrate the sample, in fact, material in biological samples that can interfere with analysis, the chromatographic column or the detector includes proteins, salts, endogenous macromolecules, small molecules and metabolic by-products [115]. A goal with the sample preparation is also to exchange the analyte from the biological matrix into a solvent suitable for injection into the chromatographic system. If done efficiently, sample preparation enhances selectivity and sensitivity of the LC-MS/MS methods, leads to higher reproducibility of data, and increases lifetime of column and instrumentation. In addition to purification from interfering substances, main objectives of the clean-up procedure are the concentration of the analyte to increase detection limits, and dissolution of the analyte in a suitable solvent for instrumental analysis [125,126]. The most common preparation procedures will be described below:

- Dilution is a rapid clean-up procedure, in which biological samples are simply diluted with water or mobile phase solution prior to injection into the LC-MS. This type of procedure is simple and time-efficient, but the are some disadvantages, such as the fact that there isn't the step of removing interfering compounds and the lack of an analyte pre-concentration step, which may lead to insufficient selectivity and/or sensitivity [127].
- Protein precipitation (PP) is an efficient technique, where the proteins in the biological matrix are denatured by the use of a strong acid/base (resulting in a change of pH), by the application of heat, or by the addition of organic solvents such as methanol or acetonitrile [128,129]. During the denaturation process, proteins undergo a change in their tertiary and secondary structure, and analytes become thus freely soluble in the denaturing solvent. After centrifugation of samples, the denatured proteins form a pellet at the bottom of the tube, while the analyte is dissolved in the supernatant. After evaporation of the supernatant to dryness, and subsequent reconstitution in mobile phase or injection solvent, the sample is ready for LC-MS/MS analysis [126]. PP is simple, fast, and inexpensive [123].
- Liquid-liquid extraction (LLE) is based on the different solubility and equilibrium of partition between an aqueous and an organic phase.

Analytes are extracted from the original sample in into organic phase which is immiscible with the water phase [20]. The LLE technique has a number of disadvantages: the extraction of hydrophilic analytes is limited, recoveries may be variable, and relatively large biological sample volumes are needed [128].

- **Solid-phase extraction (SPE)** is a selective method for sample preparation where the analyte is bound onto a solid support, interferences are washed off and the analyte is selectively eluted. Due to many different choices of sorbents, SPE is a very powerful technique. SPE consists of four steps; conditioning, sample loading, washing and elution. In solid-phase extraction (SPE), analytes are separated from the biological matrix by means of a solid (stationary) phase. [115]
- **Supported-liquid extraction (SLE)** is performed using commercial 96-well plates (e.g. Isolute® SLE+ from Biotage) [130]. Each well is packed with a modified form of diatomaceous earth with a high capacity for retaining aqueous samples [129]. The biological samples are loaded onto the well, then the aqueous portion of the sample adsorbs to the hydrophilic surface of the packing material and analytes can successively be eluted applying appropriate eluent [130]. SLE offers high recovery and reproducibility, but is more expensive than PP and LLE [130].

1.6.2 DEVELOPMENT AND VALIDATION OF LC-MS/MS METHOD

Develop LC-MS/MS method means take in consideration different phase that requires time and funds, but contributes considerably to a successful method validation.

First of all is important investigate the **physicochemical properties** of the analyte, such as solubility, lipophilicity, thermal and light stability and molecular structure, then must be selected the solvents for sample processing.

Then appear to be fundamental select the suitable **internal standard** (I.S.), a compound at known concentration to add at every quantification sample, that can correct every variation in sample extraction, transfer/injection volumes, ionization efficiency, and detector response [131]. Isotopic-labeled analytes should be selected as I.S., when is possible, because it the same physico-chemical characteristics of the analyte and, of course the equal behaviour during all phases of the analytical procedure. When is not possible use the isotopic-labelled analytes, for example, for natural compounds, structurally

similar compounds with small differences in functional groups and similar chromatographic properties may be employed [132].

After the selection of the I.S., **MS/MS parameters** (MRM transitions, cone voltage, collision energy etc.) for both analyte and I.S. are tested and optimized, then is possible to start with the development of a chromatographic method for the separation of the analyte from other compounds in the sample. So different stationary phases (HPLC columns) and mobile phase (eluents) are tested and the best gradient, flow, column temperature. must be selected Appear to be very important, in this step of development, that the retention times of the analyte and I.S. are relatively close, in order to compensate the matrix effect. At this point is possible select the suitable technique for **sample preparation** to extract the compound(s) of interest from the matrix. The traditional approach is to start with the simplest extraction method such as PP or dilution [133], then more sophisticated extraction methods such as LLE, SPE, and SLE may be evaluated.

The concluding steps are the determination of the **quantification range**, and the estimation of **the carry-over** for analyte and I.S. The quantification range should be based on the sample concentrations estimated for our study. The lower limits of quantification (LLOQ; calibration standard with the lowest concentration) in the pg/mL range can be done in LC-MS/MS, depending on the type of triple quadrupole detector, HPLC separation, and sample clean-up procedure. The carry-over should be evaluated by injecting a blank sample (pure matrix) after the upper limit of quantification (ULOQ; calibration standard with the highest concentration). According to EMA guidelines, carry-over should not exceed 20% for the analyte and 5% for the I.S. [134]. If these acceptance criteria are not seen, apposite actions should be taken to reduce the carry-over (e.g. change of washing needle solution, injection of blank samples after each sample containing analyte, adaption of the quantification range as higher LLOQ or lower ULOQ).

At the end of the development of the LC-MS/MS method, it can be validated according to good laboratory practice (GLP) guidelines defined by regulatory agencies. The European Medicines Agency (EMA) “Guideline on Bioanalytical Method Validation” (2009) and the US Food and Drug Administration (FDA) “Guidance for Industry, Bioanalytical Method Validation” (2001; new draft in 2013) are the most used ones [134–137]. A harmonized global guideline, however, does not yet exist [138].

The EMA and FDA have different grades of **bioanalytical method validation** in their guidelines: full validation, partial validation, and cross-validation. The first is required if a method is applied for the first time, or if new analytes are added to an already existing method. Partial validation of a method may include intra-assay accuracy and precision determination. Cross-validation is required if samples from one single study are analyzed in two different laboratories, or if two or more different bioanalytical techniques (e.g. ELISA and LC-MS/MS) are employed for sample analysis [134,135].

International guidelines describe different validation parameters, as reported:

- **Calibration curve and LLOQ:** A calibration curve should consist of calibration standards (calibrators) and quality controls (QCs) at a minimum of three concentrations levels (low = QCL, middle = QCM, high = QCH) [134,135]. QCL should be within 3x of the lowest calibrator, QCM should be in the middle of the quantification range, and QCH should be approaching the high end of the range [134,135]. Calibrators and QCs should be prepared in the same biological fluid as the study samples by spiking the matrix with known concentrations of the analyte [135]. The calibration curve should be recorded as follows: a blank sample, a zero sample (sample processed with I.S., but without analyte), and six to eight calibrators covering the selected concentration range [135]. After the highest calibrator (upper limit of quantification, ULOQ), another blank sample should be injected for carry-over assessment. The calibrator with the lowest concentration is defined as lowest limit of quantification (LLOQ). For this, the following conditions need to be met: the analyte response of the LLOQ should be at least 5 times higher than the analyte response in the blank sample, and the signal to noise (S/N) ratio should be > 10 [134,135,139]. Each analytical run should begin and end with a calibration series (bracketed between blank samples) which are injected in increasing concentration. Between the two sets of calibrators, six QCs should be inserted randomly into the analytical run. The simplest model that is able to appropriately describe the concentration versus MS response curve should be applied [135]. For 75% of calibrators and 67% QCs (four out of six), the back-calculated concentrations should be ± 15% nominal values, with exception of the

LLOQ, for which a deviation ± 20% is allowed [135]. The coefficient of correlation (R2) should furthermore be higher than 0.96 [135].

- Carry-over: Carry-over of analyte and I.S. should already be assessed during method development by injecting a blank sample after each ULOQ. If carry-over occurs, it should be minimized as best as possible [134,136]. According to EMA guidelines, carry-over is not allowed to exceed 20% for the analyte and 5% for the I.S. [134]. During method validation and application, carry-over needs to be further monitored [134,136].
- Selectivity and specificity: Selectivity is defined as the ability of an analytical method to differentiate and quantify the analyte in the presence of endogenous matrix components or other compounds in the sample [135]. It should be ensured at the LLOQ by using different batches of the same biological matrix [134,135]. Specificity of the method should be proven by using independent sources of the same matrix [135]. It should be noted that selectivity is not the same as specificity. While selectivity can be graded, specificity cannot. It is an absolute characteristic that may be regarded as ultimate selectivity [140].

- Matrix effects: In LC-MS, a common problem is the occurrence of matrix effects. This phenomenon is caused by molecules originating from the biological matrix that co-elute with the analyte and may interfere with the ionization process in the mass spectrometer (leading to ion suppression or enhancement) [141,142]. Matrix effects can occur in diverse and unexpected forms and may have a negative impact on precision and accuracy of a bioanalytical method. Therefore, they should be carefully investigated in the course of method validation to ensure that precision, selectivity, and sensitivity of the assay are not compromised [134,135].

- Accuracy and precision: Accuracy of a bioanalytical method describes the closeness of mean test results obtained by the method to the nominal (true) value (concentration) of the compound. It is expressed as relative error (RE%). Precision describes the closeness of repeated individual measures, and is expressed as coefficient of variation (CV%).

$$RE\ (\%) = \frac{Experimental\ conc. - Nominal\ conc.}{Nominal\ conc.} \times 100$$

$$CV\ (\%) = \frac{Standard\ deviation\ (S.D.)}{Mean\ experimental\ conc.} \times 100$$

Accuracy and precision of a method can be subdivided into within-run and between-run accuracy and precision. The latter (between-run) reflects the reproducibility of a method [134,135]. During method validation, both within-run and between-run accuracy and precision should be assessed by replicate analysis of samples (at least five) at a minimum of three different concentration levels [135]. Mean values and S.D. values should be calculated, from which RE% and CV% can be deduced. RE% should be ± 15% (± 20% at the LLOQ), and CV% should not exceed 15% (20% at the LLOQ).

- Recovery (extraction efficiency): The recovery is a ratio of the detector response of an analyte from an extracted sample to the detector response of the analyte from an unextracted sample containing the same amount of analyte that was added to the extracted sample [143]. According to FDA guidance, recovery does not need to be 100%, but it should be consistent, precise, and reproducible [135].

- Dilution integrity: Study samples may need to be diluted if they have a higher concentration than the ULOQ. However, dilution of samples should not have an impact on accuracy and precision of the bioanalytical method. Therefore, representative dilution tests should be carried out during method validation in order to demonstrate that dilution of study samples later on does not interfere with the method [134,135].

- Stability: During the entire bioanalysis chain (beginning with sample collection and ending with sample analysis after long and short-term storages), stability of the analyte in the biofluid should be guaranteed. Therefore, various stability tests should be carried out during method

validation. According to FDA/EMA guideline, these include: freeze and thaw (F/T) stability, benchtop stability (at room temperature), long-term stability at planned storage conditions, post-preparative stability (autosampler stability), and stock solution stability [135]. Importantly, conditions used in all these stability tests should reflect the conditions expected to be encountered during real sample handling and analysis.

1.7 NATURAL COMPOUNDS *VS* NEURODEGENERATION

1.7.1 SALVIANOLIC ACID B

Salvia miltiorrhiza Bge is a very important herbal drug (HD) of traditional Chinese medicine. Bioactive constituents are represented by two main groups of secondary metabolites, the lipophilic diterpenic quinones known as tanshinones and the hydrophilic depsides known as salvianolic acids. The extracts of radix and rhizome and single constituents have been shown to have positive effects in CNS neuronal injury and degeneration in several animal models by various biological mechanisms. The models used are cerebral injury, streptozocin-induced diabetes, hyperlipidemia, and an Alzheimer's model (Aβ peptide injection), while the methods of evaluation of the neurological functions include behavioral tests (Morris water maze, Y maze, and passive avoidance tests), neurological deficits score, and specific histological and biochemical investigations such as measurement of the brain water content, infarction size, and apoptotic neurons, BBB disruption, and invasion of brain tissues.

In recent years, much attention has been directed to the water-soluble components that represent the major constituents of *S. miltiorrhiza* Bge decoction used in traditional medicine [144].

SalB was selected because is a promising molecule in the protection of neuro degeneration but its poor chemical stability and low bioavailability limits a clinical application for CNS neuronal injury and degeneration, for this reason Sal B was loaded into NPs (Figure 12).

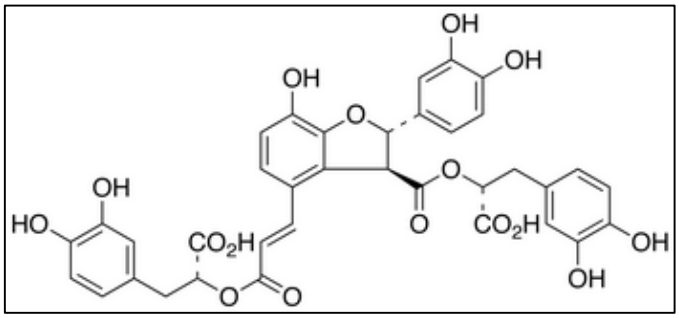

FIGURE 12: CHEMICAL STUCTURE OF SALB

Different papers report interesting results about the activity of Sal B. It was tested as a blocking agent of Aβ-induced Ca^{2+} intake in PC-12 cells. This study showed that 15 μM Aβ25–35 caused about 40% additional LDH release from Aβ-treated cells compared with normal cells, and the cotreatment with SalB inhibited the LDH release from Aβ-treated cells [145].

Lin and coworkers [146] investigated the neuroprotective effects of SalB on the expression of BPRP. Treatment of the PC12 cells with SalB significantly ($p < 0.05$) reversed the expression of BPRP and cell viability while it decreased ROS production and intracellular calcium. In a further study of rats pretreated with 10 mg/kg SalB, the number of GFAP and OX-42 positive cells were reduced. Subchronic SalB administration decreased iNOS and COX-2 expression [147]. Tian et al. [146] investigated the neuroprotective effects of SalB against 6-hydroxydopamine-induced cell death in human neuroblastoma SH-SY5Y cells. SalB significantly ($p < 0.05$) reduced the 6-hydroxydopamine-induced generation of ROS and prevented 6-hydroxydopamine-induced increases in intracellular calcium. The data demonstrated that SalB reduced the 6-hydroxydopamine-induced increase of caspase-3 activity, and cytochrome C translocation into cytosol from mitochondria. The protective effects of SalB in traumatic brain injury in mice was investigate by Chen et al. [148] and SalB treatment significantly suppressed the expression of proinflammatory cytokines TNF-α and IL-1β, and enhanced the expression of anti-inflammatory cytokines IL-10 and TGF-β1 after traumatic brain injury. Recently, Jiang and coworkers [149] examined the effects of SalB in a mouse model of cerebral ischemia and reperfusion injury with sodium nitroprusside. Pretreatment with SalB decrease the MDA content and NOS activity, and increased the T-AOC level in the cortical area of I/R. SalB also improved pathological changes of hippocampal CA1 neurons by preventing neuronal loss, increasing Bcl-2 protein expression,

inhibiting Bax protein expression, and enhancing the ratio of Bcl-2-IR to Bax-IR. Kim and coworkers, observed that SalB ameliorated the memory impairments induced by scopolamine or the Aβ25–35 peptide. SalB can inhibit GABA-induced Cl^- currents in a single hippocampal neuron in a concentration-dependent manner. Therefore, the scopolamine-induced amnesic animal model might be the result of the inhibition of GABA signalling [150]. Finally, itwas demonstred that SalB inhibits fibril aggregation and destabilizes preformed Aβ fibril in a dose- and time-dependent manner. SalB might interact with the peptide side chain to inactivate fibril aggregation [151].
The biochemical mechanisms related to SalB are recently summarized by Bonaccini et al. [144] and reported below:

- Antiapoptotic mechanisms:
  - ↓ caspase-3 expression
  - ↓ cytochrome c translocation into cytosol from mitochondria
  - ↓ intracellular calcium
  - ↑ Bcl-2 expression
  - ↓ Bax expression
  - ↑ EPO and EPOR expression
  - ↑ CD31 expression via the JAK2/STAT3 and VEGF/Flk-1 pathways
- Anti-oxidant mechanisms:
  - ↓ ROS production
  - ↓ level of MDA
  - ↓ T-AOC
- Anti-inflammatory mechanisms
  - ↓ GFAP and OX-42
  - ↓ iNOS and COX-2 expression
  - ↓ proinflammatory cytokines (TNF-α and IL-1)
  - ↑ anti-inflammatory cytokines (IL-10 and TGF-β 1)
  - ↓ NO activity
- Other mechanisms:
  - ↓ BPRP expression
  - ↓ release of LDH
  - ↑ cholineacetyltransferase (ChAT)

↑ BDNF

↓ GABA-induced Cl currents

↓ fibril aggregation and destabilize preformed Aβ fibril

1.7.2 ANDROGRAPHOLIDE

Andrographis paniculata L. is a native plant from Southeast Asian countries. For centuries, this plant has been used as an official herbal medicine in China for the treatment of various human illnesses, including acute hepatitis, meningitis, choriocarcinoma, malaria, and many other acute inflammatory conditions that can be studied using different animal models [152]. Earlier studies have indicated that AG, the main diterpene of the labdane family present in the leaves, is responsible for most of the biological effects of *Andrographis paniculata* (Figure 13).

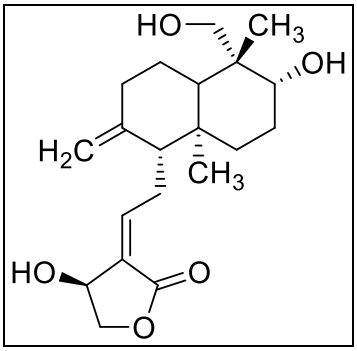

FIGURE 13: CHEMICAL STRUCTURE OF AG

Recent studies have suggested that AG might exercise neuroprotective effects, i.e., against damage induced by dopamine in mesencephalic neuronglial cultures associated with a protective effect on inflammation-mediated neurodegeneration, oxidative stress induced by nicotine in the brain, and cerebral ischemia by inhibiting certain pathways related to inflammation and apoptosis, including Akt, NF-κB and MAPK signaling. AG could be efficient molecule with a potential property for various CNS's treatments [152].

More recently, Serrano and co-authors have investigated the role of AG in neurodegeneration. They demonstrated that AG decreases Aβ depositions in young AβPPswe/PS-1mice while Tau phosphorylation decreased after AG treatment in both young and mature AβPPswe/PS-1 mice. Additionally, AG recovered the synaptic functions in AβPPswe/PS1 mice of different ages, the

spatial memory in AβPPswe/PS-1 double transgenic mice of different ages and finally inhibits GSK-3β, preventing LTD induction [152].

The interest regards the activity of this molecule increased in last years to understand the mechanism of action of AG. This year Tapia-Rojas and co-workers published a paper [152] in which they evaluate Wnt/β-catenin signalling and the possible role of AG. Wnt/β-catenin is an important pathway that regulates various biological processes, including cell adhesion and determination of cell fate during animal development; in the adult nervous system it regulates the structure and function of synapses. Dysfunction of this signalling is associated with several neurodegenerative diseases such as schizophrenia and AD. The paper reports that AG is a potent activator of Wnt signaling, inducing the transcription of Wnt target genes by a mechanism that bypasses Wnt ligand binding to its receptor. *In vitro* AG inhibits glycogen synthase kinase (GSK)-3β by a non-ATP-competitive, substrate-competitive mode of action. *In silico* AG interacts with the substrate-binding site of GSK-3β, while *in vivo* is observed the increase in the levels of GSK-3β phosphorylated at Ser^{9} as the result of an autoregulatory mechanism of the kinase, although not through activation of protein phosphatase type 1. This last study suggest that AG could be used as a potential therapeutic drug for neurodegenerative diseases [153].

Nevertheless, AG is poorly soluble in water, stable under neutral and acidic conditions, but unstable under alkaline conditions. Moreover, it is rapidly metabolized in the duodenum and jejunum to form a sulphate conjugate that is hydrophilic and likely to be impermeable [154]. So, all these factors led to the poor oral absorption and poor bioavailability of the drug.

Till now there aren't evidences in literature that AG free can cross BBB, thus, for all this reasons, in this PhD work, AG was loaded into NPs.

1.8 Reference

[1] H.L. Wong, X.Y. Wu, R. Bendayan, Nanotechnological advances for the delivery of CNS therapeutics, Adv. Drug Deliv. Rev. 64 (2012) 686–700. doi:10.1016/j.addr.2011.10.007.

[2] E. a Neuwelt, B. Bauer, C. Fahlke, G. Fricker, C. Iadecola, D. Janigro, et al., Engaging neuroscience to advance translational research in brain barrier biology., Nat. Rev. Neurosci. 12 (2011) 169–182. doi:10.1038/nrn2995.

[3] B. V Zlokovic, The blood-brain barrier in health and chronic neurodegenerative disorders., Neuron. 57 (2008) 178–201. doi:10.1016/j.neuron.2008.01.003.

[4] B.B. Weksler, E.A. Subileau, N. Perriere, P. Charneau, K. Holloway, M. Leveque, et al., Blood-brain barrier-specific properties of a human adult brain endothelial cell line, FASEB J. 19 (2005) 1872–1874.

[5] N.J. Abbott, L. Rönnbäck, E. HaNPson, Astrocyte-endothelial interactions at the blood-brain barrier., Nat. Rev. Neurosci. 7 (2006) 41–53. doi:10.1038/nrn1824.

[6] N.J. Abbott, Astrocyte-endothelial interactions and blood-brain barrier permeability., J. Anat. 200 (2002) 629–38. http://www.pubmedcentral.nih.gov/articlerender.fcgi?artid=1570746&tool=pmcentrez&rendertype=abstract (accessed August 15, 2015).

[7] B.T. Hawkins, T.P. Davis, The blood-brain barrier/neurovascular unit in health and disease., Pharmacol. Rev. 57 (2005) 173–85. doi:10.1124/pr.57.2.4.

[8] R. Bendayan, G. Lee, M. Bendayan, Functional expression and localization of P-glycoprotein at the blood brain barrier., Microsc. Res. Tech. 57 (2002) 365–80. doi:10.1002/jemt.10090.

[9] R. Bendayan, P.T. Ronaldson, D. Gingras, M. Bendayan, In situ localization of P-glycoprotein (ABCB1) in human and rat brain., J. Histochem. Cytochem. 54 (2006) 1159–67. doi:10.1369/jhc.5A6870.2006.

[10] J.F. Deeken, W. Löscher, The blood-brain barrier and cancer: transporters, treatment, and Trojan horses., Clin. Cancer Res. 13 (2007)

1663–74. doi:10.1158/1078-0432.CCR-06-2854.

[11] W. Löscher, H. Potschka, Drug resistance in brain diseases and the role of drug efflux transporters., Nat. Rev. Neurosci. 6 (2005) 591–602. doi:10.1038/nrn1728.

[12] P.T. Ronaldson, Y. Persidsky, R. Bendayan, Regulation of ABC membrane transporters in glial cells: relevance to the pharmacotherapy of brain HIV-1 infection., Glia. 56 (2008) 1711–35. doi:10.1002/glia.20725.

[13] H. Kusuhara, Y. Sugiyama, Efflux transport systems for drugs at the blood-brain barrier and blood-cerebrospinal fluid barrier (Part 2)., Drug Discov. Today. 6 (2001) 206–212. http://www.ncbi.nlm.nih.gov/pubmed/11173268 (accessed November 19, 2015).

[14] S. Dallas, D.S. Miller, R. Bendayan, Multidrug resistance-associated proteins: expression and function in the central nervous system., Pharmacol. Rev. 58 (2006) 140–61. doi:10.1124/pr.58.2.3.

[15] R. Spector, C.E. Johanson, The mammalian choroid plexus., Sci. Am. 261 (1989) 68–74. http://www.ncbi.nlm.nih.gov/pubmed/2479097 (accessed November 19, 2015).

[16] D.R. Groothuis, R.M. Levy, The entry of antiviral and antiretroviral drugs into the central nervous system., J. Neurovirol. 3 (1997) 387–400. http://www.ncbi.nlm.nih.gov/pubmed/9475111 (accessed November 19, 2015).

[17] M.B. Segal, The choroid plexuses and the barriers between the blood and the cerebrospinal fluid., Cell. Mol. Neurobiol. 20 (2000) 183–96. http://www.ncbi.nlm.nih.gov/pubmed/10696509 (accessed November 19, 2015).

[18] R.H. Enting, R.M. Hoetelmans, J.M. Lange, D.M. Burger, J.H. Beijnen, P. Portegies, Antiretroviral drugs and the central nervous system., AIDS. 12 (1998) 1941–55. http://www.ncbi.nlm.nih.gov/pubmed/9814862 (accessed November 19, 2015).

[19] H. Davson, G. Hollingsworth, M.B. Segal, The mechanism of drainage of the cerebrospinal fluid., Brain. 93 (1970) 665–78. http://www.ncbi.nlm.nih.gov/pubmed/5490270 (accessed November 19, 2015).

[20] N.R. Saunders, M.D. Habgood, K.M. Dziegielewska, Barrier mechanisms in the brain, I. Adult brain., Clin. Exp. Pharmacol. Physiol. 26 (1999) 11–9. http://www.ncbi.nlm.nih.gov/pubmed/10027064 (accessed November 19, 2015).

[21] E.C.M. de Lange, Potential role of ABC transporters as a detoxification system at the blood-CSF barrier., Adv. Drug Deliv. Rev. 56 (2004) 1793–809. doi:10.1016/j.addr.2004.07.009.

[22] C. Garner, P.D. Brown, Two types of chloride channel in the apical membrane of rat choroid plexus epithelial cells., Brain Res. 591 (1992) 137–45. http://www.ncbi.nlm.nih.gov/pubmed/1332800 (accessed November 19, 2015).

[23] H. Kusuhara, Y. Sugiyama, Active efflux across the blood-brain barrier: role of the solute carrier family., NeuroRx. 2 (2005) 73–85. doi:10.1602/neurorx.2.1.73.

[24] S. Bhaskar, F. Tian, T. Stoeger, W. Kreyling, J.M. de la Fuente, V. Grazú, et al., Multifunctional Nanocarriers for diagnostics, drug delivery and targeted treatment across blood-brain barrier: perspectives on tracking and neuroimaging., Part. Fibre Toxicol. 7 (2010) 3. doi:10.1186/1743-8977-7-3.

[25] C. Spuch, O. Saida, C. Navarro, Advances in the Treatment of Neurodegenerative Disorders Employing Nanoparticles, Recent Pat. Drug Deliv. Formul. 6 (2012) 2–18. doi:10.2174/187221112799219125.

[26] D. Morgan, Immunotherapy for Alzheimer's disease., J. Intern. Med. 269 (2011) 54–63. doi:10.1111/j.1365-2796.2010.02315.x.

[27] M.D. Pasic, E.P. Diamandis, J. McLaurin, D.M. Holtzman, G. Schmitt-Ulms, R. Quirion, Alzheimer disease: advances in pathogenesis, diagnosis, and therapy., Clin. Chem. 57 (2011) 664–9. doi:10.1373/clinchem.2011.161828.

[28] J.F. Morley, H.I. Hurtig, Current understanding and management of Parkinson disease: five new things., Neurology. 75 (2010) S9–15. doi:10.1212/WNL.0b013e3181fb3628.

[29] G.G. Glenner, C.W. Wong, Alzheimer's disease: initial report of the purification and characterization of a novel cerebrovascular amyloid

protein. 1984., Biochem. Biophys. Res. Commun. 425 (2012) 534–9. doi:10.1016/j.bbrc.2012.08.020.

[30] Z.T. Kincses, L. Vecsei, Pharmacological therapy in Parkinson's disease: focus on neuroprotection., CNS Neurosci. Ther. 17 (2011) 345–67. doi:10.1111/j.1755-5949.2010.00150.x.

[31] A. Gustavsson, M. SveNPson, F. Jacobi, C. Allgulander, J. Alonso, E. Beghi, et al., Cost of disorders of the brain in Europe 2010., Eur. Neuropsychopharmacol. 21 (2011) 718–79. doi:10.1016/j.euroneuro.2011.08.008.

[32] C. Henchcliffe, W.L. Severt, Disease modification in Parkinson's disease., Drugs Aging. 28 (2011) 605–15. doi:10.2165/11591320-000000000-00000.

[33] W.W. Seeley, J. Zhou, E.-J. Kim, Frontotemporal dementia: what can the behavioral variant teach us about human brain organization?, Neuroscientist. 18 (2012) 373–85. doi:10.1177/1073858411410354.

[34] J. Götz, A. Eckert, M. Matamales, L.M. Ittner, X. Liu, Modes of Aβ toxicity in Alzheimer's disease., Cell. Mol. Life Sci. 68 (2011) 3359–75. doi:10.1007/s00018-011-0750-2.

[35] J.D. Rohrer, Structural brain imaging in frontotemporal dementia., Biochim. Biophys. Acta. 1822 (2012) 325–32. doi:10.1016/j.bbadis.2011.07.014.

[36] M. da G. Portugal, V. Marinho, J. Laks, Pharmacological treatment of frontotemporal lobar degeneration: systematic review., Rev. Bras. Psiquiatr. 33 (2011) 81–90. http://www.ncbi.nlm.nih.gov/pubmed/21537725 (accessed November 19, 2015).

[37] L. Osona-Núñez, J.A. Guisado-Macías, M. Pons, Cognition and Lewy body disease., Actas Españolas Psiquiatr. 39 267–70. http://www.ncbi.nlm.nih.gov/pubmed/21769751 (accessed November 19, 2015).

[38] G.J. Ho, W. Liang, M. Waragai, K. Sekiyama, E. Masliah, M. Hashimoto, Bridging molecular genetics and biomarkers in lewy body and related disorders., Int. J. Alzheimers. Dis. 2011 (2011) 842475.

doi:10.4061/2011/842475.

[39] K.A. Jellinger, J. Attems, Prevalence and pathology of dementia with Lewy bodies in the oldest old: a comparison with other dementing disorders., Dement. Geriatr. Cogn. Disord. 31 (2011) 309–16. doi:10.1159/000327360.

[40] A.-M. Enciu, S.N. Constantinescu, L.M. Popescu, D.F. Mureşanu, B.O. Popescu, Neurobiology of vascular dementia., J. Aging Res. 2011 (2011) 401604. doi:10.4061/2011/401604.

[41] J. Lasiene, K. Yamanaka, Glial cells in amyotrophic lateral sclerosis., Neurol. Res. Int. 2011 (2011) 718987. doi:10.1155/2011/718987.

[42] S.L. Perlman, Spinocerebellar degenerations., Handb. Clin. Neurol. 100 (2011) 113–40. doi:10.1016/B978-0-444-52014-2.00006-9.

[43] H.A.G. Teive, Spinocerebellar ataxias., Arq. Neuropsiquiatr. 67 (2009) 1133–42. http://www.ncbi.nlm.nih.gov/pubmed/20069236 (accessed November 19, 2015).

[44] P. Gambetti, I. Cali, S. Notari, Q. Kong, W.-Q. Zou, W.K. Surewicz, Molecular biology and pathology of prion strains in sporadic human prion diseases., Acta Neuropathol. 121 (2011) 79–90. doi:10.1007/s00401-010-0761-3.

[45] The Royal Society & The Royal Academy of Engineering, Chapter 4. Nanomanufacturing and the industrial application of nanotechnologies, Nanoscience and nanotechnologies: opportunities and uncertainties, 2004, pp. 25–34., (n.d.). https://royalsociety.org/~/media/Royal_Society_Content/policy/publications/2004/9693.pdf (accessed November 20, 2015).

[46] J. Kreuter, Drug delivery to the central nervous system by polymeric nanoparticles: What do we know?, Adv. Drug Deliv. Rev. 71 (2014) 2–14. doi:10.1016/j.addr.2013.08.008.

[47] V. Schäfer, H. von Briesen, H. Rübsamen-Waigmann, A.M. Steffan, C. Royer, J. Kreuter, Phagocytosis and degradation of human serum albumin microspheres and nanoparticles in human macrophages., J. Microencapsul. 11 261–9. doi:10.3109/02652049409040455.

[48] K. Gao, X. Jiang, Influence of particle size on transport of methotrexate across blood brain barrier by polysorbate 80-coated polybutylcyanoacrylate nanoparticles., Int. J. Pharm. 310 (2006) 213–9. doi:10.1016/j.ijpharm.2005.11.040.

[49] Efficacy and Safety Doxorubicin Transdrug Study in Patients Suffering From Advanced Hepatocellular Carcinoma - Full Text View - ClinicalTrials.gov, (n.d.). https://clinicaltrials.gov/show/NCT01655693 (accessed November 20, 2015).

[50] F. Landry, Degradation of poly(?-lactic acid) nanoparticles coated with albumin in model digestive fluids (USP XXII), Biomaterials. 17 (1996) 715–723. doi:10.1016/0142-9612(96)86742-1.

[51] A. Zensi, D. Begley, C. Pontikis, C. Legros, L. Mihoreanu, S. Wagner, et al., Albumin nanoparticles targeted with Apo E enter the CNS by transcytosis and are delivered to neurones., J. Control. Release. 137 (2009) 78–86. doi:10.1016/j.jconrel.2009.03.002.

[52] Chitosan Nanoparticles: A Promising System in Novel Drug Delivery, (n.d.). https://www.jstage.jst.go.jp/article/cpb/58/11/58_11_1423/_pdf (accessed November 20, 2015).

[53] K. Goyal, V. Koul, Y. Singh, A. Anand, Targeted Drug Delivery to Central Nervous System (CNS) for the Treatment of Neurodegenerative Disorders: Trends and Advances, Cent. Nerv. Syst. Agents Med. Chem. 14 (2014) 43–59. doi:10.2174/18715249146661410301459 48.

[54] A. Azadi, M. Hamidi, M.-R. Rouini, Methotrexate-loaded chitosan nanogels as “Trojan Horses” for drug delivery to brain: preparation and *in vitro*/*in vivo* characterization., Int. J. Biol. Macromol. 62 (2013) 523–30. doi:10.1016/j.ijbiomac.2013.10.004.

[55] T. Gerson, E. Makarov, T.H. Senanayake, S. Gorantla, L.Y. Poluektova, S. V Vinogradov, Nano-NRTIs demonstrate low neurotoxicity and high antiviral activity against HIV infection in the brain., Nanomedicine. 10 (2014) 177–85. doi:10.1016/j.nano.2013.06.012.

[56] K.A. Potter, M. Jorfi, K.T. Householder, E.J. Foster, C. Weder, J.R. Capadona, Curcumin-releasing mechanically adaptive intracortical implants improve the proximal neuronal density and blood-brain barrier stability., Acta Biomater. 10 (2014) 2209–22.

doi:10.1016/j.actbio.2014.01.018.

[57] S. Wohlfart, S. Gelperina, J. Kreuter, Transport of drugs across the blood–brain barrier by nanoparticles, J. Control. Release. 161 (2012) 264–273. doi:10.1016/j.jconrel.2011.08.017.

[58] J. Kreuter, Mechanism of polymeric nanoparticle-based drug transport across the blood-brain barrier (BBB)., J. Microencapsul. 30 (2013) 49–54. doi:10.3109/02652048.2012.692491.

[59] J. Kreuter, Nanoparticulate systems for brain delivery of drugs, Adv. Drug Deliv. Rev. 64 (2012) 213–222. doi:10.1016/j.addr.2012.09.015.

[60] J. Kreuter, Nanoparticulate systems for brain delivery of drugs, Adv. Drug Deliv. Rev. 47 (2001) 65–81. doi:10.1016/S0169-409X(00)00122-8.

[61] J. Kreuter, V.. Petrov, D.. Kharkevich, R.. Alyautdin, Influence of the type of surfactant on the analgesic effects induced by the peptide dalargin after its delivery across the blood–brain barrier using surfactant-coated nanoparticles, J. Control. Release. 49 (1997) 81–87. doi:10.1016/S0168-3659(97)00061-8.

[62] I. Reimold, D. Domke, J. Bender, C.A. Seyfried, H.-E. Radunz, G. Fricker, Delivery of nanoparticles to the brain detected by fluorescence microscopy., Eur. J. Pharm. Biopharm. 70 (2008) 627–32. doi:10.1016/j.ejpb.2008.05.007.

[63] P. Ramge, J. Kreuter, B. Lemmer, Circadian phase-dependent antinociceptive reaction in mice determined by the hot-plate test and the tail-flick test after intravenous injection of dalargin-loaded nanoparticles., Chronobiol. Int. 16 (1999) 767–77. http://www.ncbi.nlm.nih.gov/pubmed/10584177 (accessed November 20, 2015).

[64] P. Calvo, B. Gouritin, H. Chacun, D. Desmaële, J. D'Angelo, J.-P. Noel, et al., Long-Circulating PEGylated Polycyanoacrylate Nanoparticles as New Drug Carrier for Brain Delivery, Pharm. Res. 18 (n.d.) 1157–1166. doi:10.1023/A:1010931127745.

[65] I. Brigger, J. Morizet, G. Aubert, H. Chacun, M.-J. Terrier-Lacombe, P. Couvreur, et al., Poly(ethylene glycol)-coated hexadecylcyanoacrylate nanospheres display a combined effect for brain tumor targeting., J.

Pharmacol. Exp. Ther. 303 (2002) 928–36. doi:10.1124/jpet.102.039669.

[66] M. Huang, W. Wu, J. Qian, D.-J. Wan, X.-L. Wei, J.-H. Zhu, Body distribution and in situ evading of phagocytic uptake by macrophages of long-circulating poly (ethylene glycol) cyanoacrylate-co-n-hexadecyl cyanoacrylate nanoparticles., Acta Pharmacol. Sin. 26 (2005) 1512–8. doi:10.1111/j.1745-7254.2005.00216.x.

[67] N.J. Abbott, Prediction of blood–brain barrier permeation in drug discovery from in vivo, *in vitro* and in silico models, Drug Discov. Today Technol. 1 (2004) 407–416. doi:10.1016/j.ddtec.2004.11.014.

[68] L. Di, E.H. Kerns, G.T. Carter, Strategies to assess blood–brain barrier penetration, Expert Opin. Drug Discov. 3 (2008) 677–687.

[69] D.E. Eigenmann, PhD Thesis, University of Basel, 2015.

[70] P. Naik, L. Cucullo, *In vitro* blood-brain barrier models: current and perspective technologies., J. Pharm. Sci. 101 (2012) 1337–54. doi:10.1002/jps.23022.

[71] W. Pardridge, Transport of small molecules through the blood-brain barrier: biology and methodology, Adv. Drug Deliv. Rev. 15 (1995) 5–36.

[72] D.E. Clark, In silico prediction of blood-brain barrier permeation, Drug Discov. Today. 8 (2003) 927–933.

[73] S.D. Krämer, Absorption prediction from physicochemical parameters, Pharm. Sci. Technolo. Today. 2 (1999) 373–380.

[74] A.M. ter Laak, R.S. Tsai, G.M. Donné-Op den Kelder, P.-A. Carrupt, B. Testa, H. Timmerman, Lipophilicity and hydrogen-bonding capacity of H1-antihistaminic agents in relation to their central sedative side-effects, Eur. J. Pharm. Sci. 2 (1994) 373–384.

[75] W.M. Pardridge, Log(BB), PS products and in silico models of drug brain penetration, Drug Discov. Today. 9 (2004) 392–393.

[76] Z. Rankovic, CNS Drug Design: Balancing Physicochemical Properties for Optimal Brain Exposure, J. Med. Chem. 58 (2015) 2584–2608.

[77] J.C. Kalvass, T.S. Maurer, G.M. Pollack, Use of Plasma and Brain Unbound Fractions to Assess the Extent of Brain Distribution of 34 Drugs:

Comparison of Unbound Concentration Ratios to *in Vivo* P-Glycoprotein Efflux Ratios, Drug Metab. Dispos. 35 (2007) 660–666. doi:10.1124/dmd.106.012294.

[78] F. Joó, The blood-brain barrier *in vitro*: Ten years of research on microvessels isolated from the brain, Neurochem. Int. 7 (1985) 1–25.

[79] J.A. Nicolazzo, S.A. Charman, W.N. Charman, Methods to assess drug permeability across the blood-brain barrier, J. Pharm. Pharmacol. 58 (2006) 281–293.

[80] J.G. Prudhomme, I.W. Sherman, K.M. Land, A. V. Moses, S. Stenglein, J.A. Nelson, Studies of Plasmodium falciparum cytoadherence using immortalized human brain capillary endothelial cells, Int. J. Parasitol. 26 (1996) 647–655.

[81] L. Xiao, C. Yang, K. Dorovini-Zis, N.N. Tandon, E.W. Ades, A.A. Lal, et al., Plasmodium falciparum: Involvement of Additional Receptors in the Cytoadherence of Infected Erythrocytes to Microvascular Endothelial Cells, Exp. Parasitol. 84 (1996) 42–55.

[82] A. Muruganandam, L. Moorhouse Herx, R. Monette, J.P. Durkin, D.B. Stanimirovic, Development of immortalized human cerebromicrovascular endothelial cell line as an *in vitro* model of the human blood-brain barrier, FASEB J. 11 (1997) 1187–1197.

[83] M.F. Stins, J. Badger, K.S. Kim, Bacterial invasion and transcytosis in transfected human brain microvascular endothelial cells, Microb. Pathog. 30 (2001) 19–28.

[84] X. Gu, J. Zhang, D.W. Brann, F.-S.X. Yu, Brain and retinal vascular endothelial cells with extended life span established by ectopic expression of telomerase, Invest. Ophthalmol. Vis. Sci. 44 (2003) 3219–3225.

[85] N. Ketabi-Kiyanvash, C. Herold-Mende, F. Kashfi, S. Caldeira, M. Tommasino, W.E. Haefeli, et al., NKIM-6, a new immortalized human brain capillary endothelial cell line with conserved endothelial characteristics, Cell Tissue Res. 328 (2007) 19–29.

[86] Y. Sano, F. Shimizu, M. Abe, T. Maeda, Y. Kashiwamura, S. Ohtsuki, et al., Establishment of a new conditionally immortalized human brain

microvascular endothelial cell line retaining an *in vivo* blood-brain barrier function, J. Cell. Physiol. 225 (2010) 519–528.

[87] A. Kamiichi, T. Furihata, S. Kishida, Y. Ohta, K. Saito, S. Kawamatsu, et al., Establishment of a new conditionally immortalized cell line from human brain microvascular endothelial cells: A promising tool for human blood-brain barrier studies, Brain Res. (2012) 113–122.

[88] T. Maeda, Y. Sano, M. Abe, F. Shimizu, Y. Kashiwamura, S. Ohtsuki, et al., Establishment and characterization of spinal cord microvascular endothelial cell lines, Clin. Exp. Neuroimmunol. 4 (2013) 326–338.

[89] S. Lundquist, M. Renftel, J. Brillault, L. Fenart, R. Cecchelli, M.-P. Dehouck, Prediction of Drug Transport Through the Blood-Brain Barrier in Vivo: A Comparison Between Two *in Vitro* Cell Models, Pharm. Res. 19 (2002) 976–981.

[90] K. Takahashi, Y. Sawasaki, J.-I. Hata, K. Mukai, T. Goto, Spontaneous transformation and immortalization of human endothelial cells, Vitr. Cell. Dev. Biol. 26 (1990) 265–274.

[91] M.A. Deli, Blood-Brain Barrier Models, in: A. Lajtha, M.E.A. Reith (Eds.), Handb. Neurochem. Mol. Neurobiol., 3rd ed., Springer Verlag, Berlin Heidelberg, 2007: pp. 29–55.

[92] J. Mensch, J. Oyarzabal, C. Mackie, P. Augustijns, In vivo, *in vitro* and in silico methods for small molecule transfer across the BBB, J. Pharm. Sci. 98 (2009) 4429–4468.

[93] R.N. Hull, W.R. Cherry, G.W. Weaver, The origin and characteristics of a pig kidney cell strain, LLC-PK1, *In Vitro*. 12 (1976) 670–677.

[94] B. Veronesi, Characterization of the MDCK Cell Line for Screening Neurotoxicants, Neurotoxicology. 17 (1996) 433–444.

[95] S.G. Summerfield, K. Read, D.J. Begley, T. Obradovic, I.J. Hidalgo, S. Coggon, et al., Central nervous system drug disposition: the relationship between in situ brain permeability and brain free fraction, J. Pharmacol. Exp. Ther. 322 (2007) 205–213. doi:10.1124/jpet.107.121525.

[96] A. Braun, S. Hämmerle, K. Suda, B. Rothen-Rutishauser, M. Günthert, S.D. Krämer, et al., Cell cultures as tools in biopharmacy, Eur. J. Pharm. Sci.

11, Supple (2000) S51–S60.

[97] L. Di, E.H. Kerns, I.F. Bezar, S.L. Petusky, Y. Huang, Comparison of blood-brain barrier permeability assays: in situ brain perfusion, MDR1-MDCKII and PAMPA-BBB, J. Pharm. Sci. 98 (2009) 1980–1991.

[98] F. Roux, P.-O. Couraud, Rat Brain Endothelial Cell Lines for the Study of Blood–Brain Barrier Permeability and Transport Functions, Cell. Mol. Neurobiol. 25 (2005) 41–57.

[99] C. Förster, C. Silwedel, N. Golenhofen, M. Burek, S. Kietz, J. Mankertz, et al., Occludin as direct target for glucocorticoid-induced improvement of blood-brain barrier properties in a murine *in vitro* system, J. Physiol. 565 (2005) 475–486.

[100] Y. Omidi, L. Campbell, J. Barar, D. Connell, S. Akhtar, M. Gumbleton, Evaluation of the immortalised mouse brain capillary endothelial cell line, b.End3, as an *in vitro* blood–brain barrier model for drug uptake and transport studies, Brain Res. 990 (2003) 95–112.

[101] E.F. Wagner, W. Risau, Oncogenes in the study of endothelial cell growth and differentiation, Semin. Cancer Biol. 5 (1994) 137–145.

[102] T. Yang, K.E. Roder, T.J. Abbruscato, Evaluation of bEnd5 cell line as an *in vitro* model for the blood–brain barrier under normal and hypoxic/aglycemic conditions, J. Pharm. Sci. 96 (2007) 3196–3213.

[103] R. Cecchelli, S. Aday, E. Sevin, C. Almeida, M. Culot, L. Dehouck, et al., A Stable and Reproducible Human Blood-Brain Barrier Model Derived from Hematopoietic Stem Cells, PLoS One. 9 (2014) 1–11.

[104] E.S. Lippmann, S.M. Azarin, J.E. Kay, R.A. Nessler, H.K. Wilson, A. Al-Ahmad, et al., Derivation of blood-brain barrier endothelial cells from human pluripotent stem cells, Nat. Biotechnol. 30 (2012) 783–791.

[105] D.B. Stanimirovic, M. Bani-Yaghoub, M. Perkins, A.S. Haqqani, Blood-brain barrier models: *in vitro* to *in vivo* translation in preclinical development of CNS-targeting biotherapeutics, Expert Opin. Drug Discov. 10 (2015) 141–155.

[106] Q.R. Smith, Brain Perfusion Systems for Studies of Drug Uptake and Metabolism in the Central Nervous System, in: R.T. Borchardt, P.L. Smith,

G. Wilson (Eds.), Model. Assess. Drug Absorpt. Metab., Springer US, 1996: pp. 285–307.

[107] Y. Takasato, S.I. Rapoport, Q.R. Smith, An in situ brain perfusion technique to study cerebrovascular transport in the rat, Am. J. Physiol. - Hear. Circ. Physiol. 247 (1984) H484–H493.

[108] A.K. Deo, F.-P. Theil, J.-M. Nicolas, Confounding Parameters in Preclinical Assessment of Blood–Brain Barrier Permeation: An Overview With Emphasis on Species Differences and Effect of Disease States, Mol. Pharm. 10 (2013) 1581–1595.

[109] T.S. Maurer, D.B. DeBartolo, D.A. Tess, D.O. Scott, Relationship between exposure and nonspecific binding of thirty-three central nervous system drugs in mice, Drug Metab. Dispos. 33 (2005) 175–181. doi:10.1124/dmd.104.001222.

[110] N. Plock, C. Kloft, Microdialysis—theoretical background and recent implementation in applied life-sciences, Eur. J. Pharm. Sci. 25 (2005) 1–24. doi:10.1016/j.ejps.2005.01.017.

[111] A. Reichel, Addressing central nervous system (CNS) penetration in drug discovery: basics and implications of the evolving new concept, Chem. Biodivers. 6 (2009) 2030–2049.

[112] Y. Deguchi, Application of *In Vivo* Brain Microdialysis to the Study of Blood-Brain Barrier Transport of Drugs, Drug Metab. Pharmacokinet. 17 (2002) 395–407.

[113] Z. Redzic, Molecular biology of the blood-brain and the blood-cerebrospinal fluid barriers: similarities and differences, Fluids Barriers CNS. 8 (2011) 3.

[114] L. Di, H. Rong, B. Feng, Demystifying Brain Penetration in Central Nervous System Drug Discovery, J. Med. Chem. 56 (2013) A–K.

[115] S. Murugan, N. Pravallika, P. Sirisha, K. Chandrakala, a Review on Bioanalytical Method Development and Validation By Using Lc-Ms / Ms, 6 (2013) 41–45.

[116] J.R. Mazzeo, U. D.Neue, M. Kele, R.S. Plumb, Advancing LC Performance with Smaller Particles and Higher Pressure, Anal. Chem. 77 (2005) 460 A–467 A.

[117] R.N. Xu, L. Fan, M.J. Rieser, T.A. El-Shourbagy, Recent advances in high-throughput quantitative bioanalysis by LC–MS/MS, J. Pharm. Biomed. Anal. 44 (2007) 342–355.

[118] W.M.A. Niessen, Progress in liquid chromatography–mass spectrometry instrumentation and its impact on high-throughput screening, J. Chromatogr. A. 1000 (2003) 413–436.

[119] J.H. Gross, Electrospray Ionization, in: Mass Spectrom., 2nd ed., Springer Verlag, New York Heidelberg Dordrecht London, 2011: pp. 561–620.

[120] R.A. Yost, C.G. Enke, Triple quadrupole mass spectrometry for direct mixture analysis and structure elucidation, Anal. Chem. 51 (1979) 1251–1264.

[121] J.H. Gross, Instrumentation, in: Mass Spectrom., 2nd ed., Springer Verlag, New York Heidelberg Dordrecht London, 2011: pp. 117–221.

[122] E.B. Jones, Quadrupole, Triple-Quadrupole, and Hybrid Linear Ion Trap Mass Spectrometers for Metabolite Analysis, in: R. Ramanathan (Ed.), Mass Spectrom. Drug Metab. Pharmacokinet., John Wiley & Sons, New Jersey, 2009: pp. 123–157.

[123] J.-S. Kang, Principles and Applications of LC-MS/MS for the Quantitative Bioanalysis of Analytes in Various Biological Samples, in: J.K. Prasain (Ed.), Tandem Mass Spectrom. - Appl. Princ., InTech, Rijeka, Croatia, 2012: pp. 441–492.

[124] J.N. and J. Rowe, Topics on Drug Metabolism, InTech, 2012. doi:10.5772/1180.

[125] L.A. Berrueta, B. Gallo, F. Vicente, A review of solid phase extraction: Basic principles and new developments, Chromatographia. 40 (1995) 474–483.

[126] S. Devanshu, M. Rahul, G. Annu, S. Kishan, N. Anroop, Quantitative Bioanalysis by LC-MS/MS: A Review, J. Pharm. Biomed. Sci. 7 (2010) 1–9.

[127] V. Viette, M. Fathi, S. Rudaz, D. Hochstrasser, J.-L. Veuthey, Current role of liquid chromatography coupled to mass spectrometry in clinical toxicology screening methods, Clin. Chem. Lab. Med. 49 (2011) 1091–

1103.

[128] P.L. Kole, G. Venkatesh, J. Kotecha, R. Sheshala, Recent advances in sample preparation techniques for effective bioanalytical methods, Biomed. Chromatogr. 25 (2011) 199–217.

[129] M. Meng, P.K. Bennett, Method Development, Validation, and Sample Analysis for Regulated Quantitative Bioanalysis Using LC-MS/MS, in: Q.A. Xu, T.L. Madden (Eds.), LC-MS Drug Bioanal., Springer Science+Business Media, New York Heidelberg Dordrecht London, 2012.

[130] J. Pan, X. Jiang, Y.-L. Chen, Automatic Supported Liquid Extraction (SLE) Coupled with HILIC-MS/MS: An Application to Method Development and Validation of Erlotinib in Human Plasma, Pharmaceutics. 2 (2010) 105–118.

[131] D.M. Ramanathan, R.M. LeLacheur, Evolving Role of Mass Spectrometry in Drug Discovery and Development, in: R. Ramanathan (Ed.), Mass Spectrom. Drug Metab. Pharmacokinet., John Wiley & Sons, New Jersey, 2009: pp. 1–85.

[132] J. Wieling, LC-MS-MS experiences with internal standards, Chromatographia. 55 (2002) S107–S113.

[133] Q.A. Xu, Madden, eds., LC-MS in Drug Bioanalysis, Springer Science+Business Media, New York Heidelberg Dordrecht London, 2012.

[134] Guideline on bioanalytical method validation, European Medicines Agency (EMEA/CHMP/EWP/192217/2009), London, 21 July 2011,

[135] Guidance for Industry: Bioanalytical Method Validation, US Food and Drug Administration (FDA), Center for Drug Evaluation and Research, May 2001,

[136] Guidance for Industry: Bioanalytical Method Validation, US Food and Drug Administration (FDA), Center for Drug Evaluation and Research, Draft Guidance September 2013, (n.d.).

[137] L. V. Sonawane, B.N. Poul, S. V. Usnale, P. V. Waghmare, L.H. Surwase, Bioanalytical Method Validation and Its Pharmaceutical Application- A Review, Pharm. Anal. Acta. 5 (2014) 1–7.

[138] B. DeSilva, F. Garofolo, M. Rocci, S. Martinez, I. Dumont, F. Landry, et al.,

2012 White Paper on Recent Issues in Bioanalysis and Alignment of Multiple Guidelines, Bioanalysis. 4 (2012) 2213–2226.

[139] Validation of Analytical Procedures: Text and Methodology Q2 (R1), International Conference onf Harmonisation of Technical Requirements for Registration of Pharmaceuticals for Human Use (ICH) Harmonised Tripartite Guideline, November 1996, (n.d.).

[140] E. Rozet, R.D. Marini, E. Ziemons, B. Boulanger, P. Hubert, Advances in validation, risk and uncertainty assessment of bioanalytical methods, J. Pharm. Biomed. Anal. 55 (2011) 848–858.

[141] P. Kebarle, L. Tang, From ions in solution to ions in the gas phase, Anal. Chem. 65 (1993) 972A–986A.

[142] A. Van Eeckhaut, K. Lanckmans, S. Sarre, I. Smolders, Y. Michotte, Validation of bioanalytical LC–MS/MS assays: Evaluation of matrix effects, J. Chromatogr. B. 877 (2009) 2198–2207.

[143] S. Bansal, A. DeStefano, Key elements of bioanalytical method validation for small molecules, AAPS J. 9 (2007) E109–E114.

[144] L. Bonaccini, A. Karioti, M.C. Bergonzi, A.R. Bilia, S. Fiorentino, Effects of Salvia miltiorrhiza on CNS Neuronal Injury and Degeneration : A Plausible Complementary Role of Tanshinones and Depsides *, (2015) 1003–1016. doi:10.1055/s-0035-1546196.

[145] Y. Zhou, W. Li, L. Xu, L. Chen, In Salvia miltiorrhiza, phenolic acids possess protective properties against amyloid β-induced cytotoxicity, and tanshinones act as acetylcholinesterase inhibitors., Environ. Toxicol. Pharmacol. 31 (2011) 443–52. doi:10.1016/j.etap.2011.02.006.

[146] L.-L. Tian, X.-J. Wang, Y.-N. Sun, C.-R. Li, Y.-L. Xing, H.-B. Zhao, et al., Salvianolic acid B, an antioxidant from Salvia miltiorrhiza, prevents 6-hydroxydopamine induced apoptosis in SH-SY5Y cells., Int. J. Biochem. Cell Biol. 40 (2008) 409–22. doi:10.1016/j.biocel.2007.08.005.

[147] Y.W. Lee, D.H. Kim, S.J. Jeon, S.J. Park, J.M. Kim, J.M. Jung, et al., Neuroprotective effects of salvianolic acid B on an Aβ25-35 peptide-induced mouse model of Alzheimer's disease., Eur. J. Pharmacol. 704 (2013) 70–7. doi:10.1016/j.ejphar.2013.02.015.

[148] T. Chen, W. Liu, X. Chao, L. Zhang, Y. Qu, J. Huo, et al., Salvianolic acid B attenuates brain damage and inflammation after traumatic brain injury in mice., Brain Res. Bull. 84 (2011) 163–8. doi:10.1016/j.brainresbull.2010.11.015.

[149] Y. Jiang, Z. Liu, W. Cui, W. Zhang, J. Gong, X. Wang, et al., Antioxidant effect of salvianolic acid B on hippocampal CA1 neurons in mice with cerebral ischemia and reperfusion injury., Chin. J. Integr. Med. 21 (2015) 516–22. doi:10.1007/s11655-014-1791-1.

[150] D.H. Kim, S.J. Park, J.M. Kim, S.J. Jeon, D.-H. Kim, Y.-W. Cho, et al., Cognitive dysfunctions induced by a cholinergic blockade and Aβ 25-35 peptide are attenuated by salvianolic acid B., Neuropharmacology. 61 (2011) 1432–40. doi:10.1016/j.neuropharm.2011.08.038.

[151] S.S.K. Durairajan, Q. Yuan, L. Xie, W.-S. Chan, W.-F. Kum, I. Koo, et al., Salvianolic acid B inhibits Abeta fibril formation and disaggregates preformed fibrils and protects against Abeta-induced cytotoxicty., Neurochem. Int. 52 (2008) 741–50. doi:10.1016/j.neuint.2007.09.006.

[152] F.G. Serrano, C. Tapia-Rojas, F.J. Carvajal, J. Hancke, W. Cerpa, N.C. Inestrosa, Andrographolide reduces cognitive impairment in young and mature AβPPswe/PS-1 mice., Mol. Neurodegener. 9 (2014) 61. doi:10.1186/1750-1326-9-61.

[153] C. Tapia-Rojas, A. Schüller, C.B. Lindsay, R.C. Ureta, C. Mejías-Reyes, J. Hancke, et al., Andrographolide activates the canonical Wnt signalling pathway by a mechanism that implicates the non-ATP competitive inhibition of GSK-3β: autoregulation of GSK-3β in vivo., Biochem. J. 466 (2015) 415–30. doi:10.1042/BJ20140207.

[154] T. Yang, H.-H. Sheng, N.-P. Feng, H. Wei, Z.-T. Wang, C.-H. Wang, Preparation of andrographolide-loaded solid lipid nanoparticles and their *in vitro* and *in vivo* evaluations: characteristics, release, absorption, transports, pharmacokinetics, and antihyperlipidemic activity., J. Pharm. Sci. 102 (2013) 4414–25. doi:10.1002/jps.23758.

CHAPTER 2

DEVELOPMENT OF BLOOD–BRAIN BARRIER PERMEABLE NANOPARTICLES AS POTENTIAL CARRIERS FOR SALVIANOLIC ACID B TO CENTRAL NERVOUS SYSTEM

This work was carried out in collaboration with Cristina Grossi[1], Benedetta Isacchi[2], Maria Camilla Bergonzi[2], Ilaria Luccarini[1], Fiorella Casamenti[1], Anna Rita Bilia[2]

[1] Department of Neuroscience, Psychology, Drug Research and Child Health, Division of Pharmacology and Toxicology, University of Florence, 50139 Florence, Italy

[2] Department of Chemistry, University of Florence, Via Ugo Schiff 6, 50019 Sesto Fiorentino, Florence, Italy

2.1 ABSTRACT

BBB hinders the passage of systemically delivered therapeutics and the brain extracellular matrix limits the distribution and durability of locally delivered agents. Drug-loaded nanocarriers represent a promising strategy to overcome these barriers and address specific drug delivery challenges, due to their small size and versatile design. We synthetized fluorescent poly (ethyl-cyanoacrylate) nanoparticles (PECA-FITC-D-TW80 NPs) by emulsion polymerization method to target and reach the brain after intravenous and intraperitoneal administration. NPs were characterized in terms of dimensional analysis, polydispersity (PDI) and Zeta Potential (ζ-potential); morphology, encapsulation efficacy (EE) and loading capacity (LC) were evaluated too. After intracerebral injection in healthy rats, NPs were distributed within the injected hemisphere and mainly they interacted with microglial cells, presumably involved in their clearance by phagocytosis. Furthermore, NPs were able to pass BBB after systemic administration in rats and the lack of toxicity in C57/B6 mice chronically administered was highlighted. These evidences contribute to clarify NPs distribution, accumulation, fate and toxicity into the brain supporting the observation that the selected NPs may represent a biocompatible promising carrier to be further investigated as brain delivery systems. SalB from the *Salvia miltiorrhiza* Bge*,* is a promising molecule in the protection of degeneration in several animal models by various biological mechanisms but its poor chemical stability and low bioavailability limits a clinical application for CNS neuronal injury and degeneration. NPs were loaded with SalB obtaining an EE% and LC% of 98.70 % ± 0.45 and 53.3% ± 0.24 respectively. They were suitable for parental administration because their mean diameter was smaller than 300 nm, with a PDI of 0.04 ± 0.03, and a ζ-potential of -8.38 mV± 3.87. The *in vitro* studies pointed out that the release of SalB from the NPs was sustained and prolonged during 8 hours, a suitable performance for a promising clinical application.

2.2 INTRODUCTION

SalB (Figure 12) represents the most abundant constituent among the water-soluble compounds of roots and rhizome of Danshen (*Salvia miltiorrhiza* Bge.), a medicinal plant widely used in Asia for the treatment of a variety of diseases, in particular cardiovascular diseases such as angina pectoris, myocardial infarction and stroke [1]. Numerous studies have revealed multiple pharmacological actions SalB acting with various molecular targets suggesting an important role

in the different CNS pathologies, both the acute ones such as cerebral ischemia, traumatic brain injury, and epilepsy, but also chronic diseases such as multiple sclerosis, AD, Parkinson's disease, schizophrenia.

Besides the extensive studies reporting these mechanisms, pharmacokinetic studies are still very limited and not conclusive, reporting that oral administration give a rapid absorption, quick clearance, and poor absolute bioavailability; after i.v. administration, it is extensively metabolized and degraded rapidly.

A unique trial on humans, a randomized, open-label, single-dose study, was conducted in 12 healthy Chinese volunteers receiving a single intravenous infusion of a 100- or 200-mg of a mixture of depside salts (SalB ca. 88%), a preparation marketed in China for the treatment of coronary heart disease, and it disclosed that SalB is methylated rapidly in the liver and most of the metabolites (M1, M2, and M3 detected in the plasma with very low concentrations between 50 and 170 ng/ mL) are excreted into bile and faeces. In a further study, SalB (50 mg/kg BW) administrated intragastrically, was not detected in blood and brain microdialysates, collected at 15- and 30-min time intervals for 4 h, respectively [1].

Aim of this study was to develop blood brain barrier (BBB) permeable nanocarriers for the delivery of molecules that might be of therapeutic value in the treatment of neurodegenerative and psychiatric disorders. Nanovectors (NVs) can cross the BBB using several mechanisms including the aperture of the tight junctions between endothelial cells, transcytosis and endocytosis, inhibition of the transmembrane efflux systems (i.e., P-glycoprotein), induction of local toxic effects on the brain vasculature leading to a limited permeability of the brain endothelial cells [2].

Natural and synthetic polymers have been used to produce NPs, all these materials are very versatile for the transport of drugs, which may be bound either as a solid solution or as dispersion, can be adsorbed to the surface or chemically attached. Nanoparticulate brain delivery systems should not damage the BBB and drug delivery should be targeted to the site of intended action in the brain. Moreover, the vectors should have an adequate shelf-life for a sustained and controlled drug delivery, they should be biodegradable after the drug release, not toxic and antigenic [3]. Poly (alkyl cyanoacrylates), in particular PBCA and poly(isohexyl cyanoacrylate) (PIHCA), represent suitable polymers for this therapeutic approach, because they have a quite rapid elimination, due to

an enzymatic cleavage of the ester bond of the alkyl side chain of the polymer and resulting in the formation of the low-toxic water-soluble products-poly(cyanoacrylate) acid and appropriate alcohol. The BBB crossing of poly(alkyl cyanoacrylates) NPs is acquired by overcoating NPs with certain surfactants such as TW80 or poloxamer 188 (Pluronic® F68) [4]. Studies with PBCA NPs have been assessed that doxorubicin and temozolomide could be transport across only in rats treated with surfactant-coated NPs. These observations demonstrate the great potential of surface-coated PBCA NPs for the delivery of drugs to the central nervous system. This delivery should be achieved by covalent coupling with apolipoprotein E, A-I, or B-100, followed by receptor-mediated endocytosis of the NPs by the brain capillary endothelial cells [5,6] However, *in vivo* data concerning NPs uptake, distribution, time-dependent accumulation, tropism, fate and toxicity inside the brain is still almost unclarified. To the best of our knowledge, Fricker's group has recently investigated the PBCA NPs's biocompatibility by *in vitro* and *ex vivo* studies. No cell death or loss of metabolic activity was observed for nanoparticle-concentrations ≤500 µg/ml up to 3 h of treatment. Metabolic activity was tested by the AlamarBlue®-assay and cell viability by LDH-assay. Integrity of the BBB was analyzed *in vitro* by measuring the trans-endothelial electrical resistance using the CellZscope®. Additionally, an *in vitro* test (Multi-Analyte ELISArray™ Kit Human Inflammatory Cytokines) was used to evaluate the release of inflammatory cytokines in human blood after 24 h incubation of NPs. Only interleukin-8 was released significantly. No severe inflammatory processes or organ damages were identified in rats in an *ex vivo* model [7].

In the present work we developed and optimized fluorescent-labeled PECA NPs to target and reach brain tissues. This polymer is less investigated then PBCA. NPs distribution and fate in the brain parenchyma were evaluated in healthy rats, after NPs intracerebral injection into the *nucleus basalis magnocellularis* (NBM) of the basal forebrain. Furthermore, we report the ability of NPs to reach the brain after an acute systemic administration in rats and the lack of their toxicity in C57/B6 mice NPs-administered for two weeks, supporting the observation that these NPs may represent a promising carrier for drug delivery to the CNS. Hence, Sal B (88.2%), isolated from Danshen was loaded into optimized PECA NPs and their performance evaluated *in vitro*.

2.3 RESULTS

2.3.1 *Development and characterization of PECA NPs*

PECA NPs were prepared and optimized by emulsion polymerization method. The dimensional analysis, PDI and ζ-potential of PECA NPs, PECA NPs coated with Tween 80 (PECA-TW80 NPs), PECA-FITC-D NPs, PECA-FITC-D-TW80 and PECA NPs loaded with SalB, are reported in Table 6. The mean diameter of PECA-TW80 NPs was 303±8 nm, 248±1 nm for PECA-FITC-D-TW80 and both resulted suitable for the systemic administration. The dimensional analysis was not affected by the coating. The mean ζ-potentials of PECA NPs coated or not with 1% Tween 80 was ca. -4 mV and -3 mV, respectively. This characteristic was very interesting because NPs with slightly negative surface charge encompasses reduced plasma protein adsorption and low rate of nonspecific cellular uptake [8]. The yields of preparative process for PECA-TW80 and PECA-FITC-D-TW80 NPs were very high, as reported.

Table 6: Characterization of PECA-based NPs in terms of mean diameter, Polidispersity (PDI), Zeta-potential, Yield of preparative process, Encapsulation efficiency and Loading Capacity

PECA NPs	Size (nm)	PDI	Z-Potential (mV)	Yield %	EE%	LC%
PECA	288± 7	0.19 ± 0.01	-2.85 ± 1.18	92± 9.51		
PECA-TW80	303 ± 8	0.36 ± 0.04	-4.07 ± 0.05	-		
PECA-FITC-D	247 ± 2	0.14 ±0.04	-2.83 ± 0.55	66± 0.01		
PECA-FITC-D-TW80	248 ± 1	0.11 ±0.07	-3.38 ± 0.55	-		
PECA- SalB	205±2	0.07±0.02	-7.18±2.84	59.73±7.00	98.70±0.45	53.3±0.24
PECA- SalB-TW80	288±1	0.04±0.03	-8.38±3.87	-	-	-

TEM analyses provided important details on the morphology and the dimension of the NPs giving a different electronic cloud between the NPs core and the coating (Figure 14). As showed in the Figure 15, PECA-FITC-D-TW80 NPs were sphere-shaped, with a regular and narrow size distribution comparable to DLS analysis. PECA-SalB NPs were obtained with mean diameter smaller than 300 nm, with similar results to empty NPs, so the selected molecule didn't impact on the optimized formulation. The sample appears to be very homogenous, with

very low PDI and the yield of preparative process is comparable with fluorescent NPs.

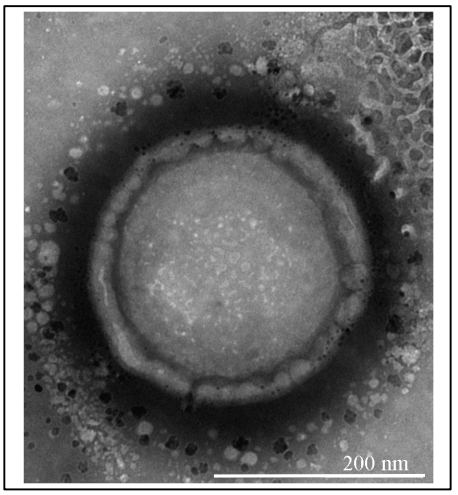

FIGURE 14: TEM MICROGRAPH OF PECA-FITC-D-TW80 NPS

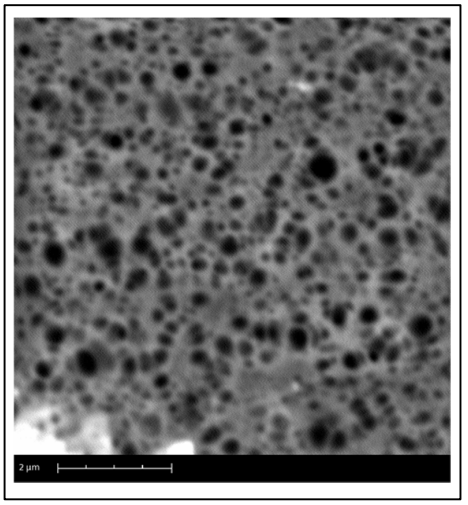

FIGURE 15: SEM MICROGRAPH OF PECA-SAL B NPS COATED WITH TWEEN 80

2.3.2 IN VIVO EXPERIMENTS

2.3.2.1 Fluorescein-labelled PECA NPs injection into the rat NBM

Firstly, 1µl (8µg/µl) of PECA-FITC-D-TW80 NPs was directly injected into the Nucleus Basalis Magnocellularis (NBM) of adult rats to follow the cellular distribution of NPs within the brain, the occurrence of general toxicity for the animals as well as NPs-induced inflammatory response in terms of glia reaction.

Histochemical analysis revealed at the injection site (asterisk), a large amount of fluorescent NPs (green) at one, three and seven days after injection (Figure 16 b,d,g). The day after surgery some NPs were detected close to cellular nuclei (DAPI, blue) in the injection site surroundings (Figure 16 c, arrows). Three and seven days after injection, PECA-FITC-D-TW80 were detected, in addition to the injection site, in a large number of cells with glial morphology (Figure 16 e and h, arrows) and inside blood vessels (inset in Figure 16 g) in the ipsilateral injected hemisphere. In particular, seven days after injection NPs moved and distributed in the ipsilateral brain parenchyma in a roughly 800μm distance from the injection site. Notably, fourteen days after injection PECA-FITC-D-TW80 fluorescent staining was strongly reduced at the injection site (Figure 16 i, asterisk) and few cells with glial morphology were FITC-labeled (Figure 16 j, arrow). NPs uptake mediated by glial cells could, likely, result in the removal/phagocytosis of NPs from brain tissue, ensuring their clearance and biocompatibility. No PECA-FITC-D-TW80 NPs were almost detected in the contralateral un-injected hemisphere (Figure 16 a and f). Immunohistochemical analysis did not reveal any astrocytosis either at the site of injection or in its vicinity, as shown by the resting morphology of GFAP-immunopositive cells (Figure 17, red) in PBS (Figure 17 a) and NPs injected groups (Figure 17 c), as exemplified at seven days after injection. By contrast, microglial cells (red) increased in number with time at the injection site and in its proximity 1, 3 and 7 days after surgery (as shown for the 7 day time-point in Figure 17 d) as compared to PBS-injected controls (Figure 17 b). Fluorescent NPs uptake mediated by microglial cells was revealed by the widespread colocalization (yellow) between FITC-labelled NPs (green) and Iba 1-immunopositive cells (red) (Figure 17 d, f). At 14 days after injection, the strong reduction in FITC NPs staining at the injection site, likely due to microglia phagocytosis and removal from the brain, was accompanied by very few Iba-1 immunopositive cells co-stained with PECA-FITC-D-TW80 NPs (Figure 17 e, arrows). In particular, the colocalization (yellow) between fluorescent NPs (green) and Iba 1 and OX6 staining (red) demonstrates that the cellular uptake of PECA-FITC-D-TW80 NPs was mainly mediated by activated microglial cells, that exhibit enlarged cell bodies, thickened and retracted processes or losses of branches in all injected groups, as shown for animals sacrificed 7 days after injection (Figure 17 f, g). PECA-FITC-D-TW80 NPs partially interacted with GFAP-immunopositive astrocytes (arrows), as shown in Fig. 4 for the 7-day time point; no interactions

with NeuN positive neurons (red) and ChAT positive neurons (red) of the NBM (Figure 17 I, j) were mostly detected. Overall, these data indicate that *in situ* administration of NPs was well tolerated, didn't induce astrogliosis and favoured microglial cells migration to the injection site for phagocytosis of NPs, ensuring their elimination from brain tissue and their biocompatibility. Consequently, as clearly shown in Figure 17, microglial cells were numerous and activated 7 days after NPs administration. In addition, a large amount of NPs co-localizes in microglial cells, suggesting an early role of microglia in removing NPs from the brain parenchyma. At 14 days after NPs intracerebral injection, the presence of reactive microglia was much reduced in parallel with the reduction of NPs. These data indicate an important role of microglia in the immune defence of the CNS.

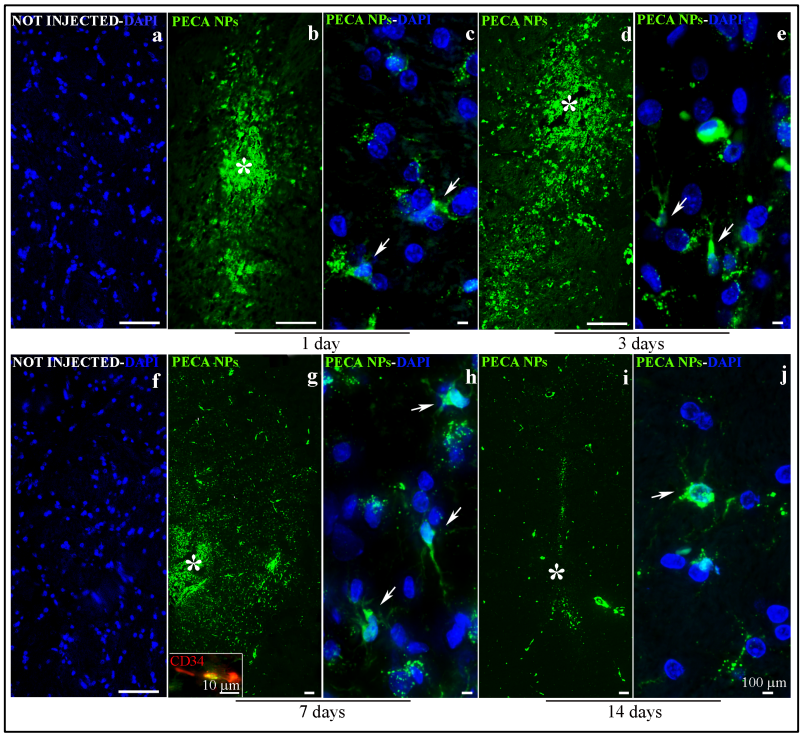

FIGURE 16: INTRACEREBRAL INJECTION OF PECA-FITC-D-TW80 NPS IN THE RAT NBM (B-E; G-J) TIME DEPENDENT NPS (GREEN) MOBILIZATION FROM THE INJECTION SITE (ASTERISK) ONE (B,C), THREE (D,E), SEVEN (G,H) AND FOURTEEN (I,J) DAYS AFTER SURGERY. THE MAGNIFIED IMAGES (C,E,H,J) SHOW NPS UPTAKE BY CELLS WITH GLIAL MORPHOLOGY (INDICATED BY THE ARROWS, DAPI IN BLUE). THE INSET IN PANEL (G) SHOWS THE COLOCALIZATION (YELLOW) BETWEEN PECA-FITC-D-TW80 NPS (GREEN) AND THE ENDOTHELIAL MARKER CD34 (RED).

PECA-FITC-D-TW80 NPs LABELLING IS ABSENT IN THE UN-INJECTED HEMISPHERE (A,F). SCALE BARS:100 MM APPLIED TO ALL IMAGES AND 10 MM TO THE INSET IN PANEL (G).

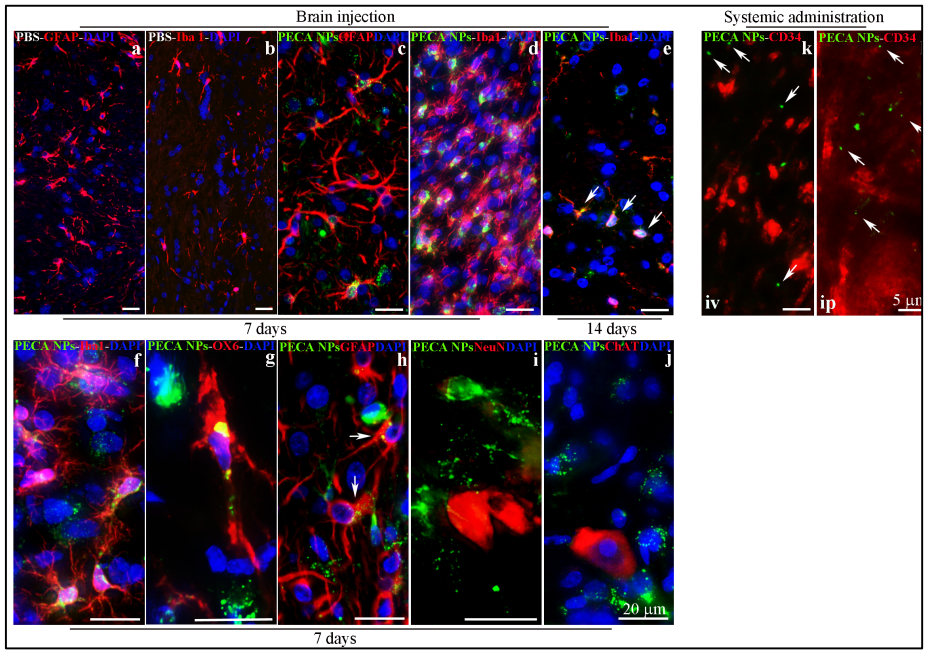

FIGURE 17: INTRACEREBRAL INJECTED PECA-FITC-D-TW80 NPS INTERACTION WITH GLIAL CELLS AND NPS BBB CROSSING AFTER SYSTEMIC ADMINISTRATION

(C-J) DOUBLE LABELLING EXPERIMENTS BETWEEN PECAFITC-D-TW80 NPS (GREEN) AND GLIAL MARKERS GFAP/IBA-1/OX6 (RED, ARROWS) OR NEURONAL NEUN/CHAT ABS (RED) PLUS DAPI (BLUE) IN INJECTED RATS, SEVEN (C-D; F-J) AND FOURTEEN (E) DAYS AFTERSURGERY. GFAP- AND IBA 1-IMMUNOPOSITIVE CELLS (RED) WITH RESTING MORPHOLOGY AND NO PECAFITC-D-TW80 NPS (GREEN) SIGNAL WERE DETECTED IN PBS-INJECTED RATS (A, B). (K,L) THE LACK OF COLOCALIZATION BETWEEN PECA-FITC-D-TW80 NPS (GREEN, INDICATED BY THE ARROWS) AND THE BRAIN VASCULAR ENDOTHELIUM MARKER CD34 (RED) DEMONSTRATED THEIR ABILITY TO CROSS THE BBB AFTER AN ACUTE IV (K) AND IP (L) ADMINISTRATION.

2.3.2.2 Intravenous and intraperitoneal administration of fluorescent PECA-FITC-D-TW80 NPs in rats

The ability of fluorescent PECA-FITC-D-TW80 NPs to cross the BBB was evaluated in rats administered acutely with 100 mg/kg iv and ip of FITC-labelled NPs. Three hours after administration (Figure 17 k, l), FITC-labelled NPs (green, arrows) were detected in the brain parenchyma outside the vascular bed (CD34, red) indicating the ability of the developed nanoformulation to cross the BBB after systemic administration. No apparent differences were evident in crossing BBB with the two routes of administration.

2.3.2.3 Systemic administration of fluorescent PECA-FITC-D-TW80 NPs in mice and behavioral test

To exclude NPs toxicity and behavioural alterations, PECA-FITC-D-TW80 NPs (200 mg/kg, ip) were daily administered to C57/B6 mice for two weeks. During this period, the nanoformulation was well tolerated, no evident side effects were revealed, as also shown by the body weight trend graph of NPs-treated mice as compared to controls (Figure 18 a) and no animals died. At the end of the treatment, mice were behaviourally evaluated in the ORT test, to check for their locomotor-exploratory abilities and cognitive functions. As shown in Figure 18 b, no locomotor (path length) nor cognitive impairments (discrimination score) were detected in NPs-treated mice as compared to controls ($P>0.05$). Overall these data provide an evidence on the biocompatibility and potential delivery of molecules to the CNS of this nanoformulation.

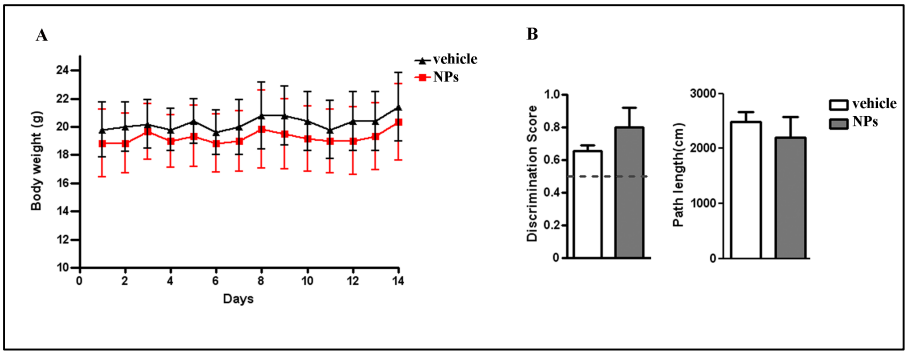

FIGURE 18: BODY WEIGHT AND BEHAVIOURAL EVALUATIONS ON MICE CHRONICALLY ADMINISTERED WITH PECA-FITC-D-TW80 NPS FOR TWO WEEKS
(a-b) PECA-FITC-D-TW80 NPs did not affect either ponderal (a) or ORT (b) cognitive and locomotor parameters.

2.3.3 ISOLATION OF SALB

The method of extraction and isolation of SalB was rapid and easy to reproduce. The dried crude extract (2g) of the roots and rhizome of *Salvia miltiorrhiza* Bge was firstly submitted to exclusion-size chromatography (Sephadex LH-20) using hydro-alcoholic solutions with descending polarity for a rapid separation and refinement of SalB thanks to the difference in molecular size of the tetramer SalB compared to other monomers, dimers and trimers of caffeic acid that are in the extract. Then, to have pure SalB, liquid-liquid extraction and acidification at

pH=2 were performed, obtaining 829.7 mg of SalB pure at 88,2%. The presence of SalB in the extract was assessed by comparison of retention time and UV spectra with the reference standard and the data present in the literature.

TABLE 7: FRACTIONS OBTAINED AFTER EXCLUSION-SIZE CHROMATOGRAPHY (SEPHADEX LH-20) AND COMBINED AFTER MONITORING BY HPLC-DAD

Fractions	Solvent	Constituent
A	EtOH 20%	3,4-dihidrossi acid phenyl-lactic
B	EtOH 20%	Mixture of phenolic acids
C	EtOH 20%	Lithospermic acid impure
D	EtOH 20%	Lithospermic acid pure
E	EtOH 20%	Lithospermic acid + SalB (salt)
F	EtOH 40%	SalB (salt)
G	EtOH 60%	SalB (salt) + Rosmarinic acid
H	EtOH 60%	Rosmarinic acid + Sal B (neutral)
I	EtOH 80%	Sal B (neutral)
J	MeOH 100%	Sal A + Salvianolic Acid A

2.3.4 PREPARATION AND CHARACTERIZATION OF SALB LOADED-PECA NPS

PECA-SalB NPs were developed dissolving SalB in the 0.1 N HCl/dextran 70,000 solution, before ECA polymerization. Coated and uncoated PECA-SalB NPs were characterized as shown in Table 6. A slight increment of ζ-potential, from -2 to -8 mV, was probably related to the interaction of SalB with the superficial charge and was useful to stabilize the formulation. After freeze-drying, NPs were suspended with PBS at concentration of 20 mg / ml with vortex. The size and the PDI didn't change. The value obtained in term of EE% was too high (ca. 98%), as show in the Table 6, and the LC resulted ca. 50 %.

2.3.4.1 *In vitro* release study of SalB

The test provided a comprehension of the kinetics of release of SalB loaded in uncoated or coated with Tween 80 PECA NPs, during 8 hours.

To calculate the % of SalB released in the medium at pH 7.4 at each point time the following formula was used:

$$\% \ SalB \ released_t = (mg \ SalB_t \times 100) / mg \ SalB_{tot}$$

where:

- mg $SalB_t$ = mg SalB released for each timepoint *t*
- mg $SalB_{tot}$ = total mg of SalB loaded in NPs (10.8mg)

NPs were loaded with 10.8 mg of SalB. The release profile of the drug-loaded PECA NPs is shown in Figure 19. A typical sustained drug release was found and a biphasic release profile for both PECA NPs was assessed. The initial fast release rate may be due to smaller particle size of NPs which is associated with smaller diffusion path, so drug accessible to the solid/ dissolution medium interface can diffuse easily to the surface. Thereafter, the release rate decreased that reflects the release of drug entrapped in the polymer. In the second phase, the release rate is assumed to be controlled by diffusion of drug across the polymer matrix. These release studies fit with others concerning Rivastigmine NPs successfully developed to treat Alzheimer's disease [9, 10]. In addition, the lower release of PECA-SalB-TW80 NPs was probably due to the presence of Tween 80, which can decrease the release percentage of hydrophilic drugs from NPs.

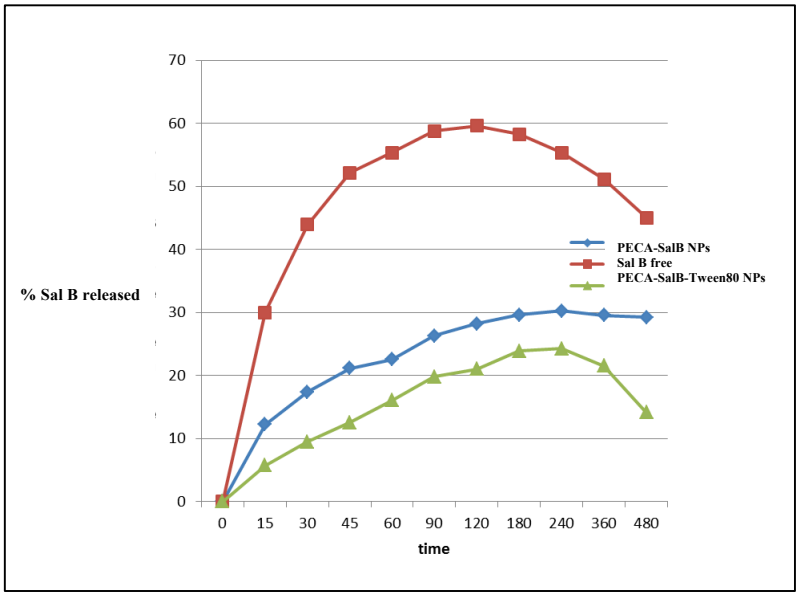

FIGURE 19: IN VITRO RELEASE STUDIES OF SALB FREE AND LOADED IN PECA NPS UNCOATED AND COATED WITH TWEEN 80 AT PH 7.4

2.4 CONCLUSIONS

Nanotechnology is an emerging field that can offer new tools and opportunities to provide more focused and fine-tuned treatments of diseases, enhancing the therapeutic potential of drugs by altering their biodistribution. In the present study we develop and optimize a novel 250 nm fluorescent-labelled PECA NPs to

target the CNS crossing the BBB, using the nonionic surfactant TW80 as coating agent. A simple, relatively inexpensive, and highly reproducible method of preparation, with an ease scaling-up production was performed. The *in vivo* study demonstrated the biocompatibility and biodegradability of PECA-FITC-D-TW80 NPs. Chronic NPs administration in mice didn't induce mortality, nor locomotor activity or cognitive dysfunctions. The decrease of FITC-labelled NPs over time may be related with their clearance made by microglial cells, resident macrophages in the CNS, which, when activated, can migrate to the site of injury, proliferate, and perform phagocytosis. Moreover, the presence of NPs in the brain parenchyma didn't induce astrocytosis. Among the various NPs, biocompatible and biodegradable polymeric NPs are the safest and most versatile vehicles for drug delivery to the brain. Our studies contribute to depict a clearer picture of PECA NPs distribution, time-dependent accumulation, fate and toxicity inside the CNS. According to our findings, PECA-TW80 NPs are useful to deliver a variety of therapeutics in the brain, achieving improved distribution, efficacy and sustained drug delivery to treat brain diseases and disorders. In this investigation, we successfully developed PECA-SalB NPs coated with Tween 80, suitable for parental administration, with high encapsulation efficiency and a sustained release behaviour, which could be valuable for CNS clinical applications. These studies represent the starting point for future investigations to understand the potential application *in vivo* of PECA-SalB NPs in the treatment of neurodegenerative disease.

2.5 Materials and Methods

2.5.1 Materials

The monomer ethyl cyanoacrylate (ECA), dextran 70,000 (D), fluorescein isothiocyanate dextran 70,000 (FITC-D), D-(+)-glucose, TW80 PBS (phosphate buffered saline) were purchased from Sigma-Aldrich, (Milan, Italy). *S. miltiorrhiza* Bge. (Lamiaceae) roots and rhizome were purchased by Shenzhou Medical Center, Rome, Italy. SalB standard CRS was kindly provided by China's National Institute for the Control of Pharmaceutical and Biological Products (NICPBP), ($C_{36}H_{30}O_{16}$; MW 718.6; purity 98.5%).

All other materials and reagents used in the study were Analytical/HPLC grade. Ethanol was analytical reagent grade from Riedel-de Haen (Seelze, Germany). All solvents used were HPLC grade; CH_3CN and MeOH were purchased from Merck

(Darmstadt, Germany). HCOOH (85%) was provided by Carlo Erba (Milan, Italy). Water was purified by a Milli-Q_{plus} system from Millipore (Milford, MA, USA).

2.5.2 *Extraction and isolation of SalB from Salvia Miltiorrhiza Bge.*

The isolation was carried out as previously reported [12]. Briefly, powdered dried roots of *S. miltiorrhiza* Bge. were extracted with H_2O:EtOH (4:1) and partitioned with *n*-hexane and dichloromethane, acidified to pH=2 with HCOOH, and partitioned with ethyl acetate. The solvent soluble fraction was dried and dissolved in 20% EtOH. Then the solution was subjected to size-exclusion chromatography over Sephadex LH-20 using hydroalcoholic mixtures of decreasing polarity (EtOH:H_2O 20:80, 40:60, 60:40, 80:20) and MeOH 100%. Pure SalB (829.7 mg) was obtained after liquid-liquid extraction of the acidified fractions.

2.5.3 *Analytical HPLC-DAD analysis of SalB*

The HPLC system consists of HP 1100 L instrument with Diode Array Detector and managed by HP900 workstation (Agilent Technologies, Palo Alto, CA, USA). The analytical method was previously developed and validated in our group, as previously reported [12]. For the quantification of SalB, internal standard method was applied. The HPLC-DAD method consented to monitor the fractionations and to evaluate the purity of SalB, to calculate the EE and LC of SalB into NPs and the amount of compound released from the formulations during the time. For the calibration curve, SalB reference standard (CRS, purity 98%) was dissolved in MEOH in the range from 0.37 ng to 1.11 µg; the linearity was expressed as $R^2 = 0.999$. The purity was 88.2%.

2.5.4 *Production and Coating of PECA NPs*

PECA NPs were prepared by emulsion polymerization. Briefly, 100 µl of the monomer ECA were added drop by drop under magnetic stirring (500 rpm) to 10 ml of acidic polymerization medium (0.1 N HCl) containing 100 mg of dextran 70,000. The monomer ECA is a clear liquid, which undergoes polymerization in contact with water. The mixture was stirred magnetically for 4 h to facilitate NPs formation. The resulting suspension was neutralized with 0.1 N sodium hydroxide solution and filtered through a sintered glass filter (pore size 10 µm) to remove agglomerates. Anhydrous glucose (0.1% w/v) was added as cryoprotector to improve redispersibility of the NPs after lyophilisation. The NPs

suspension was then lyophilized using a freeze-drier overnight. Fluorescent NPs were prepared as described above, using 100 mg FITC-D instead of un-substituted dextran 70,000. After lyophilisation, NPs dimensional analysis was optimised by applying 20 min of ultrasonication probe (cycles of 5 min, amplitude 60%). PECA NPs were resuspended in PBS at a concentration of 20 mg/ml under constant stirring for 1 hour. Then, Tween 80 was added to a final concentration of 1%, the mixture was incubated for 30 min at 500 rpm and finally lyophilized.

PECA-SalB NPs were developed dissolving SalB (drug:monomer ratio 2:1) in the 0.1 N HCl/dextran 70,000 solution, before ECA polymerization. The process yield of PECA NPs was determined as the weight percentage of the final product after drying, with respect to the initial total amount of polymer and other materials used for the preparation.

2.5.5 *Characterization of PECA NPs in terms of particle size, polydispersity index and Z- potential*

Particle size of the developed NPs was measured by a Dynamic Light Scattering (DLS), Zetasizer Nano series ZS90 (Malvern Instruments, Malvern, UK) equipped with a JDS Uniphase 22 mW He– Ne laser operating at 632.8 nm, an optical fibre-based detector, a digital LV/LSE-5003 correlator and a temperature controller (Julabo water-bath) set at 25°C. Time correlation functions were analysed to obtain the hydrodynamic diameter of the particles (Zh) and the particle size distribution using the ALV-60X0 software V.3.X provided by Malvern. Autocorrelation functions were analysed by Distribution, fitting a multiple exponential to the correlation function to obtain particle size distributions. In particular, PDI values were calculated for each peak as peak width/mean diameter. Scattering was measured in an optical quality 4 mL borosilicate cell at a 90° angle, diluting the samples 30-folds in PBS.-potentials of the NPs were measured using a Malvern Instruments Zetasizer Nano series ZS90. For all samples, an average of three measurements at stationary level was taken. The temperature was kept constant at 25°C by a Haake temperature controller. The **ζ-**potential was calculated from the electrophoretic mobility, µE, using the Henry correction to Smoluchowski's equation.

2.5.6 *Morphological analysis of PECA NPs*

NPs dispersions were analysed in terms of morphology and mean diameter by transmission electron microscope (TEM, Jeol Jem 1010) and by scanning

electron microscope (SEM, Phenom G2 ProX, Phenom-World, Alfatest, Italy). Ten µL of NPs dispersion diluted 10-times was applied to a carbon film-covered copper grid. Most of the dispersion was blotted from the grid with filter paper to form a thin film specimen, which was stained with a phosphotungstic acid solution 1% w/v in sterile water. The samples were dried for 3 min and then were examined under a JEOL 1010 electron microscope and photographed at an accelerating voltage of 64 kV.

2.5.7 *Purification of PECA-SalB NPs*

NPs were purified from *free drug* by ultracentrifugation for 30, 60 and 90 min at 14000 rpm, after resuspension at the concentration of 20 mg/mL in PBS. The amount of SalB loaded into NPs was calculated using an indirect method, analysing, by HPLC-DAD, the supernatants obtained after the centrifugations.

2.5.8 *Determination of encapsulation efficacy and loading capacity of PECA-SalB NPs*

After freeze-drying, NPs were resuspended in PBS at the concentration of 20 mg/ml, the amount of SalB (*Total Drug*) loaded in 1 ml of NPs (or in 20 mg of NPs) was calculated as follow:

[SalB BL]: [NPs BL]= [SalB AL]: [NPs AL]

where:

- [SalB BL] is the amount of SalB before the lyophilisation
- [NPs BL] is the concentration of NPs before the lyophilisation
- [SalB AL] is the amount of SalB after the lyophilisation (*Total Drug*)
- [NPs AL] is the concentration of NPs after the lyophilisation

The evaluation of EE% and LC% were performed using an indirect method, by detracting the mg total of SalB used in the preparation of NPs (*Total Drug*) to the amount of SalB free (*Free drug*) quantified in the supernatant after purification of the NPs, as already described.
The EE% and the LC% were calculated using the following equations [13]:

$$EE\% = \frac{(Total\ Probe - Free\ Probe)}{Total\ Drug} \cdot 100$$

$$LC\% = \frac{(Total\ Probe - Free\ Probe)}{Weight\ of\ NPs} \cdot 100$$

2.5.9 *In vitro Release Studies*

SalB NPs loaded with (drug:monomer ratio 2:1) were subjected to the *in vitro* release studied, using the dialysis bag method. The suspensions of NP coated and uncoated with 1% of Tween 80, and SalB free were inserted in dialysis bags and placed in PBS at pH 7.4 to mime the *sink-conditions.* The volume of PBS (medium of release) was calculated according to [14]. The bags were placed inside a thermostatic bath at 37 °C ± 0.5 °C, under magnetic stirring at 200 rpm, for8 hours. The release was monitored at 15, 30, 45, 60, 90,120,180, 240, 360 and 480 minutes; aliquots of one millilitre were withdraw in duplicate, replaced with fresh PBS maintained at 37 °C, and analysed by HPLC for the quantification of released drug.

2.5.10 *Evaluation of stability of probe linked to PECA NPs*

The initial amount of fluorescent label present in NPs was determined by hydrolysis in 4N NaOH solution and the fluorophore released was determined using FITC-D for the calibration curve. The HPLC system consisted of a HP 1200 L instrument with a Diode Array Detector and fluorimetric detector and managed by a HP 9000 workstation (Agilent Technologies, Palo Alto, CA, USA). The column was a Lycrosorb C18, (100 mm x 4.6 mm) with a 5 µm particle size (Agilent) maintained at 27 °C. Eluents were H_2O at pH 3.2 by formic acid (A) and acetonitrile (B) at a flow rate of 0,8 ml/min. The gradient condition was: 0–10 min, 87-85% B; 10–23 min, 85–75% B; 23– 28 min 75–5% B; 28–31 min, 5–87% B, with a 10 min equilibration time. Injected volume of the samples was 10 µl. The UV spectra were recorded between 200 and 600 nm. Chromatographic profile of fluorescein was registered at 240 nm and λ_{ex}=495 nm and λ_{em}=525 nm. For the stability studies, the NPs were incubated in PBS, pH 7.4, for 7 days at room temperature under gentle mixing (100 rpm). After this period, samples were centrifuged at 10.000 rpm for 10 min, and the supernatant (500 µl) was transferred in 4 N NaOH solution (100 µl) for the determination of fluorescent label released [15]. In PECA-FITC-D NPs (λ_{ex}=495 nm and λ_{em}=525 nm.; UV spectrum at 240 nm; FITC-D 186 µg/mg NPs) the amount of probe released was 13.8%±0.08, n=3.

2.5.11 *In vivo Experiments*

2.5.11.1 Animals

Three-month-old, 230-250 grams, Wistar rats (Harlan, Milan, Italy) (n=3/group) and three-month-old, 15-25 grams, C57/B6 mice (Harlan, Milan, Italy)

(n=8/group) were used (male and female were equally divided within treatment groups). Animals were housed in macrolon cages with ad libitum food and water and maintained on a 12-hour (h) light/dark cycle at 23 °C. All experiments were carried out according to the European Community Directive 86/609/EEC for animal experiments and National guidelines for animal care (Permit Number: 152/2014-B). All efforts were made to minimize the number of animals used and their suffering.

2.5.11.2 Brain injections of fluorescent PECA NPs

One-microliter of PECA-FITC-D-TW80 NPs (8 mg/ml) or PBS (control group) was injected into the right NBM of anesthetized (chloral hydrate, 400 mg/kg, ip plus Carprofen, 5 mg/kg, sc) rats, at the following stereotactic coordinates: AP=-0.2; L=-2.8 and H=6.8 from Bregma as previously described [16]. One, three, seven and fourteen days after injection, rats were deeply anesthetized with chloral hydrate (400 mg/kg, ip) and sacrificed by decapitation.

2.5.11.3 Intravenous and intraperitoneal administration of fluorescent PECA NPs

To study the ability of NPs to cross the BBB rats were acutely dosed with PECA-FITC-D-TW80 NPs (100 mg/kg) or vehicle (0.9% NaCl) by i.v. injection by the tail vein and also by i.p. injection. Three hours after systemic administration rats were perfused transcardially with saline solution (0.9%) and then with 4% ice-cold paraformaldehyde in 0.1 M PBS, pH 7.2, under deep anaesthesia (chloral hydrate, 400 mg/kg, ip, plus Carprofen, 5 mg/kg, s.c.).

2.5.11.4 Animal Tissue Processing

After sacrifice, brains were quickly extracted and fixed in phosphate-buffered 4% paraformaldehyde (pH 7.4) for 48 hs (after decapitation) or 4 hs (after transcardial perfusion) at 4 °C. Subsequently brains were rinsed with PBS, dehydrated using an automated machine, and embedded in paraffin. Coronal sections (5.0 μm) were cut using a microtome and mounted on slides.

2.5.11.5 Immunohistochemistry

Sections were subjected to antigen retrieval by microwave incubation in 10 mM Na-citrate buffer, pH 6.0, and immunostained as previously described [17]. Polyclonal ionized calcium binding adaptor molecule 1 (Iba1) (1:250 dilution, Wako, Osaka, Japan), monoclonal anti-RT1B (anti-OX6, 1:100 dilution, BD Biosciences Pharmingen, Franklin Lakes, New Jersey) antibodies (Abs) were used

to detect total (resting and activated) and activated microglia, respectively and anti glial fibrillary acid protein (GFAP) (1:1000 dilution, Dako Cytomation, Glostrup Denmark) Ab was used to visualize astrocytes. Monoclonal anti-neuronal nuclei (NeuN) Ab (1:100 dilution, Millipore, Billerica, USA) was used to detect neurons, polyclonal anti-choline acetyltransferase (ChAT) Ab (1:200 dilution, Millipore, Billerica, USA) was used to stain cholinergic neurons and monoclonal anti CD34 Class II Ab (1:200 dilution, Dako Cytomation, Glostrup Denmark) was used for the identification of vessels. Co-localization experiments were performed as previously reported [18], sections were coverslipped using ProLong (Lyfe Technologies, New York, USA) mounting medium with or without DAPI for nuclear staining. An Olympus BX63 microscope coupled to CellSense Dimension Software (Olympus, Milan, Italy) was used to acquire representative images.

2.5.11.6 PECA NPs toxicity and behavioural studies in C57/B6 mice

To reduce the amount of NPs to be employed, the *in vivo* toxicity was investigated in C57/B6 mice daily dosed with either PECA-FITC-D -TW80 NPs solution (200 mg/kg, ip) or vehicle for 2 weeks. The animals were weighed once a day and the body weight recorded. At the end of the sub-chronic treatment, C57/B6 mice treated with PECA-FITC-D-TW80 NPs or vehicle were behaviourally tested to evaluate their locomotor, explorative and cognitive functions by a widely used non spatial memory task: the novel object recognition test (ORT) as described in [19]. Briefly, we used a white box (60X50X25 cm) with a grid floor covered by white filter paper. A 75-Watt lamp was suspended 50 cm above the box. The day before testing, mice were allowed to explore the box for 5 min. A session of two trials (T1 and T2) at 60 min interval was given on the test day. In T1, the time spent by each mouse exploring two identical 8.0 cm side grey cubes presented for 10 min in two opposite corners of the box was recorded. During T2, one of the cubes was replaced by a 8.0 cm side grey cylinder, and the mice were left in the box for 5 min. The time spent for the exploration of the familiar (F) and the new (N) object was recorded and a discrimination score (D = N/N+F) was calculated. A discrimination score above 0.5 indicates the ability of mice to discriminate between the familiar and novel objects while a score below or equal to 0.5, reflecting a novel object exploration time less or equal to the half of the total [20, 21] time spent between the two objects, indicates memory impairment in this task. Mouse behaviour was recorded by a video-tracking/computer-digitizing system (HVS Image, UK) and the path length

crossed during T1 exploration was recorded (HVS Image, Hampton, UK) and analysed as a measure of locomotor activity.

2.5.11.7 Statistical analysis

Differences in the body weight between vehicle-and PECA-FITC-D-TW80 NPs treated mice were analyzed by two-way ANOVA plus Bonferroni's post comparison test. ORT data were evaluated by Student's t test (two-tailed probability). All calculations were performed using GraphPad Prism version 5.0 for Windows, with statistical significance established at $P<0.05$. Data were expressed as mean ± standard error of the mean (S.E.M).

2.6 REFERENCES

[1] Bonaccini L, Karioti A, Bergonzi MC, Bilia AR. Effects of Salvia miltiorrhiza on CNS Neuronal Injury and Degeneration: A Plausible Complementary Role of Tanshinones and Depsides. Planta Med 2015; 81:1003-1016.

[2] Barbu E, Molnar E, Tsibouklis J, Gorecki DC. The potential for nanoparticle-based drug delivery to the brain: overcoming the blood-brain barrier. Expert Opin Drug Deliv 2009; 6:553-565.

[3] Wohlfart S, Gelperina S, Kreuter J. Transport of drugs across the blood-brain barrier by nanoparticles. J Control Release 2012; 161:264-273.

[4] Kreuter J, Ramge P, Petrov V, Hamm S, Gelperina SE, Engelhardt B, Alyautdin R, von Briesen H,Begley DJ. Direct evidence that polysorbate-80-coated poly(butylcyanoacrylate) nanoparticles deliver drugs to the CNS via specific mechanisms requiring prior binding of drug to the nanoparticles. Pharm Res 2003; 20:409-416.

[5] Wohlfart S, Khalansky AS, Gelperina S, Begley D, Kreuter J. Kinetics of transport of doxorubicin bound to nanoparticles across the blood-brain barrier. J Control Release 2011; 154:103-107.

[6] Tian XH, Lin XN, Wei F, Feng W, Huang ZC, Wang P, Ren L, Diao Y. Enhanced brain targeting of temozolomide in polysorbate-80 coated polybutylcyanoacrylate nanoparticles. Int J Nanomedicine 2011; 6:445-452.

[7] Kolter M, Ott M, Hauer C, Reimold I, Fricker G. Nanotoxicity of poly(n-butylcyano-acrylate) nanoparticles at the blood–brain barrier, in human whole blood and in vivo. J Control Rel 2015; 197:165-179.

[8] Alexis F, Pridgen E, Molnar LK, Farokhzad OC. Factors affecting the clearance and biodistribution of polymeric nanoparticles. Mol Pharm 2008 ; 5: 505-515.

[9] Shrinidh AJ, Sandip SC, Krutika KS. Rivastigmine-loaded PLGA and PBCA nanoparticles: Preparation, optimization, characterization, in vitro and

pharmacodynamic studies. European Journal of Pharmaceutics and Biopharmaceutics 2010; 76: 189–199.

[10] Wilson B, Samanta MK, Santhi K, Kumar KPS, Paramakrishnan N, Suresh B. Poly(*n*-butylcyanoacrylate) nanoparticles coated with polysorbate 80 for the targeted delivery of rivastigmine into the brain to treat Alzheimer's disease. Brain Research 2008; 1200: 159-168.

[12] Isacchi B, Fabbri V, Galeotti N, Bergonzi MC, Karioti A, Ghelardini C, Vannucchi MG, Bilia AR. Salvianolic acid B and its liposomal formulations: Anti-hyperalgesic activityin the treatment of neuropathic pain. European Journal of Pharmaceutical Sciences 2011; 44: 552–558.

[13] Gulyaev AE, Gelperina SE, Skidan IN, Antropov AS, Kivman GY, Kreuter J. Significant transport of doxorubicin into the brain with polysorbate 80-coated nanoparticles. Pharmaceutical research 1999;16: 1564-1569.

[14] Nimesh S, Manchanda R, Kumar R, Saxena A, Chaudhary A, Yadav V, Mozumdar S, Chandra R. Preparation, characterization and in vitro drug release studies of novel polymeric nanoparticles. International Journal of Pharmaceutics 2006; 323: 146-152.

[15] Costantino L, Gandolfi F, Tosi G, Rivasi F, Vandelli MA, Forni F. Peptide-derivatized biodegradable nanoparticles able to cross the blood-brain barrier. J Control Release 2005 ;108:84-96.

[16] Baglioni S, Casamenti F, Bucciantini M, Luheshi LM, Taddei N, Chiti F, Dobson CM, Stefani M. Prefibrillar amyloid aggregates could be generic toxins in higher organisms. J Neurosci 2006 ; 26:8160-8167.

[17] Rosi MC, Luccarini I, Grossi C, Fiorentini A, Spillantini MG, Prisco A, Scali C, Gianfriddo M, Caricasole A, Terstappen GC, Casamenti F Increased Dickkopf-1 expression in transgenic mouse models of neurodegenerative disease. J Neurochem 2010; 112:1539-1551.

[18] Fiorentini A, Rosi MC, Grossi C, Luccarini I, Casamenti F. Lithium improves hippocampal neurogenesis, neuropathology and cognitive functions in APP mutant mice. PLoS One 2010; 5: e14382.

[19] Grossi C, Rigacci S, Ambrosini S, Ed DT, Luccarini I, Traini C, Failli P, Berti A, Casamenti F, Stefani M. The polyphenol oleuropein aglycone protects TgCRND8 mice against Ass plaque pathology. PLoS One 2013; 8:e71702.

[20] Hammond RS, Tull LE, Stackman RW. On the delay-dependent involvement of the hippocampus in object recognition memory. Neurobiol Learn Mem 2004; 82:26-34.

[21] Greco SJ, Bryan KJ, Sarkar S, Zhu X, Smith MA, Ashford JW, Johnston JM, Tezapsidis N, Casadesus G. Leptin reduces pathology and improves memory in a transgenic mouse model of Alzheimer's disease. J Alzheimers Dis G 2010; 19:1155-1167.

CHAPTER 3

ALBUMIN-BASED NANOPARTICLES FOR BRAIN DELIVERY: A COMPARISON OF CHEMICAL *VS* THERMAL PREPARATION METHODS AND *IN VIVO* BEHAVIOUR

This work was carried out in collaboration with Maria Camilla Bergonzi[1], Cristina Grossi[2], Vieri Piazzini[1], Andrea Torracchi[1], Ilaria Luccarini[2], Fiorella Casamenti[2], Anna Rita Bilia[1]

[1] Department of Chemistry, University of Florence, Via Ugo Schiff 6, 50019 Sesto Fiorentino, Florence, Italy

[2] Department of Neuroscience, Psychology, Drug Research and Child Health, Division of Pharmacology and Toxicology, University of Florence, 50139 Florence, Italy.

3.1 ABSTRACT

HSA NPs have gained considerable attention owing to their high loading capacity of various drugs and being well tolerated without any serious side effects. The aim of this work was the investigation of two different methods of cross-linking in order to produce HSA NPs without using unsafe organic solvents, obtaining useful drug delivery systems to cross the BBB. NPs were obtained by coacervation using both chemical (HSAC NPs) and thermal cross-linking (HSAT NPs). NPs were developed and optimised to target brain tissues after intravenous and intraperitoneal administration in healthy rats. Furthermore, their distribution, cellular uptake and fate were investigated *in vivo* after intracerebral injection into the NBM of the basal forebrain of healthy rats. In addition, the toxicity of the developed carriers was estimated by behavioural test. All NPs were characterized by DLS, TEM and HPLC-DAD-FLD analyses. HSAT NPs were superior than HSAC NPs in terms of formulation parameters, while the *in vivo* performance was very similar. Distribution and fate of NPs in the brain were evaluated by fluorescent microscope images. NPs were able to cross the BBB and reach brain tissue and did not induce inflammatory response. Behavioural test demonstrated no locomotor, explorative and cognitive functions impairment induced by NPs in rats.

3.2 INTRODUCTION

BBB restricts the transport from the blood into the brain of many therapeutically important drugs, including anticancer drugs, antibiotics and a wide variety of central nervous system (CNS)-active drugs, especially macromolecules such as neuropeptides and proteins. The limitations imposed by BBB and the non-selective distribution of drugs in the brain have hindered the effective treatment of brain diseases and may result in severe side effects on the healthy tissues of brain. A number of different strategies have been devised to overcome this barrier and nanocarriers have emerged as versatile vectors for the specific delivery of drugs to brain tissues [1,2]. Various macromolecular substances such as synthetic and natural polymers can be used for nanoparticle preparation [3,4]. Among these, HSA is a promising material because it is the most abundant plasma protein, has been shown to be non-toxic, non-immunogenic, biocompatible and biodegradable, it is extremely robust towards pH, temperature and organic solvents. These properties as well as its preferential

uptake in tumour and inflamed tissue, its ready availability, biodegradability and lack of toxicity make it an ideal candidate for drug delivery to brain.

Moreover, HSA NPs have gained considerable attention owing to their high binding capacity of various drugs [5-6]. Albumin nanoparticles are widely used as carriers for delivering drugs to a variety of organs but only a very few studies are concerning *in vivo* brain delivery of albumin NPs without any surface modification. The endogenous transport mechanisms to cross BBB are diverse and include paracellular aqueous pathway, transcellular lipophilic pathway, proteins transport (carriers)-mediated, RMT and AMT. The AMT is a nonspecific process, which originated from the observation that policationic proteins, as protamine, can bind not only to the endothelial surface, but they can also penetrate the BBB. The AMT is triggered by electrostatic interactions between the positively charged parts of protein and the negatively charged brain membrane [7]. Nevertheless, almost all *in vivo* studies concerning HSA NPs for CNS delivery are overcoated nanoparticles with certain surfactants that adsorb specific apolipoproteins from the blood after intravenous injection or with the covalent attachment of such apolipoproteins, or containing transferrin or anti-transferrin-receptor monoclonal antibodies covalently coupled. These surface modifications or decorations enable the interaction of HAS NP with the respective receptors on the brain capillary endothelial cells to cross the BBB [3].

The aim of this work was the development and optimisation of HSA NPs as drug delivery systems to cross BBB using two different cross-linking methods, the most studied chemical cross-linking and the lesser-known thermal cross-linking. All the preparation steps including extent of the polymerization process, concentration of reagents, time and temperature of cross-linking, NPs purification methods, type and concentration of cryoprotectants were optimised to obtain suitable NPs for the parental administration. Additionally, NPs were loaded with fluorescein sodium salt (NAF) as a florescent probe to evaluated their *in vivo* performance. All NPs were characterized in terms of dimension, polydispersity and ζ-potential by DLS; their morphology was evaluated by TEM while EE%, loading capacity LC% and the stability of probe were measured by HPLC-DAD-FLD.

HSA NPs distribution, cellular uptake and fate were studied in healthy rats by fluorescent microscope images, after NPs intracerebral injection into the NBM of the basal forebrain. The occurrence of a potential general toxicity for the animals, as well as NPs-induced inflammatory response in terms of glia reaction,

were deeply investigated. In addition, the ability of NPs to cross the BBB was evaluated after intravenous and intraperitoneal administration in healthy rats and the potential toxicity of the carriers was estimated by behavioural test in healthy mice.

3.3 MATERIALS AND METHODS

3.3.1 MATERIALS

HSA, glutaraldehyde 25%, sodium chloride (NaCl), D-(+)-glucose anhydrous, sucrose, NAF, PBS pH 7.4 were purchased from Sigma-Aldrich (Milan, Italy). All solvents used were HPLC grade: CH_3CN and MeOH were purchased from Merck (Darmstadt, Germany). EtOH was analytical reagent grade from Riedel-de Haen (Seelze, Germany). HCOOH (85%) was provided by Carlo Erba (Milan, Italy). Phosphotungstic acid was obtained by Società Italiana Chimici (Rome, Italy). Water was purified by a Milli-Q_{plus} system from Millipore (Milford, MA, USA).

3.3.2 HSAC NPS PREPARATION

Empty HSAC NPs were prepared modifying a previously proposed desolvation technique[7-9]. HSA at a concentration of 20 mg/ml (2% w/v) was dissolved in 3 ml of 10 mM NaCl solution under magnetic stirring (500 rpm, 30 minutes). NPs were obtained by continuous addition of 6 ml of the desolvating agent ethanol to HSA solution, at constant rate of 1 ml/min (ratio NaCl-ethanol 1:2 v/v) under stirring (500 rpm) at room temperature. After the desolvation process, 60 μl of a solution of 0.5 w/v of glutaraldehyde in ethanol (5 μg/mg protein) were added to induce particle crosslinking. The crosslinking process was performed under magnetic stirring for 2 hours at room temperature. The resulting NPs were purified by centrifugation (4500 rpm, 30 min x 3). Then, NPs were re-suspended in 3 ml of 10 mM NaCl solution containing 3% w/v sucrose as cryoprotective agent and freeze-dried.

3.3.3 FLUORESCENT HSAC NPS PREPARATION

HSAC NAF NPs were prepared using the same method optimized for non-fluorescent NPs, using NAF as fluorescent probe (λ_{ex}=460 nm; λ_{em}=515 nm). NAF (10 mg/ml, 1% w/v) was incubated with 3 ml of an HSA solution (20 mg/ml, 2% w/v) under magnetic stirring (500 rpm) for 2 h. NPs were obtained by the continuous addition of the ethanol at constant rate of 1 ml/min (ratio NaCl-ethanol 1:2 v/v) under stirring (500 rpm) at room temperature. Glutaraldehyde

(5 μg/mg protein) was added under magnetic stirring at room temperature for 2 h to induce particle crosslinking. Fluorescent HSA NPs were purified by centrifugation (4500 rpm, 30 min x 3 times). Then, NPs were re-suspended and dispersed in the original volume of 10 mM NaCl solution containing 3% w/v sucrose as cryoprotective agent, then the samples were lyophilized.

3.3.4 HSAT NPS PREPARATION

Empty HSAT NPs were prepared modifying and optimizing a thermal cross-linking method proposed by [10]. Briefly, HSA at a concentration of 5 μg/ml (0.5% w/v) was dissolved in 20 ml of 10 mM NaCl solution under magnetic stirring (700 rpm, 30 min). Polymerization process was performed by continuous addition of 20 ml of the ethanol at a rate of 1 ml/min (ratio NaCl-ethanol 1:1 v/v) under stirring (500 rpm) at room temperature. Magnetic stirring (500 rpm) was continued at 90°C for 1 hour to yield an aqueous suspension of thermally cross-linked HSA NPs. They were allowed to cool at room temperature and then were purified by centrifugation (4500 rpm, 30 min x 3 times). Pellets were suspended in the 10 ml of 10 mM NaCl solution containing 2% w/v anhydrous D-glucose and after freeze-dried.

3.3.5 FLUORESCENT HSAT NPS PREPARATION

Fluorescent HSAT NPs were prepared by the same method optimized for non-fluorescent NPs. The probe (NAF) (5 mg/ml, 0.5% w/v) was incubated with 3 ml of HSA solution (5 mg/ml, 0.5% w/v) for 2 h under magnetic stirring at 500 rpm. Ethanol was added at constant rate of 1 ml/min (ratio NaCl-ethanol 1:1 v/v) under magnetic stirring (500 rpm) at room temperature. The stirring was continued at 90°C for 1 h to obtained an aqueous suspension of thermally cross-linked HSA NPs. NPs were allowed to cool at room temperature, then were centrifuged (4500 rpm, 30 min x 3 times). Pellets were dispersed in the original volume of 10 mM NaCl solution containing 2% w/v anhydrous D-glucose as cryoprotective agent, then were freeze-dried.

3.3.6 NPS YIELD

The yield of the process of preparation for both NPs was expressed as the weight percentage of the final product after drying, with respect to the initial total amount of protein and other materials used for the preparation.

3.3.7 Characterization of NPs: Size, Polydispersity Index and Zeta Potential

Particle size of the developed NPs was measured by a DLS, Zetasizer Nano series ZS90 (Malvern Instruments, Malvern, UK) equipped with a JDS Uniphase 22 mW He-Ne laser operating at 632.8 mm, an optical fiber-based detector, a digital LV/LSE-5003 correlator and a temperature controller (Julabo water-bath) set at 25°C. Time correlation functions were analysed to obtain the Z_h and the PDI using the ALV-60X0 software V.3.X provided by Malvern. Autocorrelation functions were analysed by the Cumulants method, fitting a single exponential to the correlation function to obtain particle size distribution. Scattering was measured in an optical quality 4 ml borosilicate cell at a 90° angle, diluting the samples in 10 nM NaCl solution. ζ-potentials of the NPs were measured using a Malvern Instruments Zetasizer Nano series ZS90. For all samples, an average of three measurements at stationary level was taken. The temperature was kept constant at 25°C by a Haake temperature controller. The ζ-potential was calculated from the electrophoretic mobility, μ_E, using the Henry correction to Smoluchowski's equation.

3.3.8 Morphological characterization

NPs were analysed in terms of morphology, polydispersity, shape and dimensions by TEM. NPs dispersion diluted 10-times was applied to a carbon film-covered copper grid. Most of the dispersion was blotted from the grid with filter paper to form a thin film specimen, which was stained with a phosphotungstic acid solution 1% w/v in sterile water. The samples were dried for 3 min and then were examined under a JEOL 1010 electron microscope and photographed at an accelerating voltage of 64 kV.

3.3.9 Purification of NPs

NPs were purified from free probe by ultracentrifugation for 75 min at 18000 rpm, 4°C.The amount of NAF loaded into NPs was calculated using an indirect method.

3.3.10 HPLC-DAD-FLD analyses

The HPLC system consisted of a HP 1200 L instrument with a Diode Array Detector and fluorimetric detector and managed by a HP 9000 workstation (Agilent Technologies, Palo Alto, CA, USA). The column was a LiChrosorb C18, (100 mm x 4.6 mm) with a 5μm particle size (Agilent) maintained at 27 °C.

Eluents were H_2O at pH 3.2 by formic acid (B) and acetonitrile (A) at a flow rate of 0.8 ml/min. The gradient condition was: 0-10 min, 87-85% B; 10-23 min, 85-75% B; 23-28 min 75-5% B; 28-31 min, 5-87% B, with a 10 min equilibration time. Injected volume of the samples was 10 or 20 μl. Chromatographic profile of NAF was registered at λ_{ex} = 460 nm and λ_{em} = 515 nm.

3.3.10.1 Quantification of NAF Fluorescein sodium salt HPLC analysis

After freeze-drying, HSA fluorescent NPs were resuspended in 10 mM NaCl at the concentration of 20 mg/ml. The amount of NAF (*Total Probe*) loaded in 1 ml of NPs (or in 20 mg of NPs) was calculated as follow [11]:

$$[\mathbf{NAF}]_{\mathbf{bl}}:[\mathbf{NPs}]_{\mathbf{bl}} = [\mathbf{NAF}]_{\mathbf{sl}}:[\mathbf{NPs}]_{\mathbf{sl}}$$

where:

- $[\mathbf{NAF}]_{\mathbf{bl}}$concentration of NAF before freeze-drying
- $[\mathbf{NPs}]_{\mathbf{bl}}$ concentration of NPs before freeze-drying
- $[\mathbf{NAF}]_{\mathbf{sl}}$concentration of NAF subsequent freeze-drying (*Total Probe*)
- $[\mathbf{NPs}]_{\mathbf{sl}}$concentration of NPs subsequent freeze-drying

Total Probe in the HSAC is 2.63 mg in 1 ml of NPs or 2.63 mg in 20 mg of NPs.
Total Probe in the HSAT is 2.47 mg in 1 ml of NPs or 2.47 mg in 20 mg of NPs.

The evaluation of EE% and LC% were performed using an indirect method, by detracting the mg total of NAF used in the preparation of NPs (*Total Probe*) to the amount of NAF free (*Free Probe*) quantified in the supernatant after purification of the NPs by ultracentrifugation, as described in the Section 3.3.9. *Free Probe* determined by HPLC/FLD was: 0.0395 ± 0.002 mg in the case of HSAC NPs and 0.0154 ± 0.002 mg in the case of HSAT NPs.
The EE% and the LC% were calculated by using the following equations:

$$EE\% = \frac{(Total\ Probe - Free\ Probe)}{Total\ Drug} \cdot 100$$

$$LC\% = \frac{(Total\ Probe - Free\ Probe)}{Weight\ of\ NPs} \cdot 100$$

3.3.11 NAF STABILITY

The stability of NAF was evaluated with *in vitro* release test. The suspensions of NPs were inserted in a dialysis bag and were placed in a PBS solution at pH 7.4

to mime the *sink-conditions.* The volume of PBS was calculated according to [12]. The bags were placed inside a thermostatic bath at 37 °C ± 0.5 °C, under magnetic stirring at 200 rpm. Test time was set to 3 hours, according to time of the *in vivo* tests. The release was monitored at 10, 20, 30, 60, 120, 180 minutes; aliquots of one millilitre were withdraw in duplicate, replaced with fresh PBS at pH 7.4 maintained at 37 °C ± 0.5 °C, and analysed by HPLC-FLD for the quantification of released fluorescent probe.

3.3.12 IN VIVO EXPERIMENTS

3.3.12.1 Animals

One-month-old, 180-200 g, Wistar rats (Harlan, Milan, Italy) (n=3/group) and three-month-old, 15-25 g, C57/Bl6 mice (Harlan, Milan, Italy) (n=8/group) were used (male and female were equally divided within treatment groups). Animals were housed in macrolon cages with ad libitum food and water and maintained on a 12-h light/dark cycle at 23 °C. All experiments were carried out according to the EC Directive 86/609/EEC for animal experiments and National guidelines for animal care (Permit Number: 152/2014-B). All efforts were made to minimize the number of animals used and their suffering.

3.3.12.2 Brain injections of fluorescent HSAC NPs

One-microliter of HSAC NPs (10 mg/ml) or PBS (control group) was injected into the right NBM of anesthetized (chloral hydrate, 400 mg/kg, intraperitoneally (ip) plus Carprofen, 5 mg/kg, subcutaneously) rats, at the following stereotactic coordinates: AP=-0.2; L=-2.8 and H=6.8 from Bregma [13] as previously described [14].Twenty-four hours, seven and fourteen days after injection, rats were deeply anesthetized with chloral hydrate (400 mg/kg, ip, plus Carprofen, 5 mg/kg, subcutaneously) and sacrificed by decapitation.

3.3.12.3 Systemic administration of fluorescent HSAC NPs and fluorescent HSAT NPs

To study the ability of NPs to cross the BBB rats were acutely dosed with HSAT NPs (100 mg/kg) or vehicle (0.9% NaCl) by intravenous (iv) injection by the tail vein. Three hours after systemic administration rats were perfused transcardially with saline solution (0.9%) and then with 4% ice-cold paraformaldehyde in 0.1 M PBS, pH 7.2, under deep anaesthesia (chloral hydrate, 400 mg/kg, ip, plus Carprofen, 5 mg/kg, subcutaneously).

3.3.12.4 Animal Tissue Processing

After sacrifice, brains were quickly extracted and fixed in phosphate-buffered 4% paraformaldehyde (pH 7.4) for 48 h (after decapitation) or 4 h (after transcardial perfusion) at 4 °C. Subsequently brains were rinsed with PBS, dehydrated using an automated machine, and embedded in paraffin. Coronal sections (5.0 µm) were cut using a microtome and mounted on slides.

3.3.12.5 Immunohistochemistry

Sections were subjected to antigen retrieval by microwave incubation in 10 mM Na-citrate buffer, pH 6.0, and immunostained. Polyclonal ionized calcium binding adaptor molecule 1 (Iba1) (1:250 dilution, Wako) antibody–(Ab) was used to detect resting and activated microglia and anti glial fibrillary acid protein (GFAP) (1:1000 dilution, Dako Cytomation) Ab was used to visualize astrocytes. Polyclonal anti-choline acetyltransferase (ChAT) Ab (1:200 dilution, Millipore) was used to stain cholinergic neurons and monoclonal anti CD34 Class II Ab (1:200 dilution, Dako Cytomation) was used for the identification of vessels. Co-localization experiments were performed. Sections were coverslipped using ProLong (Lyfe Technologies, New York, USA) mounting medium with or without DAPI for nuclear staining. An Olympus BX63 microscope coupled to *CellSense Dimension* Software (Olympus, MI, Italy) was used to acquire representative images.

3.3.12.6 *In vivo* HSAC NPs toxicity and behavioural studies in C57/Bl6 mice

To reduce the amount of NPs to be employed, the *in vivo* toxicity was investigated in C57/Bl6 mice daily dosed with either HSAC NPs solution (100 mg/kg, ip) or vehicle for 2 weeks. The animals were weighed once a day and the body weight recorded. At the end of the sub-chronic treatment, C57/Bl6 mice treated with HSAC NPs or vehicle were behaviourally tested to evaluate their locomotor, explorative and cognitive functions by a widely used non spatial memory task: the novel ORT. Briefly, we used a white box (60X50X25 cm) with a grid floor covered by white filter paper. A 75-Watt lamp was suspended 50 cm above the box. The day before testing, mice were allowed to explore the box for 5 min. A session of two trials (T1 and T2) at 60 min interval was given on the test day. In T1, the time spent by each mouse exploring two identical 8.0 cm side grey cubes presented for 10 min in two opposite corners of the box was recorded. During T2, one of the cubes was replaced by a 8.0 cm side grey

cylinder, and the mice were left in the box for 5 min. The time spent for the exploration of the familiar (F) and the new (N) object was recorded and a discrimination score (D=N/N+F) was calculated. A discrimination score above 0.5 indicates the ability of mice to discriminate between the familiar and novel objects while a score below or equal to 0.5, reflecting a novel object exploration time less or equal to the half of the total time spent between the two objects, indicates memory impairment in this task [15,16]. Mouse behaviour was recorded by a video-tracking/computer-digitizing system (HVS Image, UK) and the path length crossed during T1 exploration was recorded (HVS Image, Hampton, UK) and analysed as a measure of locomotor activity.

3.3.12.7 Statistical analysis

Differences in the body weight between vehicle and HSAC NPs treated mice were analysed by two-way ANOVA plus Bonferroni's post comparison test. ORT data were evaluated by Student's t test (two-tailed probability). All calculations were performed using GraphPad Prism version 5.0 for Windows, with statistical significance established at $P < 0.05$. Data were expressed as mean ± standard error of the mean (S.E.M).

3.4 Results and Discussion

3.4.1 Preparation of HSA NPs with chemical cross-linking method (HSAC)

HSAC NPs were prepared with chemical cross-linking method by using glutaraldehyde as described in section 3.3.2. The pre-formulative study was focused on the optimization of different parameters in order to improve technological characteristics of NPs. The following steps were investigated and optimised: polymerization process parameters (time, temperature), concentration of reagents (principally glutaraldehyde), purification process of NPs, method for the optimization of size and homogeneity of the sample (ultrasonic bath or ultrasonication probe), choice of the type and concentration of cryoprotectant (2% w/v of mannitol or 3% w/v of sucrose). Accordingly, best results were obtained after 2 h of polymerization at room temperature with a glutaraldehyde concentration of 5 μg/mg HSA and no sonication or ultrasonication process were further used to optimize the sizes. Purification process was performed by centrifugation with three cycles of 10 minutes at 4500 rpm.

Table 8 shows the final characterization of developed HSAC NPs. Results in terms of size and homogeneity are reproducible and derived from the acceptable autocorrelation curves, dimensions are suitable for systemic administration. A dilution factor (DF) between 5 and 30 was applied in the DLS analysis.

TABLE 8: PHYSICAL CHARACTERIZATION OF HSAC AND HSAT NPS (DATA ARE MEAN VALUE ±SD, N = 3).

NPs	Size (nm)	PDI	ζ -Potential (mV)	Yield (%)
HSAC	151.67±1.53	0.28±0.01	-15.7±0.20	89.60±3.60
HSAT	143.80±0.56	0.23±0.02	-11.80±4.09	81.40±0.41

The extension of the polymerization time from 3 to 24 h does not affected PDI value, but a significant increase of size was observed (from 400 to 500 nm, for each time, respectively).

In the next step, the concentration of the cross-linking agent was evaluated. In particular, a lower amount of cross-linking agent with respect to that used routinely in the literature was tested, also to reduce the employment of chemicals. The methods reported in the literature employ 100 μl of solutions of glutaraldehyde to 8% or 4% per ml of the HSA solution (concentration 100 mg/ml or 5 mg/ml, respectively) [1,4,17-19]. In our study, the optimized formulation was obtained with 60 μl of 0.5% of glutaraldehyde solution per ml of the HSA solution (concentration 20 mg/ml). These experimental conditions (corresponding to 5 μg of glutaraldehyde per mg HAS) produced sizes of about 150 nm with a PDI=0.28. NPs show mean diameter of 250 nm and PDI > 0.3 with an amount still lower of crosslinking agent (1.56 μg/mg HAS) and using a single cycle of centrifugation for 10 minutes at 4500 rpm. The increase of polymerization time up to 24 h produced larger particles (approximately 330 nm and PDI=0.1). The samples obtained with ultrasonication bath and probe sonication resulted highly polydispersed because it modifies the sample. Table 9 reports the results obtained with cycles of 1 or 2 minutes of ultrasonication probe (amplitude max 50%). The samples without sonication or at most only one cycle of 2 min resulted the best in terms of size, but they were not homogenous. Ultrasonication bath (8 cycles of 15 minutes) reduced diameter up to about 190 nm, with PD=0.34.

TABLE 9: SIZE AND PDI OF HSAC NPS BY USING 1 AND 2 MINUTE'S CYCLES OF ULTRASONICATION PROBE
(DATA ARE MEAN VALUE ±SD, N = 3)

Number of cycles of 2 min	SIZE (nm)	PDI	Number of cycles of 1 min	SIZE (nm)	PDI
0	250±2.34	0.30±0.02	0	250±2.34	0.30±0.02
1	175.50±42.71	0.34±0.06	1	374.70±21.66	0.43±0.03
2	377.87±20.19	0.41±0.08	2	346.13±54.05	0.53±0.11
3	449.70±98.71	0.34±0.14	3	200.60±92.91	0.66±0.38
4	594.30±80.57	0.30±0.23	4	386.63±205.94	0.39±0.06
5	535.77±129.55	0.47±0.21	5	401.23±45.88	0.34±0.04

The purification of NPs was optimised by centrifugation. Different intervals of centrifugation were tested (1 cycle of 10 minutes at 4500 rpm or 3 cycles of 10 minutes at 4500 rpm). One cycle resulted not sufficient to reduce PDI of NPs to a value less than 0.3. Finally, type and concentration of cryoprotectors were considered in order to obtain a stable and easy to re-suspend lyophilised sample. Mannitol (2% w/v) and sucrose (3% w/v) were tested. Sucrose had a protective effect preventing NPs aggregation and NPs were easely re-suspended: lyophilisation process didn't affect the size and the PDI of the sample. In the case of addition of 2% of mannitol the NPs mean diameter was 350 nm and PDI was 0.3.

In order to test NPs *in vivo,* they were loaded with NAF at two different gravimetric ratio, namely 1:1 and 2:1 HSA:NAF (HSAC NAF NPs). NAF shows a very high aqueous solubility (500 g/l at 20 °C) and it does not possess the characteristics to cross the BBB. The probe was added to the solution of HSA in NaCl before polymerization, and left 2 hours under magnetic stirring at 500 rpm. HSA:NAF 2:1 given the greatest reproducibility, with smaller particles and more homogeneous, as reported in the Table 3. These particles showed an EE% of 98.50 ± 0.05 and a LC% value of 13.50 ± 0.07. For DLS analysis, a DF as 20 has been applied. The size was optimized by 2 cycles of 5 minutes of ultrasonication probe, more cycles contribute to the loss of stability of the system. The mean diameter of fluorescent NPs increases marginally in comparison with the diameter of the empty NPs, instead there are not changes regarding the homogeneity of the system, as reported in Table 10. It is also notable that ζ-potential increases in the absolute value. The values obtained were reproducible in terms of size and homogeneity and suitable for systemic administration.

TEM analyses confirmed the results obtained by DLS analysis: NPs showed spherical shape, with a regular and narrow size distribution (Figure 20).

TABLE 10: TECHNOLOGICAL CHARACTERIZATION OF HSAC NAF NPS (DATA ARE MEAN VALUE ±SD, N = 3)

HSA:NAF	Size (nm)	PDI	ζ -Potential (mV)	Yield (%)
1:1	268.33±16.15	0.30±0.01	-17.40±0.50	80.40±3.00
2:1	247.10±17.11	0.29±0.01	-18.20±0.40	79.00±5.00

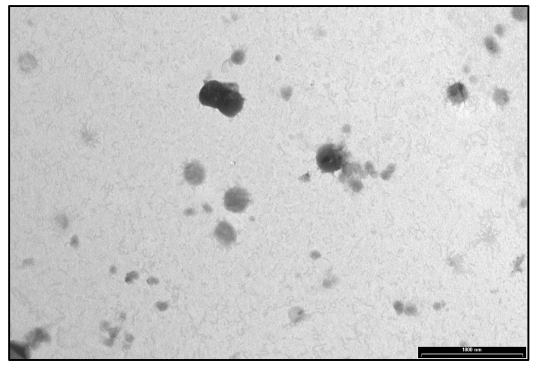

FIGURE 20: TEM MICROGRAPH OF HSAC-NAF NPS

3.4.2 PREPARATION OF HSA NPS WITH THERMAL CROSS-LINKING METHOD (HSAT)

In this work, thermal cross-linking was also investigated in order to find a suitable synthetic approach with the criteria of green chemistry and to minimize the use of unsafe substances. In our study, the optimization of different preparation parameters were investigated: polymerization process (time and temperature), purification method (solvent evaporation or centrifugation at different times), process of resuspension of the pellets (type of the dispersing medium and its volume), method of optimization of size and homogeneity (ultrasonication bath or probe), choice of the type of cryoprotector (2% w/v of mannitol or 2% w/v of anhydrous glucose). The final optimised method resulted to be: polymerization performed for 1h at 90 °C; purification process of 3 cycles of 30 minutes of centrifugation at 4500 rpm; medium of resuspension was 10 ml

of 10 mM NaCl solution; concentration of cryoprotectant was 2% of D-anhydrous glucose.

Table 8 shows the complete characterization of developed and optimised HSAT NPs: the results in terms of size and homogeneity are reproducible and derived from the acceptable autocorrelation curves. For the analysis, a DF between 0 and 20 was applied. NPs have acceptable narrow size distribution, with PDI around 0.2. The mean diameter of HSAT NPs resulted suitable for the *in vivo* systemic administration, was less than 150 nm, and the process yields of NPs was ≈80%.

The first reaction of polycondensation was conducted at 75 °C for 1h. In this case, size and PDI decrease to 192.9±1.10 nm and PDI 0.23±0.02.

The influence of temperature was considered. In particular, the polymerization at 90°C for 30 minutes or 60 minutes was tested. The NPs obtained with 60 minutes of polymerization are the smallest and homogeneous (size 143.8±0.60 nm; PDI 0.23±0.02) with respect to 30 min process (size 187.2±3.90 nm; PDI 0.32±0.01). Also in this preparative process the size reduction with sonication or ultrasonication is not necessary because small and monodispersed particles are obtained and the process results to be reproducible (data are mean value ±SD, n = 3).

The evaporation of the ethanol under vacuum at 30 °C was also studied as a simple and easy to perform purification method. This method involves serious problems in terms of stability, compromising the yield of NPs and producing risk of contamination. DLS analysis confirmed this hypothesis, by obtaining mean diameter around 350 nm with PDI=0.45. As centrifugation conditions, 3 cycles of 15 minutes at 4500 rpm and 3 cycles of 30 minutes at 4500 rpm were tested. The last method resulted the most efficient.

The process of resuspension of the pellets was considered and optimized in terms of type and volume of dispersing medium. The highest ability of dispersion of pellets requires 10 mM NaCl in equal volume as that used as desolating agent.

NPs were lyophilized overnight using as a cryoprotectant agent. D-mannitol (2% v/v) was tested and the considerable increasing of size was observed (mean diameter around 300 nm with PDI 0.48). D-anhydrous glucose prevents the aggregation of NPs compared to other cryoprotectant agents, with a higher protective effect.

The thermal method resulted to be superior in term of reduction of chemical substances used and time necessary for the NPs preparation: the polymerization time was 1 hour, compared to an hour and a half of chemical method.
After, fluorescent HSAT NPs were prepared by investigating two different gravimetric ratios HSA:NAF (1:1 and 1:2). The ratio HSA:NAF 1:1 gave smaller particles and more homogeneous, as shown in Table 11.These particles had an EE% of 99.40 ± 0.04 and a LC% value of 24.50 ± 0.26. A DF between 10 and 20 has been applied for DLS analysis. The size was reduced by 3 cycles of 5 minutes of ultrasonication probe; more cycles contribute to the loss of stability of the system.

TABLE 11: TECHNOLOGICAL CHARACTERIZATION OF HSAT NAF NPS (DATA ARE MEAN VALUE ±SD, N = 3)

HSA:NAF	Size (nm)	PDI	ζ-Potential (mV)	Yield (%)
1:1	145.60 ± 13.7	0.18 ± 0.04	- 11.7 ± 2.66	72.4 ± 0.34
2:1	286.3 ± 20.8	0.55 ± 0.10	- 10.7 ± 1.70	70.4 ± 0.54

The size of fluorescent NPs increases marginally in comparison with empty NPs, but no changes in homogeneity of the system are reported, proving that the probe does not alter the optimized formulation. It is also notable that ζ-potential increased, indicating greater system stability.
TEM investigation provided details on the morphology: NPs had a sphere-like shape with a regular and narrow size distribution, which was comparable with the dimensional distribution results obtained from DLS analysis (Figure 21).

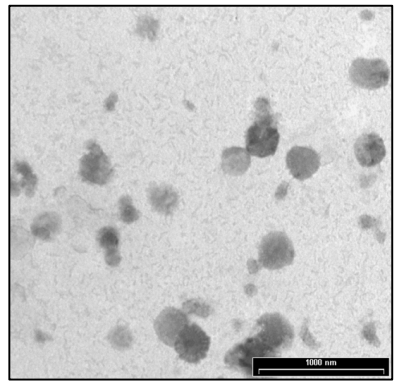

FIGURE 21: TEM MICROGRAPH OF HSAT NPS

The results in terms of size and homogeneity are similar to those obtained with chemical polymerization, but HSAT NPS resulted to be greater in term of formulative parameters, such as saving reagents, reduction of costs and the time necessary for the NPs preparation. NPs were both produced with very good yields (89.6% for HSAC and 81.4% for HSAT). The mean diameter of fluorescent NPs was 247 nm (PDI=0.3) for HSAC NPs and 145 nm for HSAT NPs (PDI=0.2). NPs showed a good EE (≈ 98%) and LC too (≈ 13 % for HSAC NPs and ≈ 24% for HSAT NPs). From the stability study on fluorescent NPs, probe was stably linked to both NPs for 3 hours. Both NPs are suitable for the *in vivo* systemic administration.

3.4.3 In vivo Experiments

3.4.3.1 Fluorescein-labelled HSAC NPs injection into the rat NBM

1µl (10µg/µl) of HSAC NAF NPs was directly injected into the NBM of adult rats to follow the cellular distribution of NPs within the brain, the occurrence of local toxicity as well as NPs-induced inflammatory response in terms of glia reaction. Histochemical analysis revealed, at the injection site (asterisk), a large amount of fluorescent HSAC NPs (green) one and seven days after injection (Figure 22). The day after surgery some NPs were detected close/within the cellular nuclei (DAPI, blue) in the injection site surroundings (Figure 22, arrows, and inset). Seven days after injection some NPs co-localized (yellow) with Iba-1 positive microglial cells (red) (Figure 3), while no HSAC NAF NPs were either found within ChAT-positive neurons (red) (Figure 3) or inside GFAP-positive astrocytes (blue) (Figure 3) in the ipsilateral injected hemisphere. Of relevance, fourteen days after injection, HSAC fluorescent staining was strongly reduced at the injection site (Figure 22, asterisk); NPs uptake mediated by microglial cells could likely result in their removal/phagocytosis from brain tissue.

No NPs were almost detected in the contralateral un-injected hemisphere (data not shown). Immunohistochemical analysis did not reveal any astrocytosis either at the site of injection or in its vicinity, as shown by the resting morphology of GFAP-immunopositive cells (Figure 22, blue) in PBS and NPs injected groups, as exemplified for 7 days after the injection. By contrast, 1 and 7 days after surgery microglial cells (red) increased in number with time at the injection site and in its proximity as compared to PBS-injected controls Figure 23). Overall, these data indicate that *in situ* administration of NPs was well tolerated, didn't induce astrogliosis and favoured microglial cells migration to the injection site for

phagocytosis of NPs, ensuring their elimination from brain tissue and their biocompatibility.

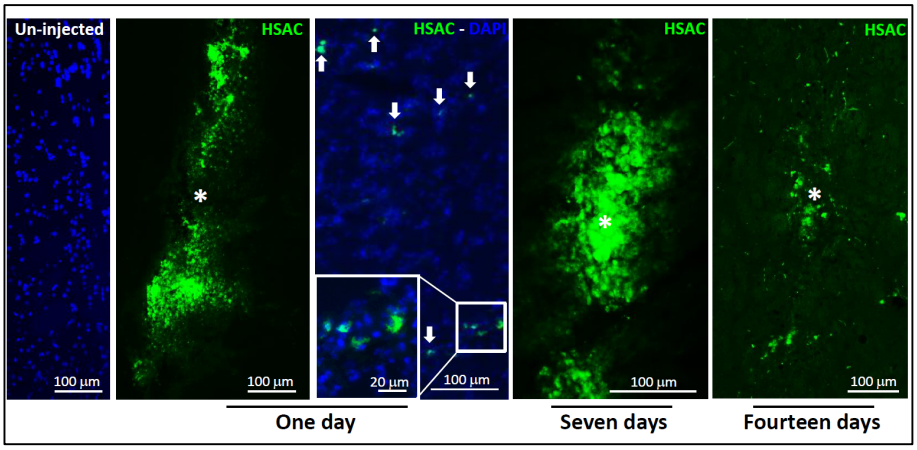

FIGURE 22: INTRACEREBRAL INJECTION OF HSAC NPS INTO THE RAT NUCLEUS BASALIS MAGNOCELULARIS

REPRESENTATIVE PHOTOMICROGRAPHS SHOWING NPS (GREEN) AT THE INJECTION SITE (ASTERISK) ONE, SEVEN AND FOURTEEN DAYS AFTER SURGERY. NPS WERE DETECTED CLOSE/WITHIN THE CELLULAR NUCLEI (DAPI, BLUE) IN THE INJECTION SITE SURROUNDINGS (ARROWS, AND INSET) ONE DAY AFTER SURGERY. NO HSAC NPS LABELLING WAS DETECTED IN THE UN-INJECTED HEMISPHERE. SCALE BARS: 100 µM

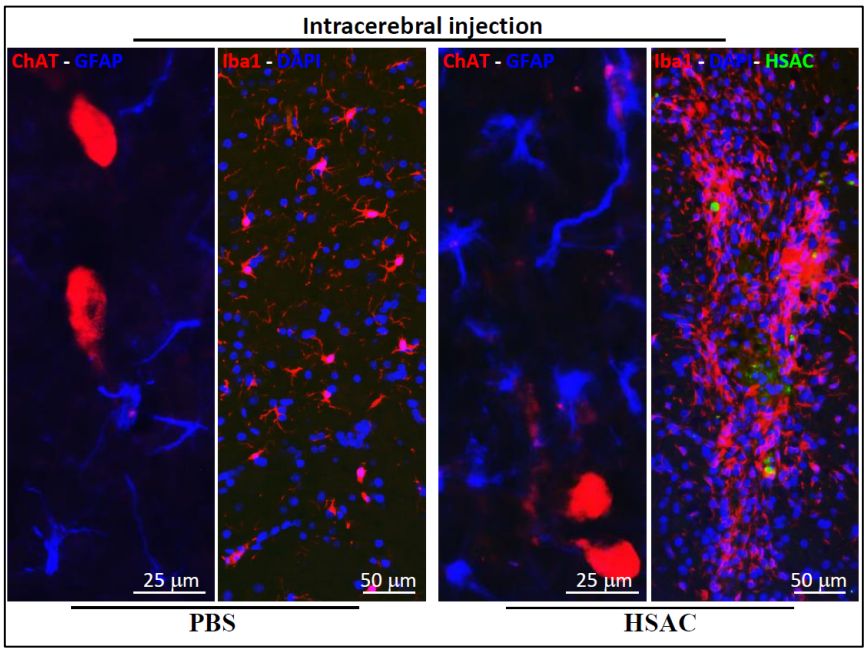

FIGURE 23: INTRACEREBRAL INJECTION OF HSAC NPS
REPRESENTATIVE PHOTOMICROGRAPHS BETWEEN HSAC NPS (GREEN) LABELLING AND GFAP (BLUE), IBA-1 (RED) AND CHAT (RED) ABS PLUS DAPI (BLUE) IN INJECTED RATS SEVEN DAYS AFTER SURGERY. IN THE NBM INJECTED WITH HSAC NPS (GREEN) CLUSTERS OF IBA-1 POSITIVE CELLS (RED) WERE DETECTED, LIKELY INDICATING A PHAGOCYTOSIS BY MICROGLIAL CELLS OF NPS AND NO HSAC NPS WERE DETECTED WITHIN GFAP POSITIVE ASTROCYTES AND CHAT POSITIVE NEURONSGFAP AND IBA 1 IMMUNOPOSITIVE CELLS WITH RESTING MORPHOLOGY WERE DETECTED IN THE NBM OF RATS INJECTED WITH PBS

3.4.3.2 Systemic administration of fluorescent HSAC and HSAT NPs in rats

The ability of fluorescent HSAC and HSAT NPs to cross the BBB was evaluated in rats administered acutely with 500 µl of HSA NPs (20 mg/ml) loaded with NAF. Four hours after iv or ip administration of fluorescent HSAC NPs and iv administration of fluorescent HSAT NPs (Figure 24), both HSA formulations (green, arrows) administered ip or iv, were detected in the brain parenchyma outside the vascular bed (CD34, red) indicating the ability of these novel nanoformulations to cross the BBB after systemic administration. Interestingly, as reported in Figure 24 the two different formulations had a very similar behaviour in crossing BBB.

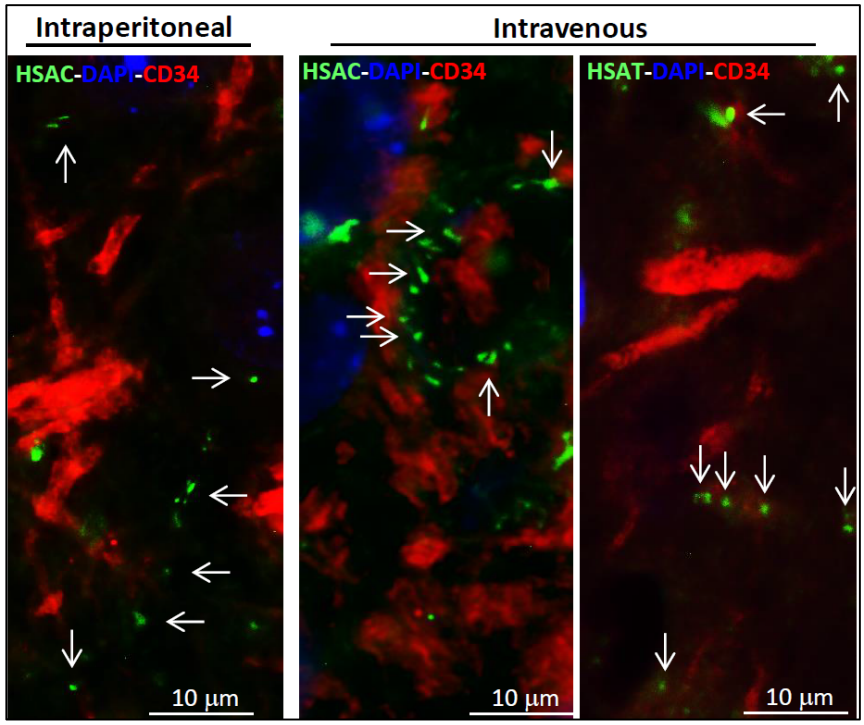

FIGURE 24: BBB CROSSING OF HSAT AND HSAC NPS IN RATS
THE LACK OF COLOCALIZATION BETWEEN HSAC AND HSAT NPS (GREEN, ARROWS) AND CD34 (RED), THE BRAIN VASCULAR ENDOTHELIUM MARKER, INDICATES THE ABILITY OF THE TWO NANOFORMULATIONS TO CROSS THE BBB AFTER AN ACUTE SYSTEMIC ADMINISTRATION

3.4.3.3 Systemic administration of fluorescent HSAC NPs in mice

To exclude potential NPs toxicity and behavioural alterations, fluorescent HSAC NPs (100 mg/kg, ip) were daily administered to C57/Bl6 mice for two weeks. During this period, the nanoformulation was well tolerated, no evident side effects were revealed, as also shown by the body weight trend graph of NPs-treated mice as compared to controls (Figure 25) and no animals died. At the end of the treatment, mice were behaviourally evaluated in the ORT test, to check for their locomotor-exploratory abilities and cognitive functions. As shown in Figure 25, no locomotors (path length) or cognitive impairments (discrimination score) were detected in NPs-treated mice as compared to controls ($P>0.05$). Overall, these data provide strong evidence on the

biocompatibility and potential delivery of molecules to the CNS of this nanoformulation.

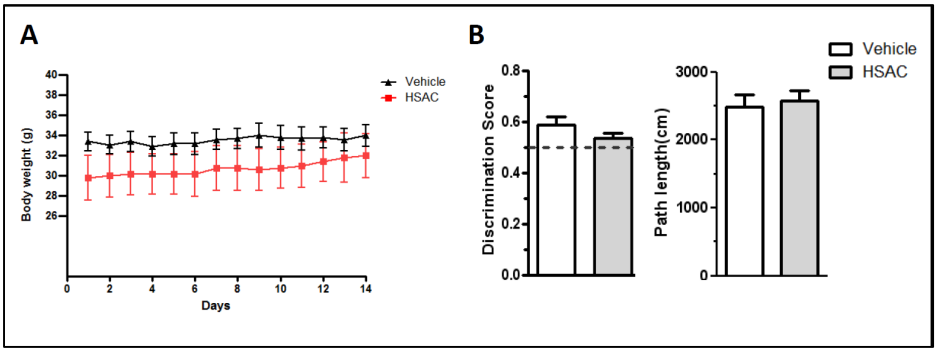

FIGURE 25: BODY WEIGHT AND BEHAVIOURAL EVALUATIONS ON MICE CHRONICALLY ADMINISTERED WITH HSAC NPS FOR TWO WEEKS
HSAC NPS DID NOT AFFECT PONDERAL (A) AND ORT (B) COGNITIVE AND LOCOMOTOR PARAMETERS

3.4.4 CONCLUSION

Albumin NPs are widely used as carrier for drug delivery to a variety of organs, but only a very few studies have been reported as vectors to brain delivery subsequent to different modifications of the NPs surfaces. In this study, HSA NPs using two cross-linking methods were developed and optimised to investigate their *in vivo* behaviour in brain tissues targeting, crossing BBB, brain distribution and fate. A first set of studies evaluated *in vivo* distribution, cellular uptake and fate HAS NPs in healthy rats, after intracerebral injection. The ability of HAS NPs to cross the BBB was investigated both by intravenous and intraperitoneal administration in healthy rats, while the potential toxicity of the developed carriers was estimated by behavioural tests. HSA NPs were produced with very good yields, with a sphere-like shape and regular and narrow size distribution. Both fluorescent HSAC NPs and HSAT NPs resulted suitable for the *in vivo* systemic administration. In the chemical polymerisation NPs were optimized by using a very low amount of cross-linking agent compared to the methods reported in the literature (0.5% vs 4%). Moreover, the thermal polymerization method of HSA was also investigated and optimized, according to green chemistry criteria. These NPs result to be superior than those obtained *via* chemical method in term of formulative parameters, such as reduction of chemical substances used, reduction of costs and the time necessary for NPs

preparation. The *in vivo* performance of both HSA nanoparticles is comparable: as assumed in the choice and design of formulation strategy, the fluorescent NPs are able to cross the BBB by adsorptive transcytosis.

Biodistribution studies showed that NPs did not induce inflammatory response after intracerebral injection and they were able to cross the BBB and reach brain tissue, while behavioural test demonstrated no locomotor, explorative and cognitive functions impairment induced by NPs. All *in vivo* tests confirmed the excellent biocompatibility and biodegradability of NPs. The developed nanocarriers represent valuable and safe vectors for brain delivery.

Since the developed HSA NPs are able to cross the BBB and are larger than 200 nm, this opens up new possibilities for all types of drugs even up to the size of nucleotides and genes and including enzymes for replacement therapy. At the moment, it appears that any drug or larger biologically active compound or complex can be transported across the BBB if it can be efficiently bound to the BBB-transcytosable NPs and is released within the brain in a therapeutically relevant concentration and time profile. Further studies will be oriented to the investigation of the BBB crossing properties of the developed HSA NPs loaded with different drugs.

3.5 REFERENCES

[1] Langer, K., Anhorn, M.G., Steinhauser, I., Dreis, S., Celebi, D., Schrickel, N., Faust, S., Vogel, V., 2008. Human serum albumin (HSA) nanoparticles: Reproducibility of preparation process and kinetics of enzymatic degradation. Int. J. Pharm. 347, 109-117.

[2] Couvreur, P. and Vauhtier, C., 2006. Nanotechnology: intelligent design to treat complex disease. Pharm. Res. 23, 1417–1450.

[3] Kreuter, J., 2014. Drug delivery to the central nervous system by polymeric nanoparticles: What do we know? Adv. Drug Del. Rev. 71, 2-14.

[4] Dadparvar, M., Wagner, S., Wien, S., Kufleitner, J., Worek, F., von Briesen, H., Kreuter, J., 2011. HI 6 human serum albumin nanoparticles-Development and transport over an in vitro blood–brain barrier model. Toxicol. Lett. 206, 60-66.

[5] Elzoghby, A.O., Samy, W.M.. Elgindy, N.A., 2012. Albumin-based nanoparticles as potential controlled release drug delivery systems. J. Controll. Rel. 157, 168–182.

[6] Santhi, K., Dhanaraj, S.A., Joseph, V., Ponnusankar, S., Suresh, B., 2002. A study on the preparation and anti-tumor efficacy of bovine serum albumin nanospheres containing 5-fluorouracil Drug Dev. Ind. Pharm. 28, 1171–1179.

[7] Hervé, F., Ghinea, N., Scherrmann J.M., 2008. CNS delivery via adsorptive transcytosis. AAPS J. 10(3), 455-472.

[8] Weber, C., Kreuter, J., Langer K., 2000. Desolvation process and surface characteristics of HSA-nanoparticles, Int. J. Pharm. 196(2), 197-200.

[9] Merodio, M., Arnedo, A., Renedo, M.J., Irache, J.M., 2001. Ganciclovir-loaded albumin nanoparticles: characterization and in vitro release properties, Eur. J. Pharm. Sci. 12(3), 251-259.

[10] Luppi, B., Bigucci, F., Corace, G., Delucca, A., Cerchiara, T., Sorrenti, M., Zecchi, V., 2011. Albumin nanoparticles carrying cyclodextrins for nasal delivery of the anti-Alzheimer drug tacrine, Eur. J. Pharm. Sci. 44(4), 559-565.

[11] Gulyaev, A.E., Gelperina, S.E., Skidan, I.N., Antropov, A.S., Kivman, G.Y., Kreuter J., 1999. Significant transport of doxorubicin into the brain with polysorbate 80-coated, nanoparticles. Pharm. Res. 16(10), 1564-1569.

[12] Chavanpatil M.D., Khdair A., Patil Y., Handa H., Mao G., Panyam J., Polymer surfactant nanoparticles for sustained release of water-soluble drugs, J. Pharm. Sci.. 96(12) (2007), 3379-3389.

[13] Paxinos, G., Watson, C. 2006. The Rat Brain, Academic Press, New York.

[14] Baglioni, S., Casamenti, F., Bucciantini, M., Luheshi, L.M., Taddei, N., Chiti, F., Dobson C.M., Stefani, M., 2006. Prefibrillar amyloid aggregates could be generic toxins in higher organisms. J. Neurosci. 26, 8160-8167.

[15] Hammond, R.S., Tull, L.E., Stackman, R.W., 2004. On the delay-dependent involvement of the hippocampus in object recognition memory, Neurobiol. Learn. Mem. 82, 26-34.

[16] Greco, S.J., Bryan, K.J., Sarkar, S., Zhu, X., Smith, M.A., Ashford, J.W., Johnston, J.M., Tezapsidis, N., Casadesus, G., 2010. Leptin reduces pathology and improves memory in a transgenic mouse model of Alzheimer's disease, J. Alzheimers Dis. 19, 1155-1167.

[17] Anhorn, M.G., Mahler, H.-C., Langer, Klaus., 2008. Freeze drying of human serum albumin (HSA) nanoparticles with different excipients. Int. J. Pharm. 363, 162-169.

[18] Yedomon, B., Fessi, H., Charcosset, C., 2013. Preparation of Bovine Serum Albumin (BSA) nanoparticles by desolvation using a membrane contactor: A new tool for large scale production. Eur. J. Pharm. Biopharm. 85, 398-405.

[19] Wilson, B., Lavanya, Y., Priyadarshini, S.R.B., Ramasamy, M., Jenita J.L., 2014. Albumin nanoparticles for the delivery of gabapentin: Preparation, characterization and pharmacodynamic studies. Int. J. Pharm. 473, 73–79.

CHAPTER 4

PREPARATION AND ANALYSIS OF NANOVECTORS FOR BRAIN DELIVERY OF ANDROGRAPHOLIDE AS NEUROPROTECTIVE AGENT

This work was carried out in collaboration with Mouhssin Oufir[1], Vieri Piazzini[2], Daniela Elisabeth Eigenmann[1], Evelyn Andrea Jähne[1], Volha Zabela[1], Maria Camilla Bergonzi[2], Martin Smiesko[3], Matthias Hamburger[1] and Anna Rita Bilia[2]

[1]Pharmaceutical Biology, Department of Pharmaceutical Sciences, University of Basel, Klingelbergstrasse 50, CH-4056 Basel, Switzerland

[2]Department of Chemistry, University of Florence, via Ugo Schiff, 6, 50019 Sesto Fiorentino, Florence, Italy

[3]Molecular Modeling, Department of Pharmaceutical Sciences, University of Basel, Klingelbergstrasse 50, CH-4056 Basel, Switzerland

4.1 ABSTRACT

AG is a major diterpenoid of *Andrographis paniculata* (Burm. f.) Nees which has been clinically demonstrated in the treatment of inflammation-related neurodegenerative disorders. Nevertheless, low bioavailability and poor water solubility limit further developments of this compound. In order to overcome these limitations, we loaded AG into HSA NPs and into PECA NPs. HSA NPs were prepared by coacervation and both thermal cross-linking (HSAT AG NPs) and chemical cross-linking (HSAC AG NPs) were investigated. PECA AG NPs were produced by emulsion-polymerization. Both NPs appeared as spherically shaped under transmission electron microscopy. After the study of release of AG and the results in terms of size, ζ-potential and polydispersity, the ability of free AG and AG-loaded in PECA and HSAT NPs to cross the blood-brain barrier (BBB) was assessed with an *in vitro* BBB model based on human hCMEC/D3 endothelial cells. For BBB drug permeability assays, a quantitative UPLC-MS/MS method for AG in Ringer HEPES buffer was successfully developed and validated according to international regulatory guidelines for industry. Our results show that free form of AG free does not permeate the BBB, HSA NPs improve the permeation of AG maintaining the integrity of cell layer while PECA NPs permanently disrupt the BBB integrity.

4.2 INTRODUCTION

The BBB is composed of cerebral endothelial cells with tight junctions formed by a complex of intramembranous proteins, such as claudin and peripheral membrane proteins like *zonula occludens* proteins. It restricts paracellular passage of small molecules and aids in the transport of several nutrients and proteins into the brain. On the other hand, the BBB limits the delivery of neurotherapeutics to the CNS. Crossing the BBB is a major challenge for drugs, as more than 98% of small-molecules, and almost 100% of large drugs do not cross the BBB[1]. Many factors influence the permeability of molecules, such as molecular weight, the number of hydrogen bonds, pharmacokinetic properties, and the presence of active efflux transporters[2]. The BBB prevents the delivery of neurotherapeutics to the CNS not only as mechanical fence, but also like a dynamic biological barrier in which active metabolism and carrier mediated transport occur[3]. The development of nanodrug delivery systems for the controlling of neurological diseases seems promising and is still awaited to provide sufficient drug permeability into the brain. The possibility for drugs to

reach the brain, when loaded into nanovectors, is based on the fact that their crossing will depend completely on the physiochemical and biomimetic features of the carrier and will not depend anymore on the chemical structure of the drug, which is hindered inside the NPs[3].

In our study, two different mechanisms to cross the BBB were investigated with the employment of PECA and HSA NPs. In the first case, NPs were done by emulsion polymerization method, and coated with the non-ionic surfactant TW80. Several mechanisms have been proposed for the transport of these NPs across the BBB: the receptor-mediated transcytosis was supported by many studies[4–8]. TW80 acts as an anchor for the apolipoprotein-overcoated NPs thus would mimic lipoprotein particles and could interact with their receptors and then be taken up by the brain capillary endothelial cells [9].

HSA was selected as ideal material to fabricate NPs for drug delivery because it is non-toxic, non-immunogenic, biocompatible and biodegradable; therefore, have high binding capacity of various drugs and is well tolerated without any serious side-effects[10]. In this case, the rationale for the design of NPs was based on the observation that cationic proteins can bind the endothelial cell surface and cross the BBB through adsorptive-mediated transcytosis (ATM)[3], this mechanism involves electrostatic interaction. HSA NPs were prepared by coacervation and both chemical and thermal cross-linkings were investigated.

Developed nanovectors were loaded with AG, a diterpene of the labdane family, responsible of most of the biological effects of *Andrographis paniculata* (Burm. f.) Nees (Acanthaceae). AG is used in clinics in China, and has been reported to exhibit a wide spectrum of biological activities[11]. Recent reports suggest that AG protects against damage induced by dopamine, with protective effects against inflammation-mediated neurodegeneration, against oxidative stress by nicotine in the brain, and against cerebral ischemia via inhibition of pathways related to inflammation and apoptosis, including NF-kB and MAPK signaling [12–14]. Recently, Serrano and coworkers[15] showed that AG protected against damage induced by amyloid-β oligomers *in vitro,* reduced α-β levels and *tau* phosphorylation in mice, modulated the formation of amyloid plaques, and recovered spatial memory functions.

By contrast, its poor water solubility and instability resulted in lower bioavailability and seriously limited its pharmacological function. AG is slightly soluble in water and chloroform with a solubility rancing from 0.07 to 0.21mg/mL, respectively, while the solubility was relatively higher in methanol

(14.5 mg/mL). It is stable under neutral and acidic conditions, but unstable under alkaline conditions. Furthermore, it is rapidly metabolized in the duodenum and jejunum to form a sulfate conjugate that is hydrophilic and likely to be impermeable. The formulation of nanodelivery systems could improve the pharmacokinetic characteristics of problematic drugs. Many researchers have designed different new dosage forms for AG such as dropping pills, dispersible tablets, oral micro emulsion, cyclodextrin inclusion complex, liposomes and certain effects were obtained for improving the bioavailability but the clinical application was still restricted for the lower drug-loading rate, entrapment rate, and the poor stability of pharmaceutical dosage forms[11,16,17]. Up to now, there is no evidence in literature that the BBB permeability of AG itself is sufficient to possibly achieve therapeutically relevant concentrations in the CNS.
We evaluated whether loaded NPs could be used to potentially deliver AG to the human brain endothelium using hCMEC/D3 cell line [18,19], a well-known established human *in vitro* based BBB model, which expresses LRP1, and if the compound in the free form is BBB permeable.
For the permeability assays, we developed a quantitative ultra-performance liquid chromatography tandem mass spectrometry (UPLC-MS/MS) method in Ringer HEPES buffer (RHB) for AG and validated it in terms of selectivity, specificity, precision, accuracy, and reliability according to the US FDA and EMA regulatory guidelines for industry[20,21]. Our results demonstrated that free AG did not cross the BBB at the concentration of 5 μM, HSA NPs improve the permeability of AG maintaining the integrity of cell layer, while PECA NPs coated with 1% TW80 permanently altered cell layer integrity.

4.3 EXPERIMENTAL SECTION

4.3.1 MATERIALS

NAF, TW80, ECA, HSA, bovine serum albumin (BSA), glutaraldehyde 25%, PBS, NaCl, sodium hydroxide, hydrochloric acid 37%, sulfuric acid 97%, D-(+)-glucose anhydrous, sucrose and dextran 70000 were purchased from Sigma-Aldrich (Steinheim, Germany). Acetonitrile, methanol, formic acid (FA), trifluoroacetic acid (TFA), and ammonium formate were all HPLC grade and were purchased from BioSolve (Valkenswaard, the Netherlands). Dimethyl sulfoxide (DMSO) was purchased from Scharlau (Scharlab AG, Sentmenat, Spain). Analytical grade ethanol (EtOH) was from Riedel-de Haen (Seelze, Germany). Phosphotungstic acid was obtained by Società Italiana Chimici (Rome, Italy). HPLC grade water

was obtained by a Milli-Q integral water purification system (Millipore Milford, USA). RHB (150 mM NaCl, 2.2 mM $CaCl_2$, 0.2 mM $MgCl_2$, 5.2 mM KCl, 2.8 mM glucose, 5 mM HEPES, 6 mM $NaHCO_3$) was prepared in-house, adjusted to pH 7.4, filtered, and stored at 4°C. 24-Well plates and inserts (transparent PET membrane, 3.0 µm pore size, 0.6×10^6 pores/cm^2) were obtained from Greiner Bio-one® (Frickenhausen, Germany). Immortalized hCMEC/D3 cells were obtained from Prof. Pierre-Olivier Couraud (Institut Cochin, Université René Descartes, Paris, France), Prof. Babette Weksler **(**Weill Cornell Medical College, New York, NY, USA) and Prof. Ignacio A Romero **(**Department of Life, Health and Chemical Sciences, Open University, Milton Keynes, U.K).

4.3.2 DESIGN AND OPTIMIZATION OF NANOVECTORS LOADED WITH AG

4.3.2.1 Production and coating of PECA AG NPs

PECA NPs were prepared by emulsion polymerization, as described by Kreuter[22], with some modifications to the original method. Briefly, 100 µl of the monomer ECA were added drop by drop under magnetic stirring (500 rpm) to 10 ml of acidic polymerization medium (60:40 methanol:water pH 2) containing 1% of dextran 70,000 and 0.1% w/v or 0.5% w/v of AG. The monomer ECA is a clear liquid, which undergoes polymerization in contact with water. The mixture was stirred magnetically for 4 h to facilitate NPs formation. The resulting suspension was neutralized with NaCl 0.1 N and filtered through a sintered glass filter (pore size 10 µm) to remove any agglomerates. In order to eliminate methanol, the suspension was centrifuged for 10 minutes, 3 times at 4500 rpm at 4 °C. The pellet with NPs was resuspended with the same volume of RHB. Anhydrous glucose (0.1% w/v) was added as cryoprotector to improve redispersibility of the NPs after lyophilization. The NPs suspension was lyophilized overnight and resuspended in RHB at a concentration of 5 mg/ml by vortex. The non-ionic surfactant TW 80 was added to a final concentration of 1% v/v and the mixture was incubated for 30 min at 500 rpm and finally lyophilized.

4.3.2.2 HSAC-AG NPs preparation

HSA NPs were prepared modifying a previously proposed desolvation technique[23–25]. In principle, HSA (2% w/v) was dissolved in a solution of NaCl 10 mM under magnetic stirring (500 rpm, 15 minutes). The resulting HSA solution was transformed into NPs by the continuous addition of EtOH at a defined rate of 1 ml/min (ratio NaCl- EtOH 1:2 v/v) under stirring (500 rpm) at room temperature. After the desolvation process glutaraldehyde (5 µg/mg

protein) was added to induce particle crosslinking. The process was performed under magnetic stirring for 2 hours at room temperature. The resulting NPs were centrifugated (4500 rpm, 10 min x 3 times, 4°C) to separate the supernatant, containing free HSA and glutaraldehyde, from the pellet containing HSA NPs. The pellet was dispersed in the original volume of 10 mM NaCl solution containing 3% w/v sucrose as cryoprotective agent and freeze-dried overnight. HSAC NPs loaded with AG were obtained using the same method and solubilized AG in the EtOH (ratio 1:1 w/w with HSA) with one hour of incubation.

4.3.2.3 HSAT-AG NPs preparation

HSA NPs were prepared modifying and optimizing thermal cross-linking method[26,27]. HSA (0.5% w/v) was dissolved in a solution of NaCl 10 mM under magnetic stirring (500 rpm, 15 min). The resulting HSA solution was transformed into NPs by the continuous addition of the desolvating agent EtOH at a defined rate of 1 ml/min (ratio NaCl-EtOH 1:1 v/v) under magnetic stirring (500 rpm) at room temperature. Stirring was continued at 90°C for 1 hour to obtain NPs thermal cross-linked. The suspension was centrifuged (4500 rpm, 30 min x 3 times, 4°C) and the pellet contained NPs was dispersed in the original volume of NaCl solution 10 mM with 2% w/v anhydrous D-glucose as cryoprotector, then was freeze-dried overnight. NPs loaded with AG were prepared using the same method, incubating AG (ratio 1:1 w/w with HSA) in EtOH for one hour.

4.3.2.4 NPs yield

The yield of the processes of preparation were determined as the weight percentage of the final product after drying, with respect to the initial total amount materials used for the preparation[28].

4.3.2.5 Characterization of NPs in terms of size, polydispersity index and ζ potential

Particle size of the developed NPs were measured by a DLS, Zsizer Nano series ZS90 (Malvern Instruments, Malvern, UK) equipped with a JDS Uniphase 22 mW He-Ne laser operating at 632.8 mm, an optical fiber-based detector, a digital LV/LSE-5003 correlator and a temperature controller (Julabo water-bath) set at 25°C. Time correlation functions were analysed to obtain the Zh and the particle size distribution using the ALV-60X0 software V.3.X provided by Malvern. Autocorrelation functions were analysed by the Cumulants method, fitting a single exponential to the correlation function to obtain particle size distribution.

Scattering was measured in an optical quality 4 ml borosilicate cell at a 90° angle, diluting the samples in 10nM NaCl solution or RHB for HSA NPS and PBS or RHB for PECA NPs. ζ potentials were measured using the same instrument; for all samples, an average of three measurements at stationary level was taken. The temperature was kept constant at 25°C by a Haake temperature controller. ζ potential was calculated from the electrophoretic mobility, using the Henry correction to Smoluchowski's equation.

4.3.2.6 Morphological characterization

NPs were analyzed in terms of morphology, polydispersity, shape and dimensions by TEM. The dispersions diluted 10-times were applied to a carbon film-covered copper grid. Most of the dispersion was blotted from the grid with filter paper to form a thin film, which was stained with a phosphotungstic acid solution 1% w/v in sterile water. The samples were dried for 3 min and then were examined under a JEOL 1010 electron microscope and photographed at an accelerating voltage of 64 kV.

4.3.2.7 Purification of NPs, Encapsulation Efficiency and Loading Capacity

The amount of AG entrapped into nanocarriers was calculated using the indirect method. NPs were purified from free drug by ultracentrifugation for 75 min at 18000 rpm and 4°C. EE% and the LC% of NPs were calculated by the difference between the total amount of the drug loaded and the amount of AG determined in the supernatants obtained after the purification of the NPs, using the following equations[29]:

$$EE\% = (\text{Total Drug} - \text{Free Drug})/(\text{Total Drug}) \cdot 100$$

$$LC\% = (\text{Total Drug} - \text{Free Drug}))/(\text{Weight of NPs}) \cdot 100$$

4.3.2.8 *In vitro* release of AG

The ability of NPs to provide a controlled or sustained release of AG was evaluated using the dialysis bag method, in a PBS solution at pH 7.4 to mimic the sink conditions. The volume of medium of release was calculated according to Yang et al [11].The systems were placed in a thermostatic bath at 37 °C ± 0.5 °C, under magnetic stirring at 200 rpm. The release was measured for 24 hours. Aliquots of one milliliter were withdraw in duplicate at the following time point: 20, 40, 60, 120, 240, 360, 480 end 1440 minutes and replaced with the fresh PBS, maintained at 37 °C.

4.3.3 UPLC- MS/MS ASSAY FOR THE QUANTIFICATION OF AG

4.3.3.1 Stock solutions, calibration standards, and quality controls (QCs)

Stock solutions (SS) of AG as analyte and forskolin as I.S. were prepared separately by dissolving at least 2 mg of compound in 10 mL of DMSO. Weightings were done on an analytical microbalance (Sartorius, Switzerland). Working solutions (WSs) of analyte and I.S. at concentrations of 50 µg/mL were prepared by further diluting the respective SSs. For analytes, calibration standards (calibrators) and quality controls (QCs) in RHB at low, medium, and high concentrations (QCL, QCM, and QCH) were prepared by serial dilution of the respective WSs (range 10.0–2000 ng/mL). The first concentration level of the calibrators was defined as lower limit of quantification (LLOQ), and the last level as upper limit of quantification (ULOQ). Calibrators and QCs were aliquoted into polypropylene tubes and stored below -65°C until analysis. For the I.S., a second working solution (WS2) was freshly prepared on the day of the analytical run by further diluting the I.S. WS1 at the concentration of 2000 ng/mL.

4.3.3.2 Sample extraction from Ringer HEPES buffer

Analytes and corresponding I.S. (Figure 26) were extracted from RHB by means of protein precipitation.

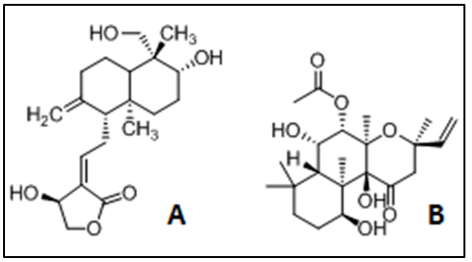

FIGURE 26: CHEMICAL STRUCTURES OF (3E,4S)-4-HYDROXY-3-{2-[(1R,4AS,5R,6R,8AS)-6-HYDROXY-5-(HYDROXYMETHYL)-5,8A-DIMETHYL-2-METHYLENEDECAHYDRO-1-NAPHTHALENYL]ETHYLIDENE}DIHYDRO-2(3H)-FURANONE (ANDROGRAPHOLIDE) (A) AND INTERNAL STANDARD, (3R,4AR,5S,6S,6AS,10S,10AR,10BS)-6,10,10B-TRIHYDROXY-3,4A,7,7,10A-PENTAMETHYL-1-OXO-3-VINYLDODECAHYDRO-1H-BENZO[F]CHROMEN-5-YL ACETATE (FORSKOLIN) (B).

Sample aliquots (200 µL) were spiked with a freshly prepared working solution (WS2) of the I.S. (100 µL). Subsequently, samples were spiked with a BSA

solution (60g/L) (200 µL) and then subjected to protein precipitation with ice-cold acetonitrile (800 µL). The mixture was briefly vortexed, then stirred for 10 min at 1400 rpm on a Eppendorf Mixmate (Vadaux-Eppendorf, Schönenbuch, Switzerland), and subsequently centrifuged for 20 min at 13200 rpm (MiniSpin plus, Vaudaux-Eppendorf, Schönenbuch, Switzerland). The supernatant (1100 µL) was transferred into a 96-deep well plate, dried under nitrogen (Evaporex EVX-96, Apricot Designs, Monovia, CA, USA) and thereafter reconstituted with the injection solvent (200 µL) (Table 12).

TABLE 12: OPTIMIZED UPLC PARAMETER. INJECTION SOLVENT: 65% A1 + 35% B1; A1: HIGH PURITY WATER + 0.1% FA ACID; B2: ACETONITRILE + 0.05% FA

Analyte	Gradient	Total run time (min)	Eluents	Injection volume (µL)	Column	Column temperature (°C)	Flow rate (mL/min)
AG	10–100% B1 in 4 min 100–10% B1 from 5.01 min	6.00	A1+B1	10.0	Waters Acquity CSH ™ Phenyl-hexyl	75.0	0.500

For optimal reconstitution, the 96-deep well plate was stirred on an Eppendorf Mixmate (45 min at 1500 rpm) and subsequently centrifuged for 4 min at 3000 rpm (Megafuge, Heraeus Instruments AG, Switzerland). Samples were then injected into the UPLC-MS/MS in full loop mode (injection volumes see in Table 12).

4.3.3.3 UPLC-MS/MS settings

Method validation was performed on a Waters Acquity UPLC system coupled to a Waters Acquity triple quadrupole (Waters, Milford, MA, USA). The UPLC system included a binary pump, a cooling autosampler (set at 10°C, protected from light), and a column heater. Separation of analytes and I.S. was achieved with an Acquity (Waters, Milford, MA, USA) UPLC Phenyl-Hexyl column (C18; 2.1 x 50 mm; 1.8 µm particle size) stored at 75°C. Mobile phase A was 0.1% formic acid (FA) in water, and mobile phase B was 0.1% FA in acetonitrile (Table 12). Total run time was 6 min; the flow rate of the mobile phase was set at 0.5 mL/min (Table 12). Gradients for all analytes are listed in Table 12. Weak wash solution was a mixture of acetonitrile and water (50/50, v/v) containing 0.2%

TFA. Strong wash solution was a mixture of acetonitrile, isopronanol, and acetone (40/30/30, v/v/v) containing 0.2% TFA. Seal wash solution was a mixture of acetonitrile and water (10/90, v/v). The MS system was equipped with an ESI interface, and measurements were performed in negative ion mode (ESI-) with multiple reaction monitoring (MRM). Nitrogen, provided by a nitrogen generator N2-Mistral (Schmidlin AG, Neuheim, Switzerland), was used both as desolvation gas and as cone gas. Argon was used as collision gas. Source temperature was set at 150°C. MS/MS transitions and parameters were generated using Waters IntelliStart software and subsequently optimized manually. Transitions, cone voltage, and collision energy for analytes and I.S. are listed inTable 13. Data were acquired with MassLynx V4.1 software and quantification was done using QuanLynx software (Waters, Milford, MA, USA).

TABLE 13: OPTIMIZED MS/MS PARAMETERS (SRM TRANSITIONS, CONE VOLTAGE, COLLISION ENERGY AND DWELL TIME) IN ESI NEGATIVE MODE FOR ANDROGRAPHOLIDE AND FORSKOLIN (I.S.)

Compounds	SRM transitions	Cone voltage (V)	Collision energy (eV)	Dwell time (ms)
AG	Quant: 394.8 > 287.1	20	18	95
	Qual: 394.8 > 331.1	20	10	95
I.S. Forskolin	409.0 > 349.0	21	9	195

4.3.3.4 Method validation

Method validation for the quantification of AG by UPLC-MS/MS was performed according to international regulatory guidelines[20,21]. Imprecision in all validation tests was expressed by CV%. According to both guidelines, the CV % had to be below 15% of the nominal values at all concentration levels (exception below 20% at the LLOQ level). Inaccuracy in all validation tests was expressed by RE %, and had to be within ± 15 % of the nominal value at all concentration levels (exception within ± 20 % at the LLOQ level) according to both guidelines[20,21].

- Calibration curve and regression parameters

Seven calibrators were injected with increasing concentration after a blank sample (blank RHB) and a zero sample (RHB only spiked with I.S.). Each validation run, performed on different days, consisted of a set of calibrators at the beginning and at the end of the run. The calibration curve was validated

through six QCs (duplicates of QCL, QCM, and QCH), which were inserted randomly into the analytical run. The weighting factor was determined during the first run to obtain a consistent dispersion of measure errors across the range. According to FDA guidance, a run was considered to be valid if the coefficient of determination (R^2) was higher than 0.96 and if at least 75 % of all calibrators were used to generate the calibration curve. For the LLOQ and the ULOQ, at least one replicate had to be accepted. For the six QCs, at least four replicates in total and at least one replicate at each level had to be accepted[20].

- Carry-over

To assess the carry-over of both analyte and I.S. in each analytical run, blank samples were injected after the ULOQ. Peak areas of analyte and I.S. in these blank samples were then compared to the peak areas at the LLOQ. Mean carry-over in each analytical run, expressed in %, had to be below 20 % for analytes and below 5% for I.S. [21]

- Specificity

A total of six blank samples (duplicates, three different batches of RHB) without the addition of analyte or I.S. were injected into the UPLC-MS/MS within an analytical run. Peak areas were assessed using a valid calibration curve, and they had not to exceed 20 % of the mean peak area of both replicates at the LLOQ.

- Selectivity

Six samples at the LLOQ (duplicates, three different batches of RHB) were injected into the UPLC-MS/MS within a validation run. Concentrations were calculated using a valid calibration curve. Selectivity imprecision (CV %) had to be below 20 % and inaccuracy (RE %) had to be within ± 20 % of the nominal values.

- Within-run and between-run reproducibility

Six replicates at five concentration levels (LLOQ, QCL, QCM, QCH, and ULOQ) were injected into the UPLC-MS/MS within three validation runs on three different days. In each validation run, within-run imprecision (CV %) of each QC series had to be below 15 % (below 20 % at the LLOQ) and within-run

inaccuracy (RE %) had to be within ± 15 % (within ± 20 % at the LLOQ) of the nominal values. Between-run imprecision (CV %) and inaccuracy (RE %) were then assessed calculating the overall means and standard deviations (S.D.). The acceptance criteria for imprecision (CV %) and inaccuracy (RE %) were the same as described above.

- Dilution test

To assess the reliability of the method at concentration levels outside the calibration ranges, a dilution test was performed. From the WS of the analytes, a solution at a concentration 5-fold higher than the ULOQ was prepared. This solution was first diluted to give a solution at a 10-fold lower concentration, then further diluted to give a second solution at 100-fold lower concentration. Six replicates of both levels were injected into the UPLC-MS/MS system. For all replicates of both QC series, the concentration was assessed using a valid calibration curve and subsequently multiplied with the corresponding dilution factor. Resulting mean concentrations, imprecision, and inaccuracy were calculated. According to FDA guidance, the imprecision (CV %) had to be below 15% and the inaccuracy (RE %) had to be within ± 15% of the nominal values[20].

- Extraction yield (recovery)

The extraction yield of the analytes was determined using six replicates spiked with analyte at three different concentration levels (QCL, QCM, and QCH) before extraction, and spiked with I.S. after extraction, compared to six replicates of blank RHB samples spiked after extraction with analyte at three different concentration levels (QCL, QCM, and QCH) and with I.S. The extraction yield of I.S. was determined using six replicates spiked with I.S. before extraction and with analyte at medium concentration after extraction, compared to six replicates of blank RHB spiked after extraction with I.S. and analyte at medium concentration. According to FDA guidance, recovery does not need to be 100%, but the extent of recovery of an analyte and of the internal standard should be consistent, precise, and reproducible[20].

- Freeze and thaw (F/T) stability

Six replicates of QCL and QCH were subjected to three freeze and thaw (F/T) cycles, processed, and subsequently analyzed using a valid calibration curve. At

both concentration levels, the imprecision (CV %) had to be below 15% and the inaccuracy (RE %) had to be within ± 15% of the nominal values.

- Short-term stability on benchtop

Six replicates of QCL and QCH were stored for 2 hours at room temperature (RT), processed, and quantified using a valid calibration curve. At both concentration levels, imprecision (CV %) had to be below 15% and inaccuracy (RE %) had to be within ± 15 % of the nominal values.

- Processed sample stability at autosampler conditions

Six replicates of QCL and QCH were injected into the UPLC-MS/MS after processing and quantified using a valid calibration curve. All QCs were stored in the autosampler (set at 10°C, protected from light) and after a defined time period reassessed using a new calibration curve. At both concentration levels, imprecision (CV %) had to be below 15 % and inaccuracy (RE %) had to be within ± 15 % of the nominal values.

- Long-term stability below -65°C

Three replicates of QCL, QCM, and QCH were quantified using a valid calibration curve at time zero (t=0), and three replicates at the same concentration levels (QCL, QCM, and QCH) were stored below -65°C. After one week of storage, the samples were processed and quantified using a valid calibration curve generated by freshly prepared calibrators and QCs. Results from samples stored below -65°C were plotted in function of results from time zero (t=0), and a curve was fitted by linear regression (forced through zero). Samples were considered as stable when the slope was within 1 ± 0.15.

- Stock solution stability

Fresh stock solutions for analytes and I.S. were prepared and kept at RT for 2 hours. Old stock solutions which were stored below -65°C for various time periods were thawed, and similarly kept at RT for 2 hours. Subsequently, working solutions for each compound at 5.00 µg/mL in the injection solvent were prepared in 6 replicates and injected into the UPLC-MS/MS system, and peak areas from old and fresh stock solutions were compared. The eventual degradation had to be ≤ 5%.

4.3.4 IN SILICO PREDICTION OF BBB PERMEABILITY

Three-dimensional computer model of AG was built in Maestro modeling environment[30]. The global minimum geometry identified in a conformational search was used as an input for the QikProp [31] application, to evaluate various descriptors relevant for compound permeability through the BBB. PSA and the logarithm of partition coefficient (LogP) descriptors were calculated also using the Calculator plugin of Chemaxon Marvin application[32].

4.3.5 BLOOD-BRAIN BARRIER DRUG PERMEABILITY ASSAYS

4.3.5.1 Human *in vitro* BBB model

The human mono-culture *in vitro* BBB model based on hCMEC/D3 cell line was prepared as reported previously[33]. As culture medium, EBM-2 supplemented with hydrocortisone, ascorbic acid, heparin, antibiotic-antimycotic solution, and 5% FBS (heat inactivated at 56°C for 30 min) was used (Single-Quots). After 5–7 days of incubation of hCMEC/D3 monolayers (at a maximal TEER, Table 14), the permeability assays for the compounds were carried out.

TABLE 14: APPARENT PERMEABILITY COEFFICIENTS APICAL TO BASOLATERAL ($P_{APP\ A>B}$) FOR AG AND NAF AS BARRIER INTEGRITY CONTROL (N = 3)

Assays	Mean P_{app} AG ± SEM ($\times 10^{-6}$ cm/s)	Mean NAF P_{app} ± SEM ($\times 10^{-6}$ cm/s)	Time of withdrawal (min)	Recovery (%) for AG	Recovery (%) for NAF
Free form of AG	**9.51±0.707**	**7.85 ±0.188**	60	85.3	90.7
HSAT AG NPs	**18.7±3.31**	**9.34±0.611**	60	96.2	94.2
PECA AG NPs	**32.6±1.62**	**29.9±4.38**	60	102.8	88.9

Briefly, the tissue culture inserts were transferred into a 24-well plate containing 1200 µL of pre-warmed (37°C) RHB in each well (basolateral compartment). Medium in inserts (apical compartment) was subsequently replaced with 300 µL of a pre-warmed (37°C) working solution containing the test compound (5 µM) and NAF as integrity control marker (10 µg/mL) in RHB. The 24-well plate was incubated at 37°C on an orbital shaker (ELMI DTS-2, Riga, Latvia) with moderate speed (300 rpm), and aliquots of 270 µL of both apical and basolateral compartments were collected after several timepoints (15, 30, 60, and 120 min) (one insert per timepoint) and stored below -65°C until analysis. All experiments were performed at least in triplicate. Quantification of NAF fluorescence was

carried out using a Chameleon microplate reader (Hidex, Turku, Finland). Quantification of AG was performed by means of the validated UPLC-MS/MS methods.

4.3.5.2 Calculation of permeability coefficients

The apparent permeability coefficient (P*app*) for AG and NAF was calculated in centimeters per second (cm/s) according to the equation[34]:

$$Papp\ (cm/s) = V_R/AC_{D0} \times (\Delta C_R/\Delta t)$$

where:

- V_R is the volume in the receiver compartment,
- A is the surface area of the filter membrane (0.336 cm^2 for 24-well inserts),
- C_{D0} is the initial concentration in the apical compartment,
- $(\Delta C_R/\Delta t)$ is the change of concentration over time in the basolateral compartment.

Recovery for AG and NAF was calculated according to the equation:

$$Recovery\ (\%) = C_{Df}\ V_D + C_{Rf}\ V_R\ /\ (C_{D0}V_D) \times 100$$

where:

- C_{Df} and C_{Rf} are the final concentrations of the compound in the donor and receiver compartments, respectively,
- C_{D0} is the initial concentration in the donor compartment,
- V_D and V_R are the volumes in the donor and receiver compartments, respectively.

All results are expressed as means ± SD. To confirm that AG and NAF did not attach to the plastic material and that the diffusion barrier was only provided by the cells, control experiments were performed using collagen coated inserts without cells.

Endothelial permeability coefficients (P_e) for AG and NAF were calculated as follows. For each replicate (controls and samples), the cleared volume was calculated according to the following equation[35,36]:

$$Clearance\ (\mu L) = \frac{C_B V_B}{C_A}$$

where:

- CB and VB are the concentration and volume in the basolateral compartment, respectively,
- CA is the concentration in the apical compartment.

The mean cleared volume was plotted as a function of time (30, 60, and 120 min), and the slope was estimated by linear regression analysis. Permeability-surface area product (PS) and Pe values were subsequently calculated according to the following equations:

$$\frac{1}{PS_{total}} - \frac{1}{PS_{filter}} = \frac{1}{PS_e}$$

$$\frac{PS_e}{A} = P_e$$

where:

- PS_{total} is the slope of the clearance curve of cell monolayer with filter inserts,
- PS_f is the slope of the clearance curve of control filter inserts without cells,
- PS_e is the slope of the the clearance curve for the endothelial monolayer, and A is the surface area of the filter membrane (0.336 cm^2).

Recovery (mass balance) was calculated according to the following equation:

$$Recovery\ (\%) = \frac{C_{Af}V_A + C_{Bf}V_B}{C_{A0}V_A} \times 100$$

where:

- C_{Af} and C_{Bf} are the final concentrations of the compounds in the apical and basolateral compartments, respectively,
- C_{A0} is the initial concentration in the apical compartment,
- V_A and V_B are the volumes in the apical and basolateral compartments, respectively.

All results are expressed as means ± SD.

4.4 RESULTS AND DISCUSSION

4.4.1 CHARACTERIZATION OF PECA NPS

The results obtained in term of dimensional analysis, PDI and ζ-potential of PECA NPs are reported in the following Table 15.

TABLE 15: CHARACTERIZATION OF PECA-BASED NPS IN TERMS OF MEAN DIAMETER, POLYDISPERSITY, Z –POTENTIAL, YIELD OF PREPARATIVE PROCESS, ENCAPSULATION EFFICIENCY AND LOADING CAPACITY. (MEAN±SD; N=3)

PECA NPs	Size (nm)	PDI	ζ -Potential (mV)	Yield (%)	EE%	LC%
PECA	288 ± 7.00	0.19 ± 0.01	-2.85 ± 1.18	81.40±0.41	-	-
PECA-TW80	303 ± 8.00	0.36 ± 0.04	-4.07 ± 0.05	81.40±0.41	-	-
PECA AG 0.1%	221.20±3.20	0.20 ± 0.05	-2.78 ± 0.10		96.04±0.21	4.61±0.20
PECA AG 0.1% TW80	242.85±4.10	0.20 ± 0.05	-5.22 ± 0.10		96.04±0.21	4.61±0.20
PECA-AG 0.5%	232.90±8.2	0.22 ± 0.02	-3.85 ± 0.10	86.95±3.50	94.60±0.41	13.20±0.36
PECA-AG 0.5%- TW80	**255.40±8.9**	**0.19 ± 0.02**	**-4.77 ± 0.18**	**86.95±3.50**	**94.60±0.41**	**13.20±0.36**

The data were obtained by DLS analysis; a dilution factor between 10 and 50 was applied for measurement. The sizes were not affected after coating with 1% TW 80. PECA AG NPs done with a modified method of preparation have satisfactorily narrow size distribution, with PDI around 0.2. The yields of NPs's preparation were ≈90% for empty NPs and for PECA AG 0.5% NPs too, while ≈70% for PECA AG 0.1%. TEM analyses provided important details on the morphology and the dimension of the NPs(Figure 27).

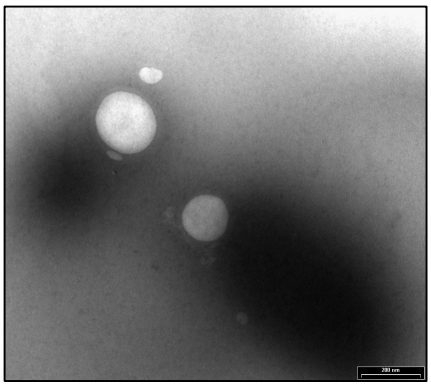

FIGURE 27: TEM ANALYSIS OF PECA AG NPS

PECA AG NPs were sphere-shaped, with a good size distribution comparable to DLS analysis, suitable for systemic administration. Changing the polymerization medium does not affect the properties of NPs. The suspension becomes opalescent after the addition of the monomer ECA as soon as started the process of polymerization. After freeze-drying, NPs were suspended with RHB at concentration of 5 mg / ml for the NPs containing 0.1% w /v of AG and 20 mg / ml for the NPs containing AG at 0.5% w / v with vortex. The size and the PDI did not change. The increase of concentration of AG loaded did not negatively impact on the formulation. This indicates that the selected molecule does not alter the optimized nanocarriers. The value obtained in term of EE% are too high (≈ 95%) for both concentration of AG, NPs size increased when AG concentration increased with lower EE%.

4.4.2 CHARACTERIZATION OF HSA NPS

At the beginning, HSA AG NPs were prepared using the method of chemical cross-linking, trying to reduce the % of glutaraldehyde. In the preparation phase, was observed a considerable turbidity of the HSA solution during the addition of ethanol with subsequent formation of a coacervate of white colour, that became even more evident by the addition of glutaraldehyde which acts as cross-linker for the formation of NPs. The size, the homogeneity and the ζ potential of optimized HSAC NPs were determined by DLS. A dilution factor between 5 and 30 was applied. NPs have acceptable narrow size distribution, with PDI around 0.3; the process yields of NPs were ≈90%. The Table 16shows the final characterization of HSAC NPs.

TABLE 16: CHARACTERIZATION OF HSAC NPS IN TERMS OF MEAN DIAMETER, POLYDISPERSITY, Z –POTENTIAL, YIELD OF PREPARATIVE PROCESS, ENCAPSULATION EFFICIENCY AND LOADING CAPACITY. (MEAN±SD; N=3)

HSAC NPs	Size (nm)	PDI	ζ –Potential (mV)	Yield (%)	EE%	LC%
HSAC	151.67±1.53	0.28±0.01	15.7±0.20	89.60±3.60	-	-
HSAC-AG 2:1	335.10±1.12	0.06±0.05	11.25±0.20	77.33±0.01	99.22±0.01	7.76±0.01
HSAC-AG 1:1	225.20±3.10	0.24±0.01	12.30±0.10	86.88±0.34	98.50±0.01	14.09±0.01

The size of the NPs loaded with AG, does not change respect to the diameter of the empty NPs. In particular, increasing the concentration of AG, the formulative parameters became superior. The acceptable values obtained, in terms of size, homogeneity and surface charge were constantly reproducible and suitable for systemic administration. TEM analyses confirm the data obtained by the DLS, in particular show the spherical shape of NPs Figure 28.

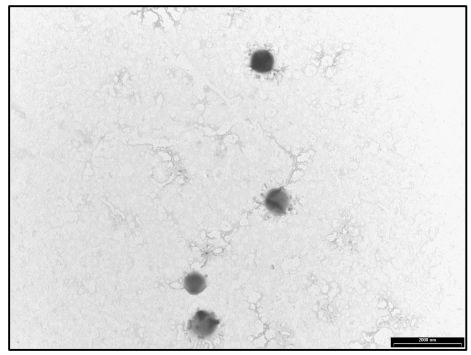

FIGURE 28: TEM ANALYSIS OF HSAC AG NPS

In order to find a safe method of preparation of NPs and according with the criteria of green chemistry, thermal cross-linking was investigated to minimize the use and the generation of unsafe substances by replacing solvents and toxic elements with biocompatible and non-toxic ones. The chemical cross-linkers glutaraldehyde was substituted by temperature. The size, the homogeneity of the sample and the ζ potential of optimized HSAT AG NPs were determined by DLS. Tem analysis confirmed the results in term of size and homogeneity and showed the spherical shape of HSAT AG NPs (Figure 29).

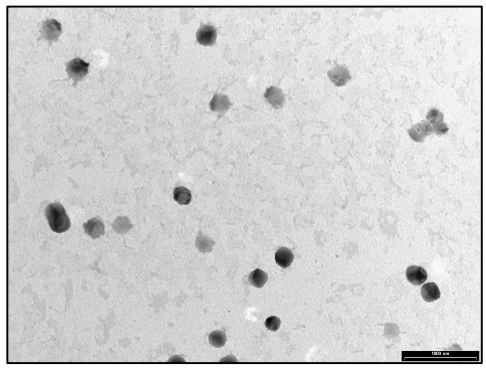

FIGURE 29: TEM ANALYSIS OF HSAT AG NPS

For analysis a dilution factor between 20 and 50 was applied. Table 17 shows the final characterization of HSAT NPs: the results in terms of size and homogeneity are reproducible and derived from the acceptable autocorrelation curves. NPs have good size distribution, with PDI around 0.2; the process yield of NPs was ≈95%. The data obtained in term of EE% and LC% are very satisfactory for all NPs developed, very high for this type of nanocarriers.

TABLE 17: CHARACTERIZATION OF HSAT NPS IN TERMS OF MEAN DIAMETER, POLYDISPERSITY, Z -POTENTIAL, YIELD OF PREPARATIVE PROCESS, ENCAPSULATION EFFICIENCY AND LOADING CAPACITY. (MEAN±SD; N=3)

HSAT NPs	Size (nm)	PDI	ζ–Potential (mV)	Yield (%)	EE%	LC%
HSAT	143.80±0.56	0.23±0.02	11.80±4.09	81.40±0.41	-	-
HSAT-AG 2:1	257.60±1.25	0.17±0.01	9.75±0.10	96.25±0.01	98.40±0.01	5.53±0.01
HSAT-AG 1:1	**202.15±6.15**	**0.17±0.01**	**10.20±0.15**	**94.65±0.45**	**98.21±0.01**	**8.50%±0.01**

The second method of preparation of HSA NPs is more safe, biocompatible and obviously easy to scale up. The result in term of characterization by DLS and TEM analysis and, of course, as EE% and LC% show comparable value, for this reason, to screen the best formulation to deliver AG in the brain, were selected the non-toxic HSAT NPs and the synthetic PECA AG NPs.

4.4.3 IN VITRO RELEASE STUDY

The test provides to comprehend the kinetics of release of the AG from the different drug delivery systems, during 24 hours. To calculate the percentage of AG released in the medium at pH 7.4 at each point time the following formula was used:

% AG released = (mg AG*t* x 100) / mg AG tot

where:

- mg AGt = mg AG released for each timepoint *t*,
- mg AG tot = mg of AG Total loaded in NPs.

NPs loaded with the higher amount of AG were selected for the test. The shows the comparison of the % of AG released to the time.

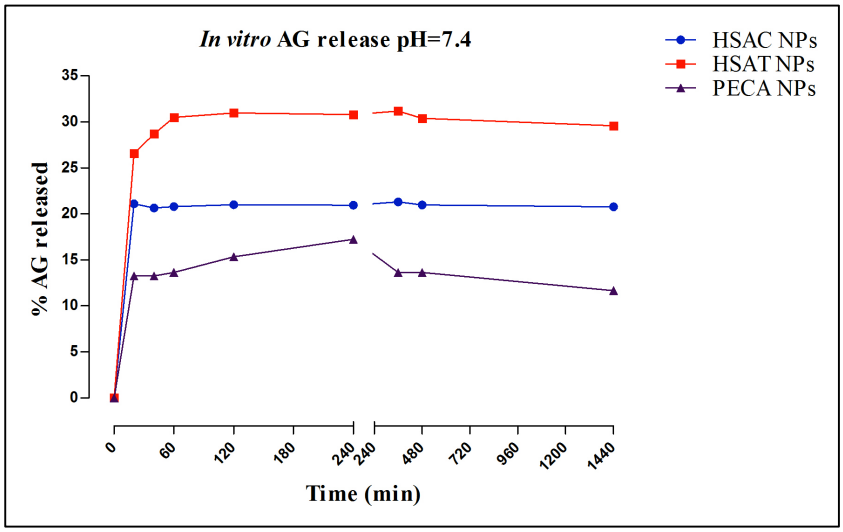

FIGURE 30: RELEASE OF AG FROM NPS IN PBS, PH 7.4. DATA DISPLAYED AS MEAN ± SD (N=3)

Controlled end sustained release of AG can be detected when the compound is entrapped into NPs, in this case is not be observed a burst effect at the beginning of test. PECA AG NPs releases the compound slowly in the first 20 minutes and then a plateau can be observed. The highest % of drug released is 17.23% ± 0.01 corresponding to about 0.50 mg of AG. In the case of HSA NPs, we can see a modulate release of AG. A plateau of concentration 40 minutes later in the case of HSAC NPs and 60 minutes in the case of HSAT NPs can be observed. The maximum amount of drug released is the 31.17% ± 0.02, corresponding to 0.55 mg for HSAT NPs and the 21.29% ± 0.01 for the HSAC NPs equal to 0.60 mg. The results indicate that the systems are able to release AG for prolonged times. The encapsulation of AG improves the solubility and consents to administer higher concentration of molecule.

4.4.4 METHOD VALIDATION

- **Chromatographic performance**

Calibration curves in the range of 10.0–2000 ng/mL were fitted by least-squares quadratic regression, and weighting factors of $1/X^2$ were applied (Table 18).

TABLE 18: CALIBRATORS AND CALIBRATION CURVE PARAMETERS FOR AG METHOD IN RHB (N=14).RESPONSE: A X CONC.^{2} + B X CONC. + C, QUADRATIC REGRESSION, WEIGHTING FACTOR $1/X^2$, ORIGINS: INCLUDED. * >15% ACCEPTANCE CRITERIA, NOT USED FOR CALCULATIONS

Run number	Nominal concentration (ng/mL)							Regression parameters			
	10.0	50.0	100	200	500	1000	2000	A	B	C	R^2
1	11.4	*61.9	*120	229	503	942	2038	-0.000000911	0.00532	0.0182	0.996
	8.88	57.4	*117	228	485	918	2108				
2	10.4	*58.7	*115	227	501	927	2089	-0.000000898	0.00525	0.0156	0.997
	9.49	55.9	111	216	457	*836	2006				
3	9.80	*61.1	114	224	484	934	*2376	-0.00000121	0.00640	0.0212	0.995
	9.50	55.6	110	216	451	*820	1866				
4	10.3	*60.1	111	227	486	974	2285	-0.00000884	0.00512	0.0154	0.997
	10.0	*61.7	113	209	482	929	1879				
5	10.4	*59.8	112	223	480	963	2109	-0.00000759	0.00491	0.0178	0.996
	9.6	*60.0	115	226	484	915	2013				
6	9.55	52.6	104	209	492	972	2065	-0.00000297	0.00341	0.00762	0.999
	9.21	56.1	110	211	499	950	1984				
7	10.6	52.3	105	199	511	996	2163	-0.00000464	0.00367	0.00758	0.998
	9.46	53.9	103	205	494	949	1884				
Mean	9.90	54.8	110	218	486	947	2038	-0.00000387	0.00487	0.0148	0.997
S.D.	0.660	1.93	3.98	9.77	16.6	25.0	120	0.00000330	0.00110	-	-
CV%	**6.66**	**3.52**	**3.62**	**4.49**	**3.41**	**2.64**	**5.89**				
RE%	**-1.00**	**9.70**	**9.85**	**8.90**	**-2.72**	**-5.26**	**1.89**				

- **Carry-over assessment**

Mean carry-over in blank RHB samples injected after the ULOQ was 0.0295 % for andrographolide and 0.00439 % for forskolin as I.S. (Table 19, for the carry-over of AG see Figure 31). Acceptance criteria from the EMA guidance[21] were

hence fulfilled (below 20 % for analyte, below 5 % for I.S.) and it was proved that carry-over did not affect precision and accuracy of the method[21].

TABLE 19: CARRY-OVER EVALUATION FOR AG AS ANALYTE, AND FOR FORSKOLIN AS I.S. (N=14)

Run number	Replicate	Peak response (counts)				Carry-over (%)		Mean Carry-over (%)	
		Blank sample		LLOQ					
		Analyte	IS	Analyte	IS	Analyte	IS	Analyte	IS
1	1	0.00	1.22	629	7996	0.00	0.0153	0.00	0.00764
	2	0.00	0.00	518	7913	0.00	0.00		
2	1	0.00	0.00	533	7636	0.00	0.00	0.00	0.00
	2	0.00	0.00	544	8329	0.00	0.00		
3	1	0.00	0.00	535	6386	0.00	0.00	0.00	0.00
	2	0.00	0.00	590	7205	0.00	0.00		
4	1	0.00	0.00	493	7235	0.00	0.00	0.00	0.00
	2	0.00	0.00	513	7897	0.00	0.00		
5	1	0.00	0.00	571	8279	0.00	0.00	0.00	0.00
	2	0.00	0.00	495	7646	0.00	0.00		
6	1	1.00	2.79	242	6035	0.412	0.0462	0.206	0.0231
	2	0.00	0.00	288	7378	0.00	0.00		
7	1	0.00	0.00	311	6692	0.00	0.00	0.00	0.00
	2	0.00	0.00	346	8187	0.00	0.00		
					Mean	**0.0295**	**0.00439**		

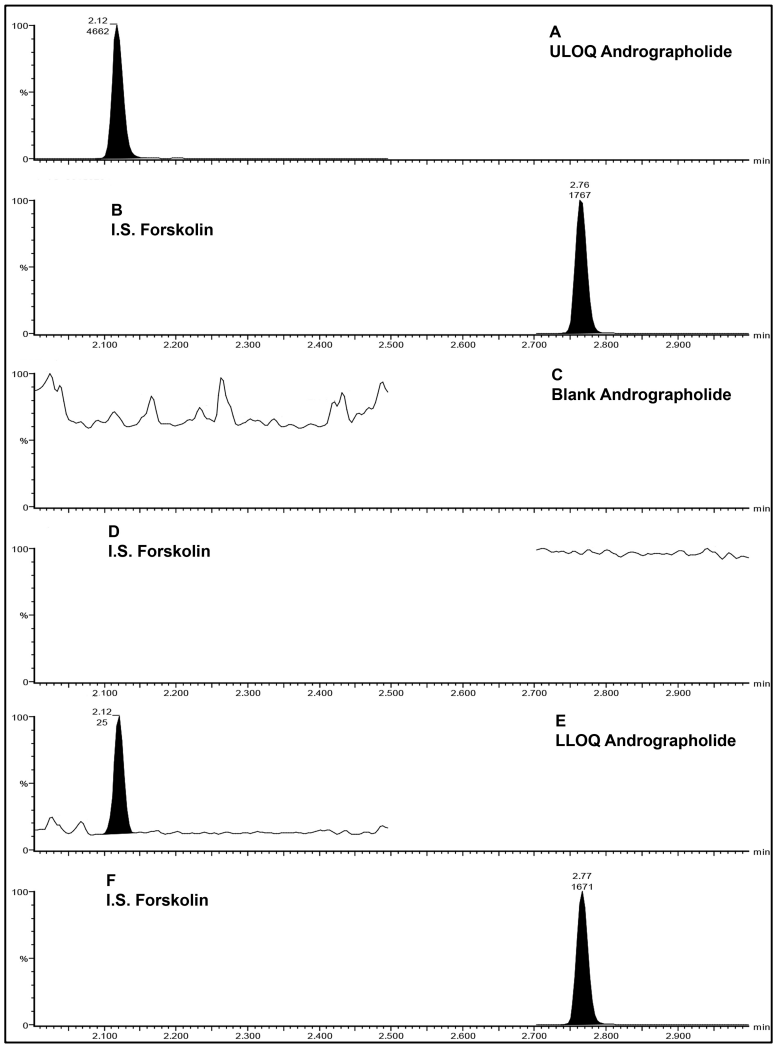

FIGURE 31: TYPICAL MRM CHROMATOGRAMS OF RHB SPIKED WITH 2000 NG/ML (ULOQ) OF AG (A), AND WITH 2000 NG/ML OF I.S. FORSKOLIN (B), OF BLANK RHB INJECTED DIRECTLY AFTER THE ULOQ AND MONITORED FOR AG (C) AND FOR I.S. FORSKOLIN (D), OF RHB SPIKED WITH 10.0 NG/ML (LLOQ) OF AG (E), AND WITH 2000 NG/ML OF I.S. FORSKOLIN (F). VALUES DISPLAYED ON TOP OF PEAKS: RETENTION TIME (MIN) AND PEAK AREA (CPS)

- **Specificity test**

Peak areas of the six blank samples (duplicates, three different batches of RHB) were equal to 0.00% of the mean peak area of the duplicates LLOQ (Table 20)

fulfilling the acceptance criteria of guidelines of industry (below 20% of LLOQ). Thus, UPLC-MS/MS method was proved to be specific for AG.

TABLE 20: SPECIFICITY TEST FOR AG, BASED ON EXTRACTED BLANK SAMPLES FROM THREE DIFFERENT BATCHES OF RHB (N=6)

Run number	Matrix Number	Peak area	LLOQ%
1	1	0.00	**0.00**
		0.00	**0.00**
	2	0.00	**0.00**
		0.00	**0.00**
	3	0.00	**0.00**
		0.00	**0.00**
	LLOQ 1	629	
	LLOQ 2	518	
	Mean	573	

- **Selectivity test**

Selectivity imprecision (CV %) for the six samples at the LLOQ (duplicates, three different RHB batches) was 6.76% (below 20 %), and inaccuracy (RE %) was 4,15% (within ± 20 %) (Table 21). Hence, the quantification method was proved to be selective for AG.

TABLE 21: SELECTIVITY TEST AT THE LLOQ FOR AG, BASED ON THREE DIFFERENT RHB BATCHES (N=6)

Nominal concentration (ng/mL)		10.0
Run number	Matrix Number	Measured conc.
4	1	10.4
		9.58
	2	8.66
		9.61
	3	8.80
		9.34
Mean		9.40
S.D.		0.636
CV%		**6.76**
RE%		**4.15**

- Intra-run and Inter-run precision assessment

Intra-run imprecision (CV %) was between 0.673 and 7.45% (below 15 %) and intra-run inaccuracy (RE %) was between -10.3 to -0.776% (within ± 15 %) at five QC levels (Table 22). Inter-run imprecision (CV %) was between 2.01 and 6.31% and inter-run inaccuracy (RE %) was between -9.10 and -1.97% at five QC levels (within ± 15 %) (Table 22). FDA/EMA requirements were hence fulfilled, and the quantification method was proved to be precise, accurate, repeatable and reproducible.

TABLE 22: INTRA-RUN (N=6) AND INTER-RUN (N=18) IMPRECISION (EXPRESSED AS CV%) AND INACCURACY (EXPRESSED AS RE%) OF CALIBRATORS AND QC SAMPLES OF AG IN RHB, BASED ON 3 SERIES OF 6 REPLICATES FOR EACH LEVEL

	LLOQ	QCL	QCM	QCH	ULOQ
Nominal concentration (ng/mL)	**10.0**	**30.0**	**1000**	**1600**	**2000**
Intra-run Mean	9.81	29.8	936	1511	1795
Intra-run S.D.	0.731	1.31	6.30	36.8	63.7
Intra-run CV%	**7.45**	**4.41**	**0.673**	**2.44**	**3.55**
Intra-run RE%	**-1.92**	**-0.776**	**-6.42**	**-5.55**	**-10.3**
Inter-run Mean	9.65	27.8	909	1485	1961
Inter-run S.D.	0.608	1.08	19.9	29.9	94.4
Inter-run CV%	**6.31**	**3.87**	**2.19**	**2.01**	**4.81**
Inter-run RE%	**-3.53**	**-7.28**	**-9.10**	**-7.19**	**-1.97**

- Dilution integrity test

For both dilution QCs diluted 10 and 100 fold, imprecision (CV %) was between 1.51 and 1.70% (below 15 %) and inaccuracy was between 8.64 % and 14.7 % (within ± 15 %) (Table 23). It could hence be proved that dilution of RHB samples up to 100-fold did not impact the precision and accuracy of the quantitative method.

TABLE 23: DILUTION INTEGRITY TEST FOR AG IN RHB AT TWO DILUTION FACTORS: 10 X AND 100 X (N = 6). *>15% ACCEPTANCE CRITERIA, USED FOR CALCULATIONS

Nominal concentration (ng/mL)	10000	10000
Dilution factor	10x	100x
Run number	Measured conc.	Measured conc.
7	10594	11522*
	10908	11771*
	10692	11280
	10982	11333
	11085	11451
	10921	11443
Mean	10864	11467
S.D.	185	173
CV%	1.70	1.51
RE%	8.64	14.7

- Extraction yield

Absolute recoveries were consistent along the quantitative range at all three levels (QCL, QCM, and QCH) AG and these recoveries (between 89.8 and 98.7%) were comparable with the recovery (97.0%) of forskolin as I.S. (Table 24 and Table 25).

TABLE 24: ABSOLUTE EXTRACTION YIELD OF AG IN RHB METHOD (N=6)

	Nominal concentration (ng/mL)					
	30.0		1000		1600	
AG	Peak ratio in processed samples	Peak ratio in unprocessed samples	Peak ratio in processed samples	Peak ratio in unprocessed samples	Peak ratio in processed samples	Peak ratio in unprocessed samples
1	0.123	0.141	3.52	3.85	4.85	4.90
2	0.134	0.146	3.49	3.89	4.93	5.00
3	0.127	0.141	3.65	3.95	4.89	4.87
4	0.132	0.140	3.40	3.86	4.66	5.09
5	0.135	0.152	3.52	3.91	5.18	5.10
6	0.137	0.144	3.47	4.00	5.07	5.01
Mean	0.131	0.144	3.51	3.91	4.93	4.99
SD	0.00532	0.00452	0.0814	0.0575	0.181	0.0942
CV%	4.05	3.14	2.32	1.47	3.67	1.89
Absolute recovery (%)	91.2		89.8		98.7	
CV%	5.12		2.75		4.13	
SD	4.67		2.46		4.07	

TABLE 25: ABSOLUTE EXTRACTION YIELD OF FORSKOLIN IN RHB METHOD (N=6)

	Internal standard conc. (ng/mL)	
	846	
Forskolin	Peak ratio in processed samples	Peak ratio in unprocessed samples
1	3.86	4.00
2	3.75	3.92
3	3.76	3.79
4	3.85	3.87
5	3.86	3.92
6	3.72	4.00
Mean	3.80	3.92
SD	0.0637	0.0820
CV %	1.68	2.09
Absolute recovery (%)	97.0	
CV%	2.68	
SD	2.60	

- **Freeze and thaw (F/T) stability test**

Imprecision (CV%) for the six replicates of QCL and of QCH subjected to three successive F/T cycles was between 2.31 and 6.94 % (below 15 %), and inaccuracy (RE %) was between -6.34 and -4.99% (within ± 15 %) (Table 26). Hence, AG was proved to be stable in RHB after three F/T cycles below -65°C.

TABLE 26: THREE SUCCESSIVE FREEZE (BELOW -65°C) AND THAW (ROOM TEMPERATURE) CYCLES STABILITY TEST IN RHB FOR AG (N = 6)

Nominal concentration (ng/mL)	30.0	1600
Run number	Measured conc.	Measured conc.
3	28.5	1415
	28.6	1501
	28.4	1519
	28.5	1453
	27.0	1719
	27.6	1514
Mean	28.1	1520
S.D.	0.649	106
CV%	**2.31**	**6.94**
RE%	**-6.34**	**-4.99**

- **Benchtop stability test at room temperature**

Imprecision (CV%) for the six replicates of QCL and QCH in RHB stored for 2 hours at RT was between 2.91 and 3.97 % (below 15%), and inaccuracy (RE%) was between 0.125 and 4.04% (within ± 15%) (Table 27). Thus, AG proved to be stable in RHB when stored for 2 hours at RT before subjection to sample preparation. AG was not stable in RHB after 4 hours at RT (data not shown).

TABLE 27: BENCHTOP STABILITY TEST OF AG IN RHB DURING 2 HOURS AT ROOM TEMPERATURE (N = 6)

Nominal concentration (ng/mL)	30.0	1600
Run number	Measured conc.	Measured conc.
2	30.2	1580
	31.0	1675
	32.7	1622
	29.9	1550
	32.7	1563
	30.7	1622
Mean	31.2	1602
S.D.	1.24	46.6
CV%	3.97	2.91
RE%	4.04	0.125

- Processed sample stability at autosampler conditions

Imprecision (CV %) for six replicates of QCL and QCH stored after extraction from RHB at autosampler conditions (10°C, protected from light) for 4 days was between 2.93 and 3.07 % (below 15 %), and inaccuracy (RE %) was between 0.802 and 6.89 % (within ± 15 %). Hence, processed RHB samples proved to be stable for 4 days at 10°C and protected from light (Table 28).

TABLE 28: AUTOSAMPLER STABILITY TEST OF PROCESSED RHB SAMPLES OF AG DURING 4 DAYS AT 10°C AND PROTECTED FROM LIGHT (N = 6)

Nominal concentration (ng/mL)	30.0	1600
Run number	Measured conc.	Measured conc.
5	32.8	1555
	32.9	1650
	33.1	1678
	31.0	1613
	31.1	1566
	31.5	1615
Mean	32.1	1613
S.D.	0.985	47.3
CV%	3.07	2.93
RE%	6.89	0.802

- **Long-term stability (LTS) below -65°C**

The slope of the calculated linear regression was 0.9372 (within 1 ± 0.15). Hence, stability of samples in RHB could be confirmed for 7 days of storage below -65°C (Figure 32).

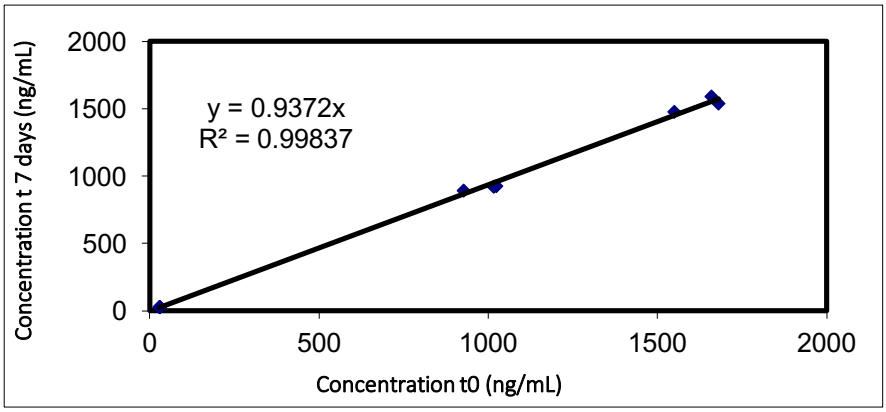

FIGURE 32: LONG-TERM STABILITY OF AG IN STORED FOR 7 DAYS BELOW -65°C

- **Stock solution stability**

Stock solutions of AG and I.S. proved to be stable for various time periods in DMSO (AG for 109 days and forskolin for 1355 days), as degradation expressed by the difference percentage was -0.996 % for AG and 0.802 % for forskolin (below 5 %) (Table 29: Stock solution stability of AG in DMSO stored below -65°C for 109 days and 2 hours at room temperature (n=6))

TABLE 29: STOCK SOLUTION STABILITY OF AG IN DMSO STORED BELOW -65°C FOR 109 DAYS AND 2 HOURS AT ROOM TEMPERATURE (N=6)

Stock solutions tested	Replicates	Peak area ratios
t=109 days	1	3.10
Old*SS AG	2	3.07
+	3	3.13
New SS I.S	4	3.10
	5	3.10
	6	3.07
Mean		3.09
S.D.		0.0224
CV%		0.724
t=0	1	3.24
New SS analyte	2	3.11
+	3	3.09
New SS I.S.	4	3.00
	5	3.02
	6	2.91
Mean		3.06
S.D.		0.110
CV%		3.60
Difference %		-0.996

* Stored below -65°C for 109 days

TABLE 30: STOCK SOLUTION STABILITY OF FORSKOLIN (I.S.) IN DMSO STORED BELOW -65°C FOR 1355 DAYS AND 2 HOURS AT ROOM TEMPERATURE (N=6)

Stock solutions tested	Replicates	Peak area ratios
t=1355days	1	0.320
Old*SS I.S.	2	0.328
+	3	0.326
New SS AG	4	0.318
	5	0.325
	6	0.328
Mean		0.324
S.D.		0.00415
CV%		1.28
t=0	1	0.309
New SS I.S.	2	0.321
+	3	0.324
New SS AG	4	0.333
	5	0.331
	6	0.343
Mean		0.327
S.D.		0.0117
CV%		3.57
Difference %		0.802

* Stored below -65°C for 1355 days

4.4.5 *IN SILICO PREDICTION OF BLOOD-BRAIN BARRIER PERMEABILITY*

The analysis of descriptors relevant for the BBB permeation (Table 31) shows that AG meets several criteria for BBB permeation: it is not too flexible (3 rotatable bonds), has a low molecular weight (MW < 450 g/mol) and a balanced lipophilicty (logP) falling into the preferred range 1.0 – 4.0 units. However, AG contains as much as five oxygen atoms (ideally the oxygen atom count should not exceed three form BBB+ drugs) accounting for its rather high molecular polar surface area (above the threshold value of 70 Å2[37,38]) clearly disfavoring BBB permeation. The QikProp model for brain/blood partitioning LogBB predicts that only a low proportion would be distributed into the brain and AG cell permeability predicted using the QikProp MDCK model is rather low, too.

TABLE 31: *IN SILICO* CALCULATIONS OF BBB PERMEATION FOR AG

	QikProp descriptors (3D based)							Marvin descriptors		
Compound	MW	Donor HB[a]	accptHB[b]	PSA (Å^2)	LogP (o/w)	LogBB[c]	QPPMDCK[e] (nm/s)	PSA (Å^2)	LogP	Rotatable bonds[d]
AG	350.5	3	8.1	100.8	1.44	-1.33	96.5	87.0	1.66	3

[a]donorHB: donor hydrogen bonds; [b]acceptor hydrogen bonds; [c]LogBB: Predicted brain/blood partition coefficient (for 95% of known drugs, values range between -3.0 and 1.2); [c]QPPMDCK: predicted apparent Madin-Darby Canine Kidney (MDCK) cell permeability in nm/s (< 25 poor, > 500 great); [d]Counting according to Veber rule

4.4.6 BLOOD-BRAIN BARRIER (BBB) DRUG PERMEABILITY ASSAYS

The first BBB drug permeability assay was done with the free form of AG at 5 μM with a co-incubation with a fluorescent barrier integrity marker NAF at 10 μg/mL as negative control. The P_{app} of AG in free form state for the apical to basolateral transport after 60 min ($P_{app\ A\to B}$) was 9.51± 0.707 x 10^{-6} cm/s (Figure 33). Compared to the $P_{app\ A\to B}$ of the negative control NAF (7.85 ± 0.188 x 10^{-6} cm/s), the free form of AG did not permeate significantly the human BBB monolayer, as confirmed by *in silico* predictions (Figure 33,Table 31). The % of recovery of AG was 85.3% in all experiments, suggesting that the obtained P_{app} value was reliable. A recovery above 80% is required for an acceptable *in vitro* prediction of P_{app} value[39]. After each permeability assay, TEER values and C_{CL} were recorded. In the case of the free form of AG, TEER values were closer to the maximum TEER values reached, indicating that the free form of AG at 5μM did not impact the cell layer integrity (Figure 33A).

The data obtained with AG 50 μM loaded into HSA NPs in term of P_{app} are reported in the Figure 33, while the TEER value and C_{CL} after and before the screening are showed in Figure 33 B. The $P_{app\ A\to B}$ of AG loaded in HSA NPs was 18.7± 3.31 x 10^{-6} cm/s (Figure 33), while the $P_{app\ A\to B}$ of the negative control NAF was 9.34 ±0.611 x 10^{-6} cm/s. These results suggest that HSA NPs AG improve the permeation of AG across the human BBB monolayer. The integrity of the barrier was preserved during the experiments as shown in Figure 33 B and recoveries for both AG and NAF were above 80 %.

In the case of PECA NPs coated with 1% of TW80 and loaded with AG at 50 μM, $P_{app\ A\to B}$ of AG was 32.6± 1.62 x 10^{-6} cm/s and $P_{app\ A\to B}$ of the negative control NAF 29.9 ±4.38 x 10^{-6} cm/s (Table 6). These data suggest that PECA NPs coated with 1% of TW80 induce a BBB disruption since low TEER values (Figure 33 C) and high Papp value of the barrier integrity marker NAF were observed. After a second exchange of culture medium which improved the removal of all TW80

traces, TEER values reached again the maximum TEER values before the assays. This temporary disturbance of the BBB monolayer integrity demonstrated that this nanocarrier appeared to be non-suitable for *in vitro* studies. Both recoveries for AG and NAF were above 80 %.

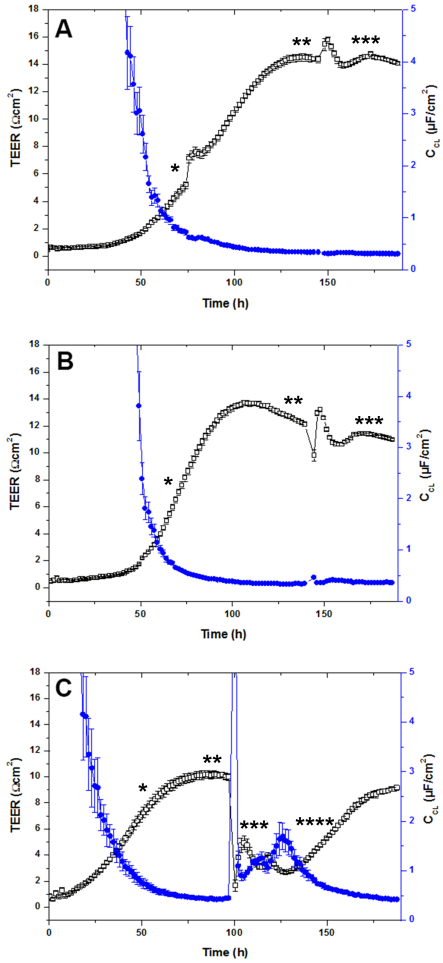

* Fresh medium exchange, **AG BBB permeability assays, *** CellZscope transferred back into incubator (37°C, 5% CO2) for barrier integrity control, **** Fresh medium exchange to discard all traces of tween 80. (A) BBB drug permeability assays with free form of AG at 5 µM and NAF at 10µg/mL, (B) BBB drug permeability assays with HSA NPs loaded with AG at 50 µM and and NAF at 10µg/mL, (C) BBB drug permeability assays with PECA NPs coated with 1% Tween 80 and loaded with AG at 50 µM and and NAF at 10µg/mL

FIGURE 33: MEAN TEER ± SD VALUES (BLACK CURVE) AND MEAN CELL LAYER CAPACITANCE (CCL) ± SD VALUES (BLUE CURVE) RECORDED IN REAL-TIME BY THE CELLZSCOPE SYSTEM OF HCMEC/D3 CELL MONOLAYERS GROWN ON 24-WELL TISSUE CULTURE INSERTS (N = 14). CCL VALUES IN THE RANGE OF 0.5–5.0 µF/CM2 INDICATE CELL CONFLUENCY AND VALIDATE TEER VALUES.

4.5 CONCLUSION

We have reported the optimization of formulative's parameters in term of size, polydispersity, surface charge, morphology and encapsulation efficacy for different types of nanocarriers able to encapsulate the neuroprotective AG, with excellent encapsulation efficiency. NPs are produced with high yield; they are easy to prepare with good reproducibility. The method of preparation of HSAT NPs is completely free of toxic agent, according with the recommendations of green-chemistry. The release of AG is controlled and sustained during one day. We developed a UPLC-MS/MS method for the analysis of AG in RHB and validated it according to EMA and FDA guidelines for industry[20,21]. Forskolin was selected as I.S. All the validation data obtained proved that the method was selective, specific, precise, accurate and capable of reproducing reliable results. A well-established immortalized mono-culture human (hCMEC/D3) BBB model was selected to test the permeability across the BBB of AG in free form and loaded in HSAT NPs and PECA NPs coated with 1% of TW80. The data obtained showed that the free form of AG did not permeate the *in vitro* BBB model, as predicted by *in silico* predictions of BBB penetration. HSAT NPs increase slightly the permeability of AG across the BBB. PECA NPs coated with 1 % of TW80 disrupt the BBB integrity, thus, further investigations are needed to improve the formulation and to clarify the real mechanism of passage across the BBB. HSAT AG NPs seem to represent a better candidate for the neurodegenerative diseases treatment. The validated UPLC-MS/MS will be used and adapted for future pharmacokinetic studies and to test the oral bioavailability of HSAT AG NPs.

4.6 REFERENCES

[1] W.M. Pardridge, The blood-brain barrier: bottleneck in brain drug development., NeuroRx. 2 (2005) 3–14. doi:10.1602/neurorx.2.1.3.

[2] Y.E. Pillay, Viness; Choonara, Advances in Neurotherapeutic Delivery Technologies Edited by Advances in Neurotherapeutic, Adv. Neurother. Deliv. Technol. (2015) 29.

[3] M. Masserini, Nanoparticles for Brain Drug Delivery, ISRN Biochem. 2013 (2013) 1–8. doi:http://dx.doi.org/10.1155/2013/238428.

[4] J. Kreuter, Drug delivery to the central nervous system by polymeric nanoparticles: What do we know?, Adv. Drug Deliv. Rev. 71 (2014) 2–14. doi:10.1016/j.addr.2013.08.008.

[5] S. Wohlfart, S. Gelperina, J. Kreuter, Transport of drugs across the blood–brain barrier by nanoparticles, J. Control. Release. 161 (2012) 264–273. doi:10.1016/j.jconrel.2011.08.017.

[6] J. Kreuter, Mechanism of polymeric nanoparticle-based drug transport across the blood-brain barrier (BBB)., J. Microencapsul. 30 (2013) 49–54. doi:10.3109/02652048.2012.692491.

[7] J. Kreuter, Nanoparticulate systems for brain delivery of drugs, Adv. Drug Deliv. Rev. 64 (2012) 213–222. doi:10.1016/j.addr.2012.09.015.

[8] J. Kreuter, V.. Petrov, D.. Kharkevich, R.. Alyautdin, Influence of the type of surfactant on the analgesic effects induced by the peptide dalargin after its

delivery across the blood–brain barrier using surfactant-coated nanoparticles, J. Control. Release. 49 (1997) 81–87. doi:10.1016/S0168-3659(97)00061-8.

[9] J. Kreuter, D. Shamenkov, V. Petrov, P. Ramge, K. Cychutek, C. Koch-Brandt, et al., Apolipoprotein-mediated transport of nanoparticle-bound drugs across the blood-brain barrier., J. Drug Target. 10 (2002) 317–25. doi:10.1080/10611860290031877.

[10] A.O. Elzoghby, W.M. Samy, N. a Elgindy, Albumin-based nanoparticles as potential controlled release drug delivery systems., J. Control. Release. 157 (2012) 168–82. doi:10.1016/j.jconrel.2011.07.031.

[11] T. Yang, H.-H. Sheng, N.-P. Feng, H. Wei, Z.-T. Wang, C.-H. Wang, Preparation of andrographolide-loaded solid lipid nanoparticles and their in vitro and in vivo evaluations: characteristics, release, absorption, transports, pharmacokinetics, and antihyperlipidemic activity., J. Pharm. Sci. 102 (2013) 4414–25. doi:10.1002/jps.23758.

[12] T. Wang, B. Liu, W. Zhang, B. Wilson, J.-S. Hong, Andrographolide reduces inflammation-mediated dopaminergic neurodegeneration in mesencephalic neuron-glia cultures by inhibiting microglial activation., J. Pharmacol. Exp. Ther. 308 (2004) 975–983. doi:10.1124/jpet.103.059683.

[13] C. Tapia-Rojas, A. Schüller, C.B. Lindsay, R.C. Ureta, C. Mejías-Reyes, J. Hancke, et al., Andrographolide activates the canonical Wnt signalling pathway by a mechanism that implicates the non-ATP competitive inhibition of GSK-3β: autoregulation of GSK-3β in vivo., Biochem. J. 466 (2015) 415–30. doi:10.1042/BJ20140207.

[14] S.J. Chan, W.S.F. Wong, P.T.H. Wong, J.S. Bian, Neuroprotective effects of andrographolide in a rat model of permanent cerebral ischaemia, Br. J. Pharmacol. 161 (2010) 668–679. doi:10.1111/j.1476-5381.2010.00906.x.

[15] F.G. Serrano, C. Tapia-Rojas, F.J. Carvajal, J. Hancke, W. Cerpa, N.C. Inestrosa, Andrographolide reduces cognitive impairment in young and mature AβPPswe/PS-1 mice., Mol. Neurodegener. 9 (2014) 61. doi:10.1186/1750-1326-9-61.

[16] A. Mukherjee, Roy, Das, Bera, Mondol, Andrographolide nanoparticles in leishmaniasis: characterization and in vitro evaluations, Int. J. Nanomedicine. (2010) 1113. doi:10.2147/IJN.S14787.

[17] A.D. Thingale, K.S. Shaikh, P.R. Channekar, U.C. Galgatte, P.D. Chaudhari, C. Bothiraja, Enhanced hepatoprotective activity of andrographolide complexed with a biomaterial, Drug Deliv. 22 (2015) 117–124. doi:10.3109/10717544.2013.871602.

[18] B.B. Weksler, E.A. Subileau, N. Perrière, P. Charneau, K. Holloway, M. Leveque, et al., Blood-brain barrier-specific properties of a human adult brain endothelial cell line., FASEB J. 19 (2005) 1872–4. doi:10.1096/fj.04-3458fje.

[19] B. Weksler, I.A. Romero, P.-O. Couraud, The hCMEC/D3 cell line as a model of the human blood brain barrier., Fluids Barriers CNS. 10 (2013) 16. doi:10.1186/2045-8118-10-16.

[20] F. and D. Administation, U.S.D. of H. and H. Services, C. for D. Evaluation, C. for V. Medicine, Guidance for Industry Bioanalytical Method Validation

Guidance for Industry Bioanalytical Method Validation, Non-Binding Recomm. by FDA. (2001) 1–25. http://www.mendeley.com/research/guidance-industry-bioanalytical-method-validation-guidance-industry-bioanalytical-method-validation-23/ (accessed November 24, 2015).

[21] European Medicines Agency, Guideline on bioanalytical method validation, EMA Guidel. 44 (2012) 1–23. doi:EMEA/CHMP/EWP/192217/2009.

[22] J. Kreuter, R.N. Alyautdin, D.A. Kharkevich, A.A. Ivanov, Passage of peptides through the blood-brain barrier with colloidal polymer particles (nanoparticles)., Brain Res. 674 (1995) 171–4. http://www.ncbi.nlm.nih.gov/pubmed/7773690 (accessed November 24, 2015).

[23] C. Weber, C. Coester, J. Kreuter, K. Langer, Desolvation process and surface characterisation of protein nanoparticles., Int. J. Pharm. 194 (2000) 91–102. doi:10.1016/S0378-5173(99)00370-1.

[24] A. Arnedo, J.M. Irache, M. Merodio, M.S. Espuelas Millán, Albumin nanoparticles improved the stability, nuclear accumulation and anticytomegaloviral activity of a phosphodiester oligonucleotide, J. Control. Release. 94 (2004) 217–227. doi:10.1016/j.jconrel.2003.10.009.

[25] M. Merodio, A. Arnedo, M.J. Renedo, J.M. Irache, Ganciclovir-loaded albumin nanoparticles: Characterization and in vitro release properties, Eur. J. Pharm. Sci. 12 (2000) 251–259. doi:10.1016/S0928-0987(00)00169-X.

[26] B. Luppi, F. Bigucci, G. Corace, A. Delucca, T. Cerchiara, M. Sorrenti, et al., Albumin nanoparticles carrying cyclodextrins for nasal delivery of the anti-

Alzheimer drug tacrine, Eur. J. Pharm. Sci. 44 (2011) 559–565. doi:10.1016/j.ejps.2011.10.002.

[27] B. Luppi, F. Bigucci, T. Cerchiara, R. Mandrioli, A.M. Di Pietra, V. Zecchi, New environmental sensitive system for colon-specific delivery of peptidic drugs, Int. J. Pharm. 358 (2008) 44–49. doi:10.1016/j.ijpharm.2008.02.009.

[28] E. Gavini, A.B. Hegge, G. Rassu, V. Sanna, C. Testa, G. Pirisino, et al., Nasal administration of carbamazepine using chitosan microspheres: in vitro/in vivo studies., Int. J. Pharm. 307 (2006) 9–15. doi:10.1016/j.ijpharm.2005.09.013.

[29] A.E. Gulyaev, S.E. Gelperina, I.N. Skidan, A.S. Antropov, G.Y. Kivman, J. Kreuter, Significant transport of doxorubicin into the brain with polysorbate 80-coated nanoparticles., Pharm. Res. 16 (1999) 1564–9. http://www.ncbi.nlm.nih.gov/pubmed/10554098 (accessed November 24, 2015).

[30] 2014 Maestro, version 9.9, Schrödinger, LLC, New York, NY.

[31] 2014 QikProp, version 4.1, Schrödinger, LLC, New York, NY.

[32] C. Marvin 15.4.13.0, 2015, Marvin 15.4.13.0, 2015, ChemAxon, http://www.chemaxon.com.

[33] D.E. Eigenmann, G. Xue, K.S. Kim, A. V Moses, M. Hamburger, M. Oufir, Comparative study of four immortalized human brain capillary endothelial cell lines, hCMEC/D3, hBMEC, TY10, and BB19, and optimization of culture conditions, for an in vitro blood-brain barrier model for drug permeability studies., Fluids Barriers CNS. 10 (2013) 33. doi:10.1186/2045-8118-10-33.

[34] K.A. Youdim, A. Avdeef, N.J. Abbott, In vitro trans-monolayer permeability calculations: often forgotten assumptions, Drug Discov. Today. 8 (2003) 997–1003. doi:10.1016/S1359-6446(03)02873-3.

[35] A. Siflinger-Birnboim, P.J. Del Vecchio, J.A. Cooper, F.A. Blumenstock, J.M. Shepard, A.B. Malik, Molecular sieving characteristics of the cultured endothelial monolayer., J. Cell. Physiol. 132 (1987) 111–7. doi:10.1002/jcp.1041320115.

[36] Y. Sano, Y. Kashiwamura, M. Abe, L.H. Dieu, J. Huwyler, F. Shimizu, et al., A stable human brain microvascular endothelial cell line retaining its barrier-specific nature, independent of the passage number, Clin. Exp. Neuroimmunol. (2012). http://edoc.unibas.ch/26290/ (accessed November 24, 2015).

[37] J. Kelder, P.D. Grootenhuis, D.M. Bayada, L.P. Delbressine, J.P. Ploemen, Polar molecular surface as a dominating determinant for oral absorption and brain penetration of drugs., Pharm. Res. 16 (1999) 1514–9. http://www.ncbi.nlm.nih.gov/pubmed/10554091 (accessed December 3, 2015).

[38] Y. Brito-Sánchez, Y. Marrero-Ponce, S.J. Barigye, I. Yaber-Goenaga, C. Morell Pérez, H. Le-Thi-Thu, et al., Towards Better BBB Passage Prediction Using an Extensive and Curated Data Set, Mol. Inform. 34 (2015) 308–330. doi:10.1002/minf.201400118.

[39] I. Hubatsch, E.G.E. Ragnarsson, P. Artursson, Determination of drug permeability and prediction of drug absorption in Caco-2 monolayers., Nat. Protoc. 2 (2007) 2111–9. doi:10.1038/nprot.2007.303.

CHAPTER 5
FINAL REMARKS

In the last years, nanotechnology is offering novel chances to enhance the therapeutic potential of poorly BBB-permeable drugs.

At the beginning of my PhD investigation, ECA was selected as synthetic monomer to made NPs, because it is less investigated then butyl cyanoacrylate, studied from many years for the synthesis of NPs from brain delivery of active compounds. Developed nanocarriers were coated with non-ionic surfactant TW80 and were produced with high yields, spherical shape and regular and narrow size distribution The *in vivo* study demonstrated the ability of NPs to cross the BBB, the biocompatibility and biodegradability of the selected monomer.
PECA-SalB NPs coated with TW80 were successfully developed and they were suitable for parental administration, with high encapsulation efficiency and a sustained release behaviour, thus, they were valuable for CNS clinical applications. These studies represented a starting point for future investigations to understand the potential application *in vivo* of PECA-SalB NPs to treat neurodegenerative disorders.

HSA was selected as material for the development of news brain delivery systems. In literature there are only few studies that report HSA NPs without surfaces modification for brain delivery. Different methods of preparations of HSA NPs, using two cross-linking methods, were developed and optimized. HSA NPs were produced with very good yields, with a sphere-like shape and reliable size distribution, suitable for systemic administration. Firstly, NPs were optimized by using a very low amount of cross-linking agent, moreover, NPs made by thermal polymerization method, according to green chemistry criteria, resulted to be superior than those obtained *via* chemical method in term of formulative parameters, safety, reduction of costs and the time necessary for NPs preparation. The *in vivo* performance of both HSA nanoparticles is comparable: NPs crossed BBB and biodistribution studies showed that did not induce inflammatory response. Further studies will be oriented to the investigation of the BBB crossing properties of the loaded HSA NPs.

The neuroprotective AG was loaded into all optimized nanocarriers, with excellent encapsulation efficiency. NPs are produced with high yield, improving the formulative's parameters in term of size, polydispersity, surface charge and

morphology. The release profile of AG showed that it is controlled and sustained during one day. For the qualitative and quantitative analysis of AG, a UPLC-MS/MS method in RHB was developed and validated according to EMA and FDA guidelines, using Forskolin as internal standard. The method was selective, specific, precise, accurate and capable to reproduce reliable results. A well-established mono-culture human (hCMEC/D3) BBB model was selected to test the permeability across the BBB of AG in free form and loaded in HSAT NPs and PECA NPs coated with 1% of TW80. AG free did not permeate the *in vitro* BBB model, as expected by *in silico* predictions of BBB penetration, while HSAT NPs increase the permeability of AG across the BBB. PECA NPs coated with 1 % of TW80 disrupt the BBB integrity, thus, further investigations are needed to improve the formulation.

HSAT AG NPs seem to represent a better candidate for the neurodegenerative diseases treatment. Future pharmacokinetic studies and bioavailability tests will be done adapting the validated UPLC-MS/MS method.

ANNEX I

DEVELOPMENT AND OPTIMIZATION OF A SIMPLE AND RAPID HPLC-DAD-MS METHOD FOR THE QUALITY CONTROL OF *CITRUS* PEELS

This work was carried out in collaboration with Maria Camilla Bergonzi[1] and Anna Rita Bilia[1]

[1]Department of Chemistry, University of Florence, via Ugo Schiff, 6, 50019 Sesto Fiorentino, Florence, Italy

I.I ABSTRACT

A chromatographic method for the qualitative and quantitative characterization of peel of different species of *Citrus* was developed in order to obtain a total evaluation of the phytocomplex and to verify the eventual content of protoalkaloids. Twenty-four constituents comprising flavones, flavanones, polymethoxyflavonoids and protoalkaloids were fully identified. Fourteen major constituents were quantified using validated HPLC method with UV–vis. The samples were analysed by HPLC-DAD and HPLC-MS, HPLC-MS/MS. The identification of the components was performed by comparing the retention times, UV-Vis and MS spectra, with these of reference standards or for comparison with the literature data. Sweet orange, lemon, mandarin and grapefruit are the analyzed matrices. Flavanones (hesperidin, naringin), flavones (lucenin-2, vicenin-2, stellarin-2, lucenin-2,4'-methylether, luteolin-7-O-rutinoside) and polymethoxyflavones (sinensetin, nobiletin, tangeretin, 3,5.6,7,8.3',4'- hepta-methoxy flavone) have been identified as the main constituents. Synephrine resulted present in all samples, except in the grapefruit.

I.II INTRODUCTION

The genus *Citrus* represents the largest sector of the world's fruit production, with more than 100 million tons produced each season, among which, the major commercially important orange fruit accounted for almost 45 million tons. Around 34% of these products were used for juice production, yielding large amounts of peels (roughly half of the fruit mass) which represent a source of molasses, pectin, and essential oil. The waste material is usually dried and sold as cattle feed, mixed with dried pulps [1].

Citrus peels have recently been considered also potential sources of other functional components, a rich source of polyphenols, in particular polymethoxyflavonoids and flavanones (mainly glycosides), having potent anti-oxidant, anti-inflammatory and antithrombogenic anti-atherogenic activities, and hypolipidemic/hypoglycaemic effects [2-12]. In addition, polymethoxyflavonoids have an antiproliferative activity [13-17]. Other health significant constituents of *Citrus* peels are phenolic acids and protoalkaloids, namely hydroxyphenethylamine alkaloids principally represented by *p*-synephrine and *p*-octopamine which are weak adrenergic agonists, active on

both α- and β-adrenoceptors, but generally orders of magnitude less active than norepinephrine [18].

Protoalkaloids have been involved in the last decade in safety issues, i.e. several reports of adverse effects due to the use of bitter orange, as a replacement for ephedra, in weight-loss dietary supplements. Synephrine and/or octopamine are speculated to play a role in the advent of such effects, mainly increasing of cardiac output and blood pressure [19]. Consequently, many health authorities of EU and non-EU countries has set a maximum limit for the daily intake of synephrine from food supplements. Therefore, the Germany's Federal Institute for Risk Assessment has set a maximum limit for the daily intake of synephrine from food supplements of 6.7 mg.

Accordingly, mostly of analytical methods reported in the literature focus on the identification of the constituents of bitter orange (*Citrus aurantium* L.). In this work other *Citrus* matrices, namely sweet orange, lemon, mandarin and grapefruit have been investigated because of their important economic value as food and feed, as a source of extracts or single constituents with medicinal and health properties.

Hence, in many regions of the world, *Citrus* peel is traditionally used for relieving stomach upset, some inflammatory syndromes and infections, and as a consequence there are official monographs of *Citrus* peels and their preparations (i.e. fluid extract, tincture, syrup). In the current European Pharmacopoeia, the oldest monograph is "Bitter orange epicarp and mesocarp" from *Citrus aurantium* L. ssp. *aurantium* (syn. *C. aurantium* L. ssp. *amara* Engl.) and the tincture produced from one part of the freshly powdered drug and 5 parts of *alcohol* (*70 per cent V/V*) by an appropriate procedure. Quality of this peel is only based on the volatile oil content (1.0-2.5 % V/m) with a main constituent, limonene (up to 90 %) [20]. In addition, there is a monograph of "Sweet orange oil" defined as essential oil obtained without heating, by suitable mechanical treatment from the fresh peel of the fruit of *Citrus sinensis* (L.) Osbeck (*Citrus aurantium* L. var. *dulcis* L.) [21]. Finally, there are two monographs of Mandarin. One is "Mandarin oil" defined as the essential oil obtained without heating, by suitable mechanical treatment, from the peel of the fresh fruit of *Citrus reticulata* Blanco [22]. The other is "Mandarin epicarp and mesocarp" defined as the dried epicarp and mesocarp of the ripe fruit of *Citrus reticulata* Blanco or its cultivars, partly free from the white spongy tissue of the mesocarp [23]. Only this *Citrus* monograph reports on the quality control

based on flavonoids, on the content of a flavanone glycoside (minimum 3.5 per cent of hesperidin) [23].

Despite the extensive pharmacological studies on the *Citrus* constituents, there are no available analytical methods able to simultaneously analyse flavones, flavanones, polymethoxyflavonoids, hydroxycynnamic acids and protoalkaloids. Up to now several analytical methods have been developed for the quantification of the content of phenethylamine alkaloids (e.g. synephrine, octopamine) in citrus peels and fruits, extracts and food supplements; most of them use chromatographic (HPLC, GC) and electrophoretic (CE) methods, including enantioselective analysis [24]. Other methods have been developed for the simultaneous characterization of protoalkaloids and organic acids [25], flavanones and protoalkaloids [26], flavanones, hydroxycinnamic acids and protoalkaloids [27], both polymethoxyflavonoids and flavonones [28], hydroxycinnamates and polymethoxylated flavones [29].

Aim of this study was to develop a simple and rapid HPLC-DAD and HPLC-MS/MS method for qualitative and quantitative standardization of all flavonoids and protoalkaloids in *Citrus* peels. The samples were analyzes by using high performance liquid chromatography (HPLC-DAD) and mass spectrometry (HPLC-MS, HPLC-MS/MS). Flavones (lucenin-2, vicenin-2, stellarin-2, lucenin-2,4'-methylether, luteolin-7-O-rutinoside), flavanones (hesperidin, naringin) and polymethoxyflavones (sinensetin, nobiletin, tangeretin, 3,5.6,7,8.3',4'- hepta-methoxyflavone) have been identified as the main constituents. Synephrine resulted present in all samples, except in the grapefruit.

I.III MATERIALS AND METHODS

I.III.I CHEMICALS

The solvents, HPLC grade acetonitrile, formic acid, dimethyl sulfoxide and methanol were purchased from Sigma-Aldrich (Steinheim, Germany) and with a purity of 96% is ethanol of HPLC grade (Riedel-de-Haën Rdh Soherchemikalien Gmbh & Co. KG Seelze, Germany). Deionized water (18 MX) was prepared by distilled water through a Milli-Q system (Millipore, Milford, MA, USA). Other reagents and chemicals are of analytical grade.

I.III.II SAMPLES OF CITRUS PEELS

Sweet orange, *Citrus sinensis* (L.) Osb. (CD 16781), lemon, *Citrus limon* (L.) Brum. fil. (R7146Z), grapefruit, *Citrus paradise* Macf (R7144Z), mandarin, *Citrus*

reticulata Blanco (R7145Z) peels were kindly offered by Amway GmbH, Puchheim, Germany.

I.III.III STANDARDS

For the qualitative and quantitative analysis of the extracts the following standards were used: naringin (naringenin-7-O-neohesperidose), hesperidin (hesperetin-7-O-rutinoside), sinensetin (3',4',5,6,7-pentamethoxyflavone), synephrine were purchased from Extrasynthèse (Genay, France), and their purity was higher than 98%.

I.III.IV HPLC/DAD/MS-MS/MS QUALITATIVE AND QUANTITATIVE ANALYSIS OF PLANT EXTRACTS

I.III.IV.I Preparation of extracts

From each peels different extract was prepared. Methanol extract of grapefruit peels was prepared by maceration of 2g of herbal drug with 100ml of MeOH 100% (thrice). Hydroalcoholic extracts of lemon and mandarin peels were prepared by maceration of 2g of herbal drugs with 100ml of EtOH:$H_2$0 70:30 (thrice), whereas hydroalcoholic extracts of sweet orange peels by maceration of 2g of peels with 100ml of EtOH:$H_2$0 80:20 (thrice). After three days, the extract were filtered and evaporated to dryness.

I.III.IV.II Sample Preparation

Dry extract were solubilized in MeOH:DMSO 4:1, ultrasonicated for 5 minutes and centrifugated for 4 min at 14.000 rpm prior to injection.

I.III.IV.III HPLC-DAD and HPLC–MS/MS analysis instrumentations

The HPLC system consisted of a HP 1100 L instrument with a Diode Array Detector and managed by a HP 9000 workstation (Agilent Technologies, Palo Alto, CA, USA). The column was a Zorbax Eclipse XDB-C18, (150 mm × 4,6 mm) with a 5 µm particle size (Agilent) maintained at 27 °C. Eluents were methanol (A), H_2O at pH 3.2 by formic acid (B) and acetonitrile (C) at a flow rate of 1 ml/min. The gradient condition was: 0–10 min, 100-85% B, 0-15% C; 10–20 min, 85–80% B, 15-10% C; 20–25 min 80–70% B, 10-20% C; 25–35 min, 70–10% B, 20-75% C; 35–40 min, 10% B, 75-80% C; 40–45 min, 10–100% B 80-0% C, with a 10 min equilibration time. Injected volume of the samples was 10 µl. The UV spectra were recorded between 200 and 600 nm. Chromatographic profiles were registered at 240, 280, 330 and 350 nm.

MS and MS/MS experiments were conducted using an HPLC Surveyor coupled to a LTQ equipped with an ESI interface (Thermo Electron, San Jose, CA, USA). Mass spectrometry and electrospray operating parameters were optimised for negative and positive polarity. ESI parameters were as follow: Sheath Gas Flow Rate (arb): 30, Aux Gas Flow Rate (arb): 9, Sweep Gas Rate (arb): 5, Capillary Temp (°C): 280.00, Capillary Voltage (V): 11.00, Tube Lents (V): 60.00, Normalised Collision Energy: 25, 20. MS spectra were acquired from *m/z* 240 to 100 in negative and in positive mode.

I.III.IV.IV Identification of peaks

Identification of marker constituents was performed by HPLC-UV, MS and MS/MS analysis by comparing the retention time, the UV, MS and MS/MS spectra of the peaks in the samples with those of authentic reference samples or literature data.

I.III.IV.V Preparation of standard solutions

Calibration curve solutions were freshly prepared by dilution of stock solutions CH_3OH/DMSO 4:1 to obtain the following concentrations: 2.285, 3.427,11.426, 13.7112 and22.852 µg/ml for hesperidin, 3.15, 1.89,1.26, 0.88, 0.25 sinensetin and 14.1, 8.46, 5.64, 3.95, 1.12 µg/ml for naringin

I.III.IV.VI Quantitative determination of constituents

The method of external standard was applied to quantify each compound. Quantification of individual constituents was performed using a regression curve, each point in triplicate. Measurements were performed at 280 and 350 nm which is the maximum absorbance for flavonoids and polymethoxyflavonoids respectively. Results were expressed as the mean ± SD of 3 separate experiments.

I.III.IV.VII Limit of detection and quantification

Limits of detection (LOD) and limits of quantification (LOQ) were determined using the linear regression equation. The LOD was defined as the lowest concentration level resulting in a peak area of three times the baseline noise (S/N=3). The LOQ was defined as the lowest concentration level resulting in a peak area of 10 times the baseline noise (S/N=10).

Synephrine, naringin, sinensetin and hesperidin were accurately weighed and dissolved in methanol. Synephrine LOD 2.46 ng; LOQ 12.3 ng. Naringin LOD 1.0

ng; LOQ 7.67 ng. Hesperidin LOD 1.32 ng; LOQ 9.86 ng. Sinensetin LOD 1.78 ng; LOQ 10.7 ng.

I.IV RESULTS AND DISCUSSION

The analytical study aimed to identify the substances present in the commercial peels of sweet orange, lemon, grapefruit, mandarin. Peels were extracted using hydroalcoholic solution for sweet orange, lemon and grapefruit and methanol for mandarin. The yields of the extraction process were 26.25%, 49.23%, 45.88% and 23.10%, respectively. The extracts were analyzed by HPLC-UV-DAD-MS for the qualitative and quantitative evaluation of the compounds of interest.

I.IV.I OPTIMIZATION OF CHROMATOGRAPHIC CONDITIONS

The selection of the chromatographic conditions was guided by the requirement for obtaining chromatograms with better resolution of adjacent peaks within a short analysis time. Formic acid was used as a mobile phase modifier, because it significantly restrained the peak tailing of phenolic acids and alkaloids in our experiments. Moreover, considering the different degrees of polarity of the compounds of the phytocomplexes, the gradient elution was used to achieve a better separation.

Under the optimum gradient conditions reported in the experimental part, the baseline separation of these peaks was achieved. As stationary phase, we tested two reverse phase columns: Zorbax® Eclipse XDB-C18 (4.6 x 150 mm, 5µm) and Vydac® C_{18}, (4.6x250 mm, 5µm). The first column has shown the best performance (Fig. 1A-1D). The optimal wavelengths for simultaneous analysis of flavones, flavanones, polymetoxyflavonoids, alkaloids and phenolic acids were set at 240 nm, 280 nm and 330 and 350 nm.

The satisfying MS response of flavones, flavanones and polymetoxyflavonoids, was mainly obtained in the negative mode, and that of alkaloids was obtained in the positive mode.

The selected ion monitoring (SIM) mode was employed to identify the target components in our experiments. The retention time, UV spectra and MS information could help identify the compounds in the plant extracts by comparison with those from authentic standards or with literature data.

I.IV.II QUALITATIVE ANALYSIS OF SWEET ORANGE PEELS

Retention times, UV-vis absorption and fragmentation profiles of MS and MS/MS of all the compounds identified in the extract of sweet orange were

showed in Table 32: altogether 10 compounds were identified (C1-C10) belonging to the chemical class of flavonoids.

TABLE 32: CONSTITUENTS OF SWEET ORANGE IDENTIFIED BY HPLC-DAD-MS AND HPLC- MS/MS

Peak	Rt	Positive ion mode	Negative ion mode	MS/MS fragmentation	UV (nm)	Identification
C1	13.0		593.4 $[M-H]^-$	593.2 $[M-H]^-$ 575.2 $[(M-H)-18]^-$ 503.1 $[(M-H)-90]^-$ 473.1 $[(M-H)-120)]^-$ 383.1 $[(M-H)-210)]^-$ 353.1 $[(M-H)-240)]^-$	271, 335	**Apigenin 6,8-di-C-glucoside (Vicenin-2)**
C2	26.3		579.4 $[M-H]^-$	579.3 $[M-H]^-$ 459.2 $[(M-H)-120)]^-$ 313.1 $[(M-H)-266)]^-$ 271.0 $[(M-H)-308)]^-$	214, 226 284, 334	**Naringin isomer**
C3	27.5	611.1$[M+H]^+$	609.4 $[M-H]^-$		228, 284, 334	**Hesperetin 7-O-rutinoside (Hesperidin)**
C4	29.3		593.4 $[M-H]^-$	285 $[(M-H)-308)]^-$	282, 330	**Isosakuranetin-7-O-neohesperidoside (Poncirin)**
C5	30.0	728.6$[M+H]^+$	726.6 $[M-H]^-$			**Citrusin III**
C6	32.0	373.4$[M+H]^+$			214,239, 269, 331	**5,6,7,3',4'-Pentamethoxyflavone (Sinensetin)**
C7	32.4	403.3$[M+H]^+$			270, 330	**Nobiletin isomer**
C8	32.8	403.3$[M+H]^+$		388.4 $[(M+H)-14]^+$ 373.3 $[(M+H)-30]^+$ 355.4 $[(M+H)-48]^+$ 313.5 $[(M+H)-90]^+$ 151.2 $[(M+H)-151]^+$	248, 270, 330	**5,6,7,8,3',4'-Examethoxyflavone (Nobiletin)**
C9	33.2	433.4$[M+H]^+$		418.4 $[8M+H)-15]^+$ 403.3 $[(M+H)-30]^+$ 165.2 $[(M+H)-268]^+$	254, 343	**3,5,6,7,8,3',4'-Eptamethoxyflavone**
C10	33.6	373.4$[M+H]^+$		358.3 $[(M+H)-15]^+$ 343.3 $[(M+H)-30]^+$ 325.3 $[(M+H)-48]^+$ 283.3 $[(M+H)-90]^+$ 151.3 $[(M+H)-222]^+$	271,336	**5,6,7,8,4'-Pentamethoxyflavone (Tangeretin)**

Next figures show the chromatographic profile (Figure 34: Chromatogram at 350 nm of Sweet orange) and TIC in positive and negative mode (Figure 35) of hydroalcoholic extract of sweet orange.

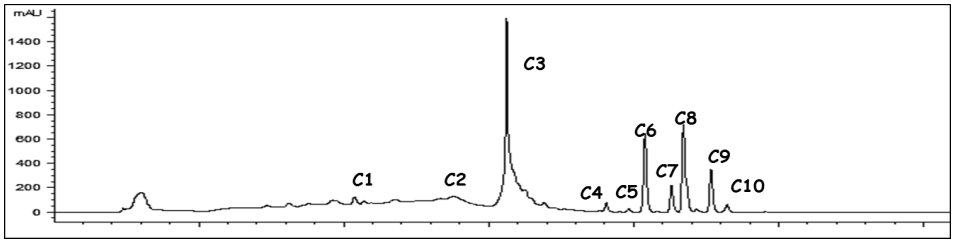

FIGURE 34: CHROMATOGRAM AT 350 NM OF SWEET ORANGE SAMPLE

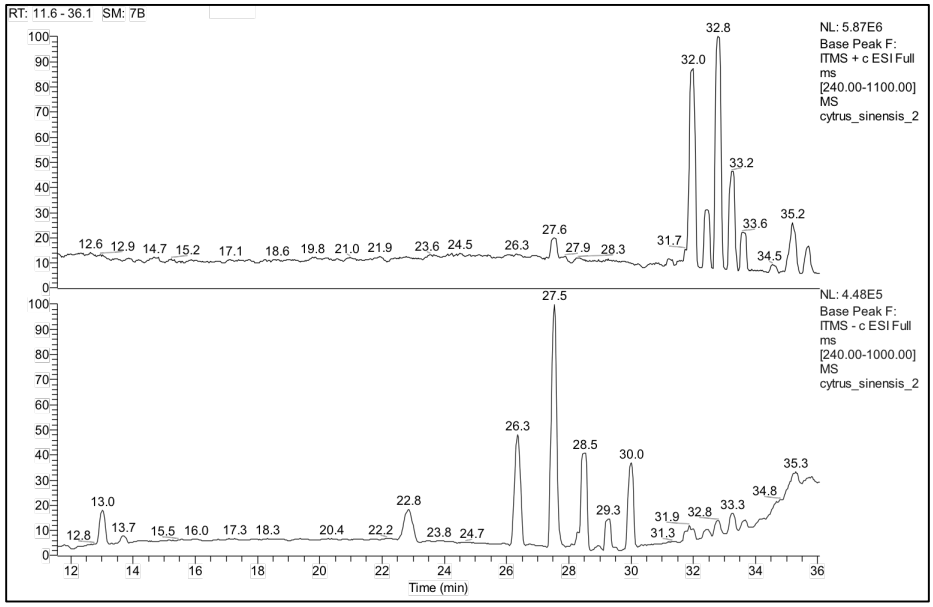

FIGURE 35: TOTAL ION CURRENT (POSITIVE TOP AND NEGATIVE BOTTOM IONIZATION) OF SWEET ORANGE SAMPLE

Vicenin-2 (PM 594) provides $[M-H]^-$ with m/z 593.4. For further confirmation, this ion was subjected to MS/MS investigation to produce secondary fragments (575 $[(M-H)-18]^-$, 503 $[(M-H)-90]^-$, 473 $[(M-H)-120)]^-$, 383 $[(M-H)-210)]^-$, 353 $[(M-H)-240)]^-$), which were in agreement with those previously reported in the literature [30-31]. The compound C2, with R*t* of 26.3 minutes, is a structural isomer of naringin (R*t* = 27.3). The MS spectrometry generates the ion with m/z 579.4 characteristic of both. Finally, as a further confirmation, the MS/MS analysis produces the same pattern of fragmentation that naringin 579 $[M-H]^-$, 459 $[(M-H)-120)]^-$, 313 $[(M-H)-266)]^-$, 271 $[(M-H)-308)]^-$ [32]. Among these fragments the most abundant resulted m/z 271.0 $[M-H]^-$, probably due to structural differences between the isomers that make this bond cleavage more

probable that the fragment with m/z 459.2, typical of naringin. The cleavage consists in the loss of the sugar (rutinose) with formation of a fragment corresponding to the aglycone naringenin. The peaks at 27.5, 32.0 minutes were identified as hesperidin (C3) and sinensetin (C6) for comparison with the standards. The next compound at 29.3 min was attributed to poncirin (C4), by comparison with UV and mass spectra. The negative ionization generates an ion with m/z 593.4 $[M-H]^-$. In fact, even if the vicenin-2, present in sweet orange, has the same molecular weight and it can generate this ion, the confirmation comes from the comparison with the literature data [28] and from different time elution and MS/MS data. Poncirin generates essentially the ion with m/z 285.2, resulting from the bond cleavage of the sugar and loss of neohesperidose (m/z 308), leaving the aglycone isosakuranetina (m/z 285[(M-H)-308)]). This ion is not observed in the case of vicenin-2 because, in this case the fragments characteristic are due to the sugars ring opening. The peak at 30.0 minutes is the superposition of three substances with m/z 726.6 [M-H]-, 696.6 $[M-H]^-$ and 711.2 $[M-H]^-$. Among these, the only possible identification was that of the ion with m/z 726.6 attributed to Citrusina III (C5), a cyclic peptide consisting of seven aminoacids: Gly-Ser-Pro-Leu-Leu-Pro-Tyr. The compount at 32.0 min is the sinensetin (C6), confirmed by comparison with the standard. The peak at 32.4 minutes is a structural isomer of nobiletin (C7), with the same UV spectrum and the same ions generates in positive mode (*m/z* 403.3 $[M+H]^+$; *m/z*: 388.4 $[(M+H)-14]^+$; 373.3 $[(M+H)-30]^+$; 355.4 $[(M+H)-48]^+$; 313.5 $[(M+H)-90]^+$; 151.2 $[(M+H)-151]^+$. Nobiletin was identified at 33.8 min. (C8). The C9 peak with R*t* of 33.2 min corresponds to 3,5,6,7,8,3',4'-eptametossiflavone as can be evidenced by its characteristic UV and MS spectrum [33]. The last compound identified in sweet orange was the tangeretin C10 (R*t* 33.6 min). In fact, comparing its UV, MS, MS–MS data and retention time to that already described, it was possible to obtain unambiguous structural assignment [33].

I.IV.III QUALITATIVE ANALYSIS OF LEMON PEELS

In lemon matrix 11 compounds were identified (L1-L11) belonging to the chemical class of flavonoids, as reported in Table 33:Constituents of Lemon identified by HPLC-DAD-MS and HPLC-MS/MS.

TABLE 33:CONSTITUENTS OF LEMON IDENTIFIED BY HPLC-DAD-MS AND HPLC-MS/MS

Peak	Rt	Positive mode	Negative mode	MS/MS fragmentation	UV (nm)	Identification
L1	11.9		609.4 $[M-H]^-$		270, 349	**Luteolin-6,8-di-C-glucoside (Lucenin-2)**
L2	13.0		593.2 $[M-H]^-$	593.2 $[M-H]^-$ 575.2$[(M-H)-18]^-$ 503.1$[(M-H)-90]^-$ 473.1$[(M-H)-120)]^-$ 383.1$[(M-H)-210)]^-$ 353.1$[(M-H)-240)]^-$	271, 335	**Apigenin 6,8-C-di-glucoside (Vicenin-2)**
L3	13.7		623.4 $[M-H]^-$	623.5$[M-H]^-$ 605.4$[(M-H)-18)]^-$ 533.4$[(M-H)-90)]^-$ 503.3$[(M-H)-120)]^-$ 413.4$[(M-H)-210)]^-$ 383.3$[(M-H)-240)]^-$	271, 348	**Diosmetin 6,8-di-C-glucoside (Lucenin-2,4'-methylether)**
L4	14.4		623.4 $[M-H]^-$	623.4$[M-H]^-$ 605.4$[(M-H)-18)]^-$ 533.4$[(M-H)-90)]^-$ 503.3$[(M-H)-120)]^-$ 413.3$[(M-H)-210)]^-$ 383.3$[(M-H)-240)]^-$	271, 347	**Chrysoeriol 6,8-di-C-glucoside (Stellarin-2)**
L5	22.1		595.3 $[M-H]^-$		283, 325	**Eriodictyol 7-O-neohesperidoside (Neoriocitrin)**
L6	24.5		593.4 $[M-H]^-$		260, 292, 350	**Luteolin-7-O-rutinoside**
L7	26.3	581.0 $[M+H]^+$	579.4 $[M-H]^-$	579.3$[M-H]^-$ 459.2$[(M-H)-120)]^-$ 313.1$[(M-H)-266)]^-$ 271.0$[(M-H)-308)]^-$	287, 324	**Naringin isomer**
L8	27.5	611.1 $[M+H]^+$	609.3 $[M-H]^-$		284, 326	**Hesperetin 7-O-rutinoside (Hesperidin)**
L9	32.9	403.4 $[M+H]^+$		388.4$[(M+H)-14]^+$ 373.3$[(M+H)-30]^+$ 355.4$[(M+H)-48]^+$ 313.5$[(M+H)-90]^+$ 151.2$[(M+H)-151]^+$	248, 270, 330	**5,6,7,8,3',4'-pentamethoxyflavone (Nobiletin)**
L10	33.3	433.4 $[M+H]^+$		418.4$[(M+H)-15]^+$ 403.3$[(M+H)-30]^+$ 165.2$[(M+H)-268]^+$	254, 343	**3,5,6,7,8,3',4'-eptamethoxyflavone**
L11	33.7	373.4 $[M+H]^+$		358.3$[(M+H)-15]^+$ 343.3$[(M+H)-30]^+$ 325.3$[(M+H)-48]^+$ 283.3$[(M+H)-90]^+$ 151.3$[(M+H)-222]^+$	271, 336	**5,6,7,8,4'-pentamethoxyflavone (Tangeretin)**

Next figures show the chromatographic profile (Figure 36) and TIC of positive and negative ionization (Figure 37)of hydroalcoholic extract of Lemon.

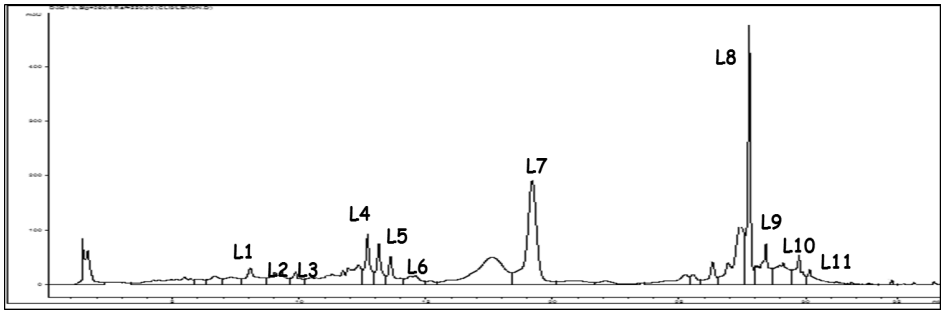

FIGURE 36: CHROMATOGRAM AT 350 NM OF LEMON SAMPLE

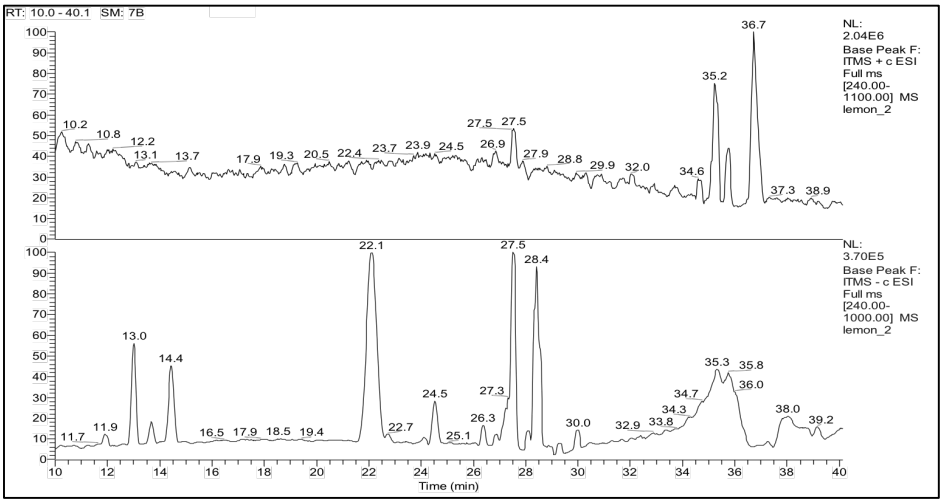

FIGURE 37: TOTAL ION CURRENT (POSITIVE AND NEGATIVE IONIZATION) OF LEMON SAMPLE

The peaks at 13.0, 26.3, 27.5, 32.9, 33.3, and 33.7 minutes correspond to compounds already identified in the sweet orange peels (Table 1). New peaks are L1 and L3 corresponding to lucenin-2 and lucenin-2,4'-methylether. Lucenin-2 showed a retention time of 11.9 minutes, identified with UV spectrum and with MS/MS analysis. Lucenin-2 generates a m/z 609.4 $[(M-H)^-]$. Others the fragments identified were: 591 $[(M-H)\ -18]^-$, 519 $[(M-H)-90]^-$, 489 $[(M-H)-120]^-$, 399 $[(M-H)-210]^-$, 369 $[(M-H)]^-240]^-$ [31]. The next compound L3 is the Lucenin-2,4'-methylether, confirmed by the characteristic UV spectrum UV, MS, MS–MS data and retention time [30-31]. The peak at 14.4 minutes corresponds to stellarin-2 (chrysoeriol 6,8-di-C-glucoside) (L4) as confirmed by UV spectrum

analysis and MS results [32]. The substance L5 (Rt: 22.1 min) was identified as the neoeriocitrin. From the MS/MS data, three ions were present: 595.3 $[M-H]^-$, 287.2 $[(M-H)-308]^-$, 459 $[(M-H)-136]^-$. The main signal is $[M-H]^-$ with m/z equal to 595.3 and $[(M-H)-308]^-$ 287.2. This compound is the aglyconeeriodictyol, resulting from the loss of the disaccharide neoesperidose. Literature data [31] report that the neoeriocitrin (a neohesperidoside) is able to form the fragment m/z 459 $[(M-H)-136]^-$ which is not observed for another compound, named eriotricin (a rutinoside), that presents same molecular weight and UV spectrum. The loss of a fragmentor of m/z 136 may correspond to a back-cyclization that involves the aglycone. The following peaks, with retention time of 24.5 and 27.5 minutes, were attributed to luteolin 7-O-rutinoside (L6) and hesperidin (L8), respectively.

I.IV.IV Qualitative analysis of Grapefruit peels

In the extract of *Grapefruit* three peaks have identified, (G1-G3) belonging to the chemical class of flavonoids, as showed in the Table 34.

Table 34: Constituents of Grapefruit identified by HPLC-DAD-MS and HPLC-MS/MS

Peak	Rt	Negative mode	MS/MS fragmentation	UV (nm)	Identification
G1	26.6	579.4 $[M-H]^-$	579.3$[M-H]^-$ 459.2$[(M-H)-120)]^-$ 313.1$[(M-H)-266)]^-$ 271.0$[(M-H)-308)]^-$	214, 226 284, 334	**Naringin isomer**
G2	27.3	579.4 $[M-H]^-$	579.3$[M-H]^-$ 459.2$[(M-H)-120)]^-$ 313.1$[(M-H)-266)]^-$ 271.0$[(M-H)-308)]^-$	214, 226 284, 334	**Naringenin 7-O-neoesperidoside (Naringin)**
G3	29.5	593.4 $[M-H]^-$		282, 330	**Isosakuranetin-O-neohesperidoside (Poncirin)**

In Figure 38 and Figure 39 we can observe the chromatographic profile and mass spectra in positive and negative ionization of an hydroalcoholic extract. G1, at 26.6 minutes, is a derivative of naringenin, already identified in the previous matrices. To prove that the molecule was an isomer of naringin was performed a standard addition of to hydroalcoholic extract of *Grapefruit*; naringenin has a retention time of 27.3 minutes.

The last molecule identified, with a retention time of 29.3 minutes, is poncirin G3 (R*t* = 29.3).

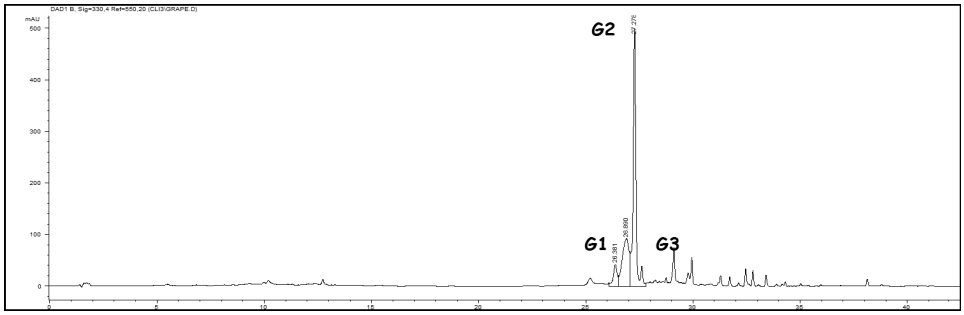

FIGURE 38: CHROMATOGRAM AT 350 NM OF GRAPEFRUIT SAMPLE

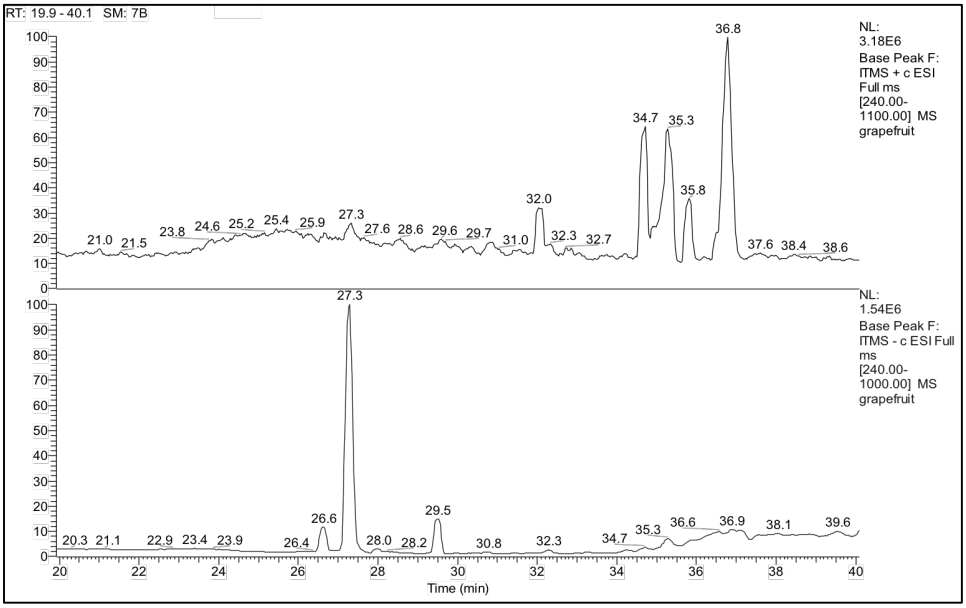

FIGURE 39: TOTAL ION CURRENT (POSITIVE AND NEGATIVE IONIZATION) OF GRAPEFRUIT SAMPLE

I.IV.V QUALITATIVE ANALYSIS OF MANDARIN PEELS

In *Mandarin peels,* 9 flavonoids (M1-M9) were identified, as reported in Table 35 .

TABLE 35:CONSTITUENTS OF MANDARIN IDENTIFIED BY HPLC-DAD-MS AND HPLC-MS/MS

Peak	Rt	Positive ion mode	Negative ion mode	MS/MS Fragmentation	UV (nm)	Identification
M1	12.9		593.2[M-H]$^-$	593.2[M-H]$^-$ 575.2[(M-H)-18]$^-$ 503.1[(M-H)-90]$^-$ 473.1[(M-H)-120)]$^-$ 383.1[(M-H)-210)]$^-$ 353.1[(M-H)-240)]$^-$	271, 335	**Apigenin 6,8-di-C-glucoside (Vicenin-2)**
M2	26.5		579.2[M-H]$^-$	579.3[M-H]$^-$ 459.2[(M-H)-120)]$^-$ 313.1[(M-H)-266)]$^-$ 271.0[(M-H)-308)]$^-$	214, 226 284, 334	**Naringin isomer**
M3	27.3	581.0[M+H]+	579.2[M-H]$^-$	579.3 [M-H]$^-$ 459.2 [(M-H)-120)]$^-$ 313.1 [(M-H)-266)]$^-$ 271.0 [(M-H)-308)]$^-$	214, 226 284, 334	**Naringenin-7-o-neohesperidoside (Naringin)**
M4	27.6		609.2[M-H]$^-$		228, 284, 334	**Hesperetin 7-O-rutinoside (Hesperidin)**
M5	29.3	595.0[M+H]$^+$	593.2[M-H]$^-$		282, 330	**Isosakuranetin-O-neohesperidoside (Poncirin)**
M6	32.0	373.0[M+H]$^+$			214,23 9, 269, 331	**5,6,7,3',4'-pentamethoxyflavone (Sinensetin)**
M7	32.8	403.2[M+H]$^+$		388.4[(M+H)-14]$^+$ 373.3[(M+H)-30]$^+$ 355.4[(M+H)-48]$^+$ 313.5[(M+H)-90]$^+$ 151.2[(M+H)-151]$^+$	248, 270, 330	**5,6,7,8,3',4'-esamethoxyflavone (Nobiletin)**
M8	33.2	433.3[M+H]$^+$		418.4[8M+H)-15]$^+$ 403.3[(M+H)-30]$^+$ 165.2[(M+H)-268]$^+$	254, 343	**3,5,6,7,8,3',4'-eptamethoxyflavone**
M9	33.6	373.2[M+H]$^+$		358.3 [(M+H)-15]$^+$ 343.3 [(M+H)-30]$^+$ 325.3 [(M+H)-48]$^+$ 283.3 [(M+H)-90]$^+$ 151.3 [(M+H)-222]$^+$	271,33 6	**5,6,7,8,4'-pentamethoxyflavone (Tangeretin)**

All compounds were also found in previous matrices and their structure has been identified as previously reported. In Figure 40 and Figure 41 we can observe the chromatographic profile and mass spectra in positive and negative mode of methanol extract.

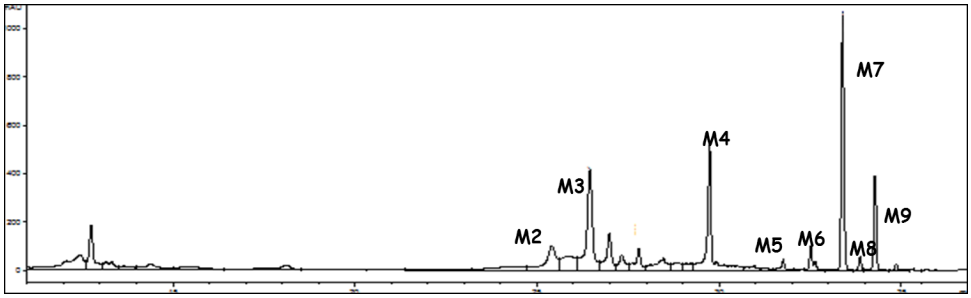

FIGURE 40: CHROMATOGRAM AT 350 NM OF MANDARIN SAMPLE

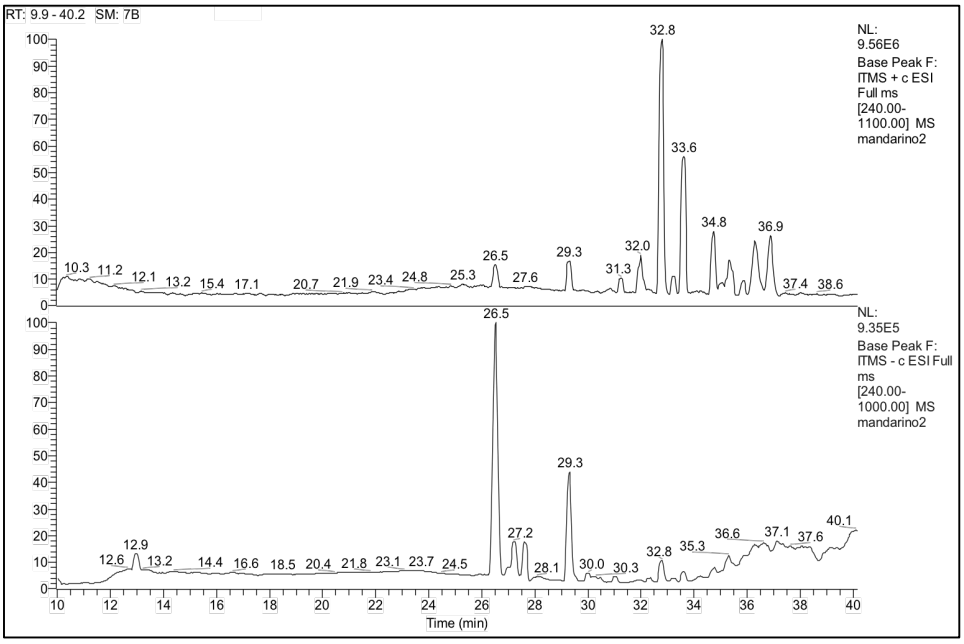

FIGURE 41: TOTAL ION CURRENT (POSITIVE AND NEGATIVE IONIZATION) OF MANDARIN SAMPLE

I.IV.VI IDENTIFICATION OF SINEPHRINE

Identification of alkaloid synephrine in the four extracts was also performed. In Figure 42 the comparison of HPLC-MS chromatograms were reported. The HPLC-DAD analysis has not made possible the identification of the compound because it resulted below the LOD. The identification of synephrine was obtained by comparing the retention times and by mass spectra of the reference standard ($[M+H]^+$ m/z 168). The molecule was present in mandarin, in

sweet orange and lemon while it is absent in grapefruit, as reported in the literature [34].

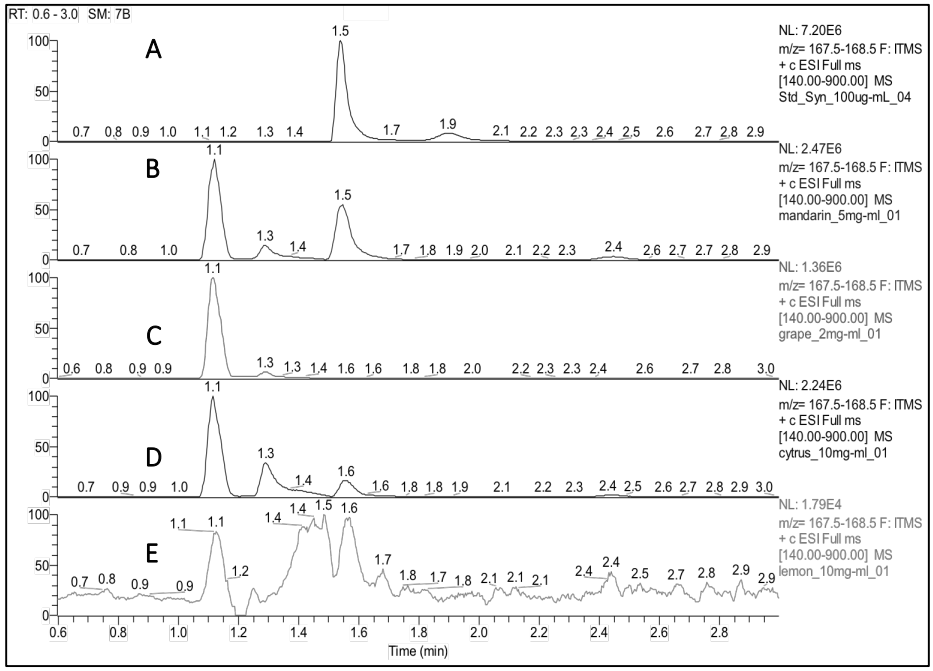

FIGURE 42: TOTAL ION CURRENT (POSITIVE IONIZATION) OF SYNEPHRINE STANDARD (A), MANDARIN (B), GRAPEFRUIT (D), SWEET ORANGE (E) AND LEMON (F) SAMPLES

I.IV.VII QUANTITATIVE ANALYSIS OF CONSTITUENTS OF PEELS' MATRICES

Grapefruit extract was the matrix with the highest content of total flavonoids (29.93%±3.25 of flavonoids and 1.36%±0.07 of polymethoxyflavonoids), while *mandarin* extract was richer in polymethoxyflavonoids (15.85%±1.79 of flavonoids and 11.55%±1.32 of polymethoxyflavonoids). The contents in *lemon* extract were 10.12%±0.98 and 0.11%±0.02 of flavonoids and polymethoxyflavonoids, respectively. *Sweet orange* resulted the poorest matrix (3.11%±0.75 of flavonoids and 2.10%±0.58 of polymethoxyflavonoids).

I.V CONCLUSIONS

The presence of polyphenols in the pericarp of some species of *Citrus*, in particular of polymethoxyflavonoids and flavonoid glycosides, with different biological activities, i.e. anti-oxidant and anti-inflammatory, have made interesting the waste from the processing of *Citrus* fruits. In this study, analytical

studies on different species of *Citrus* peels were performed in order to develop a method for the evaluation of the total phytocomplex.

Peels of four species of *Citrus*: *C. sinensin, C. limon, C. paradisii* and C. *reticulata* were considered to evaluate in particular the profile of flavonoids and the absence of synephrine and any other compounds could be related to safety.

The developed analytical method is suitable for the evaluation of all the non-volatile constituents of the peel of *Citrus*. In all tested samples the main constituents were *O*-glycosilated flavanones (hesperidin, naringin, neoeriocitrin), flavones (lucenin-2, 2-vicenin, stellarin-2, lucenin-2,4'-methyl, luteolin-7-O-rutinoside) and polymethoxyflavonoids (sinensetin, nobiletin, tangeretin, 3,5,6,7,8,3', 4'-eptametoxyflavone) and phenolic acids, while amines such as synephrine and octapamin were absent or at the limit of detection. The developed method is applicable to quality control of *Citrus* peels, or their extracts or their commercial preparations to support also their safety.

I.VI REFERENCES

[1] Khan, M.K.; Abert-Vian, M.; Fabiano-Tixier, A.S.Dangles, O.; Chemat F. Ultrasound-assisted extraction of polyphenols (flavanone glycosides) from orange (*Citrus sinensis* L.) peel. *Food Chemistry*. 2010, *119*, 851–858.

[2] Chen, Z.T.; Chu, H.L.; Chyau, C.C.; Chu, C.C.; Duh. P.D. Protective effects of sweet orange (*Citrus sinensis*) peel and their bioactive compounds on oxidative stress. *Food Chemistry.* 2012, *135,* 2119–2127.

[3] Whitman, S.C.; Kurowska, E.M.; Manthey, J.A.; Daugherty, A. Nobiletin, a citrus flavonoid isolated from tangerines, selectively inhibits class A scavenger receptor-mediated metabolism of acetylated LDL by mouse macrophages. *Atherosclerosis.* 2005, *178*, 25-32.

[4] Lin, N.; Sato, T.; Takayama, Y.; Mimaki, Y.; Sashida, Y.; Yano, M.; Ito, A. Novel antiinflammatory actions of nobiletin, a citrus polymethoxy flavonoid, on human synovial fibroblasts and mouse macrophages. *Biochemical Pharmacology*. 2003, *65*, 2065-2071.

[5] Huang, Y.S.; Ho, S.C. Polymethoxy flavones are responsible for the anti-inflammatory activity of citrus fruit peel. *Food Chemistry.* 2010, *119,* 868-873.

[6] Li, R.W.; Theriault, A.G.; Au, K.; Douglas, T.D.; Casaschi, A.; Kurowska, E.M.; Mukherjee, R. Citrus polymethoxylated flavones improve lipid and glucose homeostasis and modulate adipocytokines in fructose-induced insulin resistant hamsters. *Life Science*. 2006, *79*, 365-373.

[7] Kurowska, E.M.; Manthey, J.A. Hypolipidemic effects and absorption of citrus polymethoxylated flavones in hamsters with diet-induced hypercholesterolemia. *Journal of Agricolture and Food Chemistry*. 2004, *52*, 2879-2886.

[8] Green , C.O.; Wheatley, A.O.; Mcgrowder, D.A.; Dilworth, L.L.; Asemota, H.N. Citrus peel polymethoxylated flavones extract modulates liver and heart function parameters in diet induced hypercholesterolemic rats. *Food and Chemical Toxicology.* 2013, *51*, 306-309.

[9] Kang, S.R.; Park, K.I.; Park , H.S.; Lee , D.H.; Kim , J.A.; Nagappan , A.; Kim , E.H.; Lee , W.S.; Shin , S.C.; Park , M.K.; Han, D.Y.; Kim, G.S. Anti-

inflammatory effect of flavonoids isolated from Korea Citrus aurantium L. on lipopolysaccharide-induced mouse macrophage RAW 264.7 cells by blocking of nuclear factor-kappa B (NF-jB) and mitogen-activated protein kinase (MAPK) signalling pathways. *Food Chemistry.* 2011, *129*, 1721-1728.

[10] Oboh, G.; Ademosuni A.O. Phenolic-rich extracts from orange peels (*Citrus sinensis*) inhibit key enzymes linked to non-insulin dependent diabetes mellitus (NIDDM) and hypertension*. La rivista italiana delle sostanze grasse*. 2011, *88.*

[11] Kim, G.S.; Park, H.J.; Woo1, J.H.; Kim, M.K.; Koh, P.O.; Min, W.; Ko, Y.G.; Kim, C.H.; Won, C.K.; Cho, J.H. Citrus aurantium flavonoids inhibit adipogenesis through the Akt signaling pathway in 3T3-L1 cells. BMC *Complementary and Alternative Medicine*. 2012, *12*.

[12] Li, S.; Pan, M.H.; Lo, C.Y.; Tan, D.; Wang, Y., Shahidi, F., Ho. C.T. Chemistry and health effects of polymethoxyflavones and hydroxylated polymethoxyflavones. *Journal of Functional Foods*. 2009, *1*, 2-12.

[13] Manthey, J. A.; Guthrie, N.; Grohmann, K. Biological properties of citrus flavonoids pertaining to cancer and inflammation. *Current Medicinal Chemistry*. 2001, 8, 135-153.

[14] Benavente-García, O.; Castillo, J. Update on uses and properties of *Citrus* flavonoids: new findings in anticancer, cardiovascular, and anti-inflammatoryactivity. *Journal of Agricultural and Food Chemistry*. 2008. 56, 6185-6205.

[15] Yoshimizu, N.; Otani, Y.; Saikawa, Y.; Kubota, T.; Yoshida, M.; Furukawa, T.; Kumwi, K.; Kameyama, K.; Fujii, M.; Yano, M.; Sato, T.; Ito, A.; Kitajima, M. Antitumor effects of nobiletin, a citrus flavonoid, on gastric cancer include: antiproliferative effects, induction of apoptosis and cell cycle deregulation. *Alimentary Pharmacology Therapeutics Journal*. 2004, *20* (Suppl. 1), 95-101.

[16] Du, Q., Chen, H. The methoxyflavones in *Citrus reticulata* Blanco cv. Ponkan and their antiproliferative activity against cancer cells. *Food Chemistry.* 2010, *119*, 567-572.

[17] Righeschi, C.; Eichhorn, T.; Karioti, A.; Bilia, A.R.; Efferth, T. Microarray-based mRNA Expression Profiling of Leukemia Cells Treated with the Flavonoid Casticin. *Cancer genomics & proteomics*. 2012, *9*, 143-151.

[18] Jordan, R.; Midgley, J.M.; Thonoor, C.M.; Williams, C.M. β-Adrenergic activities of octopamine and synephrine stereoisomers on guinea-pig atria and trachea. *Journal of Pharmacy and Pharmacology.* 1987, *39*, 752-754.

[19] Stohs, S.J. Assessment of the adverse event reports associated with *Citrus aurantium* (bitter orange) from April 2004 to October 2009. *Journal of Functional Food.* 2010, *2*, 235-238.

[20] Bitter orange epicarp and mesocarp (Aurantii amari epicarpium and mesocarpium). In: *European Pharmacopoeia*. 7th Edition. Council of Europe, Strasburg, pp 1077-1078.

[21] Sweet orange oil (Aurantii dulcis olii). In: *European Pharmacopoeia*. 7th Edition. Council of Europe, Strasburg, pp 1249-1250.

[22] Mandarin Oil (Citri reticulatae aetheroleum). In: *European Pharmacopoeia*. 8th Edition. Council of Europe, Strasburg, pp. 1308-1309.

[23] Mandarin epicarp and mesocarp (Citri reticulatae epicarpium and mesocarpium). In: *European Pharmacopoeia*. 8th Edition. Council of Europe, Strasburg, pp. 1307-1308

[24] Pellati, F.; Benvenuti, S. Chromatographic and electrophoretic methods for the analysis of phenethylamine alkaloids in Citrus aurantium. *Journal of Chromatography A.* 2007, *116*, 71-88.

[25] Uckooa, R.M.; Jayaprakashaa, G.K.; Nelsonb, S.D.; Patil, B.S. Rapid simultaneous determination of amines and organic acids in citrus using high-performance liquid chromatography. *Talanta*. 2011, *83*, 948-954.

[26] Ding, L.; Luo, X.; Tang, F.; Yuan, J.; Liu, Q.; Yao, S. Simultaneous determination of flavonoid and alkaloid compounds in Citrus herbs by high-performance liquid chromatography–photodiode array detection–electrospray mass spectrometry. *Journal of Chromatography B*. 2007, *857*, 202-209.

[27] He, D.; Shan, Y.; Wu, Y.; Liu, G.; Chen, B.; Yao, S. Simultaneous determination of flavanones, hydroxycinnamic acids and alkaloids in citrus fruits by HPLC-DAD–ESI/MS. *Food Chemistry*. 2011, *127,* 880-885.

[28]Zheng, G.D.; Zhou , P.; Yang , H.; Li , Y.; Li , P.; Liu, E. Rapid resolution liquid chromatography–electrospray ionisation tandem mass spectrometry method for identification of chemical constituents in Citri Reticulatae Pericarpium. *Food Chemistry.* 2013*, 136*, 604-611.

[29]Manthey, J.A.; Grohmann, K. Phenols in citrus peel byproducts. Concentrations of hydroxycinnamates and polymethoxylated flavones in citrus peel molasses. *Journal of Agriculture and Food Chemistry*. 2001,*49*, 3268-3273.

[30]Gattuso, G.; Caristi, C.; Gargiulli, C.; Bellocco, E.; Toscano, G.; Leuzzi, U. Flavonoid Glycosides in Bergamot Juice (Citrus bergamia Risso). *Journal of Agriculture and Food Chemistry*. 2006, *54*, 3929-3935.

[31]Zhou, D.; Xu, Q.;.Xue, X.; Zhang, F.; Liang, X. Identification of O-diglycosyl flavanones in *Fructus aurantii* by liquid chromatography with electrospray ionization and collision-induced dissociation mass spectrometry. *Journal of Pharmaceutical and Biomedical Analysis.* 2006, *42*, 441–448.

[32]Shi, P.; He, Q.; Song, Y.; Qu, H.; Cheng, Y. Characterization and identification of isomeric flavonoid O-diglycosides from genus Citrus in negative electrospray ionization by ion trap mass spectrometry and time-of-flight mass spectrometry. *Analytica Chimica Acta.* 2007*. 598,* 110–118.

[33]Lin, Z.; Wang, H.; Xu, Y.; Dong, J.; Hashi, Y.; Chen, S. Identification of antioxidants in Fructus aurantii and its quality evaluation using a new on-line combination of analytical techniques. *Food Chemistry*. 2012. *134,* 1181-1191.

[34]Avula, B.; Upparapalli, S.K.; Khan, I.A. Simultaneous analysis of adrenergic amines and flavonoids in citrus peel jams and fruit juices by liquid chromatography: part 2. *Journal of AOAC International.*2007, *90,* 633-40.

ANNEX II

RAPID AND EFFICIENT EXTRACTION AND ANALYSIS OF SESQUITERPENE LACTONES FROM *AUCKLANDIA LAPPA* DECNE. ROOT

This work was carried out in collaboration with Giorgia Ros[1], Maria Camilla Bergonzi [1]and Anna Rita Bilia[1]

[1]Department of Chemistry, University of Florence, via Ugo Schiff, 6, 50019 Sesto Fiorentino, Florence, Italy

II.I ABSTRACT

Aucklandia lappa Decne. is a perennial plant of the Asteraceae family, native to East Asia, growing in the Himalayas, Burma, China and India. The root is widely used in Asian traditional medicine due to sesquiterpene lactones. The aim of this study was the development and optimisation of the extraction and analysis of sesquiterpene lactones. The current Chinese Pharmacopoeia reports a monograph of "Aucklandiae Radix", but the extraction method is very long and tedious including a maceration overnight and ultrasonications. Different extraction protocols were evaluated with the aim of optimising maceration period, solvent, shake and sonication time. The optimised method consists of only one hour of shake plus 30 minutes of sonication using 100% of MeOH as solvent. ^{1}H NMR was used as a complementary analytical tool to monitor the residual presence of sesquitepene lactones in the herbal material. A suitable LC-DAD method was set up to quantify the sesquiterpene lactones. Recovery was ca. 97% but a very high instability of constituents was found after powdering the herbal drug. A loss of about 20% of total sesquiterpenes after 15-20 days was found; as a consequence, it is strongly endorsed to use fresh powdered herbal material to avoid errors in the quantification.

II.II INTRODUCTION

Aucklandia lappa Decne. (Family of Asteraceae) is a perennial plant, native to East Asia, growing in the Himalayas, Burma, China and India. The root (木香, Muxiang, also called Costus Root) is widely used in Asian traditional medicine due to sesquiterpene lactones. Different commercial names can be found on the market, according to the origin, the root produced in Yunnan and Guangxi of China is called "Yunmuxiang", while that produced in India and Burma is called "Guangmuxiang". "Chuanmuxiang" is mainly produced in Sichuan and Tibet. "Aucklandiae Radix" is one of the fifty fundamental herbs employed in the Traditional Chinese Medicine and a monograph is reported in the current Chinese Pharmacopoeia [1]. It is mainly used for treatments of digestive ailments, including gastric and abdominal pain, loss of appetite, indigestion, diarrhoea, anorexia, nausea and vomiting [2]. The plant is also utilized to treat asthma and cough [3,4], coronary heart disease [4], acute pancreatitis, acute cholecystitis and hepatitis [5,6]. The sesquiterpene costunolide and dehydrocostuslactone (Figure 43) are considered the major active compounds [7–8] of "Aucklandia root", and many pharmacological activities have been

attributed to their presence, such as anti-ulcer [9], anti-cancer [10–11], hepatoprotective [12] and cytotoxic properties [8]. Furthermore, they also have been found to exhibit antiangiogenic [13], anti-inflammatory [14], antimicrobial, fungicidal [15,16] and immunomodulatory activities [17].

At present this plant has a vast diffusion in the European market, requiring the need of a simple and rapid HPLC method for the evaluation of quality control of the herbal drug. The HPLC assay described in the Chinese Pharmacopoeia monograph reports the quantification of the two major sesquiterpene lactones but the extraction method is very long and tedious and includes a maceration overnight and several steps of ultrasonication. The main purpose of our work was the optimization of the extraction method of the sesquiterpene lactones in the roots and the consequent quantitative analysis in real commercial samples of "Aucklandia root".

Extraction method reported in the Chinese Pharmacopoeia was used as staring point to optimise the maceration period, the duration of mechanical stirring, the application of ultrasound bath, solvent choice, shake and sonication time. NMR was used as an integrative analytical method to evaluate the performance of the developed extraction method.

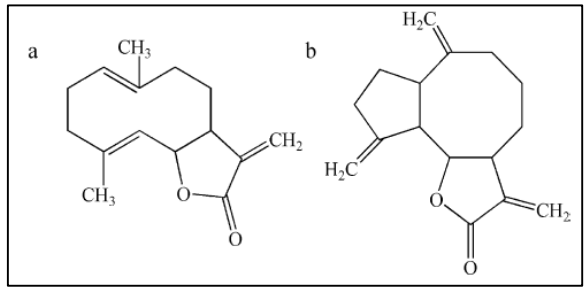

FIGURE 43: CHEMICAL STRUCTURES OF COSTUNOLIDE (A) AND DEHYDROCOSTUSLACTONE (B)

II.III MATERIAL AND METHODS

II.III.I APPARATUS

Extractions were performed using an electronic Sonorex RH 100 SH ultrasonic bath (Bandelin, Berlin, Germany) and a Bandelin electronic Sonoplus, using the mechanical shaker HS 250 BASIC (Ika Labortechnik, Staufen, Germany). A mortar of porcelain with 10 cm of diameter (reference code 1259, Galeno s.r.l.,

Carmignano, Italy) was used to powder the roots before the extraction. An Agilent 1100 HPLC system coupled with DAD detector was used for chemical profile and quantitative analysis. NMR spectra were recorded using a Bruker DRX (Koln, Germany) operating at 400.13 MHz and a Bruker Avance-600 spectrometer operating at 600.13MH (14.1T), both using a 5mm inverse probe equipped with a z-shielded gradient. Data processing was achieved using TOPSPIN software package 1.3.

II.III.II CHEMICAL AND REAGENTS

Dimethylsulfoxide-d_6 (99.9% purity) and MeOH were HPLC grade from Sigma Aldrich (Seelze, Germany). Water was purified by a Milli-Qplus system from Millipore (Milford, MA, USA). The HPLC column used was a Zorbax® Eclipse XDB C18, 150×4.6 mm, 5µm (Agilent, Palo Alto, CA, USA). The following standards were used: Costunolide, code Y0001307 and Dehydrocostulactone, code 38384 both CRS and gived by EDQM (Strasbourg, France).

II.III.III HERBAL DRUG SAMPLES

Two samples (46393, named Auck1 and 31401, named Auck2) were commercial herbal drugs from Shenyang, China, were sent by EDQM. A commercial Chinese sample, Auck3, was donated by Phytax (Schlieren, Switzerland) while five samples from China (Auck5=410079, Auck6=750079, Auck7=110079, Auck8=671375, Auck9=130079), one from Austria (Auck10=112014) and one from India (Auck11= 21657100) were provided by Plantasia (Oberndorf, Austria).

II.III.IV PREPARATION OF EXTRACTS

All the investigated samples were whole roots, firstly were cut into transverse slices and subsequently powdered with a porcelain mortar. The extracts of *Aucklandia lappa* Decne. were obtained by macerating 0.3 g of herbal drug with 50 mL of MeOH, under mechanical shake for one hour. Macerate overnight, the samples were than sonicated for 30 minutes using ultrasonic bath. The total weight of preparation were monitored at the beginning and at the end of the extraction process (after cooling of the sample) and MeOH was replenished in case of the loss of weight. The obtained liquid extracts were mix well and filtered through a membrane filter (nominal pore size 0.45 µm) before the analysis.

II.III.V PREPARATION OF SAMPLES FOR HPLC-DAD ANALYSIS

The extracts of *Aucklandia lappa* Decne. were sonicated for 10 minutes in the ultrasonic bath and then centrifuged for 4 minutes at 14,000 rpm, prior the injection. Subsequently, the standard solutions were sonicated for 2 minutes before the injection. The Reference solutions were prepared as following:

- *Reference solution (a):* 5.0 mg of Custunolide CRS were dissolved in 5 mL of MeOH, shake well and diluted to 50 mL with the same solvent and finally mixed well.
- *Reference solution (b):* 2.5 mg of Dehydrocostus lactone CRS were dissolved in 5 mL of MeOH, shake well and diluted to 25 mL with the same solvent and finally mixed well.

II.III.VI PREPARATION OF SAMPLES FOR ^{1}H NMR ANALYSIS

The herbal material before and after the extraction was freeze-dried for 12 hours in order to remove the residual water. 50 mg of the dried powdered herbal material was put in glass tubes and treated with 0.6 ml of DMSO-d_6. Tubes were manually shaken and finally filtered before analysis.

II.III.VII PROCESS OF SAMPLE SONICATION AND ULTRASONICATION

The sonication was performed using a bath and the temperature never exceeded 25°C. The ultrasonication was performed by immersion of probe directly into the sample with a maximum ampitudine of 50% and a frequency of 20kHz, at room temperature. At the end of process the samples become very hot; the extracts were in direct contact with the air with a possible increase of the oxidative processes and an evaporation of the solvent.

II.III.VIII QUALITATIVE AND QUANTITATIVE HPLC–DAD ANALYSIS

The analysis was performed using a column Zorbax® Eclipse XDB C18, 4.6 x 150 mm, 5 µm, at 24 °C. The mobile phase was composed by methanol (solvent A) and water at pH 3.2 (solvent B), 13:7 V/V. The flow rate was 1.0 mL/min and the detection wavelength was set at 225 nm. The injection volume was 10 µL. The identification of two main constituents was performed by comparison of the retention times and UV spectra of the reference standards and of the data reported in the literature.

The quantitative analysis of the constituents was performed using the external standard. The references Costunolide and Dehydrocostulactone were used to

obtain the calibration curve in a range of 0.220-2.200 µg/mL and 0.407-4.070 µg/mL, respectively. The standards were weighed accurately and dissolved in MeOH to obtain Stock Solutions, which were then diluted. The linearity of the calibration curves were expressed by the values of R^2 (0.99992) for both standards.

II.IV Results and discussion

II.IV.I Optimization of extraction method of sesquiterpenes from Aucklandia Lappa Decne. root

Different extraction methods of the powdered herbal material were evaluated. They were all identified with a number (1, 2, 3, 4, 5) and a letter indicating the type of extraction, namely "S" for sonication bath and "U" for ultrasonication probe. In parentheses the time of extraction expressed in minutes and/or hours is reported. In all the experiments 0.30 g of powdered roots were tested after addition of 50 ml of MeOH.

The following methods were investigated:

-Method 1S (30): 24 h of maceration under shake plus 30 minutes of sonication bath

-Method 1U (30): 24 h of maceration under shake plus 30 minutes of ultrasonication probe

-Method 2S (30): 30 minutes of sonication bath

-Method 2U (30): 30 minutes of ultrasonication probe

-Method 3S (15+15): 15 minutes of sonication plus 1 h of maceration under shake plus 15 minutes of sonication

-Method 3S (30): 1 h of maceration under shake plus 30 minutes of sonication

-Method 3U (15+15): 15 minutes of ultrasonication probe plus 1 h of maceration under shake plus 15 minutes of ultrasonication probe

-Method 3U (30): 1 h of maceration under shake plus 30 minutes of ultrasonication probe

-Method 4S (15+15): 15 minutes of sonication plus 16 h of maceration under shake plus 15 minutes of sonication

-Method 4U (30): 16 h of maceration under shake plus 30 minutes of ultrasonication probe

-Method 5E-S: 48 h of maceration under shake plus 30 minutes of sonication bath

-Method 5E-U: 48 h of maceration under shake plus 30 minutes of ultrasonication probe

The first set of experiments was started with the **Method 1U (30)**, which is that described in the Pharmacopoeia Chinese monograph "Aucklandiae Radix" (木香, MuXiang). This method was used as reference for a preliminary analysis of the data. Recovery of Costunolide and Dehydrocostulactone found with this method was considered 100%.

Subsequently, the possibility to reduce the time of extraction process was evaluated. Samples of roots were extracted using different intervals of time and the efficiency of the sesquiterpene extraction was evaluated. Five different methods of macerations were tested using increasing times (0, 1, 16, 24, 48 hours) of mechanical stirring and followed by 30 minutes of ultrasonication as reported in the official monograph of the Chinese Pharmacopoeia. A considerable loss of MeOH due to evaporation was observed in all samples, consequently, ultrasonication was replaced by sonication.

Preliminary experiments gave contradictory results, probably because sesquiterpene lactones degraded very quickly after powdering the herbal material due to the atmospheric oxygen.

Consequently, HPLC analyses in triplicate on the same sample during different days after the powdering were carried out. A gradual loss of the content of main constituents was observed. After 12 days residual percentage of active ingredients was ca. 90%, while after 18 days, the residual percentage was ca. 80%. The herbal material, therefore, when powdered undergoes to rapid degradation.

Accordingly, sample Auck1 was tested immediately after the pulverizing process, using the following experiments: Method 1S (30), Method 1U (30), Method 2S (30), Method 2U (30), Method 3S (15 + 15), Method 3U (15 + 15), Method 4S (15 + 15), Method 4U (15 +15).

Table 36 reported the results of quantitative analysis performed by HPLC-DAD expressed as percentages of the active constituents. Accordingly, to the above results:

- Sonication bath seems to be able to extract both Costunolide and Dehydrocostus lactone in the same way or even better than ultrasonication probe.
- Sonication or ultrasonication splitted gave the same quantitative results

- The best extraction method was 3S (30), with only one hour of shake followed by 30 minutes of sonication bath.

TABLE 36: QUANTITATIVE RESULTS OBTAINED FROM SAMPLE AUCK1 AFTER EXTRACTION ASSAYS BASED ON DIFFERENT TIMES OF MACERATION COMBINED WITH CENTRIFUGATION OR ULTRACENTRIFUGATION

Sample Auck1	% costunolide (g/100g)	% dehydrocostus lactone (g/100g)	% costunolide plus % dehydrocostus lactone (g/100g)
Method 1S (30)	1.00± 0.05	1.38± 0.09	2.37± 0.07
Method 2S (30)	0.98± 0.03	1.34± 0.05	2.32± 0.04
Method 2U (30)	0.85± 0.07	1.18± 0.08	2.02± 0.08
Method 3S (15+15)	0.96± 0.09	1.35± 0.07	2.31± 0.08
Method 3U (15+15)	0.87± 0.02	1.25± 0.04	2.12± 0.03
Method 3S (30)	1.01± 0.03	1.44± 0.02	2.45± 0.02
Method 3U (30)	0.85± 0.08	1.22± 0.05	2.07± 0.06
Method 4S (15+15)	0.96± 0.05	1.38± 0.07	2.33± 0.06
Method 4U (15+15)	0.85± 0.03	1.20± 0.03	2.05± 0.03
Method 4S (30)	0.86± 0.03	1.27± 0.09	2.13± 0.06
Method 4U (30)	0.96± 0.04	1.41± 0.06	2.37± 0.05
Method 1U (30)	0.90± 0.02	1.20± 0.03	2.10± 0.02

To further assess the influence of maceration time, the extraction methods 3S (30), 2 S (30), 1S (30) were repeated with samples Auck2 and Auck3. Data are reported in Table 37 and Table 38. The best extraction method for Auck3 resulted to be the 1S (30) corresponding to 24 hour of maceration under shake

plus 30 minutes of sonication bath. For Auck2 it seems that method 3S(30) is the best one. Similar results were obtained with Auck4 (Table 39).

TABLE 37: REPEATED ASSAYS WITH SAMPLE AUCK2

Sample Auck2	% costunolide (g/100g)	% dehydrocostus lactone (g/100g)	% costunolide plus % dehydrocostus lactone (g/100g)
Method 2S (30)	0.91± 0.08	1.36± 0.06	2.27± 0.07
Method 3S (30)	**1.01± 0.06**	**1.47± 0.04**	**2.47± 0.05**
Method 1S (30)	0.83± 0.02	1.18± 0.01	2.01± 0.01

TABLE 38: REPEATED ASSAYS WITH SAMPLE AUCK3

Sample Auck3	% costunolide (g/100g)	% dehydrocostus lactone (g/100g)	% costunolide plus % dehydrocostus lactone (g/100g)
Method 2S (30)	1.85± 0.07	1.76± 0.08	3.61± 0.05
Method 3S (30)	1.78± 0.09	1.68± 0.07	3.46± 0.06
Method 1S (30)	**2.17± 0.03**	**2.03± 0.02**	**4.21± 0.02**

TABLE 39: EXTRACTION ASSAYS WITH SAMPLE AUCK4

Sample Auck4	% costunolide (g/100g)	% dehydrocostus lactone (g/100g)	%costunolide plus %dehydrocostus lactone (g/100g)
Method 2S (30)	0.82± 0.09	1.31± 0.08	2.13± 0.07
Method 2U (30)	0.82± 0.03	1.28± 0.06	2.09± 0.04

Method 1S (30)	0.89± 0.05	1.37± 0.04	2.26± 0.05
Method 1U (30)	0.86± 0.08	1.32± 0.07	2.18± 0.04
Method 3S (30)	**0.89± 0.02**	**1.43± 0.01**	**2.32± 0.01**
Method 3U (30)	0.85± 0.02	1.32± 0.04	2.17± 0.04

^{1}HNMR experiments were performed directly on the pulverized herbal drug, to confirm the and exhaustive extraction of active constituents. Firstly, the proton NMR spectra of Costunolide and Dehydrocostuslactone were recorded. Then, the exhausted powdered sample Auck was treated with DMSO-d_6 and evaluated for the presence of the characteristic chemical shifts in the NMR proton spectra. In all the investigated samples no characteristic signals in the range between 8 and 5.5 ppm were found after extraction of the sample with methods 3S(30) (Figure 44).

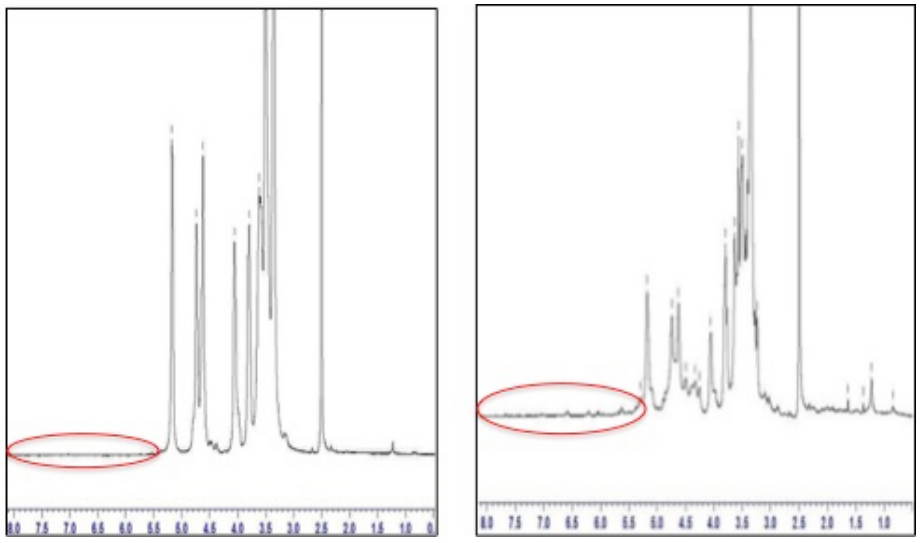

FIGURE 44: 1H NMR SPECTRA OF AUCKLANDIA LAPPA DECNE. ROOTS AFTER METHANOLIC EXTRACTION (A) WITH 3S(30) METHOD AND BEFORE THE EXTRACTION (B)

In conclusion, the sonication is less invasive then ultrasonication and the extraction method 3S(30) is the best one for the extraction of the main active constituents of Aucklandia root. The optimised method is able to extract more than 97% of the total of the active principles.

II.IV.II HPLC ANALYSIS OF AUCKLANDIA LAPPA DECNE. ROOTS EXTRACT

A simple and validated HPLC-DAD method was used for the evaluation of sesquiterpene lactones. Figure 45 shows the chromatographic profile of the methanol extract of *Aucklandia lappa* Decne. at 225 nm, obtained by the extractive method 3S (30). Both Costunolide (Rt 7.55 minutes) and Dehydrocostuslactone (Rt 8.83 minutes) were easily identified by comparison of their retention times of reference standards.

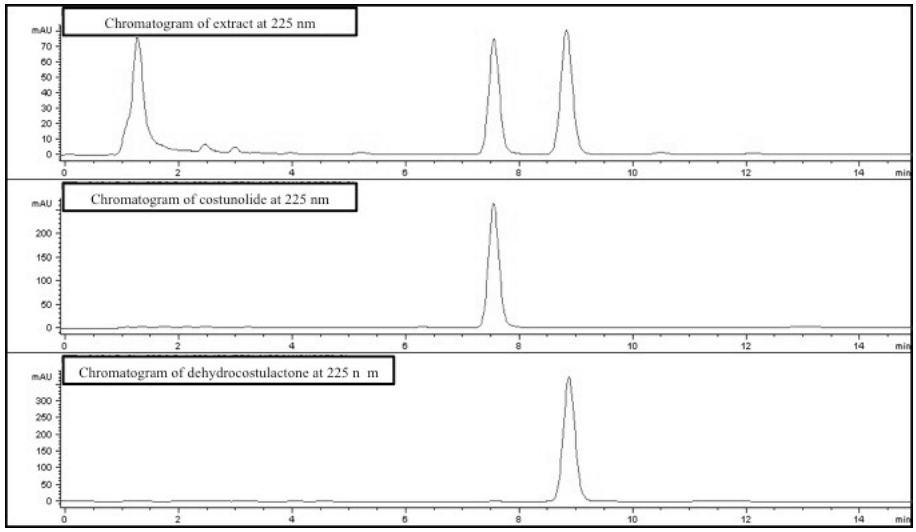

FIGURE 45: COMPARISON OF CHROMATOGRAMS AT 225 NM OF AUCKLANDIA LAPPA DECNE. ROOTS EXTRACT, COSTUNOLIDE AND DEHYDROCOSTUSLACTONE STANDARDS

II.IV.II.I Evaluation of sesquiterpene lactones in *Aucklandia Lappa* Decne. roots

Six different commercial sample of *Aucklandia Lappa* Decne. were evaluated for the content of the main active constituents. The Chinese monograph "Aucklandiae Radix" (木香, Muxiang) reports a minimum content of 0.6% of costunolide and minimum 1.8% for the sum of costunolide and dehydrocostus lactone with respect to the dried herbal drug.

Quantitative analyses were performed by HPLC–DAD and the optimized method 3S (30) was used for the extraction of the roots. All results are reported in Table 40. Among the tested samples, only the samples Auck5 and Auck7 contain less than 1.8% of active compounds.

TABLE 40: EXTRACTION ASSAYS WITH FURTHER SAMPLES

Sample	% costunolide (g/100g)	% dehydrocostus lactone (g/100g)	%costunolide plus %dehydrocostus lactone (g/100g)
Auck5	0.65± 0.02	0.95± 0.03	1.61± 0.02
Auck6	1.06± 0.05	1.30± 0.6	2.36± 0.05
Auck7	0.81± 0.03	0.68± 0.04	1.49± 0.02
Auck8	0.02± 0.04	2.15± 0.06	2.17± 0.05
Auck9	1.31± 0.06	1.35± 0.03	2.66± 0.05
Auck10	1.53± 0.08	1.46± 0.07	2.99± 0.04
Auck11	1.78± 0.04	1.56± 0.04	3.33± 0.05

II.V CONCLUDING REMARKS

HPLC-DAD and NMR were used as integrative analytical tools to optimise the extraction method of sesquiterpene lactones from *Aucklandia lappa* Decne. root.

A very high instability of both constituents was found after powdering the herbal drug with 80% residual percentage of active constituents after 15-20 days. Accordingly, it is strongly recommended to use fresh powdered herbal drug material to avoid errors in the quantification of constituents. The optimised rapid and efficient extraction method is **3S (30),** namely the powdered material is macerated for 1 h under shake followed by 30 minutes of sonication (total time of extraction is 1 h and 30 min).

The developed extraction methods and HPLC analytical method were adequate for the quality control of Aucklandia root in order to guarantee the integrity and stability of the products and assess their efficacy and safety.

II.VI REFERENCES

[1] National Commission of Chinese Pharmacopoeia, Pharmacopoeia of People's Republic of China – The First Division. China Medical Science Press, Beijing, 2010, pp 57

[2] Jiangsu New Medical College, Dictionary of Chinese Material Medica, Shanghai Scientific and Technological Press, Shanghai, 1979, pp 353

[3] Zhang, Y., Xiao, X.D. China Pharm. 2003, 12 (4), 75.

[4] Wang, X.Y., Jia, X.B., Chen, Y., Chin, J. Med. Mater. 2010, 33 (1), 153.

[5] Tian, Y., Gao, H.Y., Zhang, Y. Inform. Tradit. Chin. Med. 2000, 2, 55.

[6] Wang, R.H.J. Chin. Med. 2001, 16 (4), 44.

[7] Rao, A.S.,. Kelkar, G.R., Bhattacharyya, S.C. Tetrahedron 1960, 9, 275.

[8] Sun, C.M., Syu, W.J., Don, M.J., Lu, J.J., Lee, G.H. J. Nat. Prod. 2003, 66, 1175.

[9] Yamahara, J., Kobayashi, M., Miki, K., Kozuka, M., Sawada, T., Fujimura, H. Chem. Pharm. Bull. 1985, 33, 1285.

[10] Kawamori, T., Tanaka, T., Hara, J., Yamahara, Mori, A. H. Cancer Res. 1995, 55, 1277.

[11] Matsuda, H., Kageura, T., Inoue, Y., Morikawa, T., Yoshikawa, M. Tetrahedron. 2000, 56, 7763.

[12] Chen, H.C., Chou, C.K., Lee, S.D., Wang, J.C., Yeh, S.F. Antivir. Res. 1995, 27, 99.

[13] Jeong, S.J., Itokawa, T., Shibuya, M., Kuwano, M., Ono, M., Higuchi, R., Miyamoto, T. Cancer Lett. 2002, 187, 129.

[14] Damre, A.A., Damre, A.S., Saraf, M.N. Phytother. Res. 2003, 17, 722.

[15] Wedge, D.E., Galindo, J.C.G., Macias, F.A. Phytochemistry, 2000, 53, 747.

[16] Luna-Herrera, J., Costa, M.C., Gonzalez, H.G., Rodrigues, A.I., Castilho, P.C. J. Antimicrob. Chemother. 2007, 59, 548.

[17] Taniguchi, M., Kataoka, T., Suzuki, H., Uramoto, M., Ando, M., Arao, K., Magae, J., Nishimura, T., Otake, N., Nagai, K. Biosci. Biotechnol. Biochem. 1995, 59, 2064.

SCIENTIFIC ACKNOWLEDGEMENTS

Department of Chemistry, University of Florence:

Professor Anna Rita Bilia, for the possibility to start this adventure, to work on this very ambitious project and for her believing in my competences, her enthusiasm, her energy and all her precious advises.

Dr Maria Camilla Bergonzi

Dr Benedetta Isacchi

Dr Chiara Righeschi

Dr Karioti Anastasia

My master students *Vieri Piazzini, Andrea Torracchi, Giorgia Ros* and *Gaia Orsi Bertolini* for their help and collaboration in the experimental parts of my thesis.

All co-workers of Phytolab, University of Florence, especially *Camilla Giuliani* and *Stefano Mulas* for each funny moment, for the support and the understanding.

Department of Neuroscience, Pharmacology and Child's Health, University of Florence:

Professor Casamenti Fiorella, for her precious collaboration in the establishment of the *in vivo* studies.

Dr Cristina Grossi

Dr Ilaria Luccarini

Department of Pharmaceutical Science, University of Basel:
Professor Matthias Hamburger, to have given me the great possibility to work in his special research group, as it was my research group.

Dr Mouhssin Oufir, for his immense help and for all the tricks that he taught to me, for his big patience and for his passion for science that motivated me during all my stay in Basel.

Volha Zabela, because she was immediately a friend, for her care and laughs of everyday.

Daniela Elisabeth Eigenmann, for her explanation in laboratory, her contribution in writing my PhD thesis and for all chocolate.

Evelyn Andrea Jähne, for her support during my first experience with cell lines.

Orlando Fertig, for his excellent technical assistance.

Profs. Pierre-Olivier Couraud (Institut Cochin, Université René Descartes, Paris, France*), Babette B. Weksler* (Weill Cornell Medical College, New York, NY, USA) and *Ignacio A. Romero* (Department of Life, Health and Chemical Sciences, Open University, Milton Keynes, U.K) for kindly providing the hCMEC/D3 cell line.